RAMAN SPECTROSCOPY FOR POINT OF CARE URINARY TRACT INFECTION DIAGNOSIS

Simon Dale Dryden, MBChB, MPH

Department of Surgery and Cancer

Imperial College London

This thesis is submitted to Imperial College London in partial fulfillment of the requirements for the degree of Doctor of Philosophy. Except for where indicated, it presents entirely my own work and describes the results of my own research.

COPYRIGHT DECLARATION

ABSTRACT

Urinary tract infections (UTIs) are one of the most common bacterial infections experience by humans, with 150 million people suffering one or more UTIs each year. The massive scale at which UTIs occurs translates to a tremendous health burden comprising of patient morbidity and mortality, massive societal costs and a recognised contribution to expanding antimicrobial resistance. The considerable disease burden caused by UTIs is severely exacerbated by an outdated diagnostic paradigm characterised by inaccuracy and delay. Poor accuracy of screening tests, such as urinalysis, lead to misdiagnosis which in turn result in delayed recognition or overtreatment. Additionally, these screening tests fail to identify the causative pathogen, causing an overreliance on broad-spectrum antimicrobials which exacerbate burgeoning antimicrobial resistance. While diagnosis may be accurately confirmed though culture and sensitivity testing, the prolonged delay incurred negates the value of the information provided doing so.

A novel diagnostic paradigm is required that that targets rapid and accurate diagnosis of UTIs, while providing real-time identification of the causative pathogen. Achieving this precision management is contingent on the development of novel diagnostic technologies that bring accurate diagnosis and pathogen classification to the point of care.

The purpose of this thesis is to develop a technology that may form the core of a point-of-care diagnostic capable of delivering rapid and accurate pathogen identification direct from urine sample. Raman spectroscopy is identified as a technology with the potential to fulfil this role, primarily mediated though its ability to provide rapid biochemical phenotyping without requiring prior biomass expansion. Raman spectroscopy has demonstrated an ability to achieve pathogen classification through the analysis of inelastically scattered light arising from pathogens. The central challenge to developing a Raman-based diagnostic for UTIs is enhancing the weak bacterial Raman signal while limiting the substantial background noise.

Developing a technology using Raman spectroscopy able to provide UTI diagnosis with uropathogen classification is contingent on developing a robust experimental methodology that harnesses the multitude of experimental and analytical parameters. The refined methodology is applied in a series of experimental works that demonstrate the unique Raman spectra of pathogens has the potential for accurate classification. Achieving this at a clinically relevant pathogen load and in a clinically relevant timeframe is, however, dependent on overcoming weak bacterial signal to improve signal-to-noise ratio.

Surface-enhanced Raman spectroscopy (SERS) provides massive Raman signal enhancement of pathogens held in close apposition to noble metal nanostructures. Additionally, vacuum filtration is identified as a means of rapidly capturing pathogens directly from urine. SERS-active filters are developed by applying a gold nanolayer to commercially available membrane filters through physical vapour deposition. These SERS-active membrane filter perform multiple roles of capturing pathogens, separating them from urine, while providing Raman signal enhancement through SERS. The diagnostic and classification performance of SERS-active filters for UTIs is demonstrated to achieve rapid and accurate diagnosis of infected samples, with real-time uropathogen classification, using phantom urine samples, before piloting the technology using clinical urine samples.

The Raman technology developed in this thesis will be further developed toward a clinically implementable technology capable of ameliorating the substantial burden of disease caused by UTIs.

ACKNOWLEDGMENTS

"Success can come to you by the courageous devotion to the task lying in front of you"

C.V. Raman

I am extraordinarily grateful to my supervisors *Professor the Lord Ara Darzi, Mr Daniel Leff* and Dr *Alex Thompson* for the opportunity to take on this research and the guidance that brought this body of work together. So much more valuable was the incredible support they provided in helping me rise to the incredible challenges that life presented outside of clinical research. Completing a PhD is a considerable feat in times of stability, completing one while facing a life-changing diagnosis of my own and a global pandemic should for all intents and purposes have been insurmountable. I could not have completed this work without their wisdom and kindness. I am unable to find the words to fully express my gratitude.

The work described in this thesis spans clinical medicine, microbiology, physics, and nanotechnology. This boundary crossing research would not have been possible without the kindness and generosity of collaborators from across the Trust and College. Thank you, *Giovanni Satta*, *Ali Reza Abdolrasouli* and *Nita Fatania* at Northwest London Pathology Microbiology for welcoming me into your laboratory and patiently answering my endless microbiology questions. I am very grateful to the 10th floor laboratory team who warmly took me into their lab, and especially *Lauren Roberts* for the much-need dose of South Africa to remind me of home. I am extremely privileged to have been encouraged to use the equipment at the Hamlyn Centre, and in particular for the advice and guidance from *Jang Ah Kim* and *Florent Seichepine* in navigating the complexities of nanofabrication.

A special thanks to *Hutan Ashrafian* for being a wonderful mentor, always willing to give advice and guidance on career and life matters.

I have been beyond fortunate to have always had benefitted from the love and support of my parents, family and friends. I am blessed to have the most wonderful wife, *Andrea Barry*, whose unwavering belief and support pushes me to achieve beyond my imagination. I am so grateful to have a partner that gladly gives so much in every sphere of our life so we can both fulfil our potential. To my incredible son, *Gabriel Dryden*, who is my unparalleled greatest achievement. He is a wellspring of wonder and amusement, while being an inspiration to always do better than my best.

TABLE OF CONTENTS

ABBREVIATIONS:

ASB	Asymptomatic Bacteriuria
BHI	Brain Heart Infusion
CAUTI	Catheter Associated Urinary Tract Infection
CA-ASB	Catheter Associated Asymptomatic Bacteriuria
CCD	Charge Coupled Device
CFU	Colony Forming Units
CKD	Chronic Kidney Disease
LB	Lysogeny Broth
LDA	Linear Discriminant Analysis
LSPR	Localised Surface Plasmon Resonance
MHB	Mueller Hinton Broth
NHS	National Health Service
NHSN	National Healthcare Safety Network
NICE	National Institute for Health and Care Excellence
PBS	Phosphate Buffered Solution
PC-LDA	Principal Component – Linear Discriminant Analysis
PCA	Principal Component Analysis
PVD	Physical Vapour Deposition
PVDF	Polyvinylidene Fluoride
QCM	Quartz Crystal Monitoring
R6G	Rhodamine 6G
SCCM	Standard Cubic Centimetres per Minute
SEM	Scanning Electron Micrograph
SERS	Surface Enhanced Raman Spectroscopy
UTI	Urinary Tract Infection
UVRR	Ultraviolet Raman Resonance

LIST OF TABLES AND FIGURES

CHAPTER 1: INTRODUCTION

1.1 THE CLINICAL CHALLENGE

Urinary tract infection (UTI) is one of the most common bacterial infections, with 150 million people suffering from one or more urinary tract infections each year[1]. Half of women will suffer from UTIs in their lifetime. The pervasiveness of UTIs has normalised the infection to one of mundanity, distracting from the substantial health burden caused. The frequency with which UTIs occur rapidly translates to a massive health burden. In the United States (U.S.) alone, UTIs lead to 10.5 million consultations, a fifth of which are emergency department (ED) visits. UTIs account for $3.5 Billion in societal costs in the US alone[2].

Arguably the relatively low proportion of cases that progress to serious infections distracts from the high absolute numbers of infection sequelae. The US has 250000 cases of acute pyelonephritis annually, a condition associated with a 10% mortality risk. Worse still is the misperception of treatment reliability. Antimicrobial therapy has historically been the mainstay of UTI management despite providing little protection against serious sequalae. Where placebo controlled trials have been performed they have not demonstrated protection against upper urinary tract infection, sepsis or death[2]. There is now, however, a growing appreciation for the adverse effects of antimicrobial therapy, most notably on the risk of antimicrobial resistance (AMR), but also on the negative effects on patient microbiome. The lack of efficacy and risk of adverse outcomes has prompted the National Institute for Health and Care Excellence (NICE) to advocate against routine use of antimicrobials[3].

The underappreciation of UTI's health burden may also explain the tolerance of an antiquated diagnostic paradigm. The backbone of the UTI diagnostic paradigm is still centred on urinary Dipstix and culture, first developed in the 1950s and 1800s respectively. Screening through Dipstix and urinalysis has sensitivity and specificity of 80%, leading to delayed recognition or overtreatment respectively[4]. Gold-standard identification through culture incurs a 48-hour delay, effectively negating the value of the diagnostic information provided[5, 6].

Shortcomings in existing diagnostics has prompted the development of a new diagnostic paradigm, which aims to develop technologies with greater accuracy and faster turnaround times. Polymerase chain reaction (PCR) and mass spectrometry (MS) have received the greatest interest as a result of the highly granular diagnostic information in relatively short turnaround times, however neither is suited to the unique disease burden constraints presented by UTIs. A novel diagnostic technology able to deliver accurate diagnosis at large scale and low cost is required to address the burden of disease placed by UTI[5].

Raman spectroscopy has the potential to act as the ideal diagnostic technology for UTIs. Utilising the inelastic scattering of light, Raman spectroscopy provides real time biochemical fingerprinting. It has the potential to do so without prior biomass expansion, and so may be capable of providing UTI diagnosis along with pathogen classification at the point of care[7].

This thesis hypothesises that Raman spectroscopy can reduce the burden of disease caused by UTIs by acting as the effective diagnostic technology capable of providing rapid and accurate diagnostic information. The thesis therefore aims to develop a technology using Raman spectroscopy to diagnose UTIs and provide rapid pathogen identification.

1.2 STRUCTURE OF THESIS

Chapter 2 describes the way in which the current UTI diagnostic paradigm exacerbates the substantial burden of disease cause by UTIs. The chapter is structured as a narrative review to refine the broad epidemiologic and clinical features of UTIs down to the salient features that define burden of disease, and in so, the characteristics of the ideal diagnostic technology. Rapid, ideally point of care, and accurate diagnosis are identified as the key attributes of the ideal diagnostic technology.

Chapter 3 interrogates the hypothesis that Raman spectroscopy can perform as the ideal technology for UTI diagnosis. A narrative review covers the broad topic of Raman spectroscopy focussing on clinical diagnostics before a systematic review assess the state of the art of UTI diagnosis and classification using Raman spectroscopy. The chapter identifies the ability to provide instantaneous biochemical profiling without the need for prior biomass expansion underpins Raman spectroscopy as the basis for an effective UTI diagnostic technology. The systematic review demonstrates that the unique Raman spectra of uropathogens provides for accurate pathogens classification. It also highlights limitations of Raman spectroscopy. Published research frequently relies upon combining Raman spectroscopy with microscopy to gain spatial resolution, however the cost and physical footprint are incompatible with point of care UTI diagnosis. An additional challenge arises in that the exquisite sensitivity that underpins Raman spectroscopy's ability to provide granular classification leaves it vulnerable to misclassification when strict experimental variation is not maintained.

Recognising the exquisite sensitivity of Raman spectroscopy to the experimental parameters applied, **Chapter 4** aims to develop robust methods to be applied in further experimental work. The chapter outlines an approach to Raman research into UTIs covering sample preparation, Raman acquisition, digital spectral processing, and classification through supervised learning. Individual parameters within each section are experimentally isolated and interrogated to develop an understanding of the effect of these on the resulting spectra and final classification.

Chapter 5 interrogates the hypothesis that uropathogens have unique Raman spectra that provide for UTI diagnosis and classification. Raman spectra acquired from 100 clinical samples highlight the challenge posed by spectral variability caused by broad range of biochemical components in urine. Thereafter, Raman spectra acquired from concentrated suspensions of reference strain uropathogens demonstrate that the unique spectra thereof provide for accurate classification. Extending this to suspensions diluted to clinically relevant concentrations, Raman spectroscopy augmented by prolonged acquisition times is unable to achieve pathogen classification. These findings combined demonstrate that uropathogens have unique Raman spectra with the potential for rapid and accurate UTI diagnosis, however that methods are required to capture pathogens and enhance their signal while separating them from the overwhelming background signal of urinary components to achieve classification at clinically relevant concentrations.

Surface enhanced Raman spectroscopy (SERS) provides massive Raman signal enhancement up to 10^{14} times, providing a potential means of identifying uropathogens at clinically relevant concentrations. **Chapter 6** addresses the hypothesis that SERS using nanoparticles can identify pathogens at clinically relevant concentrations. Firstly, SERS spectra are acquired from concentrated suspensions of reference strain uropathogens with classification achieved with only 5 samples of each strain. In the second experimental work, suspensions at clinically relevant concentrations were rapidly physically processed by vacuum filtration through polyvinylidene fluoride (PVDF) membrane filters before acquisition of SERS spectra using colloidal nanoparticles. These experiments demonstrate that SERS spectra augmented by vacuum filtration can identify infected samples, however fell short of providing pathogen classification. It is postulated that inconsistency in the apposition of nanoparticles to the pathogens induces variability in the SERS spectra and improving this will provide for diagnosis with pathogen classification.

SERS-active filters are developed through physical vapour deposition of a nanolayer of gold to PVDF membrane filters. **Chapter 7** investigates the hypothesis that SERS-active filters can achieve UTI diagnosis with pathogen classification direct from urine samples. Prior to working on pathogen samples, an optimal gold nanolayer thickness of 50 µm was established through assessment of SERS enhancement using Rhodamine 6G. Experimental work demonstrated SERS-active filters diagnostic and classification performances on phantom urine samples of 93.2% and 91.7% respectively. Extending this to clinical samples, a dual filtration system was developed to separate urine particulate matters prior to capture of uropathogens on SERS-active membrane filters. The clinical pilot of 100 samples did not achieve UTI diagnosis but demonstrates signal that may be built upon in larger clinical trials.

The thesis is concluded in **Chapter 8**, summarising the finding and the limitations of the experimental work. The future directions of the work are described with the adaptations planned for a definitive clinical trial assessing the clinical performance of SERS-active filters for UTI diagnosis with uropathogen classification.

The major contributions of this thesis are:

1. Development of a Raman methodology for pathogen research using a handheld Raman spectrometer. The multistage process from sample preparation to classification encompasses clinical microbiology, quantum physics, biomedical engineering and chemometric data analysis. The exquisite sensitivity of Raman spectroscopy that provides for rapid pathogen identification, also necessitates a deep understanding across these fields and strict experimental control.
2. SERS-active membrane filters were developed and optimised for uropathogen capture and Raman enhancement. This work is the first to optimise SERS-active filters, demonstrating PVDF contributes minimal noise, and that a gold nanolayer thickness of 50 µm was provides the greatest enhancement of signal.
3. This is the first published work to validate SERS-active membrane filters on urine samples, demonstrating accurate UTI diagnosis with pathogen classification in under 10 minutes.
4. A prototype technology using dual filtration to rapidly capture uropathogens while separating these from urine components was developed and employed in a clinical pilot.

The work presented in this thesis resulted in the following publications in peer reviewed international journals, conference proceedings and presentations at international conferences:

- **Original publication:** Dryden, S. D. *et al.* Rapid uropathogen identification using surface enhanced Raman spectroscopy active filters. *Sci Rep* **11**, 8802, doi:10.1038/s41598-021-88026-9 (2021).
- **Presentation:** Dryden, S. *et al.* in *Optical Diagnostics and Sensing XX: Toward Point-of-Care Diagnostics* (2020).
- **Conference Proceeding:** Simon D. Dryden, Salzitsa Anastasova, Giovanni Satta, Alex J. Thompson, Daniel R. Leff, Ara Darzi, "Toward point-of-care uropathogen detection using SERS-active filters," Proc. SPIE 11247, Optical Diagnostics and Sensing XX: Toward Point-of-Care Diagnostics, 1124705 (14 February 2020); https://doi.org/10.1117/12.2545515

CHAPTER 2: URINARY TRACT INFECTION AND THE NEED FOR NOVEL DIAGNOSTICS

2.1 INTRODUCTION

Urinary Tract Infection (UTI) is one the most common infections worldwide, leading to a substantial health burden encompassing societal costs, patient morbidity and mortality, and a well-recognised contribution towards burgeoning antimicrobial resistance (AMR)[1, 8, 9][10]. Furthermore, any uncertainties in the diagnostic and management pathways for UTI resulting delayed or incorrect treatment exacerbate the mal-effects of UTI.

This narrative review will provide an overview of UTIs, with a special focus on the burden it creates. This review aims to demonstrate that this burden is exacerbated by insufficiencies in current diagnostics and will aim to identify how these may best be addressed to alleviate the burden of disease associated with UTI.

2.1.1 HYPOTHESIS

Novel technologies providing rapid and accurate UTI diagnosis with pathogen classification can fundamentally alter the UTI paradigm therein alleviating the burden of disease caused by UTIs.

2.1.2 AIMS

Primary:

- Define the ideal diagnostic technology to alleviate the burden of disease caused by UTIs.

Secondary:

- Describe the burden of disease caused by UTIs, specifically: the epidemiology of the condition, patient morbidity and mortality, economic costs, and antimicrobial resistance.
- Describe the pathophysiology and microbiology of UTIs with reference to both burden of disease and potential susceptibility to novel diagnostics.
- Describe the current UTI diagnostic paradigm, including currently used diagnostics, with specific reference to how this contributes toward the burden of disease.
- Describe novel and evolving diagnostic technologies with reference to how these may alleviate the burden of disease caused by UTIs.

2.2 METHODS:

This chapter consists of a narrative review of the published literature related to urinary tract infections. The review addresses the epidemiology, the pathophysiology and microbiology of UTI in addition to reviewing the current diagnostic, preventative, and treatment strategies. The review will focus on the burden posed by UTIs and how this is influenced by current diagnostic modalities.

2.3 LITERATURE REVIEW

2.3.1 DEFINITION AND CLASSIFICATION

UTI is defined as an infection anywhere in the urinary tract, including the urethra, the bladder, the ureters and the kidneys[8]. The clinical paradigm of UTI may be further subclassified in various ways, with each sub-classification having unique epidemiologic and clinical consequence.

- Asymptomatic bacteriuria (ASB) refers to infection in the absence of symptoms.
- Lower UTIs refer to infection of the urethra or bladder, while upper UTI refers to infection of the ureters or kidneys.
- Uncomplicated UTI refers to urinary tract infection in a healthy non-pregnant individual without any functional or structural abnormality, while complicated UTI refers to urinary tract infection in those with health or structural abnormalities. The majority of complicated UTIs are associated with urinary catheterisation[11]
- Community-acquired UTI differs from nosocomial-acquired UTI which include those acquired in a health facility. The majority of nosocomial UTIs are associated with catheterisation.

2.3.2 Burden of disease

UTI is one of the most common infections both in the community and in the healthcare setting. 150 million people worldwide will have one or more UTIs each year[1]. In the US 12.6% of adult females will have a UTI each year, with a total lifetime risk of 40-50%[10]. A simplified conceptual approach to UTIs is that of an ascending infection, starting as asymptomatic urethral colonisation, progressing to symptomatic infection of the lower urinary tract and ascending to the upper tract, ultimately risking systemic dissemination via the kidneys (**Figure 2.1**). While the proportion progressing passed each step is low, the constant assault of uropathogens at the urethra translates into large downstream absolute numbers for each stage of infection.

Point prevalence surveys have demonstrated that 3.7% of women in the community will have ASB, with increased numbers seen in those who with recent sexual activity[8]. While the majority of these will not progress to symptomatic infection, a large absolute number will develop a symptomatic infection over time. 12.6% of women in the US will have one or more uncomplicated lower UTIs annually, with an estimated lifetime risk of 60.4%[8]. Furthermore, UTI is likely to recur, with 30-50% of women experiencing one or more UTIs within a year of an initial infection[8]. Progression to upper urinary tract infection is an uncommon, but well recognised sequelae of lower UTI leading to a 4.4 times increased risk of pyelonephritis. The annual incidence of pyelonephritis in the community is 59 per 10000 and 12.6 per 10000 in women and men respectively[8]. Pyelonephritis risks progression to UTI associated bacteraemia and potentially life-threatening Gram-negative sepsis. *Al-Hasan et al.* demonstrated that the age adjusted incidence of UTI associated Gram-negative sepsis in the community of Olmsted County, Minnesota was 55.3 per 100000 and 44.3 per 1000000 for women and men respectively[12]. The 28 day and 1-year all-cause mortality in this group was 4.9% and 15.6% respectively.

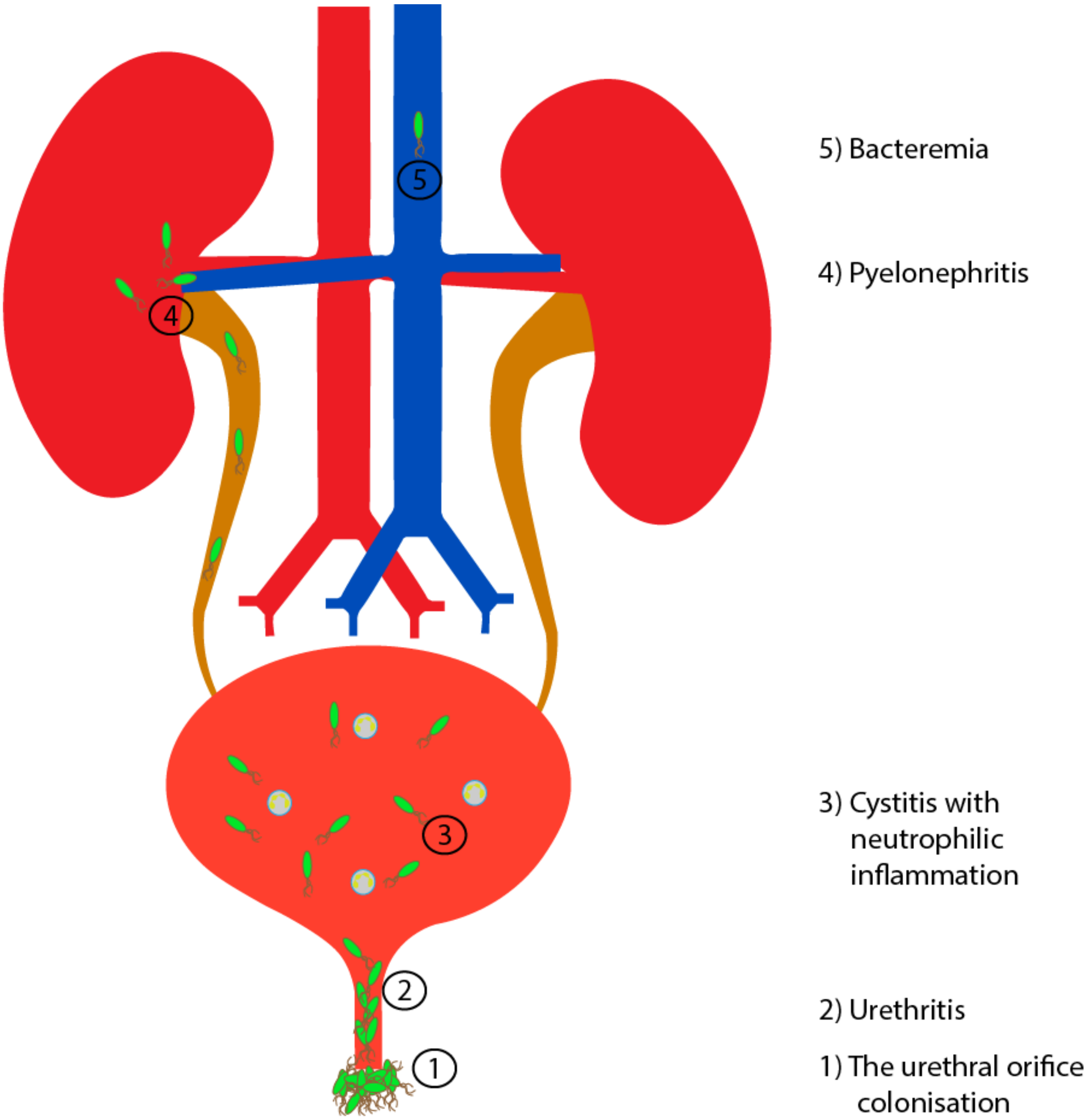

FIGURE 2. 1 THE PATHOGENESIS OF URINARY TRACT INFECTIONS AMENDED FROM FLORES MIRELES ET AL. [1]. UTIS TYPICALLY ARISE FROM ASCENDING BACTERIAL INFECTION. 1) THE URETHRAL ORIFICE IS COLONISED WITH COMMENSAL AND PATHOGENIC BACTERIA. 2) VIRULENCE FACTORS OF UROPATHOGENS ALLOW THEM TO OVERCOME IMMUNE MECHANISMS TO CAUSE URETHRITIS. 3) UROPATHOGENS GAIN ACCESS TO THE BLADDER TO CAUSE CYSTITIS WITH HOST IMMUNE RESPONSE. 4) UROPATHOGENS ASCEND THE URETERS LEADING TO PYELONEPHRITIS. 5) UROPATHOGENS TRAVERSE THE BASEMENT GLOMERULAR MEMBRANE GAINING ACCESS TO THE BLOOD STREAM LEADING TO BACTERAEMIA.

In the healthcare setting UTI is a more prominent and costly problem. UTI accounts for a third of hospital associated infections (HAIs). The prevalence of UTI on any day amongst hospitalised patients ranges from 1.1-6.6%, leading to 1 million nosocomial UTIs annually in the US alone[2, 8, 13]. Urinary catheterisation accounts for 70-80% of healthcare associated UTIs[13, 14].

Catheters present a distinctive pathophysiology, diagnostic challenge and burden within the UTI paradigm. With over 100 million catheters produced annually, urinary catheters are one of the most commonly used medical devices[15, 16]. Prevalence surveys indicate that 17.5% of European patients and 23.6% of US patient will have a catheter during their admission[15]. Catheters are frequently misused, with 40% of catheterized patients receiving one or more days of inappropriate catheterisation, and with healthcare providers unaware of 28% of urinary catheters in place[16, 17].

Urinary catheters are rapidly colonised at a rate of 3-10% per day leading to near universal colonisation within a few days[2, 8, 15]. Catheter-associated ASB (CA-ASB) is a precursor to symptomatic catheter associated UTI (CAUTI). The incidence of CAUTI varies widely by geography and department, reflecting catheter practices, ranging from 3.2 infections per 1000 catheter days in general wards going as high as 15.99 infections per 1000 catheter days in certain neurologic ICUs[11, 18, 19]. The prevalence of symptomatic CAUTI in European hospitals is 1.3 %[9]. CAUTI may lead to ascending infection and predispose to bacteraemia. In a prospective multicentre study, *Melzer et al.* demonstrated that 15% of bacteraemic episodes were associated with urinary catheterisation, and that the 7-day mortality in this group reached 30.1%[20]. A survey across 61 hospitals in Quebec showed that 21% of blood-stream infections were associated with the urinary tract, of which 71% were catheter associated[21]. A large metanalysis of CAUTI in ICUs demonstrated a 1.99 odds ratio for death associated with CAUTI, as well as a 21-day increased length-of-stay, however this may be due to unmeasured confounding[22].

UTI leads to significant morbidity and imposes a substantial cost on healthcare and society. Each uncomplicated UTI leads to a mean of 3.83 symptomatic days, and 2.89 activity limited days[8]. As discussed above, both uncomplicated UTI and CAUTI are significant contributors to blood-stream infection, sepsis and mortality in the hospital setting and community. When multiplied by the frequent occurrence of UTI this rapidly expands to large societal costs. It is estimated the US suffers $3.5 billion in societal costs annually attributed to UTIs[1, 23]. The costs imposed on healthcare systems are pushed to the extreme: healthcare associated UTIs are estimated to cost $390-450 million annually in the US, and £123.9 million in the UK[24, 25].

A highly concerning sequela of UTI is the growing recognition of its contribution toward the emergence of AMR. UTI is the second most common cause for antibiotic prescription in the community in the US[2]. In this setting half of prescribed antibiotics are not needed or are sub-optimally prescribed. Uropathogens develop antimicrobial resistance both vertically (through natural selection) horizontally (through plasmid sharing), allowing for rapid development of antimicrobial resistance[26]. Resistance rates display wide geographic variation, often reflecting prescribing practices. Resistance to ampicillin, previously used as a first line treatment for UTI ranges from 33% in Quebec to over 80% in Mexico. Resistance to ciprofloxacin, widely used as a current first line therapy, is negligible in Canada, but is found in 72% of isolates in Mexico[2].

AMR poses an interesting challenge in the setting of CAUTI. While treatment of CA-ASB is not recommended 60-80% of hospitalised patients with a catheter will receive an antibiotic for another indication[27]. The potential for development of antimicrobial resistance in catheter associated infections is enhanced by bacterial biofilms which result in subtherapeutic antibiotic doses reaching bacteria.[28] Colonised catheter collecting systems have been demonstrated sources for resistant pathogen outbreaks within hospitals[15]. The most recent National Healthcare Safety Network (NHSN) survey on antimicrobial resistance in healthcare associated infections demonstrated resistance rates of 38.4% and 16.1% for *E. coli* to fluoroquinolones and extended spectrum lactamases respectively[29].

2.3.3 THE PATHOPHYSIOLOGY OF URINARY TRACT INFECTION

Risk factors for UTI include factors that either enhance the degree of exposure to uropathogens or enhance colonisation of the urinary tract. Risk factors for uncomplicated UTI include female gender, increasing age, sexual activity, use of condoms, spermicides or diaphragms, current vaginal infection, diabetes and obesity and family history of UTI[1, 2, 8, 30]. Pregnancy increases the risk for ASB, symptomatic UTI and progression to pyelonephritis.[8]

The lead risk factor for CAUTI is the duration of catheterisation[31-33]. Other risk factors include increasing age, female gender, diabetes, obesity, insertion outside of the operating room, health worker hand hygiene practices and patient serum creatinine greater than 2mg/dl[11, 15].

Pathogenesis of urinary tract infections is illustrated in **Figure 2.1**, adapted from *Flores-Mireles et al*.[1]. The initiating event for infection differs in non-catheter associated UTIs as compared to CAUTI. Close proximity of the urethral meatus to the vagina and perineum to the urethra allow for near-constant exposure of bacteria, however host defence mechanisms including innate immunity, regular urinary flushing and nutrient-deplete urine prevent the majority of bacteria from colonising and ascending the urethra[34]. To invade the healthy urethra uropathogenic bacteria have developed mechanisms allowing colonisation and nutrient acquisition (please see virulence factors under microbiology)[34].

The presence of a catheter provides a surface for colonisation subverting normal defences. The catheter is a physical barrier which separates bacteria from the immune system. Urine flow through the catheter prevents flushing of bacteria from the urethra allowing unimpeded growth along the exterior surface, while static pooling of urine provides a growth medium for bacteria[15, 35]. Approximately two thirds of infections ascend the outer surface of the catheter, and one third arise from the lumen of the catheter[33].

Central to the pathogenesis of CAUTI is the establishment of biofilms. Normal urinary proteins such as Tamms-Horsfall protein in addition to fibrinous exudate caused by the immune reaction to foreign bodies form a coating on the catheter surface known as a conditioning membrane[1, 35]. Bacteria in a planktonic state use calcium-mediated adherence to attach to the conditioning membrane where they undergo a phenotypic change into sessile bacteria[36]. These bacteria secrete an extracellular matrix primarily composed of polysaccharides forming a complex 3-D structure[37]. Microorganisms may extend the biofilm or be shed to establish new colonies. The biofilm confers a survival advantage to bacteria. It provides a protective barrier from physical forces and immune cells. Bacteria are able to regulate the environment within the biofilm and are exposed to lower doses of antimicrobials, while bacteria in the sessile state are slower growing[35]. Crystalline biofilms, particularly those associated with *Proteus* species, may lead to catheter obstruction[38, 39].

Having gained access to the normally sterile bladder, either through urethral or catheter colonisation, bacteria multiply and establish further biofilm-protected colonies. Bacterial production of toxins and proteases leads to host cell damage, releasing nutrients and induces an immune response[1, 34, 40]. Bacteria may ascend the ureters and colonise the kidneys causing an upper UTI.

Bacteria in the kidney may cross the tubular epithelium and enter the blood stream, leading to bacteraemia. Risk factors for UTI associated blood-stream infection include male gender, number of days in hospital before bacteriuria, cigarette smoking, malignancy, immunosuppressive therapy, neutropaenia and renal disease[15, 41].

2.3.4 MICROBIOLOGY OF UTI

2.3.4.1 BACTERIAL STRUCTURE AND FUNCTION

The vast majority of UTIs are caused by uropathogenic bacteria, while a small proportion may be caused by yeasts. Bacteria are prokaryotes, meaning they lack a defined nucleus and membrane-bound cell organelles such as mitochondria. Instead, the cytoplasm contains the bacterial cell's DNA as a single ring chromosome. In addition to this the cytoplasm contains ribosomes, proteins, and metabolites. The cell membrane consists of a phospholipid bilayer surrounding the cytoplasm. Embedded in the cell membrane are enzymes such as those responsible for respiration, ion pumps and transporters[42].

Surrounding the bacterial cell membrane is the cell wall, which provides structural support, provide stability, and protect the bacteria from the environment and immune cells. Bacteria may be classified as Gram-positive or Gram-negative according to their response to Gram staining, which provides both a structural and functional differentiation of bacteria. Bacterial cell walls are unique to different bacterial species[42-44].

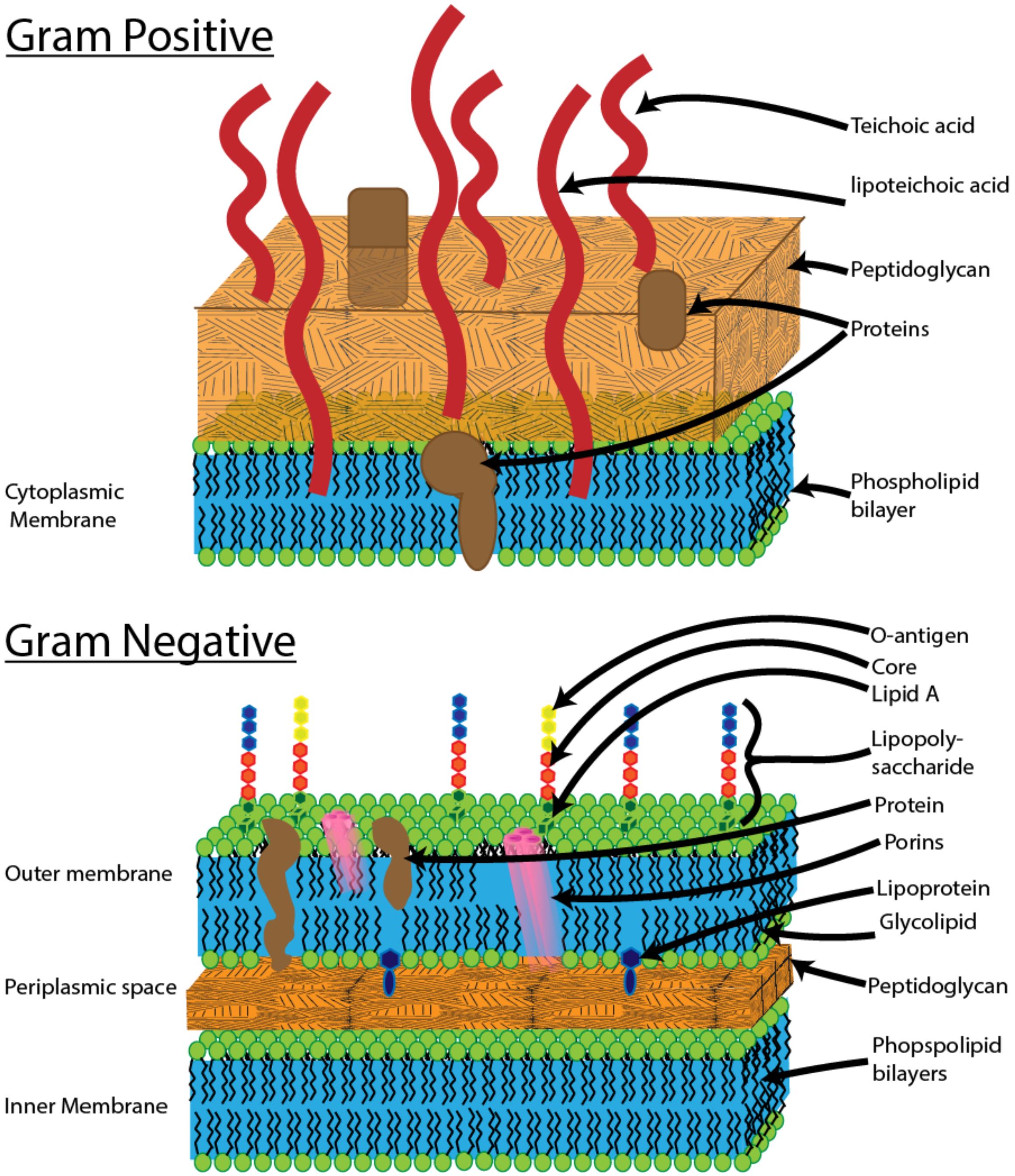

FIGURE 2. 2 GRAM-POSITIVE AND GRAM-NEGATIVE BACTERIAL CELL WALL STRUCTURE, ADAPTED FROM *MOSIER-BOSS ET AL.[45]*

The Gram-positive cell well consists of a thick peptidoglycan layer, which is a mesh-like porous layer that provides structural support while still allowing diffusion of nutrients and metabolites. Embedded in the thick peptidoglycan layer are proteins, polysaccharides and lipoteichoic acids, unique to the bacterial species and serotype[42, 46].

In contrast, the Gram-negative cell contains only a thin peptidoglycan layer not containing lipoteichoic acid. An additional outer membrane surrounds this and encloses the periplasmic space. Contained in this space are transport systems and hydrolytic enzymes that allow for nutrient acquisition as well as other enzymes such as collagenases, elastases and lactamases. The outer membrane is punctuated by porins and transport enzymes that allow uptake and excretion of metabolites. The outer membrane contains lipopolysaccharide, also known as endotoxin, a potent immune stimulator[42]. Lipopolysaccharide structure is unique between Gram negative bacterial species[43, 47]. External to the cell wall bacteria may have additional structures such as polysaccharide capsules, flagella and fimbriae[42]. These structural differences are the basis on which current diagnostic technologies identify UTIs and provide for pathogen classification, and similarly form the basis for evolving diagnostic technologies such as mass spectrometry. Rapid assessment of microbial biochemical constitution is therefore likely to be central to rapid UTI diagnosis with a granular classification of the causative pathogen.

2.3.4.2 VIRULENCE FACTORS

To colonise the urinary tract and overcome the host immune response uropathogens have developed a variety of virulence factors, described in **Table 2.1**. Virulence factors may be activated by quorum sensing – auto-activators that result in virulence factor expression once a certain critical mass of bacteria is present. Adhesion factors such as adhesins, pili and fimbriae recognise and bind to urothelial antigens, allowing for attachment and ascending colonisation[1, 34].

Uropathogens including uropathogenic *Escherichia coli* (UPEC) may form intracellular bacterial communities within urothelial cells thereby evading immune recognition. Groups of 4-10 bacteria may remain quiescent within urothelial cells for months, providing a source for recurrence[1].

Urine is a nutrient depleted medium, as such uropathogens have developed toxins and proteases to liberate nutrients from host tissue. UPEC and Proteus species produce haemolysin A, a calcium dependant toxin[1]. Iron is an important growth factor for bacteria and is depleted in urine. Bacteria use heme, enterobactin and siderophore systems to actively take up iron in urine[34].

Urease catalyses the conversion or urea into ammonia and carbon dioxide. Ammonia increases urinary pH, precipitating calcium and magnesium which are incorporated into crystalline biofilms. Furthermore, ammonia damages urothelium, releasing nutrients and allowing bacterial invasion[1, 39]. Urease is most prominent in Proteus *m*irabilis where it results in significant alkalinisation, but is also produce by *Klebsiella pneumoniae, Staphylococcus saprophyticus*, and *Pseudomonas aeruginosa*[1].

TABLE 2. 1 THE VIRULENCE MECHANISMS OF COMMON UROPATHOGENS. ADHERENCE FACTORS SUCH AS PILI ALLOW PATHOGENS TO ASCEND THE GENITAL TRACT. TOXINS DAMAGE THE UROGENITAL LINING THEREIN LIBERATING NUTRIENTS FOR THE PATHOGENS. IRON ACQUISITION FACTORS ALLOW FOR CAPTURE OR IRON WHICH IS NECESSARY OF CELL RESPIRATION. QUORUM SENSING PROVIDES A LEVEL OF COMMUNICATION BETWEEN PATHOGENS TO ALLOW SYNCHRONISED ACTIVATION OF GENES INVOLVED IN PATHOGENESIS. AIPA: ADHESION AND INVASION PROTEUS AUTOTRANSPORT; CNF1: CYTOTOXIC NECROSING FACTOR; EBP: ENDOCARDITIS AND BIOFILM ASSOCIATED; EPA: ENTEROCOCCAL POLYSACCHARIDE ANTIGEN; ESP: ENTEROCOCCAL SURFACE PROTEIN. EXOS: EXOENZYME S; F1C: TYPE 1-LIKE IMMUNOLOGICAL GROUP C; HLYA: α-HAEMOLYSIN; HPMA HAEMOLYSIN; MR/P: MANNOSE RESISTANT PROTEUS-LIKE; MR/K MANNOSE RESISTANT KLEBSIELLA-LIKE; MSR: METHIONINE SULPHIDE REDUCTASE; NAF: NON-AGGLUTINATING FIMBRIA; ND: NOT DESCRIBED; PMF: *PROTEUS MIRABILIS*-LIKE FIMBRIA; P-PILI: PYELONEPHRITIS ASSOCIATED PILI; PTA: PROTEUS TOXIC AGGLUTIN; TAAPTRIMERIC AUTOAGGLUTIN AUTOTRANSPORTER OF PROTEUS.

Uropathogen	**Virulence Factor**						**References**
	Adherence	**Toxins**	**Immune Evasion**	**Iron Acquisition**	**Urease**	**Quorum Sensing**	
UPEC	F1C Pili P Pili S Pili Type 1 Pili Dr Adhesins	HlyA CNF1	HlyA CNF1 Yersinibactin	Aerobactin Enterobactin Salmochelin Yersinibactin	ND	ND	[1, 34, 42, 48]
Klebsiella pneumoniae	Type 1 Pili Type 3 Pili	ND	Capsule	Aerobactin Enterobactin	Weakly active	ND	[1]
Proteus mirabilis	MR/P Pili MR/K Pili	HpmA HlyA Pta	Capsule ZapA IgA Protease	Proteobactin Yersiniabctin	Strongly active	Yes	[1, 34, 39]
Pseudomonas aeruginosa	Exopolysaccharides	ND	Capsule Elastase	Pyochelin Pyoverdin	ND	Yes	[1, 49]

			ExoS Phospholipase				
Staphylococcus saprophyticus	Ass Adhesin Sdrl Adhesin Uaf adhesin	Aas	ND	ND	Active	ND	[1]
Staphylococcus aureus	Adhesins	ND	ND	ND	Certain species	ND	[1]
Enterococcus faecalis	Ebp pili Ace Adhesin	ND	EpA	ND	ND	ND	[1]
Enterococcus faecium	Ebp pili Esp Adhesin	ND	ND	ND	ND	ND	[1]

2.3.4.3 UROPATHOGENS

The majority of UTIs are single organism infections, with some variation according to the type of UTI as demonstrated in **Figure 2.3.** adapted from *Flores Mireles et al*.

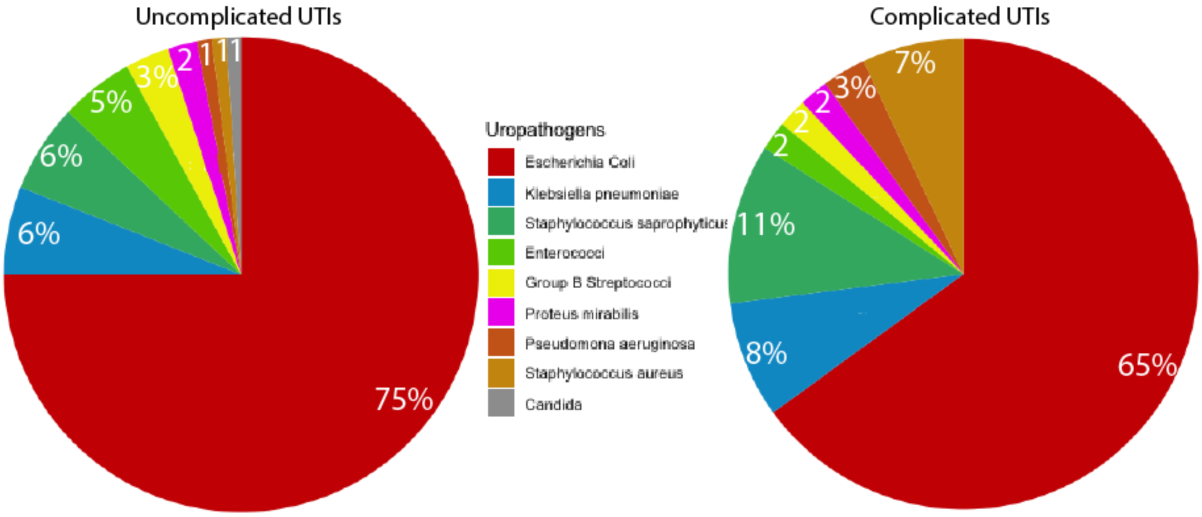

FIGURE 2. 3 PIE CHARTS DEMONSTRATED THE CAUSATIVE UROPATHOGENS FOR UNCOMPLICATED (LEFT) AND COMPLICATED (RIGHT) UTIS ADAPTED FROM *FLORES-MIRELES ET AL.* [1]

Escherichia coli is the most common causative agent in both complicated and uncomplicated UTIs. *E. coli* are Gram-negative rods (0.3-1.0μm by 1.0-6.0μm) which are rapid growing facultative anaerobes. UPEC have developed a number of virulence factors which have allowed them to colonise the urinary tract.[42, 48] *Klebsiella* species including *K. pneumoniae* and *K. oxytoca* are Gram-negative rods (0.3-1.5μm by 0.5-5.0μm) bacteria with a thick capsule. They are facultative anaerobes with simple growth media requirements. *Proteus* species, most notably *P. mirabilis* are Gram-negative rods which are facultative anaerobes. *P. mirabilis* produces a thick crystalline biofilm through urease mediated alkalinisation causing calcium and magnesium dissolution.[39, 42] Enterococci, most commonly *E. faecalis* and *E. faecium*, are Gram-positive cocci (1-2μm) and facultative anaerobes. An inherent resistance to many antibiotics, including cephalosporins, mean enterococci are seen in patients who have already received antibiotics[42]. *Pseudomonas aeruginosa* is a Gram-negative rod (0.5-1.0μm by 1.5μm). Although considered an obligate aerobic bacterium, pseudomonas may use nitrate as a terminal electron acceptor in certain circumstances[42, 49].

TABLE 2. 2 CHARACTERISTICS OF COMMON UROPATHOGENS

Uropathogen	**Stain**	**Shape**	**Size**	**Aerobic/ anaerobic**	**Denitrifying**	**Urease**
UPEC	Gram Negative	Rod	0.3-1.0X 1.0-6.0μm	Facultative Anaerobe	Yes	No
***Klebsiella* Species**	Gram Negative	Rod	0.3-1.5X 0.5-5.0μm	Facultative Anaerobe	Yes	Yes
***Proteus* Species**	Gram Negative	Rod		Facultative Anaerobe	Yes	Yes
Staphylococci	Gram Positive	Coccus	0.5-1.5um	Facultative Anaerobe	No	Yes
Group B *Streptococci*	Gram Positive	Coccus	0.6-1.2um	Facultative Anaerobe	No	No
Enterococci	Gram Positive	Coccus	1-2μm	Facultative Anaerobe	No	No
Pseudomonas aeruginosa	Gram Negative	Rod	0.5-1.0X 1.5-5.0μm	Aerobic	Yes	Yes
***Candida* species**	PAS- positive	Yeast/ oval	3-5μm	Aerobic	No	No

2.3.5 THE CURRENT DIAGNOSTIC LANDSCAPE

Clinical diagnosis of UTI follows a process of clinical assessment and screening, bacterial identification and antibiotic sensitivity testing (AST) (**Figure 2.4**). The initial step includes a clinical assessment paired with a screening urine dipstick upon which a decision for empiric management is made. While rapid, clinical assessment and screening with dipsticks are inaccurate with a sensitivity and specificity of 80%. Using dipstick testing to plan empiric treatment decisions results in 20% of patients without UTI receiving broad spectrum antibiotics where none are needed, while 20% of patients with UTI do not receive appropriate antimicrobial therapy. Furthermore, without bacterial identification broad spectrum antibiotics are required to cover the likely pathogens, increasing the risk of AMR developing.

Positive screening tests may require confirmation and identification of the causative pathogen using culture potentially augmented by matrix assisted laser desorption/ionisation – time-of-flight (MADI-TOF) mass spectrometry. The antimicrobial therapy may be refined to one likely to work based on local sensitivity profiles of the pathogen. Bacterial identification through culture may take up to 24 hours, delaying the change to narrow spectrum antibiotics and adding to workflows[5]. To this end NICE guidelines advocate not sending urine for culture for a first uncomplicated infection, citing cost-effectiveness analyses which demonstrate that the delay associated with microscopy culture and sensitivity (M,C&S) limited its value in decision making[50].

Pathogen identification is followed by phenotypic antimicrobial sensitivity testing (AST) allowing for personalised antimicrobial therapy. However, the 48-hour delay for AST results in significant exposure of uropathogens to potentially incorrect treatment[5].

Developing novel diagnostics that streamline through providing rapid and accurate microbiologic information can address these insufficiencies. A diagnostic device that provides a rapid and accurate bacterial identification at the point of care will allow for appropriate antimicrobial therapy to be prescribed at the consultation. Expedited AST will improve antibiotic stewardship by allowing for early targeted therapy[5].

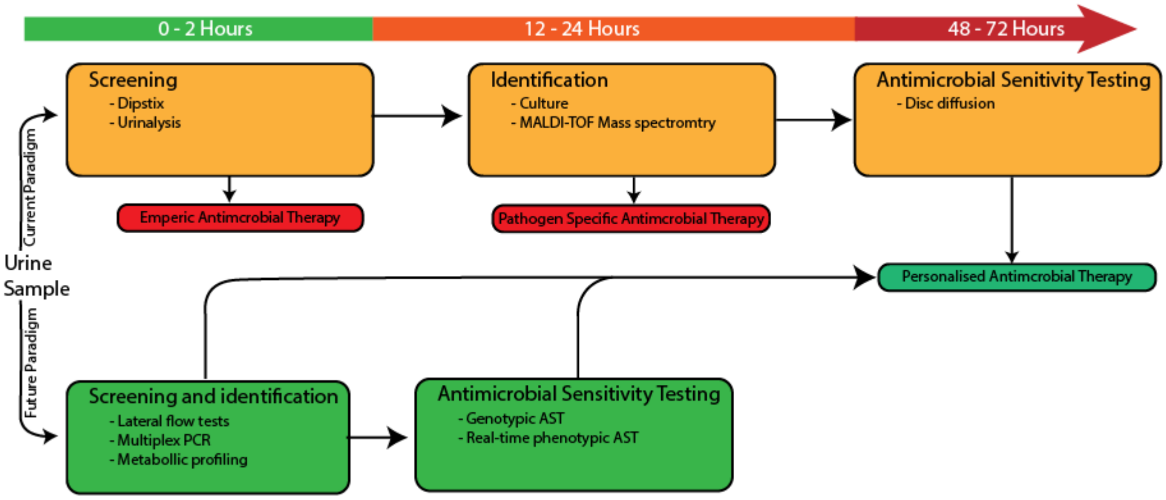

FIGURE 2. 4 EXISTING AND FUTURE DIAGNOSTIC PARADIGMS FOR UTI ADAPTED FROM *DAVENPORT ET AL*.[5].

An overview of current and investigational diagnostics can be seen in **Table 2.3**.

Clinical assessment for UTI includes assessing for symptoms of dysuria, frequency, urgency, incontinence, offensive urine, abdominal or flank pain as well as signs including fever abdominal or renal angle tenderness. Clinical assessment is required to differentiate ASB from UTI. However clinical assessment is inaccurate: clinical criteria alone has an error rate of 33%[51]. Diagnostic uncertainty arises because of poor correlation between signs and symptoms and confirmatory tests. 50% of women with classic symptoms of urgency and frequency will be culture negative, while asymptomatic bacteriuria (positive culture in the absence of symptoms) is present in 3.7% of the women at any time[2, 51].

Screening using urinary dipsticks is extremely cheap and immediately available, however it suffers from poor sensitivity and specificity. A large metanalysis demonstrated screening dipsticks to have a sensitivity and specificity of 80%[4]. Leucocyte esterase may have false positive results in the setting inflammation from another cause, such as urethritis of vaginal infection, while suffering from false negatives in immunocompromised patients. Nitrite testing will lead to false negatives in denitrifying bacteria such as *Enterococcus faecalis[51]*.

Poor performance of screening dipsticks has prompted development of novel screening tests. Lateral flow assays, such as the RapidBac, provide an inexpensive alternative to traditional dipsticks. The RapidBac uses immobilised monoclonal antibodies to *Enterobacteriacea* and a broader spectrum Gram-negative antigen to provide rapid qualitative assessment of urine for infection. While an improvement on dipsticks, the sensitivity remains low at 86%. The test does not provide bacterial identification or AST[52].

TABLE 2. 3 **CHARACTERISTICS OF EXISTING AND INVESTIGATIONAL DIAGNOSTIC TECHNOLOGIES. CORE FEATURES INCLUDE THE TIME-TO-RESULT, THE DIAGNOSTIC PERFORMANCE, AND THE INFORMATION PROVIDED SUCH AS IDENTIFICATION AND ANTIMICROBIAL SENSITIVITY.**

Test		Turnaround	Sensitivity	Specificity	Strengths	Weaknesses	ID	AST
Clinical Assessment		Immediate	NA	NA	Required to differentiate ASB from UTI	High intra observer variability	No	No
Leucocyte and nitrite dipstick (lateral flow assay)		Minutes	80%[4]	80%[4]	Fast. Cheap.	Nitrite non-producers such enterococci and staphylococci negative. Poor sensitivity and specificity	No	No
RapidBac (Lateral Flow ImmunoAssay)		20 minutes	86%[52]	94%[52]	Rapid, inexpensive, and easy to use	False negatives for some bacteria and all fungi No pathogen ID	No	No
Flow Cytometry	UF1000i	Minutes	100%[53]	60%[53]	Rapid	No pathogen ID, Cost not amenable to point of care implementation.	No	No
MALDI-TOF		1-3 hours	86%		Rapid identification of culture pathogens May be useful in polymicrobial infections	Requires pre-processing steps for direct assessment Expensive Not amenable to POCT	Yes (Known)	No
FISH		20 minutes	>96%[5]	>96%[5]	Rapid and accurate for specific pathogens	Requires specific probe development for all pathogens	Yes	No

Multiplex PCR	Septi-Fast	Hours[5]	82%[5]	60%[5]	Rapid Identification and AST	Requires further development for UTI Only identifies known pathogens Not quantitative High risk of contamination	Yes (Known)	Yes (Genotypic only)
	FilmArray	<1 hour						
	GeneXpert	90 minutes						
Real-Time Microscopy	Ocelloscope	108 minutes	NA	NA	Very rapid phenotypic AST	Not assessed in urine	Yes	Rapid
	Accelerate ID/AST	5 hours	NA	NA				
Biosensors		1 hour	89%	100%	Amenable to automation and POCT Potentially high sensitivity and selectivity	Early development. Only identifies known pathogens	Yes	Potentially
Microfluidics			NA	NA	May augment other technologies such as biosensors or time-lapse microscopy	Not widely adopted. Unclear route to market	NA	NA

Flow cytometry uses the scattering and fluorescence of labelled urine samples to provide rapid bacterial and leucocyte counts. The UF-1000i is used as a screening diagnostic in the laboratory providing excellent sensitivity, however it's poor specificity would require a rapid and accurate follow-up confirmatory test[53].

Culture is the established gold-standard for confirmation and AST of UTI, providing serotype level identification and phenotypic AST. Culture may be augmented with molecular techniques, such MALDI-TOF, to provide reduce turnaround time and provide more accurate identification. Culture is performed in centralised laboratories and is slow, taking 24 hours for bacterial identification and up to 48 hours for AST. Furthermore, the gold-standard status of M,C&S has been questioned citing discordance with clinical presentation[54].

The need for reduced time to bacterial identification sensitivity has generated interest in molecular techniques including mass spectrometry, polymerase chain reaction (PCR) and fluorescent *in situ* hybridization (FISH). MALDI-TOF mass spectrometry generates a unique mass to charge fingerprint from ionised samples, which can be compared against a reference library to deliver accurate identification on cultured samples[5]. It has already proven to be a valuable adjunct in centralised laboratories – reducing workflows and improving turnaround times. The requirement for pre-culture and large initial cost limits its use to centralised laboratories. Direct analysis of urine using MALDI-TOF has the potential to reduce bacterial identification down to a few hours, however this requires further research to optimise pre-processing and rebuild reference libraries. Direct MALDI-TOF will still be limited to centralised laboratories given the prohibitive cost of equipment[55].

PCR utilises nucleic acid amplification to identify bacterial genetics in biologic samples such as blood and stool. Early success has been demonstrated using PCR on urine samples, however, it has not been integrated into diagnostic pathways. PCR can potentially provide bacterial identification and genotypic AST within a few hours. While complicated pre-processing is required, this may be mitigated through prepared cartridges preloaded with buffer solution. The technique is highly susceptible to contamination and false positives as a result of indiscriminate amplification of all DNA. PCR may be limited to referenced genotypic signatures and so requires new libraries be developed for UTI[5, 56-58].

FISH utilised fluorescent labelled nucleic acid probes to identify known bacterial DNA and RNA targets. Kits exist for blood stream infection but require further development for use in UTI diagnostics FISH can potentially provide rapid bacterial identification, but no clear route to providing AST is available. FISH is not amenable to POCT.[5]

Emerging technologies for UTI detection include biosensors and time-lapse microscopy, both of which may be augmented using microfluidic technology. A biosensor is a device that can translate a biological signal (most commonly an analyte concentration) into a digital output. These sensors consist of a biologic recognition element that binds the target analyte, paired with a transducer which converts the degree of binding into a digital output. Biosensors are well suited to infection detection as they are potentially automatable, require limited pre-processing, and may be incorporated into POCT. An expanding array of recognition elements is available ranging from simple ion and organic molecules up to proteins and nucleic acid and even up to whole cells. Multiplexing of sensors allows for multiple different analytes to be assessed simultaneously. A challenge lies in developing sensors that are sensitive enough to identify low concentrations of bacteria while retaining selectivity in complex media such as urine. Early work has demonstrated strong potential for biosensors to provide rapid uropathogen detection, and potentially AST[59, 60].

Time-lapse microscopy takes time-lapse digital micrographs of bacteria incubated in an appropriate culture medium. Image recognition software provides real-time colony counting and morphologic assessment. This technique can be adapted to provide rapid phenotypic AST. Early work has been assessed pathogens cultured from bloods, although easy translation to urine should be possible[5, 61].

2.3.6 DIAGNOSTICS FOR CATHETER ASSOCIATE URINARY TRACT INFECTION

There is no available diagnostic or monitoring modality for catheter associated UTI. Rapid catheter colonisation results in near universal CA-ASB over a relatively short timeframe. As CA-ASB does not correlate with clinically relevant outcomes (cost, morbidity, mortality), guidelines do not recommend monitoring of ASB with dipstick or M, C&S.

CAUTI is, therefore a diagnosis made on clinical findings with microbiologic confirmation through M, C&S used only for antimicrobial guidance. The most common presentation is that of fever without localising findings and without another cause. Less commonly localising features including catheter obstruction, acute haematuria, suprapubic pain, or loin pain may be present[15, 62].

A diagnostic technology capable of providing highly resolved metabolic profiling of uropathogens could provide valuable insights into the pathophysiology of CAUTI, therein providing a much-needed means of surveillance.

2.3.7 MANAGEMENT OF UTI

National Institute for Health and Care Excellence (NICE) guidelines recommend immediate treatment of uncomplicated UTI in all children, men and pregnant women, while in women a “back-up” prescription may be considered in place of immediate treatment[63]. Nitrofurantoin is the recommended first line antibiotic, while trimethoprim may be considered in those assessed to have a low-risk of resistance.

Treatment for ASB is not recommended as the high prevalence of ASB paired with the low risk of progression to symptomatic infection leads to an unfavourable risk-benefit profile. Furthermore, treatment of ASB may precipitate symptomatic infection while increasing the risk of AMR. A notable exception is that of ASB in pregnancy, where untreated 20% of patients with ASB will progress to pyelonephritis.[8]

While antimicrobial treatment risks adverse events including gastro-intestinal upset and colitis the principal concern is the development of AMR. This has motivated research into novel treatments that may be used to treat or prevent UTI without increasing AMR. These treatments target uropathogen virulence factors, and so are should have limited unintended effects on commensal bacteria. Treatments under investigation include vaccines against adhesins, toxins, urease and siderophores as well as small molecules targeting urease and pili.[1]

The management of CAUTI should include removal or replacement of any catheter older than 7 days, paired with antimicrobial therapy[3]. Antimicrobial therapy needs to be guided by sensitivity results where available.

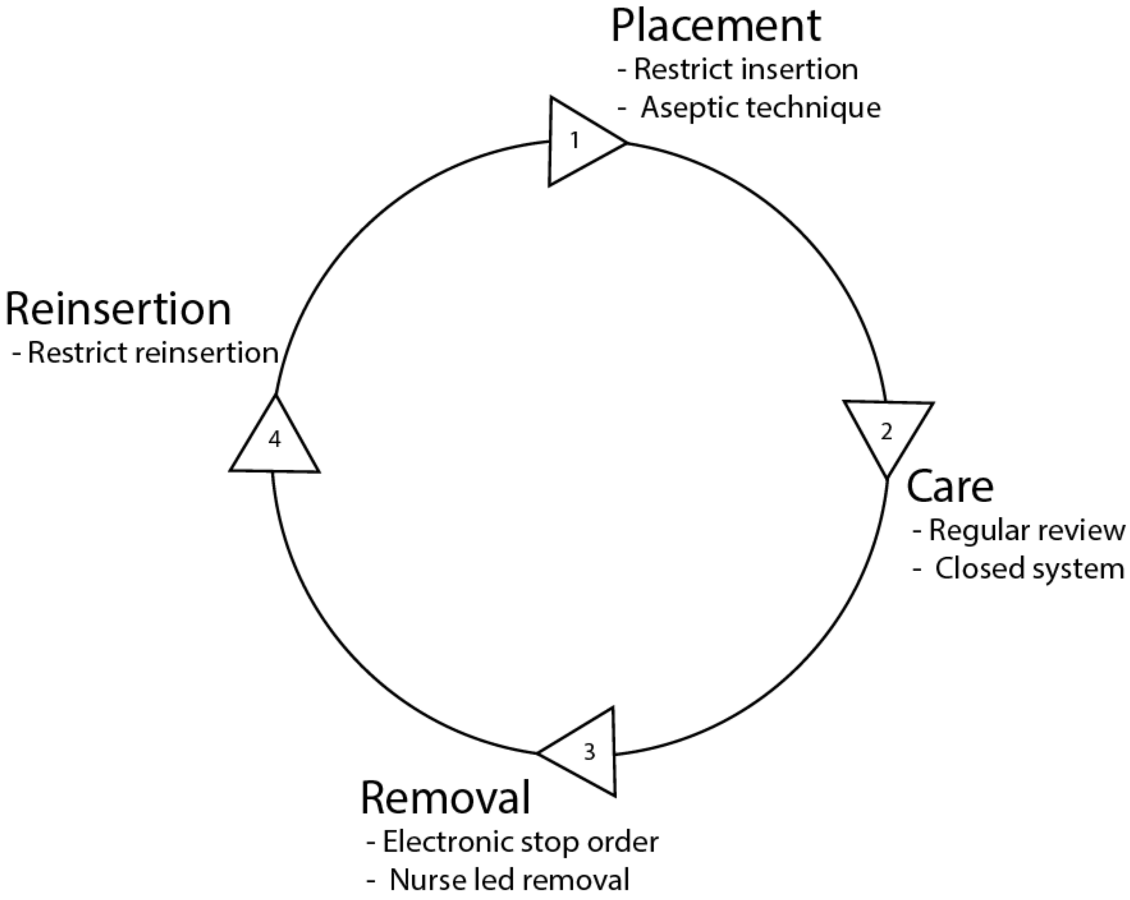

FIGURE 2. 5 THE CATHETER LIFE CYCLE ADAPTED FROM *SAINT ET AL*. [64]. METHODS DEMONSTRATED TO REDUCE CAUTIS INCLUDE: 1) RESTRICTED INSERTION AND ASEPTIC TECHNIQUE, 2) REGULAR REVIEWS AND CLOSED CATHETER SYSTEMS, 3) ELECTRONIC AND NURSE LED REMOVAL, 4) REDUCED REINSERTION

Prevention is the primary goal in CAUTI due to its potential to avoid the morbidity and costs. *Medding* and *Saint* suggested preventative efforts should aim to disrupt the catheter life cycle, as illustrated in **Figure 2.5**[64]. While there are a number of methods for CAUTI prevention, there is no established technology to monitor catheters and predict CAUTI[31] (**Table 2.4**).

Despite numerous attempts, no method has proven benefit in preventing CAUTI. These include prophylactic systemic antibiotics, bag instillation and routine meatal cleaning and catheter replacement. Early optimism for antimicrobial impregnated catheters has been met with unsatisfactory results. Silver alloy coated catheters did not reduce the incidence of CAUTI, while the small reduction afforded by nitrofuranzone impregnated catheters was overshadowed by increased discomfort requiring more frequent replacement[65, 66].

TABLE 2. 4 METHODS FOR CAUTI PREVENTION AS DESCRIBED BY *SAINT ET AL*. FOCUS ON ADDRESSING THE STAGES OF THE CATHETER LIFE CYCLE. THE GREATEST GAINS ARE ACHIEVED BY MECHANISMS REDUCING THE NUMBER OF CATHETERS INSERTED AND THE TOTAL CATHETER TIME.

Stage	**Recommended**	**Not Recommended**
Catheter Insertion	Restrict insertion to defined criteria Strict hand hygiene and aseptic technique Insertion Training Consider Alternatives (e.g., condom catheters) Meatal cleaning Smallest Catheter	Antimicrobial catheters
Catheter Care	Regular review Secure catheter Closed catheter system	Prophylactic antibiotic Antibiotic instillation Daily meatal cleaning
Catheter Removal	Electronic stop-order Nurse-led stop-order	Routine replacement
Catheter Reinsertion	Avoid unnecessary re-insertion (bladder scanners)	

2.4 THE IDEAL UTI DIAGNOSTIC

UTI is a condition pervasive throughout all societies and across all levels of healthcare. This pervasiveness underpins the substantial burden of disease attributable to UTIs. While the morbidity associated with an uncomplicated UTI and the risk of progression to severe disease may appear relatively small, when multiplied by the staggering number of UTIs occurring this presents a significant health burden. The current diagnostic paradigm, characterised by inaccuracy and delay, significantly exacerbates the burden of disease caused by UTIs.

The UTI paradigm has an abundance of areas of uncertainty and unanswered questions, which may be improved upon by novel diagnostics. Limitations in current diagnostics contributes to a paucity of clinical data for important questions including: which microbes are likely to resolve spontaneously, which microbes are likely to recur after treatment, whether different virulence mechanisms warrant different pathogen load treatment cutoffs.

A UTI diagnostic may, in fact, provide information on four questions: firstly, does the urine contain microbes (diagnosis); secondly, what microbes are present (classification); thirdly, what is the pathogen load (quantification); and finally, what are the antimicrobial sensitivities (sensitivity). The value of information provided by each of these questions differs depending on the use case. For example, UTIs are a prominent cause of morbidity and mortality in long-term care homes. In long-term care settings diagnosis has multiple nuances including, a high prevalence of bacteriuria, different symptom profiles resulting from cognitive impairment, and high prevalence of antimicrobial resistance[67]. Additionally, Gram positive uropathogen such as enterococci are considerably more prevalent in this setting, but are significantly less likely to severe disease[10]. Combining these attributes, the greatest value of information would not be provided by diagnosis of infected samples, which would risk overtreatment of asymptomatic bacteriuria, but rather microbial classification which would empower clinical decisions avoiding treatment of benign colonisation[68].

While the notion of developing a diagnostic technology capable of addressing all four diagnostic questions is appealing, it is important to set research priorities where delivery of information will have the greatest value of information under the current paradigm. A secondary goal is understanding how the paradigm is likely to advance, therein developing a strategy as to how diagnostics may contribute to evolution of disease understanding and management in the future.

Uncomplicated UTIs involving healthy women of reproductive age represent the vast majority of all UTIs. Uncomplicated UTIs are at low risk of progression to severe disease, are low risk to carry antimicrobial resistance, are likely to belong to belong to one of few uropathogens (over 90% of community acquired UTI arise from *Escherichia coli*, *Klebsiella pneumoniae*, *Staphylococcus saprophyticus* or *Enterococcus species*). Additionally, the high incidence of uncomplicated UTIs translates to a societal burden through activity limited days, health services burden and a substantial potential source given the large number of antimicrobial prescriptions.

It is reasonable therefore, for prioritise research toward developing a minimum viable product with capabilities specific to uncomplicated community acquired UTIs. The most important characteristic is accurate diagnosis, with greater importance placed on test specificity as compared to sensitivity. Greater specificity should be prioritised as the cost of a false positive, represented by development of AMR caused by overtreatment, is higher than the cost of a false negative given community acquired UTIs are unlikely to progress to severe disease irrespective of antimicrobial therapy.

As community acquired UTIs are predominantly diagnosed in the primary care setting, diagnosis at the point of care is vitally important. Transferring samples to laboratories from primary care setting incurs substantial logistical challenges, costs and delays. Additionally, where results are not available at the point of care, additional burden is placed on health services as they are required to implement procedures for following up of results.

The high incidence of community acquired UTIs necessitates the diagnostic be low-cost. Currently implemented screening modalities including Dipstix are extremely low cost, although the true cost of existing tests is likely incurred through test inaccuracies. Nevertheless, a novel diagnostic needs compete against the extremely low-cost incumbents. Importantly, the high incidence also implies that a relatively high initial capital cost may be offset if the unit cost is very low.

A minimum viable product therefore needs to prioritise low-cost, accurate point of care diagnosis, with particular importance placed on specificity. Of secondary importance to these characteristics, achieving accurate pathogen classification is likely to deliver substantial value. Knowledge of the causative pathogen may allow for more precise antimicrobial therapy, or potentially identify low risk infections not requiring antimicrobials therapy. Additionally, as community acquired uropathogens follow predictable sensitivity, classification may provide a reasonable surrogate for sensitivity testing.

An additional characteristic of secondary importance, yet with the potential to deliver substantial value would be the ability to digitally capture results. The value of the results would then extend beyond the single patient to microbial surveillance and could be made available for secondary research.

A diagnostic test with these capabilities is likely to substantially improve the management of uncomplicated UTIs. Thereafter, additional research may development the technology toward other use cases which may include hospital acquired infections or catheter associated UTIs. For these cases other characteristics such as rapid AST or quantification of pathogen load may be of greater importance.

2.5 CONCLUSION

UTI is a common infection whose pervasiveness leads to significant morbidity and massive costs to patients, healthcare providers and society as a whole. As one of the most common indications for antimicrobial prescriptions, UTI continues to contribute towards the development of AMR. This significant burden of disease is severely exacerbated by a diagnostic paradigm that is plagued by inaccuracies and delays.

Novel diagnostics are needed for UTI that will provide clinicians with reliable information at the time and place where treatment decisions are made. This will allow appropriate therapy to be given from the outset while avoiding overuse of antimicrobials. A novel point of care diagnostic also has the potential to improve workflows by reducing the need for results follow-up. A diagnostic technology whose characteristics reflect those of the ideal technology as described above has the potential fundamentally change the UTI paradigm by allowing rapid initiation of therapies specifically tailored to the causative pathogen.

Additionally, the clinical paradigm of CAUTI poses a unique challenge, where despite being the most common HAI, there is no objective and reliable means of monitoring for its development. Clinical staff must limit catheter usage and attempt pre-emptive removal, while remaining blind to the specific risk profile of the catheter. An ideal monitoring platform would provide dynamic urinary analysis, providing a personalised real-time risk profile. This would allow pre-emptive management and avoidance of the morbidity and costs associated with CAUTI.

CHAPTER 3: RAMAN SPECTROSCOPY FOR UTI DIAGNOSIS

3.1 INTRODUCTION

The ideal diagnostic for UTI would provide rapid and accurate identification of uropathogens, allowing for targeted narrow spectrum antimicrobial therapy to be provided to those patients likely to gain the greatest benefit. This entails the differentiation of infected samples at the point of care, with pathogen classification and AST in a timeframe allowing for precision antimicrobial therapy. Accurate diagnosis using current technologies is reliant on biomass amplification, therein incurring substantial delays.

Raman spectroscopy provides rapid high resolution biochemical analysis, and as such may provide real-time pathogen recognition and classification without the need for biomass amplification. Pathogen recognition using Raman spectroscopy is however challenged by weak Raman scattering and congested spectra both leading to low signal to noise ratios. A plethora of physical and analytical techniques must be potentially optimised to overcome these challenges.

Hypothesis: Raman spectroscopy, once optimised, may provide rapid and accurate UTI diagnosis with pathogen classification.

Aims:

- To review the state of the art of Raman spectroscopy with regard to pathogen identification and classification.
- To identify the opportunities and challenges of uropathogen identification and classification using Raman spectroscopy.
- To identify and understand the settings and techniques that may be employed to optimise uropathogen identification using Raman spectroscopy.
- Identify the barriers to translation of Raman spectroscopic pathogen recognition into clinical practice.

3.2 RAMAN SPECTROSCOPY

3.2.1 RAMAN SPECTROSCOPY OVERVIEW

3.2.1.1 THE RAMAN EFFECT

Raman spectroscopy utilises the inelastic scattering of light to provide rapid assessment of a target's chemical composition. Numerous potential outcomes may occur when a photon (a particle or 'single unit' of light) interacts with a molecule (**Figure 3.1)**. The photon's energy may be absorbed by the target molecule, either with no emitted photon or with later emission of a fluorescence photon. The photon may be elastically scattered (i.e. reflected or rebounded) with no change in energy or wavelength (this process is known as Rayleigh scattering and occurs when no energy is transferred between the photon and the scattering molecule). Finally, the photon may be inelastically scattered (Raman scattered), which involves an instantaneous transfer of energy between the molecule and photon during the scattering process. This transfer of energy to/from the scattering molecule means that there is a concomitant change in the energy of the scattered photon[69-71].

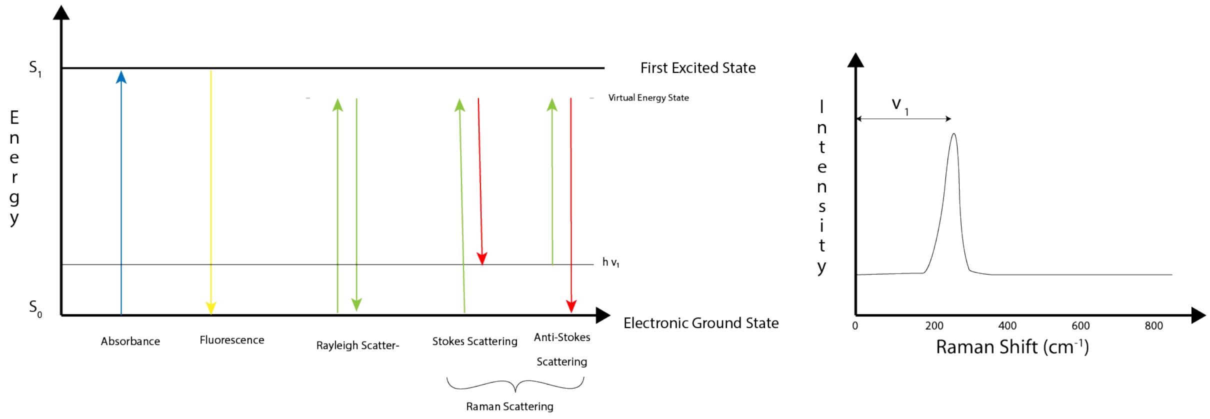

FIGURE 3. 1 JABLONSKI ENERGY DIAGRAM(LEFT) DEMONSTRATING DIFFERENT INTERACTIONS OF LIGHT WITH A MOLECULE, AND RAMAN SPECTRUM (RIGHT) DEMONSTRATING THE RELATIONSHIP OF SPECTRAL PEAKS WITH THIS CHANGE IN PHOTON ENERGY

The change in energy in the scattered photon is apparent as a change in wavelength (or frequency) after the scattering event (Equation 3.1). In Raman scattering, the scattered photons may either lose energy (Stokes scattering) or gain energy (anti-Stokes scattering). The energy difference in the target molecule arises from a change in the vibrational state of the molecular bonds of the molecule, and as such the scattered photon's energy change is unique to the molecular bonds of the target molecule. Plotting the number of photons and energy change (as described by the frequency change) of the scattered photons results in the Raman spectrum which is unique to the target molecule. The Raman effect is directly proportional to the magnitude in change in polarisability of the bond, and as such different molecules exhibit different Raman intensities, with aromatic compounds showing higher intensities than aliphatic compounds[72].

$$E = \frac{hc}{\lambda} = h\nu$$

EQUATION 3. 1 EQUATION 3. 1 BOHR'S FREQUENCY CONDITION: ENERGY OF A PHOTON AS A FUNCTION OF FREQUENCY (OR WAVELENGTH). h = PLANCK'S CONSTANT = 4.14 X 10-15 E.V.S, C = SPEED OF LIGHT = 2.998 M.S-1, λ = WAVELENGTH , v = FREQUENCY, E = PHOTON ENERGY.

3.2.1.2 A Brief History of Raman Spectroscopy for Bacterial Identification

The inelastic scattering of light was first proposed by *Smekal et al.* in 1923[73]. Chandrashekara Venkata Raman independently postulated and began work on demonstrating the inelastic scattering of light. C.V. Raman first demonstrated the inelastic scattering of light in 1927[71, 74, 75]. The demonstration of inelastic scattering of light won C.V. Raman the Nobel prize, making him the first Asian to win the prize and granting him the eponym. To overcome the infrequency of inelastic scattering Raman required a 7-foot refracting telescope to focus the sun as a light source. Technical challenges like these limited the use of Raman spectroscopy to scientific endeavour for decades.

Developments in laser technology, light capture and computing technology over the 1960s and 1970's empowered Raman spectroscopy's development as a powerful chemical analytic technique, while the development of machine learning techniques facilitated it's use in substance identification and classification[76, 77]. The 1980s saw the first use of Raman spectroscopy as a technique for bacterial investigation and classification[78].

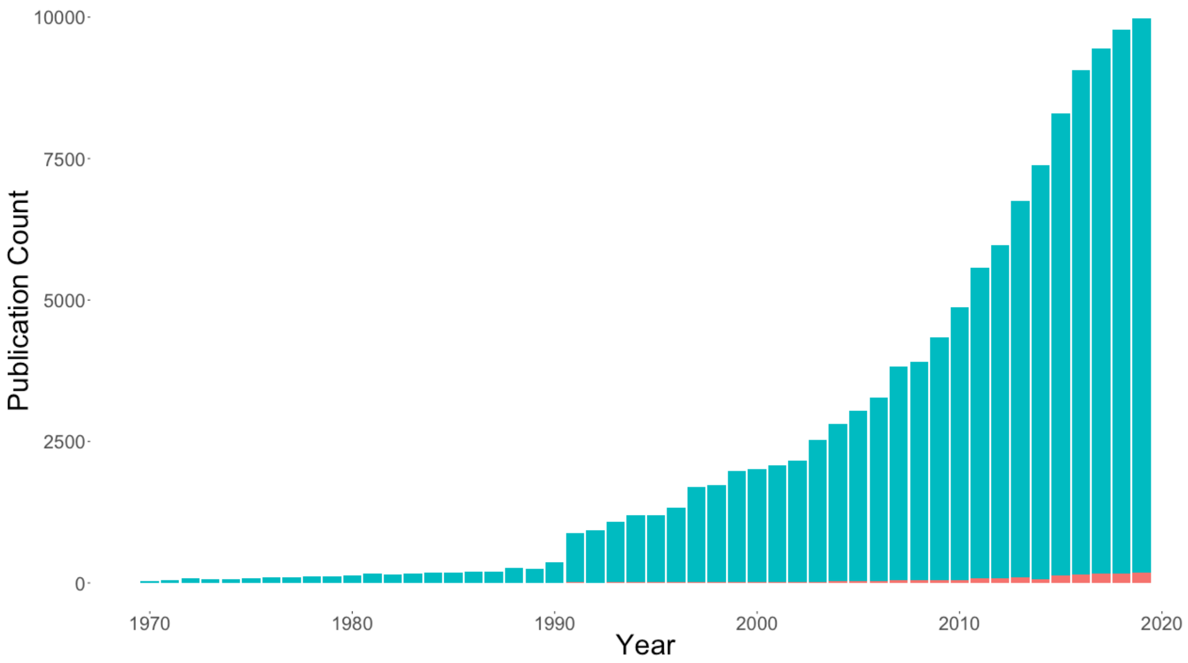

FIGURE 3. 2 WEB OF SCIENCE PUBLICATION COUNT FOR ARTICLES CONTAINING RAMAN SPECTROSCOPY (BLUE) AND CONTAINING BACTERIA (RED). THERE HAS BEEN AN INCREASE IN THE NUMBER OF ARTICLES PUBLISHED ON RAMAN SPECTRSCOPY WITH AN INCREASING PORTION OF THESE INVESTIGATING BACTERIAL RAMAN SPECTROSCOPY.

Two further developments potentiated Raman spectroscopy as a microbial diagnostic technology. In 1974 *Fleischman et al.*, stumbled upon massive Raman signal enhancements while attempting to use silver electrodes to aggregate pyridine targets[79, 80]. Four years later Jeanmarie and Van Duyne demonstrated the enhancement to have arisen from electromagnetic enhancement provided by application of the target to a roughened metal surface, therein describing surface enhanced Raman spectroscopy (SERS)[81].

Additionally, in 1972 optical microscopes were integrated with Raman spectroscopy to create Raman microscopy. Combining microscopy allowed the focusing of Raman excitation down to single cell focus, allowing the collection of single bacterial spectra known as whole organism fingerprinting.

3.2.1.3 THE CHALLENGES OF AND OPPORTUNITIES OF BACTERIAL RECOGNITION USING RAMAN SPECTROSCOPY

TABLE 3. 1 CHALLENGES AND OPPORTUNITIES FOR PATHOGEN RECOGNITION USING RAMAN SPECTROSCOPY.

Strengths	**Weaknesses**
Possible without biomass amplification	Weak Raman effect
High target sensitivity and specificity	Biologic molecules are weak Raman scattering
Little sample physical pre-processing required	Susceptibility to fluorescence
Able to identify non-cultivable organisms	Non-selective
Water Raman signal is weak	Highly sensitive to changes in Raman experimental variation

Raman spectroscopy faces multiple challenges that must be overcome before employing it for pathogen detection. The Raman effect is weak with only 1 in 10^6 incident photons being inelastically scattered.[69, 82-86] The weak Raman effect necessitates powerful laser and sensitive optical detection to bring the Raman effect up to the limit of detection. These electronics in turn contribute noise that may obfuscate the target's signal. While it is possible to overcome this challenge by increasing the number of scattered photons through increasing incident light intensity and time this may lead to photodegradation or fluorescence. A further challenge arises in that many biologic molecules are weak Raman scatterers, further compounding the challenge in identifying biologic Raman signals.

Raman scattering is in the order of 10^{14} times weaker than fluorescence[72]. Therefore, bacterial detection of pathogens may not be possible directly from media prone to fluorescence, notably urine. As such steps may be required to physically separate urine or quell urine fluorescence.

The Raman effect is non-selective, arising from all molecules that light interacts with. Raman assessment of complex samples can result in overcrowded Raman spectra not amenable to classification. This provides a significant challenge in mixed infections where overlapping Raman spectra may obscure each other[77, 87]. It is frequently necessary to amplify target molecules and reduce competing signals through physical processing steps prior to acquiring spectra.

Raman spectroscopy is highly sensitive, with minor changes in sample preparation, spectral acquisition and digital processing resulting in strikingly different spectra[82]. This necessitates strictly standardised experimental procedures during Raman investigation and poses a challenge in translation towards a clinical expansion.

Raman spectroscopy has many strengths which make it optimally suited for the clinical challenge of UTI diagnosis. Developments in laser sources, charge coupled devices and processing hardware have provided low-cost, compact and robust Raman equipment amenable to implementation at the point of care[45].

Raman spectroscopy delivers spectra with high sensitivity and specificity. High sensitivity has allowed the detection down to the level of single cells and molecules[88-91]. The high sensitivity simultaneously allows for quantitative assessment, providing a route not only for pathogen detection but also assessment of pathogen load and potentially rapid phenotypic AST[77]. The specificity is enabled by high resolution spectra with very narrow peaks as compared to Fourier transform infrared spectroscopy and fluorescence spectroscopy. High resolution spectra allow simultaneous identification of many chemical bonds allowing for accurate molecular detection. High resolution also providing for multiplex assessment, therein allowing for detection of molecules and organism with a high degree specificity[70, 82].

The ability of Raman spectroscopy to work with minute sample volumes potentially obviates the need for biomass amplification which is the single most time-consuming step in pathogen classification. The ability to circumvent biomass amplification makes Raman spectroscopy one of a handful of technologies amenable to phenotypic point of care pathogen classification[76, 77]. Similarly the ability to identify samples without preculture potentially allows Raman spectroscopy to identify non-cultivable organism, or organisms suppressed by current antimicrobial therapy, therein avoiding false negative tests[77].

Raman spectra can be acquired with little or no physical pre-processing steps. Water has a weak Raman spectrum, avoiding the need to separate pathogens from the media without losing their signal[88]. Therefore, Raman spectroscopy can potentially be reagentless and fully automatable, therein having the potential to be transformed into a point of care test.

3.2.2 ACQUIRING A SPECTRUM

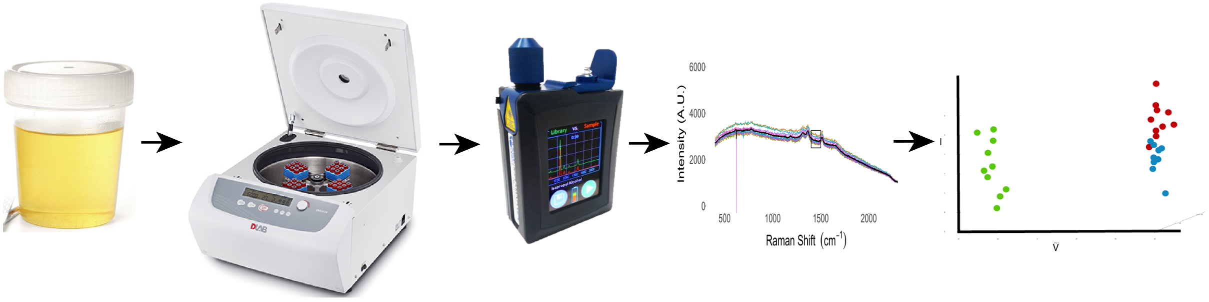

Sample Phystcal Processing Acquistion Digital Processing Classifcation

FIGURE 3. 3 PATHOGEN IDENTIFICATION FROM SAMPLE TO CLASSIFICATION.

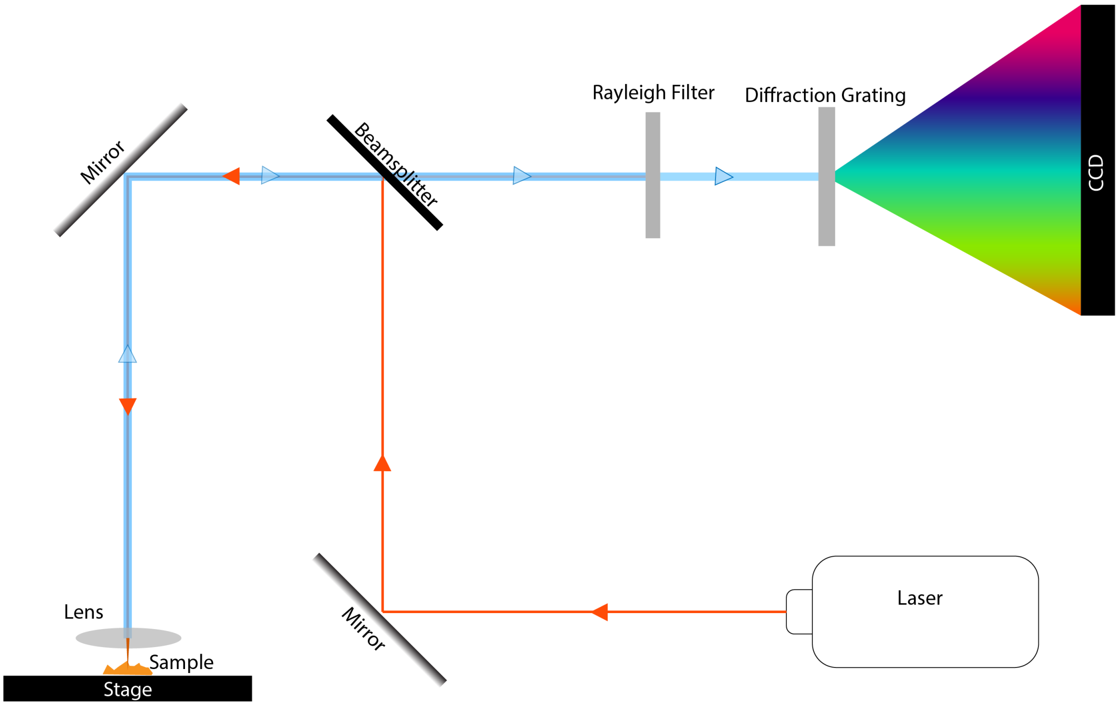

FIGURE 3. 4 THE ANATOMY OF A RAMAN SPECTROSCOPE

The complete process from sample to classification using Raman spectroscopy is depicted in **Figure 3.3.** Within each step several factors must be adjusted to optimise sample classification. Samples may be physically processed with the goal of aggregating the target within the spectroscope's focal volume and potentially separating off other substances that may overcrowd the Raman spectrum. A spectrum is captured from the sample using a Raman spectroscope. The spectrum may be digitally pre-processed with the intention of removing noise while retaining the target signal. Unsupervised chemometric machine learning techniques may identify groups without the need for prior knowledge. Certain chemometric classification techniques may require or be enhanced by preceding feature reduction. Finally, validation is employed to confirm the accuracy of the result on independent data. The identification of microorganisms requires strict standardisation of sampling procedures and strict control of spectral acquisition parameters[76].

TABLE 3. 2 FACTORS UNDER CONTROL DURING SPECTRA ACQUISITION.

Spectrum acquisition			
Factor	**Process**	**Strengths/Opportunities**	**Challenges/ weaknesses**
Laser Power	Delivery of more incident photons with a linear increase in Raman signal	Simple means of increasing signal	Non-selective Higher power laser may destroy samples or lead to photodestruction
Acquisition time	Deliver more incident photons with a linear increase in Raman signal	Simple means of increasing signal Linearly increased stability of spectra	Non-selective Increasing time may not be feasible
Laser wavelength	Selection of wavelength according to target molecule causes signal enhancement mediated by preresonance	Selective signal enhancement UVRR con provide signal enhancement up to 10^6	Minor signal enhancement Certain wavelengths are destructive UVRR not compatible with SERS
Raster orbital scanning	A narrow focal field is moved across a sample	Narrow focal field provides higher resolution spectra while limiting small sampling challenges and photodestruction	Not possible with Raman microscopes
Raman microscopy	Pairing a spectroscope with an optical microscope allows, allowing a reduce field of focus	Incident light tightly focussed on target generates high resolution spectra while avoiding competing signal from substances	Expensive. Technical user experience required for accurate focussing

Raman spectra are acquired using a Raman spectrophotometer (**Figure 3.4**). A laser provides an exciting monochromatic light source which is focused on the sample. Scattered light from the photons is passed through filter to remove elastically (Rayleigh) scattered photons before the Raman scattered photons are quantified using a charge couple device.

3.2.2.1 LASER POWER AND ACQUISITION TIME

The factors under control during spectral acquisition are summarised in **Table 3.2**. Improving the captured Raman spectrum can be achieved through increasing the number of incident photons or through control of the focal volume in which the incident photons interact with the molecules of interest, with both methods resulting in a linearly increased number of captured Raman scattered photon[76]. A greater number of incident photons can be achieved through increasing the laser power or longer acquisition times. The increase in number of scattered photons is non-selective with respect to the molecule from which they are scattered, and so these factors may not be used to selectively enhance identification of target molecules. The increased number of scattered photons results in more stable spectra as a result of effectively sampling more molecules within the sample relative to the high frequency noise generated by electronics. A challenge arises in that increasing the number of incident photons delivers more energy to the sample which may lead to sample destruction. Increased power delivers photons at a greater rate, as compared to increasing acquisition time which provides the same rate of photon delivery but over a longer period. Increased power therefore has a greater propensity toward sample degradation as the increased photon flux does not allow for the energy to dissipate[72]. This may be partially overcome by a pulsed laser sources in which intermittent delivery of photons allows energy dissipation in between pulses, or through use of a raster orbiting scanner that moves the laser focus across the sample such that it is not focussed on any one point long enough to cause damage[86, 92]. A practical approach to selection of laser power and acquisition time is to maximise the laser power without degrading the samples, and then find the minimised acquisition time that provides stable Raman spectra.

In addition to the excitation time (during which light interacts with the sample), consideration may be given to the acquisition time (during which scattered photons are captured). Time-gated Raman spectroscopy (TG-Raman) recognises that Raman scattered photons are emitted on a relatively short timescale as compared to fluorescent photons, and as such gating the acquisition time improves the relative number of Raman photons, as depicted in **Figure 3.5**[93]. While TG-Raman does not increase the total number of Raman scattered photons, the higher ratio relative to florescent photons improves the Raman signal relative to the background level. Importantly the emission time for Raman scattered photons is measured in picoseconds, and so TG-Raman requires a pulsed laser, intricate control system and highly sensitive light capture. *Kögler et al.* demonstrated TG-Raman delivered higher resolution spectra of *Escherichia coli* as compared to traditional Raman spectroscopy[94].

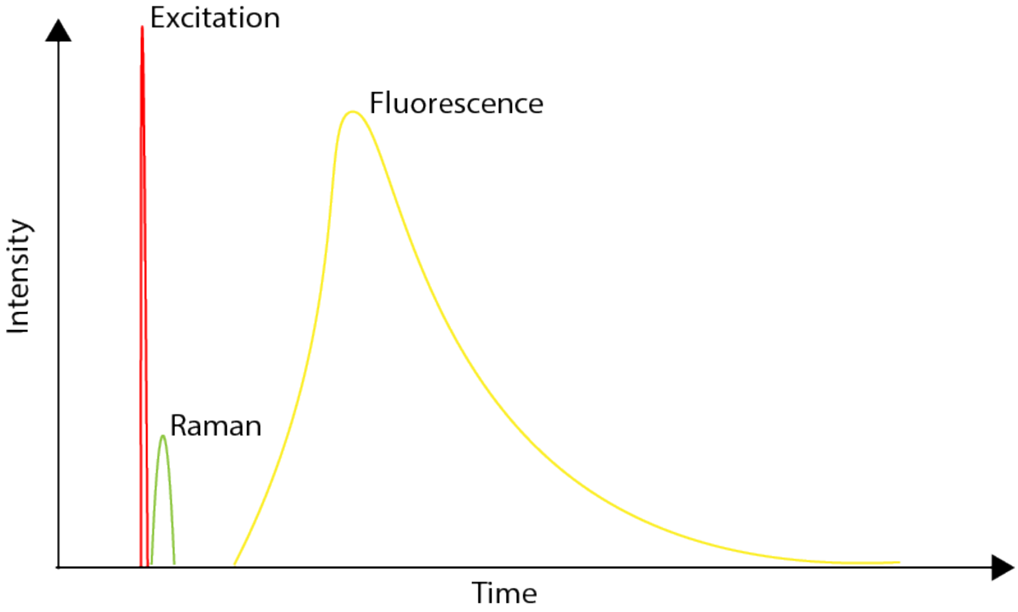

FIGURE 3. 5 TIMING OF RAMAN AND FLUORESCENT EMISSION RELATIVE TO EXCITATION ADAPTED FROM *WEI ET AL.*[26]

3.2.2.2 EXCITATION WAVELENGTH AND ULTRAVIOLET RESONANCE RAMAN

The spectral features are dependent on the excitation wavelength used. If the excitation wavelength is in the range of the absorption range of the target molecule, the electron preresonance occurs leading to signal enhancement[45]. This effect occurs over a narrow range, enhancing signal from molecules with adsorption within 10 nm of the excitation wavelength and quelling signal outside of this range[95]. Ultraviolet resonance Raman (UVRR) is a technique in which the use of UV excitation wavelengths results in electron resonance leading to signal enhancement up to 10^6 times[83, 95]. Additionally, UVRR is not subject to the fluorescence seen visible and near infrared wavelengths[76, 92, 96]. The benefits provided by UVRR are contrasted against significant limitations: UV laser sources are more expensive as compared to infrared sources; UV photons are higher energy (**Equation 3.1)** and so prone to causing sample damage; and most notably UVRR is not compatible with surface enhance Raman spectroscopy whose potential signal enhancement is much greater than that provided by UVRR[72, 82]. Rotating stages have been used to avoid photodestruction by UV light.[92]

When applied to pathogen classification, UVRR enhances the Raman signal primarily of nucleic acids and aromatic amino acids. A classification challenge arises in that the enhanced nucleic acids and amino acids are not likely to vary largely between species as compared to the cell envelope components that are preferentially enhanced by visible and near infrared wavelengths[45, 69, 83, 97]. Prior to the widespread use of SERS, UV wavelengths were more prominent in the literature but have now been superseded by visible and near infrared wavelengths. An additional potential consideration is that longer wavelengths penetrate deeper into the sample with near infrared penetrating up to 5mm, however this is unlikely to provide significant benefit in pathogen identification and classification[70, 88].

3.2.2.3 Focal volume, Raster Orbital Scanning and Raman Microscopy

Raman scattering arises non-selectively from the interaction of photons and molecules within the space in which the laser is focussed. Therefore, the resulting spectrum is highly contingent on the focal volume. A smaller focal volume will contain fewer molecules resulting in Raman spectra with well-defined peaks, while a larger focal volume will contain a greater number of molecules resulting in Raman spectra with less well-defined peaks. However, the use of smaller focal volumes may result in sampling challenges in which small sampling volumes may not contain consistent proportions of target molecules. Two techniques may be employed to utilise small volumes while ensuring accurate sampling: raster orbital scanning and Raman microscopy.

Raster orbital scanning (ROS) rapidly moves a narrowly focused laser beam across a wider area of the sample, therein capturing a Raman spectrum form a wider area while maintaining a smaller focal volume. This is technique is useful in complex mixtures including suspended pathogens or irregular samples including cultures on solid media. A precursor to ROS was first implemented by *Jarvis et al*., in which a moving stage was used to collect 50 spectra across each individual sample and averaged to create a single representative spectrum[96]. ROS is now available on most handheld spectrophotometers.

Raman microscopy combines optical microscopy with Raman spectroscopy, allowing for a narrow focal space to be accurately focussed onto a target. Raman microscopes have focal areas as small as 1 μm allowing the acquisition of high-resolution spectra from single bacteria[98, 99]. This is in contrast the focal area of spectrophotometers is 100 μm or more, and as such spectra arises from multiple bacteria in addition to a substantial volume of background media. Raman microscopy has gained greater traction in Raman bacterial classification in the published literature as a result of the high-resolution spectra generated[100]. Raman microscopy may be better suited to classification of mixed infections as a result of its ability to capture spectra from individual bacteria.

However, Raman microscopy has limitations as compared to plain Raman spectroscopy. Identifying the bacteria is time-consuming and cost-inefficient[69, 88]. Technical expertise is required for the user to identify and focus the laser on the pathogen, which is introduces inter-user variation[69, 88]. In one study, *Mircescu et al.* were required to bin 30% of spectra because of inadequate peaks resulting from imprecise focussing[101].

Furthermore, Raman microscopy is unable to answer the primary diagnostic question as to whether the samples is infected unless the user first identifies the infection. Raman microscopy is similarly unable to provide pathogen load quantification. Within samples, sequentially collected spectra of individual microorganism have differing spectral features collected using Raman microscopy introducing variation which classification algorithms need to account for[69, 83]. This effect is mitigated when using plain Raman spectroscopy due to the inclusion of multiple bacteria within the field of focus. Furthermore, the potential role of Raman microscopy for clinical identification of bacteria is significantly limited due to the prohibitive cost of Raman microscopes and their large physical footprint[88, 100].

3.2.3 ANALYSING A SPECTRUM

A Raman spectrum comprises a large volume of chemical data condensed into a single data vector. Classification by direct visual analysis of Raman spectra is rarely possible and as such chemometric techniques are required to gain accurate classification. Analysis of spectra follows a process of digital pre-processing, feature creation, classification and validation[102].

3.2.3.1 SPECTRA DIGITAL PRE-PROCESSING

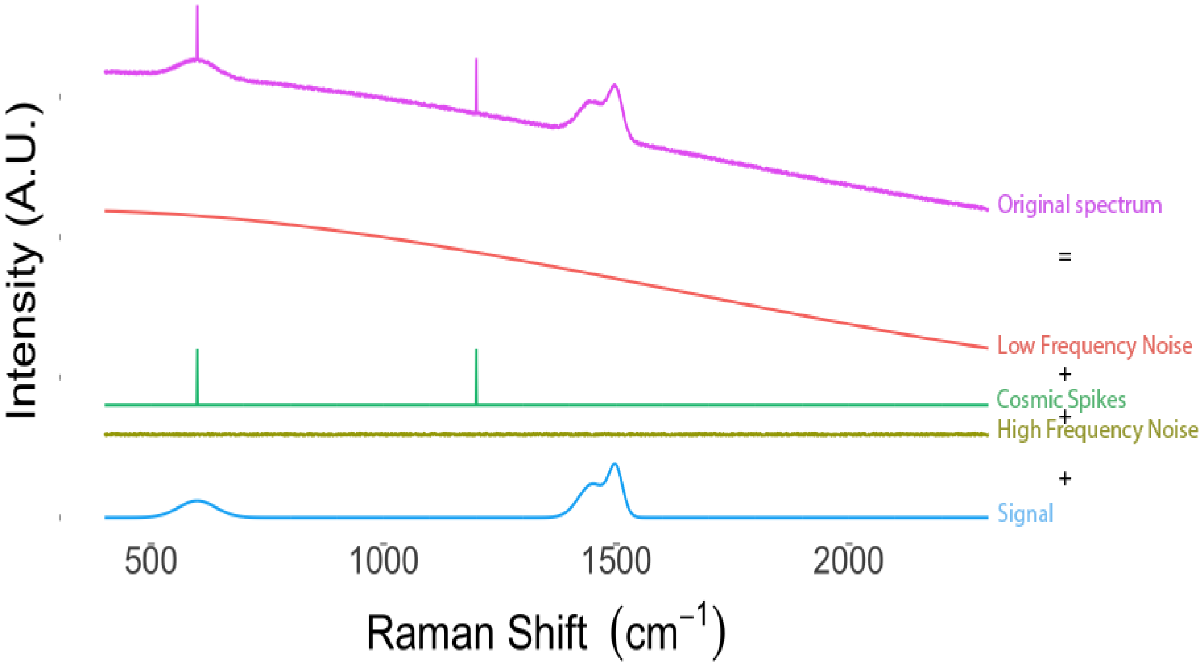

FIGURE 3. 6 DECOMPOSITION OF SIGNAL AND NOISE INCLUDED IN A RAMAN SPECTRUM.

Spectra collected sequentially from the same sample, while containing the same chemical data, display differences which if uncorrected introduce variability that leads to error when applying classification algorithms. These differences arise from noise generated by extraneous light, fluorescence, and the device electronics. Noise arises as high frequency noise from the acquisition electronics, low frequency noise from sample fluorescence, and cosmic spikes from atmospheric cosmic ray events **(Figure 3.6)**[103]. High frequency noise and cosmic spikes can be removed through smoothing algorithms such as median or Savitzky-Golay filtering. Low frequency noise may be removed by background subtraction methods such as polynomial fitting or iterative restricted least squares subtraction. Similarly, Raman spectra acquired sequentially from the same sample demonstrate additive and multiplicative shifts which may be removed by normalisation, such as highest peak, defined peak or vector normalisation[104-108]. The factors under control in digital pre-processing are summarised in **Table 3.3.**

TABLE 3. 3 FACTORS UNDER CONTROL DURING SPECTRAL DIGITAL PRE-PROCESSING.

Digital Pre-processing			
Factor	**Process**	**Strengths/Opportunities**	**Challenges/ weaknesses**
Background subtraction	Reduction of low frequency noise through subtraction of baseline	Reduces noise	May lose some of the target signal
Smoothing	Smoothing of high frequency noise and cosmic spikes	Reduces noise	May lose some target signal
Normalisation	Removes additive and multiplicative shifts of spectra	Improves comparability	

3.2.3.1.1 SMOOTHING

Smoothing algorithms are used to reduce high frequency noise and cosmic spikes. In median filtration each point on the spectrum is assigned the median value of a window of surrounding points. Similarly, in Savitsky-Golay filtering each point of the spectrum is assigned a value defined by a nth-order polynomial fitted over a bin of surrounding points[109]. Both filters have been used for Raman spectrum smoothing in microbiologic studies. The major decision for both types of filters is the bin width, with wider bins providing greater smoothing of noise but with the potential risk of smoothing off signal. A practical approach is to use the smallest bin width that provides adequate smoothing. Savitsky-Golay filtering requires an additional decision of the order of the fitted polynomial, with higher order polynomials able to maintain signal but with less smoothing effect[107, 109]. Median filtering is computationally simpler and less likely to be influenced by the outlying points present in cosmic spikes.

3.2.3.1.2 BACKGROUND SUBTRACTION

Background correction aims to remove low frequency noise (depicted in **Figure 3.6**) by subtracting a fitted baseline which approximates the low frequency noise, therein bringing the spectral baseline close to zero. The most commonly used method is a nth-order polynomial fitted by minimising the squares of the residuals. Polynomial fitting has several advantages: it is easily implemented and interpreted. The order of the polynomial is the only user input, and as is therefore less amenable to overfitting[110]. The fitted polynomial is a function of the entire spectrum, rather than specific points. Polynomial fitting however has some limitations. Fitted curves are strongly influenced by outlying spectral points, most importantly those arising from cosmic spikes. As such, removal of cosmic spikes prior to polynomial fitting is required. An additional limitation of polynomial fitting is Runge's phenomenon, oscillation of the fitted curve at the edges of the spectrum which is greater with increasing polynomial order. This oscillation induces variability at the edges of the spectrum which may obfuscate signal in these regions and is of particular importance when using principal component analysis (PCA) for feature reduction as components will be inappropriately loaded toward these areas. The effects of Runge's phenomenon can be reduced by using the lowest order polynomial possible, or by truncating the oscillating edges after baseline subtraction.

Spline interpolation is an alternative means of baseline fitting in which the spectrum to be fitted is divided into a number of windows, which are connected by the user selected interpolant points[111]. The fitted baseline consists of a number of adjacent windows which are fitted to conform to certain criteria:

- Each window is fitted to a n-th order polynomial (typically third order)
- Passes through the interpolant points
- The first-order derivative at either end of the spectrum is zero (the fitted baseline is level at either end)
- At interpolating points the first order derivatives of the adjacent fitted windows are equal, resulting in the overall baseline being continuous and smooth.

As spline interpolation fits lower order polynomials over divided windows, it provides a tighter fitting baseline as compared to polynomial fitting and it is not susceptible to Runge's phenomenon. Careful selection of interpolants is required as the fitted baseline is extremely sensitive to these points. This may be advantageous where the spectral region of interest is known, as placing the interpolating points either side provides a close baseline fit to this region. This sensitivity to the interpolating points may however be disadvantageous in two cases. Firstly, as the fitted baseline is required to pass through the interpolating points if one of these are set on a spectral band which is descriptive of the outcome of interest then informative value of the band may be reduced. Alternatively, if an interpolating point is set onto an outlier such as a cosmic spike, then the adjacent baseline fitted to this point will poorly reflect the spectral baseline. Furthermore, the need for user-selected interpolants daws a risk of overfitting data, which may be mitigated through *a priori* selection of interpolants using pilot or previous data[105, 107].

An alternative to baseline subtraction is derivative spectroscopy, in which the derivative of the spectrum is used rather than the baseline itself. As the derivative plots the rate of change, derivative spectroscopy intrinsically removes the baseline. Derivatives are easily implemented, and as the derivative order is the only user input this limits susceptibility to overfitting. A major disadvantage to derivatives is the propensity to amplify high frequency noise, and prior smoothing to remove high frequency noise is therefore required. A further potential criticism is derivative spectra are not intuitively interpretable[107, 112].

3.2.3.1.3 NORMALISATION

Raman spectrometry equipment introduces an additive and multiplicative shift such that consecutive spectra collected from the same sample can appear different. These shifts may be addressed through normalisation, in which the spectrum baseline is shifted down to zero (accounting for the additive shift), after which each band by is divided by a normalising factor (therein accounting for the multiplicative shift). A number of options are available as a normalising factor. Most used is min-max, or tallest peak, in which the normalising factor is the intensity at the highest point of the spectrum. Min-max normalisation stretches the spectrum to lie between zero and one[107]. The simplicity of this approach is countered by a number of disadvantages: as the entire spectrum is normalised upon a single automatically selected band, the normalised spectrum is highly sensitive to the choice of, and value at, this band. Notably, should an inadequately smoothed cosmic spike remain, this is likely to be the maximum and the resulting spectrum be normalised upon this noise. Similarly, as the maximum band may vary between spectra, these will be normalised upon differing bands leading to unintended variance across the spectrum[108].

An alternative is defined-peak normalisation in which the normalising factor is the intensity at a chosen peak, consistently across all normalised spectra. This method is highly sensitive to the selected peak, and as such the chosen peak should ideally have little variance between samples and not be associated with the target as unaccounted variance at this peak is extended across the rest of the spectrum during normalisation. Defined-peak normalisation is particularly advantageous when combined with internal standard, in which the spectrum may be normalised by a band arising from an included substance and therefore the spectrum will be proportional to this substance. Defined peak normalisation paired with internal standards may therefore allow for quantification of concentration of other substances, including pathogens[107].

Min-max and highest peak suffer from sensitivity variance at the band selected as a normalising factor. Alternative methods use a normalising factor derived from the entire spectrum rather than a single point. The two methods employed in the literature are the area under-the-curve (AUC), and vector normalisation. In AUC normalisation the area under the curve is calculated by summing the area under all spectral bands. In vector normalisation, each spectrum is considered a vector in hyperdimensional space which may be normalised by the vector magnitude. Both methods distribute the normalising factor across the entire spectrum, avoiding sensitivity on any single band[108].

3.2.3.2 DIMENSION REDUCTION/ FEATURE CREATION

Raman spectra consist of hyperdimensional highly co-linear data. Reducing spectra to a smaller number of uncorrelated features has a number of potential benefits. Feature reduction may improve classification accuracy through reduction of collinearity and avoiding non-contributory bands. Reducing the number of features is frequently more computationally efficient despite the additional analytical process. Working with reduced features may be less susceptible to overfitting, therein providing better generalisation. Reduced features may be computationally necessary for some learning methods such as linear discriminant analysis, in which having a greater number of features leads to a singularity error[113]. The factors under control during feature reduction are summarised in **Table 3.4.**

Principal component analysis (PCA) is the most commonly applied feature reduction method used in Raman analysis. PCA involves transforming the data into a new vector space to create a series of linear principal components (PCs) so as to maximise the variation of each component. Each PC contains a greater amount of the total variation than the next and are orthogonal to each other. Therefore, transforming the data using PCA allows for a small number of features accounting for a large proportion of the dataset variation to be used in further analysis. PCA is unsupervised, and as such the variation explained by the principal components arises agnostically both from signal (correlated with the class of interest) and the noise (not correlated with the outcome of interest). Importantly this means that while the earlier PCs will explain a greater amount of variance, these may not best correlate with the class of interest[77, 113-115].

PCA results in p-1 principal components, where p is the original number of dimensions. For example, applying PCA to a set of spectra with 2300 spectral bands will result in 2299 PCs, with each explaining decreasing amounts of the total variance. A decision on the number of these PCs passed on further analysis is required. The parsimony principal is advocated in which the smallest number of PCs used to provide the greatest classification accuracy, typically as defined by the cross-validation accuracy[92, 116]. An alternative method used in the published literature is to use the number of PCs explaining a certain amount of the total variance, however as there is no standard for this amount this method is susceptible to manipulation and overfitting[113-115]. When this method is used, the authors seldom describe how this proportion of total variance explained is decided upon.

TABLE 3. 4 FACTORS UNDER CONTROL DURING FEATURE REDUCTION

Feature Reduction			
Factor	**Process**	**Strengths/Opportunities**	**Challenges/ weaknesses**
Principal component analysis	Transforms data to a new vector space to maximise variation	Reduced features may be necessary or may improve power Assessment of component loadings may be used to identify the bands of spectra contributing toward classification Retains maximum variation using minimal features	Maximises variability in principal components which may not arise from signal Some signal is lost
Spectral band ratios	Spectrum is divided into bands and binned before creating ratios.	Self-normalising	Requires further feature reduction Not widely used Data may be lost by binning bands together Not naturally interpretable

Spectral bands ratios such as those used by *Kastanos et al.* provide an alternative method for dimensionality reduction and feature creation[69]. In this method the spectrum is divided into a number of even windows, and the mean of each window is divided by the mean of all other windows to create a new feature set. The authors advocate this method as being self-normalising while inherently removing the baseline. The user must decide on the window width (and therein the number of windows) to be used. Wider windows risk loss of signal due to signal from adjacent bands being combined into a single window. In contrast using narrow windows leads to a large number of features. For example, despite advocating spectral band ratios as a dimensionality reduction technique, their article used 25cm^{-1} windows which resulted in a greater number of dimensions after spectral band ratios were calculated. Furthermore, converting spectra to a new data structure worsens interpretability and impairs mechanistic validation through spectral band assignment.

3.2.3.3 UNSUPERVISED LEARNING

Unsupervised learning describes the application of learning algorithms to spectra without prior knowledge of the class from which they belong[111]. Unsupervised learning is to directly infer natural clustering of data without the guidance of a supervising class. PCA and hierarchical cluster analysis (HCA) are common unsupervised learning approaches applied to Raman spectra. Unsupervised learning methods re summarised in **Table 3.5.**

Unsupervised Machine Learning			
Factor	**Process**	**Strengths/Opportunities**	**Challenges/ weaknesses**
Principle component analysis	Transforms data to a new vector maximising variation	Reduces features and avoids collinearity May identify natural grouping Assessment of component loadings can identify the spectral bands that contribute to classification	Vector space with maximal variation may not maximise class separation, particularly where a high degree of noise remains
Hierarchical cluster analysis	Identifies natural clustering by proximity	Intuitive Identifies natural clusters and sub-clusters	Does not identify contributing bands Computationally inefficient

TABLE 3. 5 METHODS FOR UNSUPERVISED LEARNING

PCA involves the transformation of the data original data into a new vector space consisting of orthogonal vectors (PCs), each of which explains a greater amount of the total variance than the next. PCA has a number of advantages which make it well suited toward analysis of Raman spectra. PCA is dimensionality reducing, allowing hyperdimensional spectra to be reduced to a few descriptive PCs, which may be used for unsupervised assessment of clustering or be passed to supervised methods of classification. PCA is mathematically solvable in closed form without further user input, and as such is easily implemented and repeatable. PC loadings can be back calculated, describing the extent to which bands of the original spectra contribute to each PC[77, 111, 115].

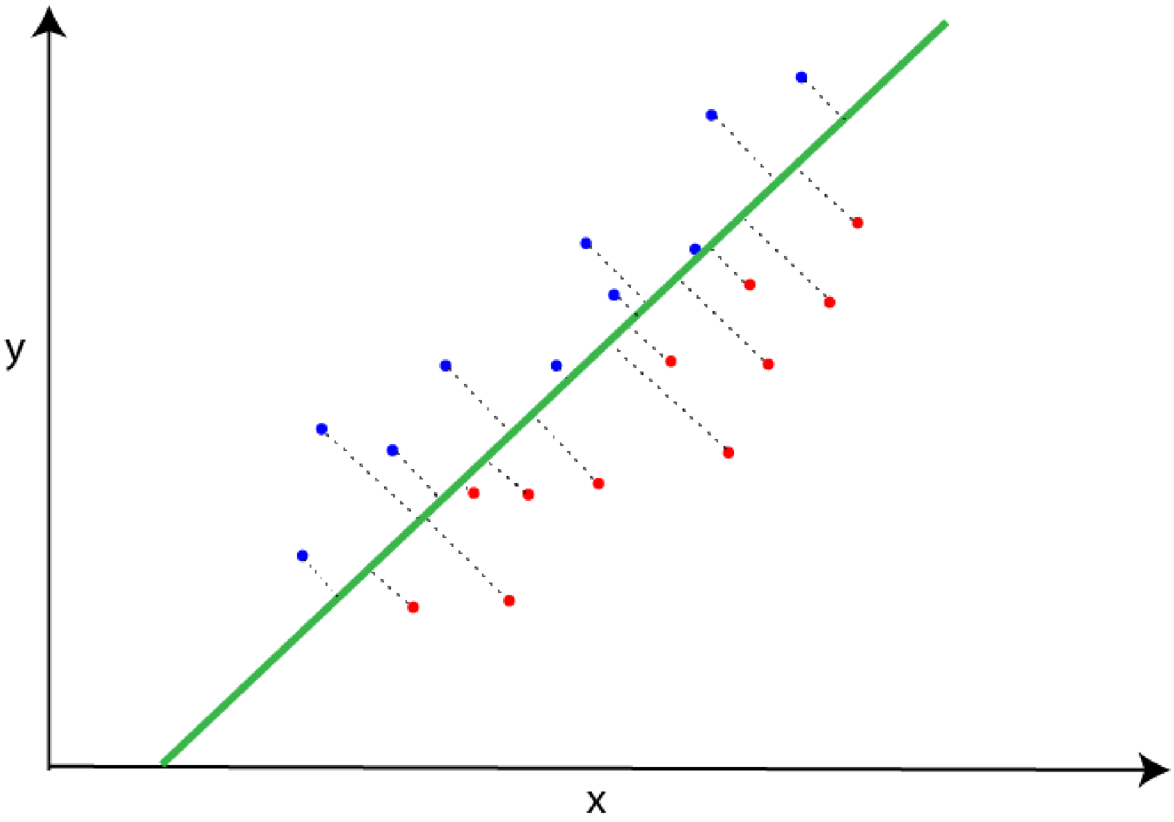

FIGURE 3. 7 SIMPLIFIED DEPICTION OF FEATURE REDUCTION BY PRINCIPAL COMPONENT ANALYSIS. TWO DIMIENSIONAL DATA POINTS (X AND Y) CAN BE PROJECTED (DOTTED LINES) TO A SINGLE DIMENTION (GREEN LINE) WHICH MAXIMISES VARIANCE. PCA IS NOT CONTINGENT ON THE CLASS OF THE DATA POINTS, REPRESENTED BY RED AND BLUE COLOUR.

HCA is an unsupervised learning method in spectra are combined into similar clusters, producing a hierarchical representation in which clusters at each level through merging the clusters from the levels below. Clusters are formed based on a user defined similarity measure such as Euclidean distance (most commonly), Manhattan distance or cosine dissimilarity. Clusters may be formed agglomeratively in which similar clusters are recursively combined to form clusters above, or divisively in which groups are split to form clusters below. HCA is advantageous in its ease of interpretability and depiction using dendrograms. It has the additional advantage that unexpected clusters may be identified[101]. They however suffer numerous limitations in spectral analysis: HCA is computationally inefficient, requiring recursive calculation of similarities between spectra. While demonstrating similarities between spectra, HCA does not provide a means of assessing which bands contribute to these similarities, and therefore no mechanistic understanding of the clustering. The need for user defined parameters such as similarity measure and clustering mechanism means the results may differ widely dependent on user choices[111].

3.2.3.3 SUPERVISED LEARNING

The primary aim of analysis of Raman spectra is frequently to provide a means of identifying the class from which the spectrum has arisen. Supervised learning uses spectra of a known class to train algorithms which may then classify spectra of unknown class. Methods for supervised learning are summarised in **Table 3.6**

TABLE 3. 6 METHODS FOR SUPERVISED LEARNING

Supervised Learning			
Factor	**Process**	**Strengths/Opportunities**	**Challenges/ weaknesses**
K- nearest neighbours	Assigns the class of the K nearest neighbouring data	Intuitive	Computationally inefficient Does not generalise well
Linear Discriminant Analysis	Transforms data to a new vector space so as to maximize between class variance	Possible with small sample set Widely used Good in set classification Multiple classes	Prone to overfitting Requires feature reduction
Support vector machines	Finds maximal class separator	Generalises well Does not require feature reduction	Binary classifier (may be extended to multiple classes)
Artificial neural networks	Multilayer perceptron identifies patterns and assigns weights to bands in the spectrum to assign class	With proper training likely to provide most accurate classification	Black box classification Requires large training set Prone to overfitting Computationally heavy

Linear discriminant analysis (LDA), also known as Fisher's discriminant analysis or discriminant function analysis) is the most commonly applied supervised method for Raman spectral classification of bacterial samples. LDA is depicted in **Figure 3.8.** LDA transforms data into a new set of linear discriminants (LDs) that maximise the ratio of between group variation to within group variation, which effectively maximises the separation of the classes in the new vectors space. [77] The LDs may then be used to identify from which class a spectrum is most likely to belong to. PCA is commonly used for dimensionality reduction and feature creation prior to LDA classification. This is because the mathematics underlying LDA requires fewer variables than observations, and because LDA performs poorly with colinear data[102]. LDA provides accurate classification with relatively little data and is therefore frequently preferred for early research. LDA has a further advantage in that it may be possible to back calculate the composition of the LDs, providing an understanding of which spectral bands provide the classification[117]. LDA however, generalises poorly which may limit its use beyond earlier stage research[111, 113, 118].

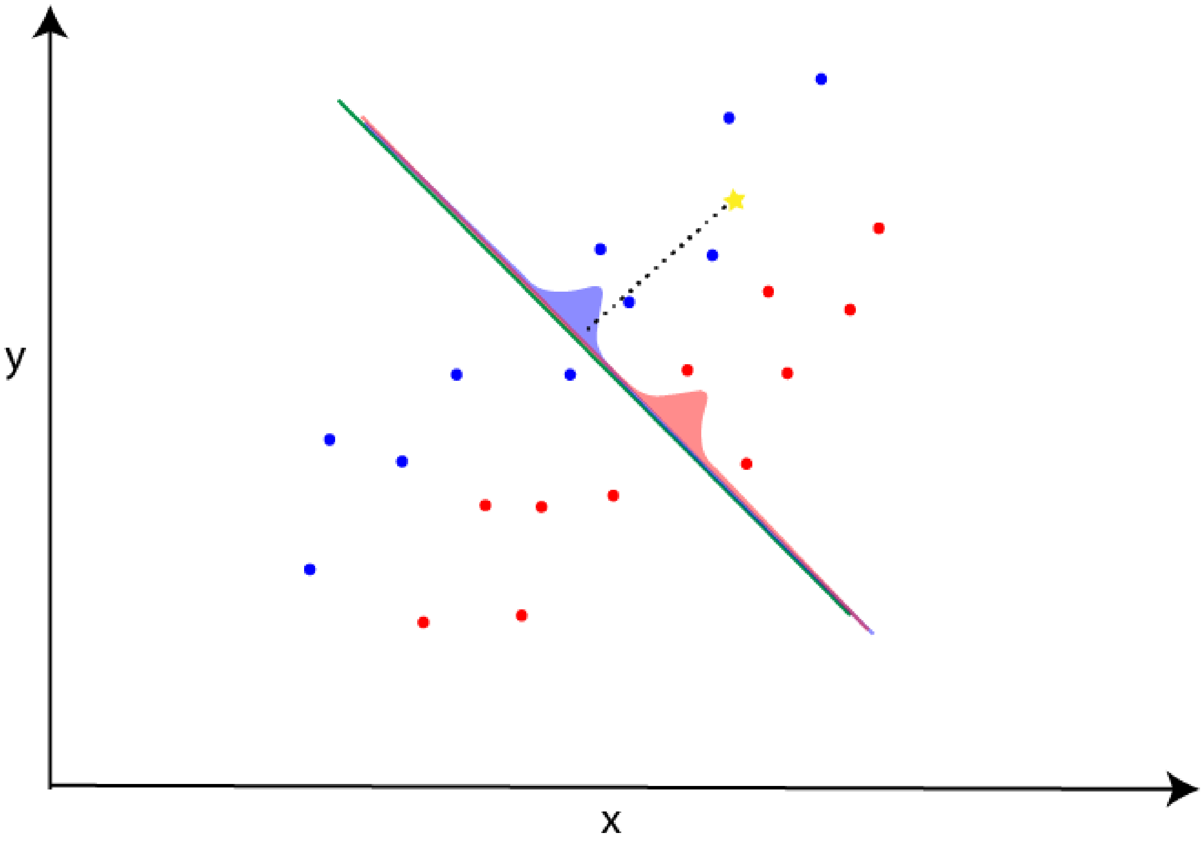

FIGURE 3. 8 SIMPLIFIED DEPICTION OF LINEAR DISCRIMINANT ANALYSIS. DATA POINTS IN TWO DIMENSIONS (X AND Y) ARE PROJECTED TO A NEW DIMENSION, OR LINEAR DISCRIMINANT (GREEN LINE), WHICH MAXIMISES THE RATIO OF THE BETWEEN GROUP VARIANCE TO THE WITHIN GROUP VARIANCE. THE UNKNOWN DATA POINT (STAR) IS ASSIGNED TO THE BLUE CLASS IN THIS DEPICTION.

Support vector machines (SVMs) have similarly been used for supervised learning of bacterial Raman spectra. SVMs are maximal margin classifiers in which data is separated into classes by a hyperplane which provides greatest separation of the classes. A two dimensional example is illustrated in **Figure 3.9**. SVMs have been demonstrated to have better generalisability as compared to LDA and as such are garnering greater interest in bacterial Raman research. A potential challenge arises in that SVMs require the data be separable by a hyperplane. Kernel methods may be employed when data is not separable, or to gain greater classification accuracy through a wider separation margin. Kernel methods use the existing data to create additional dimensions which provide greater separability of data. A major limitation arises in that SVMs require binary classifications, and are therefore not naturally suited to multi-class challenges such as bacterial classification. Two potential options are available for multi-class SVMS are one-versus-one and one-versus-all approaches, both of which have significant limitations. One-versus-one multi-class SVMs creates multiple SVMs comparing each individual class against every other individual class and assigns each spectrum to the class to which they are most commonly assigned in all of these SVMs. One-versus-one SVMs are computationally inefficient requiring each spectrum be assessed in a number of SVMs. Spectra may fail to be classified in this approach if there is disagreement between the SVMs. One-versus-all creates multiple SVMs comparing each individual class against all the other classes combined and assigning spectra to the class in which the spectra is furthest from the separating hyperplane[111, 119, 120].

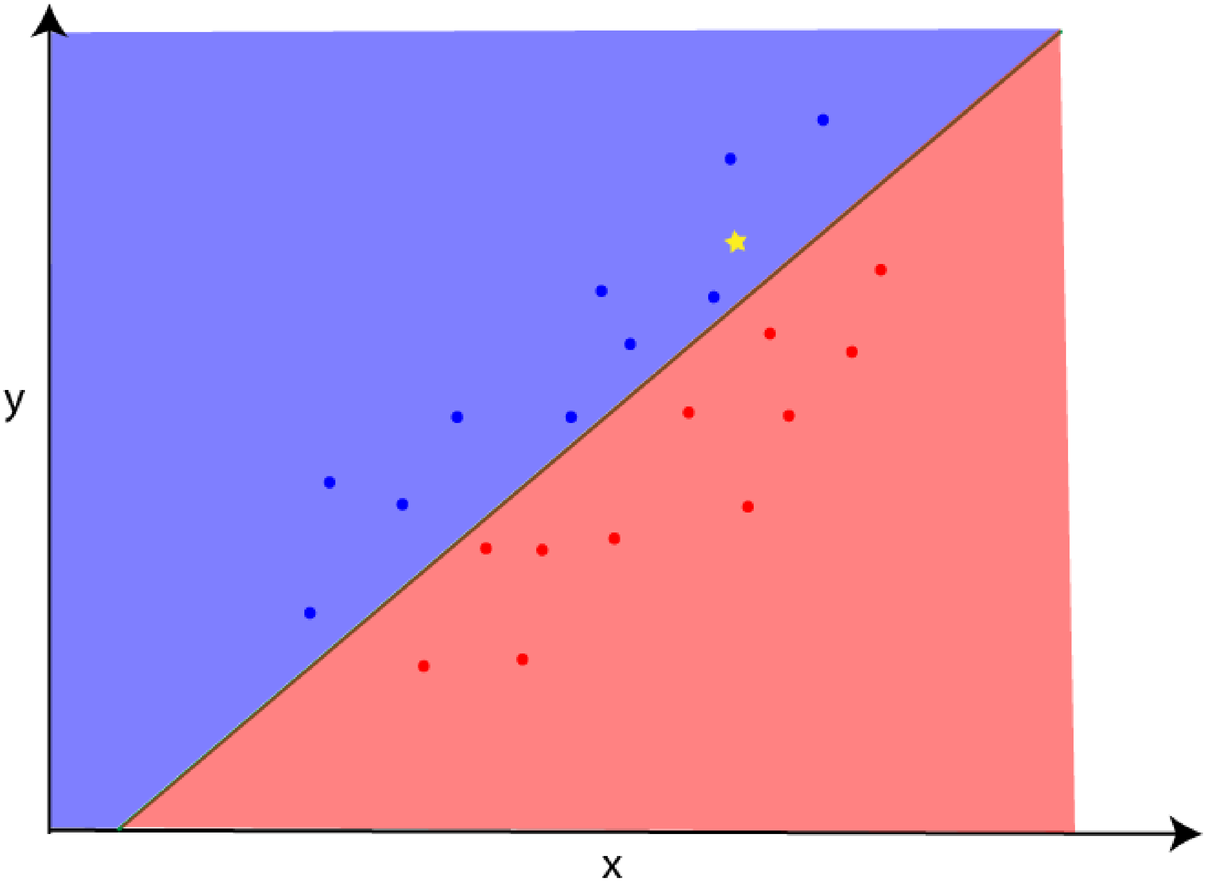

FIGURE 3. 9 A SIMPLIFIED DEPICTION OF SUPPORT VECTOR MACHINES. DATA IS SEPARATED MY A MAXIMAL MARGIN CLASSIFIER, A LINE IN THIS TWO DIMENSIONAL ILLUSTRATION, WHICH BEST SEPARATES THE CLASSES. NEW DATA (STAR) IS ASSIGNED DEPENDENT ACCORDING TO WHICH SIDE OF THIS BOUNDARY IT FALLS – BLUE IN THIS CASE.

Artificial neural networks (ANNs) hold the greatest potential for spectral classification when applied at clinical scale. ANNs use multiple layers of perceptrons to identify patterns in spectral data in a process analogous to that of neurons. ANNs have several advantages when applied to spectral analysis. ANNs have the potential to identify complex patterns in spectral data. While the traditional approach of digital pre-processing and feature creation prior to classification may be used, ANNs may classify spectra without these steps. ANNs are well suited to multi-class classification without the need for adaptation such as those required for SVMs. ANNs, however, require large amounts of training data and are therefore less favoured in early research where rapid prototyping is more important than generalisability[102]. This problem may be reduced by prior feature reduction using PCA.[102] A further potential reason ANNs are not preferred for early-stage research is that ANNs do not provide a mechanistic understanding of which spectral bands are used for classification[111, 121]. These reasons may explain why to date only *Goodacre et al.* have used ANNs for bacterial classification[102].

3.2.3.4 ASSESSING MODEL ACCURACY

The supervised learning methods applied to spectra are designed to maximise the classification accuracy on the data they are trained upon. As such these may be prone to overfitting, in which the algorithms base classification upon noise in the training data rather than signal representative of external data[76]. As such, assessing the classification accuracy is contingent on assessing algorithm performance on unseen data. Assessing data classification performance is a trade-off between the independence of the test data against the total amount of data that needs to be collected[111]. Methods for validation are summarised in **Table 3.7.**

TABLE 3. 7 METHODS FOR VALIDATION

Validation			
Factor	**Process**	**Strengths/Opportunities**	**Challenges/ weaknesses**
K-fold cross validation	Subsets collected data into k-folds, each of which is classified using algorithms trained on all other folds.	All data is used for training	Data set is not independent Still allows for some overfitting
Test Set validation	A subset is retained for testing	Test set is relatively independent	Not all data is used
Prospective validation	A diagnostic technology with trained algorithm is assessed using prospectively collected data	Test set is truly independent	Time consuming

The most robust assessment of classification performance is provided by previously trained algorithms on newly collected independent data. While providing the most robust assessment classification accuracy, this process requires the greatest amount of data as sufficient data is required to properly train the algorithm, as well as an additional separate amount of data needed to assess the classification performance. As such, independent test is reserved for completely developed technologies with previously optimised learning algorithms. While some Raman bacterial studies have assessed their technology on independent data none of these had sufficient independent testing data to robustly assess classification performance[76].

An alternative is to divide collected data into a training and a test set prior training the algorithms which maintains a degree of independence. However, as training and testing data is collected simultaneously it is not truly independent. Additionally, while it may be more efficient to collect the data simultaneously, sufficient data is still required to both train and separately test the learning algorithms[111].

Crossfold validation is a means of assessing classification performance maintaining some degree of independence without requiring collection of a separate test set. In crossfold validation the data is divided into k folds. The data in each fold is used as a test set on algorithms trained by all the other k-1 folds combined. As such all data is used for both training and testing while still maintaining independence when training algorithms. Leave-one-out cross validation (LOOCV) extends this such that each fold contains a single spectrum which is classified by algorithms trained on all other spectra. LOOCV retains the maximum possible data for algorithm training, and so is commonly used for earlier stage research[111].Importantly, LOOCV performance will always appear superior to true classification performance[69, 122].

3.2.3.5 ASSIGNING SPECTRAL BANDS

The supervised learning methods used for bacterial classification are agnostic with regards to the contents of the spectral bands upon which they determine the outputted class. As such assessing the contributions of spectral bands is not required for classification. While not necessary for the final classification of spectra, assigning and understanding the contributions of spectral bands and linking these to the molecular composition of the target is an integral part of Raman discovery and development. Assessing the contributions of spectral bands provides a mechanistic understanding of Raman-based classification therein providing a means of both forming hypotheses and testing these[76]. Careful assessment of spectral band contributions provides a strong counterargument against "black box" criticisms of supervised learning, in which a lack of mechanistic understanding underpins criticism of overfitted classification. Caution however needs to be applied as bands arising from different biochemical entities may overlap[96, 123].

An ideal method for assessing spectral band contribution would provide an accurate quantitative assessment of the location of the band, a quantitative strength of the contribution both in total magnitude and relative to noise at the spectral band. Methods for spectral band assessment should allow for pairwise comparison between groups in addition to assessment of the importance of bands across the whole population. A number of different methods have been used in the published literature to assess spectral band contribution.

Visual assessment of the spectral differences belonging to different classes has been used to assign spectral bands in the published literature, despite this method suffering a number of shortcomings. This method is reliant on user interpretation and so is subject to confirmation bias. The non-quantitative nature of visual assessment is prone to a number of challenges. Firstly, given the highly congested nature of bacterial Raman spectra, most notably in the fingerprint region, visual assessment may incorrectly assign or miss spectral bands. Secondly, as assignment of peaks is made without consideration of variability, the importance of large peaks in areas of high variability may be overestimated, while the importance of small peaks in areas of low variability may be underestimated. Finally, without quantification, visual assessment fails to demonstrate the contribution of bands relative to each other.

PC loadings are frequently used to assess the contributions of spectral bands[101, 124]. Through assessing the eigenvectors upon which the PCA transformation is performed, a quantitative assessment of the relative contribution of spectral bands to the PCs is provided. A potential limitation in this method of band assignment arises in that PCA is an unsupervised method, and therefore these loadings reflect spectral bands with greater variability which does not necessarily arise from class differences. However, where the classes separate on PCA plots it is assumed that these loadings arise from spectral differences between classes. As this only looks at the variation across all the spectra, it may underrepresent bands where small, but important, spectral differences lie in areas with little variability, or conversely over represent spectral bands where large, but meaningless, differences arise from high variation bands[77].

This method can be extrapolated to PC-LDA where the successive PC and LD transformations can be back-solved to demonstrate the spectral band contributions of the LDs. This has the advantage providing the quantitative backing behind a supervised method, and therein a greater degree of certainty the loadings arise from class differences rather than uncorrelated variation. The reliability of these spectral band assignments is inherently linked to the model fit[117].

A final approach is to centre and scale a group of spectra upon a reference group by subtracting the reference's mean at each band and dividing by the variation. The resulting plots give an indication the difference at each band relative to the reference variability. This method has a number of advantages for spectral band classification: the method is easily implemented and interpretable; quantitative spectral differences relative to reference spectral variation demonstrates the importance of the difference while ensuring small differences in low variation regions are not underrepresented; it allows for global or pairwise comparisons through selection of the reference spectra, therein allowing for interrogation of differences between specific classes or groups of classes.

3.2.3.6 A MULTILEVEL APPROACH TO SPECTRAL CLASSIFICATION

The frequent approach used for classification in which all spectra are assigned a classification from a single sample population is likely to lead to worse classification accuracy as small interclass signal is overwhelmed by the competing signal of the whole group. This has led to a number of authors employing multi-level classification approach in which a series classifications are performed on smaller groups[69, 76, 80, 85, 96]. For example, first classifying samples as infected or uninfected, then classifying infected samples as Gram-positive as compared to Gram-negative, before species level classification as illustrated in **Figure 3.10**. This approach is likely to lead to better classification as learning algorithms are allowed to focus on specific interclass signal. For example of such interclass differences is that described by *Manoharan et al.* who demonstrated Gram negative pathogens have greater intensity of tryptophan peaks[125]. This approach may have particular value when using SVMs for classification, where a series of classifications may suit the binary nature of SVMs.

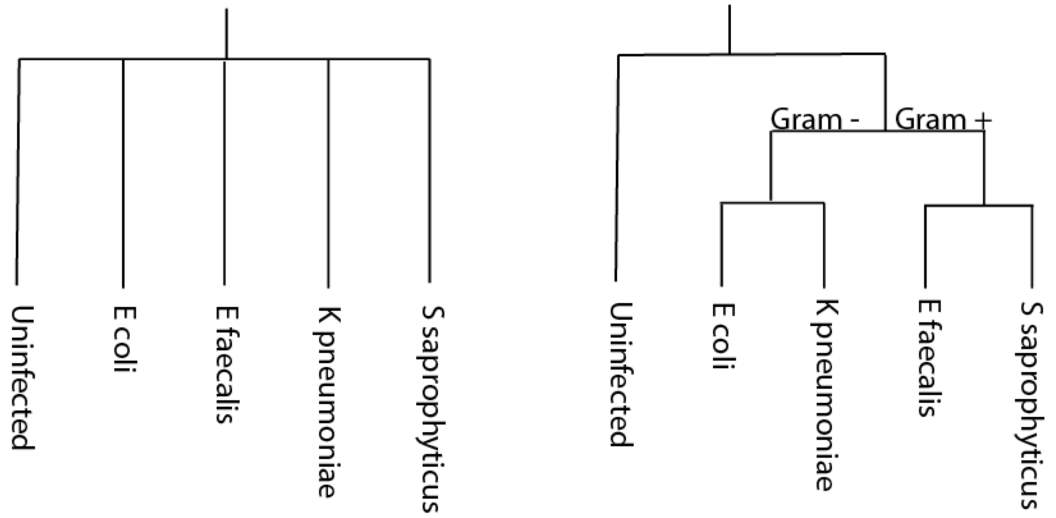

FIGURE 3. 10 DEPICTION OF STANDARD (LEFT) AND MULTILEVEL (RIGHT) CLASSIFICATION APPROACHES

In the current literature, classification levels are user-defined as a series of questions. A potential pitfall in this approach is highlighted by *Mircescu et al.*, whose work demonstrated spectral similarities between Proteus species and Gram-positive bacteria arising from chemical similarities in O-antigen and Gram-positive cell wall proteoglycan[101]. In such a case, application of a multi-level classification approach may systematically misclassify Proteus bacteria as Gram-positives. A potential alternative not yet applied in Raman based uropathogen classification is to use a combined unsupervised-supervised multi-level classification approach, in which an unsupervised approach such as HCA can be used to assign binary class decisions to be made using a supervised approach such as SVMs.

3.3 SURFACE ENHANCED RAMAN SCATTERING

The accidental discovery of surface enhanced Raman scattering (SERS) by *Fleischman et al.* provided a substantial improvement in potential for Raman spectroscopic based pathogen identification. Surface enhancement arises when the target (such as a pathogen) is placed in close proximity onto a noble metal nanostructure. Signal enhancement in the order of 10^{14} gives SERS the potential to overcome the key limitation of Raman spectroscopy of weak Raman signal levels, while the strong distance dependence provides for selective enhancement. As such, SERS is the modality of choice in the majority of Raman-based pathogen research. This extreme enhancement and strong distance relationship necessitate a careful understanding of the spatial mechanics of SERS to gain the greatest value from its use. As such SERS has been described as "combination of Raman spectroscopy and nanotechnology" by *Gao et al.*[126].

3.3.1 MECHANISM OF ACTION

The substantial enhancement provided by SERS has been attributed to two separate mechanisms: an electromagnetic mechanism (EM) and a chemical mechanism (CM). The EM arises as a result of localised surface plasmon resonance (LSPR), which occurs when the light interacts with the metal surface generating plasmons (oscillations in electron density) leading to collective oscillation. The electromagnetic mechanism generates enhancement of up to 10^5, which strongly dependent on the size and shape of the nanostructure[7, 72]. This mechanism is strongly influenced by the distance as depicted in Equation 3.2[77]. The CM is mediated by a charge transfer mechanism in which intermolecular charge transfers between the noble metal and target molecule allow for collective oscillation and resonance leading to signal enhancement. The chemical mechanism generates enhancement in the order of 10^2[70, 72, 77].

$$I \propto \frac{E^4}{d^{12}}$$

EQUATION 3.2 SERS INTENSITY (I) IS A FUNCTION OF ELECTROMAGNETIC FIELD (E) AND THE DISTANCE BETWEEN ANALYTES AND SERS SURFACE (d)

Practically applied to pathogen identification a number of factors may be controlled to optimise surface enhancement. Maximal enhancement is achieved where the frequency of the light is lower than the resonance frequency of the target molecule, and as such excitation using high frequency (lower wavelength) light, such as UV, are not used for bacterial SERS. The SERS effect decreases exponentially as distance increases and is negligible beyond 20nm. As such, while close apposition provides massive signal enhancement, poor apposition will provide no benefit and inconsistent application will lead to massive variability making classification impossible [7, 69, 72, 80, 97, 98, 123].

3.3.2 METALS

While all noble metals may be used, silver and gold are the metals most commonly used in bacterial SERS research. Gold and Silver have a number of benefits when applied to bacterial SERS. The enhancement is inversely proportional to the difference in frequencies of the metal's surface plasmons and that of the exciting photon[127]. As such, the similarity of gold and silver's plasmon frequencies to that of visible and near infrared light provide for optimal enhancement at the wavelengths used for pathogen identification.

Silver has a further advantage when applied to pathogen detection provided by its propensity to interact with the cell envelope, therein preferentially enhancing the cell envelope[128].

3.3.3 NANOSTRUCTURE

As the SERS enhancement is primarily defined by the strong localised electromagnetic fields which vary on a nanometre scale the structure of the of the SERS substrate is vitally important, both in optimising enhancement but also in ensuring reproducibility. The size, shape, and interparticle spacing must be chosen and consistently maintained to ensure consistent optimal SERS enhancement[7, 69, 72, 80, 97, 98, 123]. A number of techniques are employed to generate SERS substrates including roughened electrodes, colloidal nanoparticles and surface-confined nanostructures[72]. The SERS effect was first identified using roughened electrodes. These provide moderate enhancement in the order of 10^6. These are infrequently used in Raman bacterial research owing to challenges in maintaining consistent nanostructures as well as ensuring pathogen interaction with the substrate.

Colloidal nanoparticles are frequently favoured in SERS based pathogen research for a number of reasons: Standardised methods allow for nanoparticles of consistent size and structure; these methods can be tuned to select a nanoparticle size optimised to interact with the target; nanoparticles suspended in solution are free to interact with the target or may be encouraged to preferentially do so using techniques such as immunocapture. Challenges with nanoparticles arise in the potential for uneven dispersion or nanoparticle agglomeration, as well as chemical instability of nanoparticles in solution[45].

Surface nanostructures offer significant potential advantages for SERS based research. A number of techniques including photolithography, electron-beam lithography and additive manufacture with subsequent metal deposition, offer consistent and minute control of nanostructures specifically designed to interact optimally with the target. These surfaces may be functionalised to optimise the interaction of the target with the nanostructure[45]. Nanostructured surfaces additionally provide for greater stability and so longer shelf life as compared to colloidal nanoparticles[72].

3.4 BACTERIAL RAMAN

3.4.1 BACTERIAL STRUCTURE AND BIOCHEMICAL CONSTITUTION

An understanding of the structure and chemical composition of bacteria is needed to understand, predict and optimise Raman spectroscopy as well as predict and plan SERS enhancement.

Bacteria are prokaryotic organisms, containing no cell organelles or nucleus. Bacteria vary in shape and are substantially smaller than eukaryotic cells, with a typical diameter in the region of 1 μm as compared to 10μm and above for eukaryotic cells. Contained within the cytoplasm is a single chromosome of DNA. While unique to the bacteria in terms of the genetic information contained this DNA constitutes a miniscule proportion of the cell biomass and does not vary substantially in its overall chemical composition from cell-to-cell. Also contained within cytoplasm are the messenger RNA and ribosomes used in protein synthesis. These vary considerably in in their constitution, and the proportion of the biomass for which they account, both between cell types but also within cells[42, 45].

The cytoplasm is enclosed in a cell membrane composed of a phospholipid bilayer. In the absence of mitochondria, bacteria make use of this membrane to create the electron gradient needed for respiratory phosphorylation. The cell membrane therefore contains an abundance of respiratory enzymes, co-enzymes, intermediates and respiratory products such as proteins, cytochrome and adenosine triphosphate (ATP). These products are frequently strong Raman scatters leading to distinct Raman spectra. The cell membrane is also responsible cell nutrition and structural macromolecule synthesis, therefore containing a higher concentration of the enzymes and products associated with these processes[42].

External to the cell membrane lies the cell wall, which provides structural support, maintains a biochemical microclimate and houses proteins and macromolecules with a diverse array of functions. The cell wall is descriptive for the cell type, most notably in the composition responsible for Gram-staining but also in the contained macromolecules. The Gram-positive cell well is approximately 90% constituted by a 30-100nm thick peptidoglycan layer, a polymer consisting of repeating disaccharide subunits of N-acetyl glucosamine (NAG) and N-acetyl muramic acid (NAM) crosslinked by pentapeptide sidechains[44, 46]. The pentapeptide crosslinks are unique to bacterial types. Peptidoglycan therefore constitutes a considerable proportion of Gram-positive cell walls and is comprised of remarkably consistent repeating molecules which are strong Raman scatterers. This peptidoglycan layer therefore represents a significant opportunity to identify bacteria using Raman spectroscopy, in differentiating these from Gram negative bacteria and also in identifying bacterial species. The peptidoglycan layer is tethered by lipoteichoic acids which are covalently linked to lipids in the cell membrane[42].

The cell envelope of Gram-negative bacteria differs compared to Gram-positive bacteria most notably in that the peptidoglycan layer constitutes a much smaller proportion being only a few nanometres thick and accounting for less than 10% of the envelope biomass. A significantly thinner peptidoglycan layer is possible as Gram-negative bacteria have an additional outer membrane. Of note, in contrast to the inner membrane, this outer membrane contains glycolipids in addition to phospholipids[129]. Most notable of the glycolipids is endotoxin which plays a substantial role in the virulence of these bacteria. This outer membrane is attached to the peptidoglycan layer by murein lipoprotein (Braun's lipoprotein). This is the most abundant protein in Gram-negative bacteria such as *E. coli* and consistent in its structure[130]. The outer membrane has imbedded a number of transmembrane proteins and antigens. O-antigens are polysaccharides consisting of repeating oligosaccharides of 3-5 sugar monomers that extend out of the outer membranes are unique to bacterial strains[47]. Some bacteria, such as *Klebsiella* species, have an additional capsule beyond consisting of polysaccharides and polypeptides. These capsules are relatively variable both in their thickness and composition[42, 45].

The cell membrane and cell wall constitute the cell envelope. The cell envelope of bacteria contains consistent repeated structures which make up a substantial proportion of the biomass, are descriptive of bacteria down to the strain level, and are strong Raman scatterers. Additionally, as this the most superficial layer, the cell envelope will be preferentially enhanced by SERS substrates adjacent to the bacteria. Therefore, cell envelope components are likely to dominate Raman spectra used for bacterial identification & classification.

3.4.2 COMMON RAMAN PEAKS

Assigning the peaks used for pathogen identification and classification is an important aspect of Raman bacterial research, both building on the scientific understanding of Raman-based and providing a mechanistic validation. Researchers must optimise the many experimental and analytical factors discussed above to obtain spectra best suited toward pathogen identification and classification. As such, the discriminatory peaks of spectra are defined by the experimental conditions, and with a diverse array of contributory molecules referenced in the literature (Appendix III).

3.4.3 BACTERIAL SERS

SERS provides substantial advantages in Raman bacteriologic research in that the significant enhancement may overcome weak bacterial signal, fluorescence quenching may limit noise and the strong distance relationship may be used to preferentially target specific bacterial areas that are likely to provide better discriminatory potential. As such SERS based studies predominate the Raman bacteriologic literature with considerable focus placed on SERS optimisation. Application of SERS to bacteria is typically achieved by one of three categories of techniques: on/in bacterial nanoparticle formation, nanoparticle colloids and SERS-active surfaces.

3.4.3.1 ON/IN NANOPARTICLE FORMATION

Metal nanoparticles are achieved through reduction of a noble metal salt with a suitable reducing agent as illustrated in **Figure 3.11**. Experimental methods have been developed to localise this reaction in or adjacent to the cell membrane. Soaking the bacteria in the reducing agent such as sodium borohydride, after which the reducing agents is washed off before soaking the bacteria in a noble metal salt solution such as silver nitrate[131]. As the two solutions equilibrate across the cell membrane noble metal nanoparticles are formed on the cell wall. On wall formation provides highly resolved spectra dominated by cell wall components. A number of metal salts including silver nitrate and chloroauric acid, paired with a variety of reducing agents such as sodium borohydride hydroxylamine allow for a variety of nanoparticles with varying spectral profiles[86, 101, 128, 131].

Reversing this process, with the bacteria soaked in the noble metal salt prior to suspending in the reductant results in formation of the nanoparticles on the cell membrane as opposed to cell wall[132]. As such, the resulting spectra are dominated by cell membrane components, notably respiratory co-enzymes such as flavins and purines.

As the nanoparticles are formed directly on the cell envelope, these methods have provided valuable insights into SERS-based bacteriologic research. Despite highly resolved spectra the techniques of on/in nanoparticle formation have been confined to SERS bacteriologic basic sciences research for a number of reasons: firstly, success of these experimental procedures is contingent on strict laboratory control; secondly, the salts and reducing agents are unstable requiring fresh preparation; finally, significant delays are required during salt/ reductant absorption, washing and subsequent reaction steps making these methods impractical for clinical bacteriology.

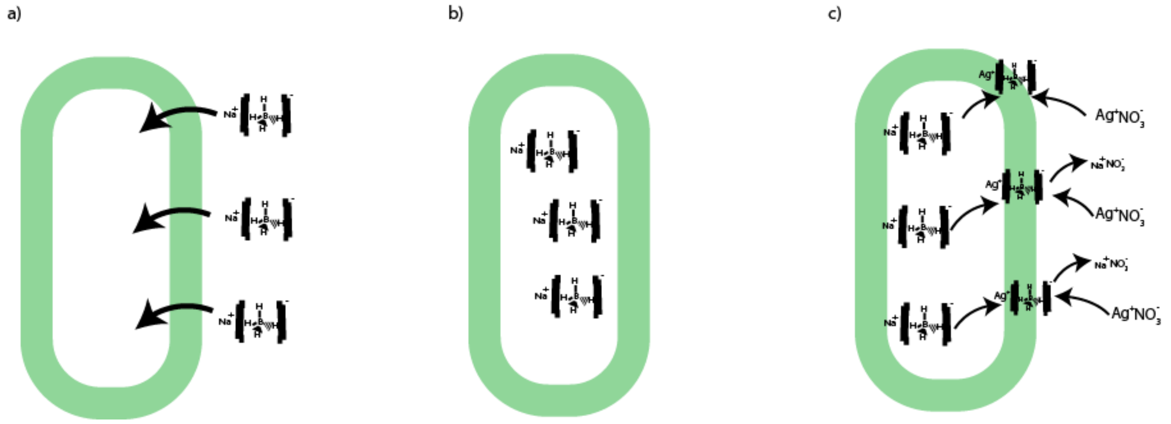

FIGURE 3. 111 FORMATION OF SERS SUBSTRATE DIRECTLY ON BACTERIAL CELL ENVELOPE INCLUDES a) ALLOWING A REDUCING AGENT TO DIFFUSE INTO THE CALL, b) BEFORE WASHING THE REDUCING AGENT OFF, AND THEN c) PLACING BATHING IN A NOBLE METAL SALT SOLUTION. THIS CAUSES THE METAL SALT TO REDUCE OUT OF SOLUTION AT THE INTERFACE PROVIDED BY THE CELL ENVELOPE

3.4.3.2 Colloids

A frequently used method for bacterial SERS is mixing bacteria suspensions with nanoparticle colloids, as illustrated in **Figure 3.12**. Nanoparticles are most frequently produced through the methods described by Leopold & Lendl[133] or that of Lee & Meisel[134]. Both methods may be adapted to produce nanoparticles varying in size, shape, size distribution and whether these are capped. Strict control is required to ensure consistency of nanoparticle size and shape.[72] Capping refers to coating the nanoparticles with an agent that avoids agglomeration, therein stabilising the colloid[135]. Capping agents contribute their own signal to the Raman spectrum which may influence classification.[136]

In the absence of employing methods to ensure adsorption of nanoparticles onto the bacteria, both are randomly distributed throughout the mixture. As such, the Raman spectra are dominated by secreted cell metabolites, with little representation of cell components [137].

The greatest challenge arises in apposing pathogens to nanoparticles[136]. The simplest method to achieve nanoparticle interaction with bacteria is time mediated[70, 136, 137]. Silver, and to a lesser extent gold, are bactericidal as a result of the metals interacting with the cell membrane[138]. This is a time-dependent process affected by the nanoparticle characteristics (smaller size, complex shapes and capping agents), environmental factors (temperature and concentration) and pathogen characteristics (Gram negatives)[136]. As a result of this time-dependent interaction, the SERS spectra of colloid-bacterial mixtures vary, initially improving in intensity as nanoparticles embed in the membrane, then deteriorating as cells lyse. Optimal SERS was achieved at approximately 3 hours. Prolonged exposure may lead to a deterioration in the spectra resulting from the bactericidal effect of nanoparticles.[45]

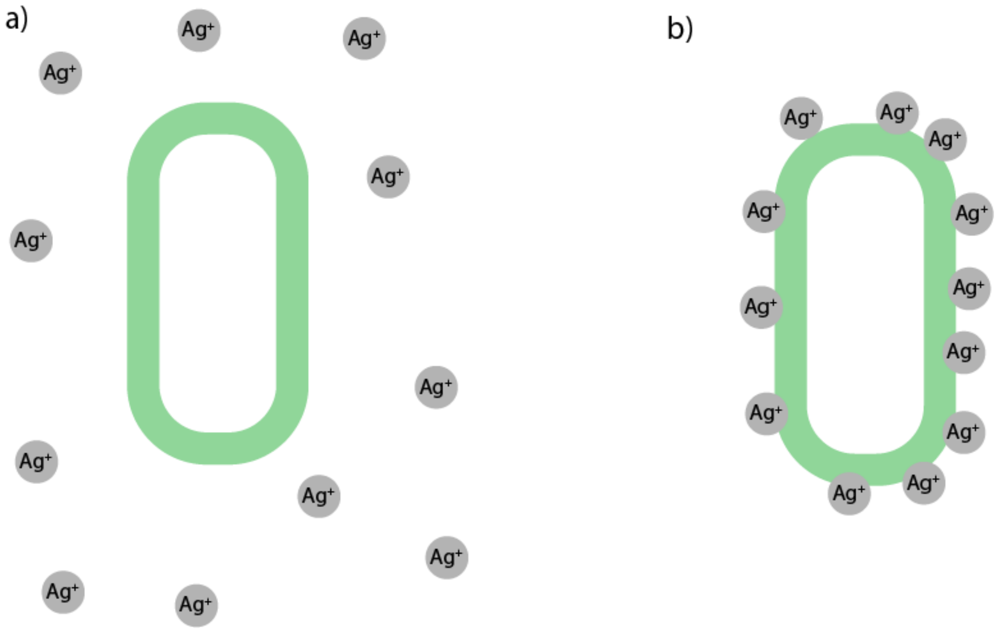

FIGURE 3. 122 SERS WITH COLLOIDAL NANOPARTICLES. a) BACTERIA IMMERSED IN COLLOIDAL NANOPARTICLES. b) NOBLE METALS NATURALLY INTERACT WITH THE CELL ENVELOPE IN A TIME DEPENDENT MANNER, WITH THE RATE DETERMINED BY FACTORS INCLUDING NOBLE METAL, NANOPARTICLE SIZE AND SHA

A range of more intricate methods have been employed to attain rapid, closer or, in some cases, targeted interaction of nanoparticles with the pathogens. This has been achieved using antibody-mediated immunocapture as well as aptamers[78, 139, 140]. Depending on the strength and specificity of the binding these techniques ensure apposition within the SERS effect range on target pathogens. This provides substantial preferential enhancement of pathogens and so is well suited to pathogen identification and identification. A potential challenge arises in that the Raman signal of the binding agent is similarly enhanced, although this is consistent across spectra and so may be accounted for during analysis. A further potential concern arises in that only pathogens onto which nanoparticles bind are enhanced, and so misclassifications will occur for any species which do not possess the specific binding site. Finally, functionalisation is a technical process which may not be amenable to cost-effective mass production or may limit the stability of nanoparticles.

3.4.3.3 SERS-ACTIVE SURFACES

A third approach is to apply the pathogens to a SERS-active substrate, as illustrated in **Figure 3.13**. Variations in the substance and manufacture of the substrate, type of SERS coating and methods for bacterial apposition allow for a diverse range of potential SERS-active surfaces that can be fine-tuned for pathogen recognition. SERS substrates provide a number of other advantages, including: the substrate may play additional roles, most notably in pathogen capture such as in SERS microfluidics; SERS substrates avoid the agglomeration challenge of colloids and so may provide better stability; and the SERS substrate also provides a consistent surface which may simplify laser focussing. A similar challenge arises to that faced by colloids in that the Raman signal of the substrate is present, although this may be minimised by the choice of substrate and remains consistent and so may be accounted for during processing[45, 128].

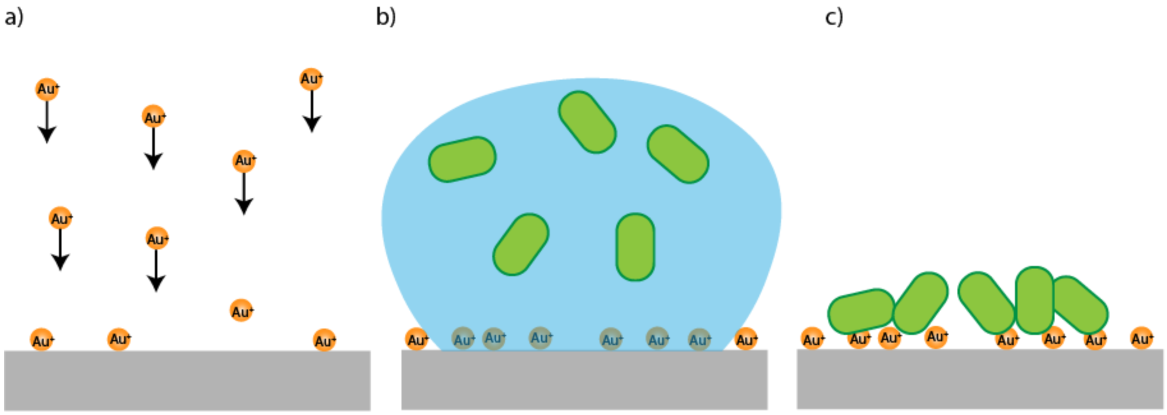

FIGURE 3. 133 SERS THROUGH ACTIVE SURFACE INCLUDE a) APPLICATION OF A NANOSTRUCTURED NOBLE METAL SURFACE USING A VARIETY OF TECHNIQUES. b) BACTERIA IN SUSPENSION ARE APPLIED TO THE SURFACE BEFORE c) USING TECHNIQUES SUCH AS AIR DRYING TO ENSURE APPOSITION OF PATHOGENS TO THE SERS SUBSTRATE

At its simplest SERS pathogen suspensions are applied to commercially available SERS-slides composed of a glass base with a roughened gold or silver layer applied[141]. Additional steps are required to bring the pathogens in apposition to the SERS substrate to gain enhancement. Apposition is frequently achieved through simple evaporation of the background solution, but a number of more rapid or selective means have been demonstrated[45, 128, 142].

SERS substrates have been produced through numerous means including lithography, electrospinning, mould compression, and additive manufacture. Differing methods have potential strengths and weakness with regards to a number of factors including: technical complexity of production process, cost of production, equipment required, resolution of the substrate and structural complexity of the substrate[45].

A similar variety of techniques are available for application of the SERS coating, including application of nanoparticles, embedding of nanoparticles into substrates, thin film deposition using physical vapour deposition. Control of these methods allow for application of SERS surfaces with varying characteristics, including SERS particle size, and spacing, film thickness and layout[72].

3.4.4 Pathogen Aggregation and Capture

Overcoming the weak Raman signal of bacteria and background fluorescence is achieved by physical methods falling into two categories. Either through increasing the amount of target biomass within the laser focus, or through SERS. Both methods are contingent on maximising the number of pathogens within a chosen space. Concentrating pathogens in the focal volume is achieved by a number of methods including culture, evaporation, centrifugation, electrostatic capture, dielectrophoresis, immunocapture, optical tweezers, magnetic coupling, microfluidics and antibiotic linking[45]. Different methods have strengths and weaknesses with regards to rate of capture, ease of implementation, equipment required, user technical experience required, selectivity of pathogens[70]

While circumventing the delay imposed by culture is the single biggest advantage to using Raman spectroscopy culture remains a commonly used technique in Raman based pathogen recognition. After passing the lag growth phase, pathogens grow exponentially, with bacteria such as *E. coli* able to double in number every 20 minutes. Raman based pathogen studies utilising culture for pathogen enhancement aim to achieve two aims: to either assess the dynamic Raman changes across growth phases, or to minimise the time to pathogen detection and classification. In addition to the delay incurred culture-based Raman detection is limited by the overwhelming background signal of culture media, although *Premasiri et al.* have demonstrated that 3 or more successive centrifuge and washing cycles are adequate to remove this background signal [143].

Filtration has been used in Raman based studies as a rapid means of capturing pathogens directly from biofluids, providing near unlimited capacity for pathogen concentration[136, 144-147]. Using filters with different pore sizes allows for physical separation of pathogens from eukaryotic cells due to different cell sizes. Additionally, filters allow for rapid separation of background signal arising from biofluids by passing through a wash fluid after pathogen capture. Filtration is widely used technique within microbiology requiring minimal technical expertise and equipment. *Lin et al.* embedded nanoparticles in mesoporous silica onto which *S. aureus* were captured for Raman analysis[136]. *Szymborski et al.* captured pathogens onto electrospun polylactic acid filters with a gold SERS thin film applied through physical vapour deposition[147]. *Dryden et al.* (Please see **Sections 6.3** and **Chapter 7**) captured uropathogens onto commercially available membrane filters with enhancement achieved by adding silver nanoparticles, and subsequently captured uropathogens directly from phantom urine samples onto gold coated filters for a single-step pathogen and Raman capture method for bacterial identification[148].

Centrifugation is commonly applied during washing steps to remove culture media but has also been used as an aggregating method for concentrating biomass for Raman analysis. Differences in pathogen size and density allow for differential centrifugation, therein allowing for selective separation of pathogens. *Tien et al.* used differential centrifugation to directly capture pathogens from urine for Raman identification[124].

Bacteria are negatively charged and so attracted to positively charged surfaces through electrostatic forces. *Mircescu et al.* used protonated glass slides to capture bacteria prior to forming SERS on the pathogens[101]. *Yang et al.* pegylated SERS slides upon which bacteria were captured directly from culture media and artificial urine[149]. This process allowed for rapid separation and Raman analysis direct from biofluids. *Prakash et al.* used positively charged bimetallic nanoparticles to identify bacteria in solution without the need for further concentrating steps. [150] The utility of this method is potentially limited by the fact that proteins and eukaryotic are also negatively charged, and as such are also bound to the SERS substrate.

Bacterial surface charge also underpins work performed by *Schroder et al.* in which custom built dielectrophoresis chips were able to concentrate uropathogens directly from suspension and human urine for Raman analysis without the need for SERS enhancement. While this work still required a Raman microscope, the relatively large focus diameter of 10-12 μm indicates that user-controlled focussing was simplified as compared to works that focused the Raman microscope onto single bacteria[117].

Liu et al. demonstrated that nanoparticles functionalised with vancomycin were able to significantly enhance susceptible bacteria directly from blood[78]. As this method relies upon the interaction of vancomycin with d-alanyl-alanine in Gram-positive peptidoglycan, this would not enhance Gram-negative pathogens or vancomycin resistant pathogens. It is therefore limited in bacterial identification or classification but could play a potential role in antimicrobial sensitivity testing in confirmed Gram-positive samples.

3.4.5 PREPARATION OF BACTERIAL SAMPLES

Fine control of many experimental and analytical parameters allows for finetuning of Raman methodology to obtain highly resolved spectra, but conversely means any experimental variation will lead to substantial differences in the spectra obtained. Similarly, methodology for Raman spectral acquisition needs to be refined for the target pathogens of interest. As such, while optimising the parameters of Raman acquisition, representative samples with minimal variability are needed. Bacterial suspensions are used as they allow for bacteria of known strain, in a consistent growth phase, at a controlled concentration suspended in a known background solution. This is in contrast to highly variable clinical samples containing pathogens from varying genera, species and serotypes, at a range of bacterial loads, with each sample containing pathogens at different growth phases and in highly variable biofluids. Bacterial suspensions for Raman research are produced culturing pathogens to a consistent growth phase, washing off culture media, followed by resuspending in a known solution and dilution to a chosen concentration.

3.4.5.1 CULTURE MEDIUM

A range of culture media including agars and broths are used in Raman pathogen research including blood agar, chocolate agar, brain hear infusion, lysogeny broth, nutrient agar and nutrient broth. The ideal growth media is non-selective, allowing for all samples to be produced in a standardised manner[110, 143].

3.4.5.2 GROWTH PHASE

Growth rates of bacterial samples are affected by environmental condition most notably temperature and time. Cultured pathogens progress through a series of growth phases: lag phase, log phase, stationary phase and death phase, reflected by dynamic changes in cell structure and function[78, 151]. These changes are reflected by dynamic Raman changes. *Avci et al.* demonstrated these dynamic shifts in uropathogens stabilised as bacteria moved into the stationary phase from 12 – 24 hours[123]. As such, Raman bacteriologic research is frequently performed in the stationary phase so as to minimise within and between sample variability. Infected clinical samples contain pathogens in varying growth phases, which are likely to lead to increased spectral variability.

3.4.5.3 CENTRIFUGE & WASHING

Culture media and biofluids have significant fluorescent and Raman spectra that may obfuscate pathogen cell signal or lead to diagnostic confounding. For example, *Premasiri et al.* demonstrated Raman spectra of different cultured pathogens cluster according to the culture medium used before washing, but after 3 or more centrifuge and wash cycles these clustered according to the pathogen present[143]. As such bacterial suspensions are washed prior to Raman analysis. As such washing is employed both during production of suspensions. Additionally, samples are frequently washed as an additional step in physical processing so as to optimise Raman signal. This is of particular value with fluorescing biofluids such as urine.

3.4.5.4 PATHOGEN LOAD AND SUSPENDING SOLUTION

Control of pathogen load may be required to reduce between sample variability, to identify limit of detection and to ensure suspensions appropriately reflect clinical samples. Gold standard assessment of pathogen load is performed using plate counting by the method defined by *Miles* and *Misra*[152]. This method is laborious entailing serial dilution and culture followed by manual counting, all repeated in triplicate. A further limitation when applied to Raman research is the delay required for culture means this method may only confirm the pathogen load rather than be used to plan bacterial loads.

Optical densitometry at 600nm (OD_{600}) is a rapid method for estimating bacterial load and for adjusting cell concentration using the suspension turbidity. *McFarland* demonstrated comparisons of suspensions turbidity against standardised solutions of barium sulphate provided a correlate of bacterial load[153]. Turbidity assessment provided by OD_{600} has become the preferred method for microbiology in view it's speed and simplicity. OD_{600} is preferable to plate counting for Raman research as pathogen load can be adjusted to the intended level before Raman assessment. OD_{600} is a surrogate measure of bacterial load with the correlation density and load varying between species as a result of differing cell size and shape[154]. Additionally, variation between devices has been demonstrated[154]. Therefore, the optical density meter used requires calibration to the chosen bacteria.

3.4.6 ANTIMICROBIAL SENSITIVITY TESTING

Gold standard AST using disc diffusion relies on demonstration of phenotypic changes, incurring substantial delays while awaiting pathogen culture and subsequent response to antimicrobials[155]. In contrast genotypic

AST provides rapid AST through identification of known mutations conferring resistance, however this may not accurately correlate with phenotypic sensitivity. Through providing rapid assessment of pathogen metabolic profile, Raman spectroscopy is ideally suited to rapid phenotypic AST[124]. Given the tendency for Raman pathogen identification to be based upon cell envelope changes, the technology is ideally suited to identify the antimicrobial mediated cell envelope degeneration. Raman-based classification has frequently been extended to provide antimicrobial sensitivity, with successful differentiation of sensitive pathogens achieved in 20 minutes or less[89, 149, 156, 157].

3.5 SYSTEMATIC REVIEW OF RAMAN SPECTROSCOPY APPLIED TO UTI DIAGNOSIS

3.5.1 INTRODUCTION

Urinary Tract Infection (UTI) is an extremely common bacterial infection in humans leading to an outsized disease burden. This burden is exacerbated by limitations in current diagnostics. Screening tests such as urinary dipsticks, while rapid, are inaccurate and fail to delineate bacterial species. Gold-standard diagnosis through cultivation, while accurate, may take as long as 48 hours. Rapid and accurate bacterial identification stand to fundamentally alter UTI management by allow for precision antimicrobial management from the point of diagnosis. While developments in microbial metabolic diagnostics including polymerase chain reaction (PCR) and mass spectrometry promise to reduce the time to diagnosis, the cost and complexity of these techniques make point of care diagnosis unfeasible[5].

Raman spectroscopy stands to fill this diagnostic gap by providing immediate speciation though whole organism metabolic fingerprinting. The application of Raman spectroscopy to bacterial identification has demonstrated success with strain level accuracy, making Raman spectroscopy an excellent candidate technology for point of care uropathogen identification.

This systematic review aims to assess the current published literature on UTI diagnosis using Raman spectroscopy: identifying the diagnostic accuracies attained, the techniques used and the progress made toward clinical detection of UTIs.

Research aims:

- **Primary**:
    - Describe the diagnostic and classification performance or Raman spectroscopy for urinary tract infections.
- **Secondary**
    - Describe the samples used in Raman spectroscopic uropathogen research, including the details of clinical samples used as well as the techniques and processes used for creating suspensions and phantoms.
    - Describe the physical methods employed for pathogen aggregation and capture prior to Raman spectral capture.
    - Describe the equipment. techniques and processes used for Raman spectral capture.
    - Describe the digital preprocessing and classification approaches applied to uropathogen Raman spectra.
    - Describe the current status of Raman UTI research including barriers to translation towards clinical implementation.

3.5.2 METHODS

A search strategy was devised with the assistance of Imperial College London librarian. The search was designed using a population, intervention, control, outcome approach, with search terms selected to ensure all pertinent studies were captured (**Table 3.8**). Searches were performed on PUBMED, Embase and Web of Science databases ensuring a cross section of clinical, engineering and basic science articles were reviewed.

TABLE 3. 8 PICO SEARCH STRATEGY

PICO	Terms
Population: UTI	UTI
	Urin* & infect*
	Cystitis OR pyelonephritis
	Uropathogen
	Urosepsis
Intervention: Raman Spectroscopy	Raman
	SERS
Comparison	None (uninfected controls not necessary)
Outcome	Diagnostic Accuracy
	Classification Accuracy

Studies selection was performed using Covidence software with inclusion and exclusion criteria listed in **Table 3.9** After removal of duplicates the remaining articles were submitted for title and abstract review. The titles and abstracts were reviewed independently against inclusion and exclusion criteria by two reviewers, with discrepancies resolved by a third independent reviewer. The full text versions were acquired and assessed for inclusion by the two independent reviewers with discrepancies resolved by a third reviewer. Papers included had data extracted into a Microsoft Excel spreadsheet by two independent reviewers, with discrepancies resolved by review and agreement. Metanalysis was not performed due to an anticipated high degree of heterogeneity.

TABLE 3. 9 INCLUSION AND EXCLUSION CRITERIA FOR SYSTEMATIC REVIEW

Inclusion	Exclusion
Studies assessing the diagnostic and/ or classification accuracy of Raman spectroscopy for uropathogens	General bacteriologic studies not for uropathogen recognition
Intended for UTI diagnosis or uropathogen identification	Non-peer-reviewed publications
2 or more uropathogens included	

3.5.3 RESULTS

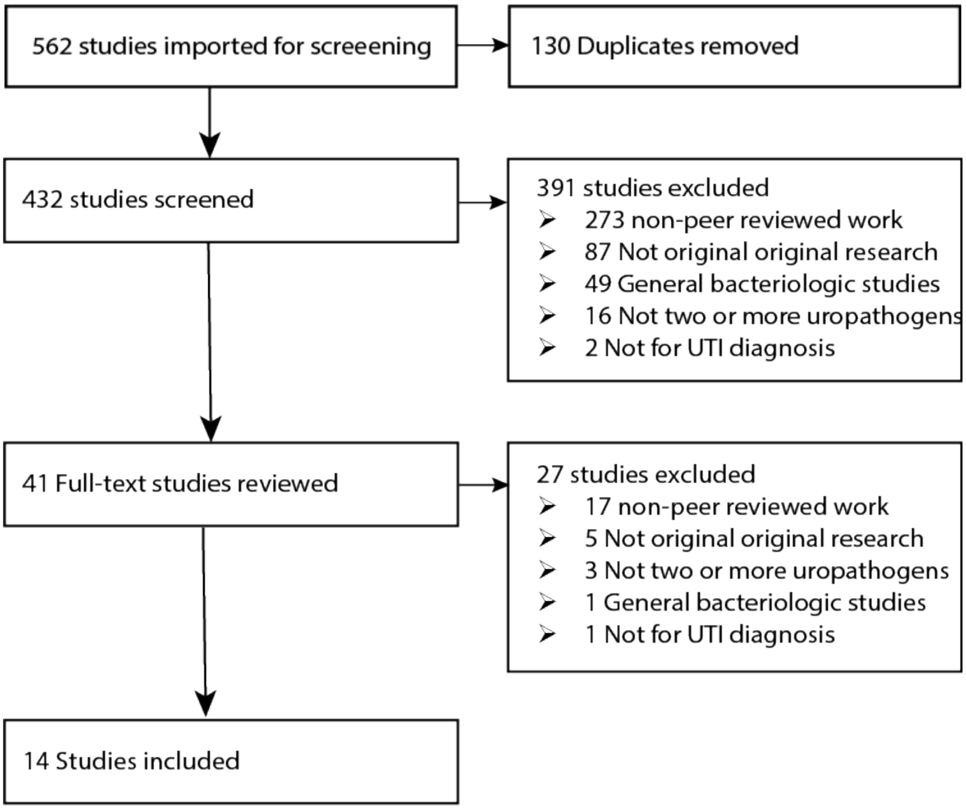

FIGURE 3. 144 PRISMA DIAGRAM FOR SYSTEMATIC REVIEW OF RAMAN SPECTROSCOPY UTI DIAGNOSTICS

Searches of Embase, PUBMED and Web of science were performed on the 8th of July 2020, with 562 search results included uploaded to Covidence. After removal of 130 duplicates 432 titles and abstracts were reviewed by two independent reviewers against inclusion and exclusion criteria. After exclusion of a further 391 studies, 41 full texts were acquired for review. After exclusion of 27 studies, 14 studies had data extracted (Table 3.10.

TABLE 3. 10 PAPERS INCLUDED IN SYSTEMATIC REVIEW

Author	**Year**	**Journal**	**Reference**
Avci	2015	Anal Bioanal Chem	[123]
Oliveira	2012	Biomedical optics	[110]
Goodacre	1998	Microbiology SGM	[102]
Jarvis$_a$	2004	Analytical Chemistry	[86]
Jarvis$_b$	2004	FEMS	[96]
Kastanos	2010	Journal of Raman Spectroscopy	[156]
Kloss	2013	Analytical Chemistry	[99]
Mircescu	2014	Anal Bioanal Chem	[101]
Yogesha	2019	Anal Bioanal chem	[158]
Premasiri	2017	Anal Bioanal chem	[159]
Schroder$_a$	2013	Analytical chemistry	[117]
Schroder$_b$	2015	Biomicrofluidics	[160]
Tien	2018	Molecules	[124]
Yang	2018	RSC Publishing	[149]

Table 3.11 captures the characteristics of the samples in the included studies. The majority of studies utilised bacterial suspensions, with only a few using urine phantoms or urine samples[99, 124, 159]. None of the included studies had negative controls, limiting these studies to pathogen classification of positive sample rather than UTI diagnosis. Many studies either did not state the number of samples[101, 160], used the same cultures to prepare multiple samples[96, 117], or else it was unclear as to whether the number quoted reflected samples or spectra[99]. *Escherichia coli* was included in all studies with a varying number of other uropathogens.

TABLE 3. 11 SAMPLE CHARACTERISTICS FROM STUDIES INCLUDED IN SYSTEMATIC REVIEW

Author	**Biofluid**																
	Studied	**Sample number**	**Source**	**EC**	**Ecl**	**EF**	**EFa**	**Esp**	**KP**	**KO**	**PA**	**PV**	**PM**	**SA**	**SE**	**SS**	**SH**
Avci	Bacterial suspension	7	Reference strain	1		1			1				1	1		1	1
Oliveira	Bacterial Suspension (10 µL)	38	Clinical Isolates	5	5			5	7		5		6	5			
Goodacre	Bacterial Suspension	59	Clinical isolates	17				12	10		10		10				
Jarvis$_a$	Bacterial Suspensions	21 samples with 4 replicates from each sample	Clinical Isolates	5				4	3	2			5				
Jarvis$_b$	Bacterial suspensions	20	clinical isolates	5				5	4	1			5				
Kastanos	bacterial suspensions	75	clinical isolates	25					25				25				

Kloss (training set)	suspensions grown in filtered urine	2951 (not stated if samples or spectra)	Reference Strain	364		441	247		233		248		247	283	234	224	221
Kloss (test set)	clinical samples	10	clinical Isolates	7		3											
Mircescu	Bacterial Suspension	Not stated	Reference strain	Yes									Yes				
Yogesha (single species)	Bacterial Suspensions	75	Clinical Isolates	15					15			15	15	15			
Yogesha (mixed samples)	Bacteria suspensions	20 (2 species) 30 (3species)	clinical isolates	50													
Premasiri	phantom urine	12 strains	clinical isolates	6		2			2							2	
Schroder$_a$ (Suspensions)	Bacterial suspensions	5 culture batches. Sample number not stated	reference strain	Yes		Yes											
Schroder$_a$ (Patient samples)	Patient samples	3	Patient samples	2 (300 spectra from each)	1 (with 300 spectra)												

Schroder$_b$ (suspensions)	bacterial suspensions			Yes		Yes											
Tien	Patient Samples	108 (97 single, 7 two , 4 three	clinical samples	Yes	Yes					Yes		Yes					
Yang	Bacterial Suspensions		Reference strain	Yes						Yes	Yes						

EC = Escherichia coli, Ecl = Enterobacter cloacae, EF = Enterococcus faecalis, Efa = Enterococcus faecium, Esp = Enterococcus species, KP = Klebsiella pneumoniae, KO = Klebsiella oxytoca, PA = Pseudomonas aeruginosa, PV = Proteus vulgaris, PM = Proteus mirabilis, SA = Staphylococcus aureus, SE = Staphylococcus epidermidis, SS = Staphylococcus saprophyticus, SH = Staphylococcus haemolyticus, Sho = Staphylococcus hominis, CF = Citrobacter freundii

TABLE 3. 12 SAMPLE PREPARATION FOR SYSTEMATIC REVIEW

Author	**Culture**			**suspension**					
	Medium	**Time**	**Temperature**	**Final Solution**	**Centrifuge speed**	**Centrifuge time**	**Wash Medium**	**Wash number**	**bacterial load**
Avci	Nutrient agar	1h, 6h, 12h, 24h	37°	1ml Deionized water	7500 rpm	5 min	Deionised water	3	10^7 (CFU/ml)
Oliveira	Mueller Hinton Agar, Blood Agar, CLED Agar	16-18h	35° +- 2		N/A				
Goodacre	Blood agar	16h	37°	Saline (0.9%)					
Jarvis$_a$	Blood Agar	16h	37 °	Saline (0.01M)					ND
Jarvis$_b$	Blood Agar	12	37°	distilled water	ND	ND	ND		ND
Kastanos	Mueller Hinton Agar	18	37°	PBS	NS	NS	PBS	3	ND
Kloss	preculture on Columbia blood agar then Filtered urine	24	37°	Deionised water	10000G	5 min	PBS	2	
Mircescu	Luria Broth	3 or 12 h	37°	Normal Saline	50000G	5 minutes (4 degrees)	Normal Saline	2	Not Diluted
Yogesha	Nutrient Agar	overnight	37°	Sterile Saline					0.5-0.7 McFarland

Premasiri	volunteer urine	NS (to chosen OD)	NS	volunteer urine					OD$_{600}$ = 0.1
Schroder$_a$ (suspensions)	CASO Agar	overnight	37°	PBS	11500G	5min	PBS	2	0.4-0.5 OD$_{600}$ (~10^8 CFU/ml)
Schroder$_a$ (patient urine)	NA	NA	NA	PBS				1	
Schroder$_b$ (patient samples)	CASO Agar	overnight	37°	PBS	11500G	5min	PBS	2	OD$_{600}$ (to concentrations of 10^7, 2*10^7. 10^8 and 2*10^8 cells/ml
Schroder$_b$ (validation)	NA	NA	NA		11500G	5min	PBS	2	
Tien	NA	NA	NA	NA	NA	NA	NA	NA	NA
Yang (suspensions)	Luria Broth or artificial urine	6h	37 °	Deionised water	4500 rpm	15min	Deionised water	2	10^5 cells/ml (by flow cytometry)
Yang (validation)	Luria Broth or artificial urine	6h	37 °	original culture medium (LB or artificial urine)	None	None	None	None	

NS = not stated, NA = Not applicable, OD = optical density, ND = Not done

Table 3.12 summarises sample preparation methods employed by the studies included in the systematic review. Preparation of suspensions typically followed a process of biomass expansion through culture pathogen, washing off the culture medium, followed by resuspension to a chosen concentration, although not all steps are included in all studies. The studies displayed a wide variation in the methods and reporting for each step. Notably, only a few studies used urine for suspensions[99, 149, 159]. Washing of cultured pathogens was frequently not performed, or performed less than 3 times and as such may be confounded by retained culture medium[143]. The pathogen load was frequently not controlled[86, 96, 99, 101, 102, 110, 156] or greater than established cut-offs[123, 158-160].

TABLE 3. 13 AGGREGATING AND SERS METHODS IN SYSTEMATIC REVIEW

Author	Physical	SERS Method
Avci	Airdrying (on CaF2 slide)	Silver Nanoparticles (Leopold and Lendl)
Oliveira	Air drying on aluminium foil	ND
Goodacre	ND	ND
Jarvis$_a$	preculture. Spotted on CaF2 slide	Nanoparticles Silver nanoparticle colloid (Lee and Meisel)
Jarvis$_b$	preculture. Spotted on CaF2 slide	ND
Kastanos	preculture. Spotted on CaF2 slide	ND
Kloss	air-dried on nickel foil	ND
Mircescu	Specially designed positively charged PEGylated slides	Silver nanoparticles (Leopold & Lendl)
Yogesha	spotted on quartz cover slip	Not done
Premasiri	Differential centrifugation	Gold nanoparticle coated silicone oxide substrate. ~80nm nanoparticles

Schroder$_a$ (suspensions)	Dielectrophoresis to aggregate and restrain pathogens	ND
Schroder$_a$ (patient)	Dielectrophoresis to aggregate and restrain pathogens	ND
Schroder$_b$ (suspensions)	v-cup microfluidic device, with centrifugation.	ND
Schroder$_b$ (patient)	Prefiltration 5um filter, wash and centrifugation. V-cup microfluidic device with centrifugation.	ND
Tien	Differential centrifugation (repeated/escalated if Raman resolution low)	Cylindrical SERS chip LabGuide Co)
Yang	Specialised pegylated (positively charged) slides.	Silver nanoparticles (*Leopold* and *Lindl*)

ND = Not done

Table 3.13 presents the aggregation and SERS methods employed by the articles included in the systematic review. These methods of enhancing Raman signal were frequently the core tenet of the research, and as such contain a variety of differing approaches. Surface enhancement was used in 6 of the 14 studies, with most using nanoparticle colloids[86, 101, 123, 124, 149, 159]. Aggregation methods fall into broad categories of basic laboratory methods[86, 96, 110, 123, 156, 158], electrostatic forces[101, 117, 149], or fluid dynamics[124, 159, 160]. The equipment used in the research included in the systematic review are presented in **Table 3.14**. The equipment specifications vary widely, likely tailored to the experimental requirements. Notably, Raman microscopes were used in most studies, with only *Kastanos et al.* and *Tien et al.* using spectrometers[124, 156].

TABLE 3. 14 RAMAN EQUIPMENT USED IN STUDIES INCLUDED IN SYSTEMATIC REVIEW

Author	Device		Wavelength	Power	Resolution	spectral limits	Acquisition time	Scans averaged	Raster Orbital Scanning/ roaming focus
	Name	Microscope/ spectrometer							
Avci	InVia Reflex, Renishaw	Microscope	830 nm	0.3-3 mW	NS		10 s		
Oliveira	Lambda P1	Spectrometer	830 nm	300 mW	2 cm^{-1}		5 s	10 (total 50 s)	
Goodacre	Renishaw	Spectroscope	780 nm	3 mW		200-2300 cm	10 s		
Jarvis$_a$	Renishaw 2000	Microscope	785 nm	~2mW	6.5cm^{-1}	403.73-986.66 cm	10 s	50 (taken from a grid)	grid scan
Jarvis$_b$	Renishaw	Microscope	244 nm	0.1mW	8cm^{-1}	780-1910 cm	120 s		rotating aluminium holder
Kastanos	Enwave Raman Analyser	Spectrometer	785 nm	180mW	4.5cm	300-2200cm	60 s	8	
Kloss	BioParticleExplorer	Microscope	532 nm	7mW	10cm^{-1}	70-3319 cm	6-30 s	2 (for spike removal)	
Mircescu	LabRam Horiba	Microscope	633 nm	14mW	2cm^{-1}	truncated to 650-1650 cm	5 s	at least 20 spectra obtained for each sample	

Yogesha	Home made	Microscope	785 nm	NS	NS	450-1800cm	NS		
Premasiri	Renishaw Rm2000	Microscope	785 nm	0.45mW	0.5cm^{-1}	200-1800cm	~10 s	10-20 scans taken	
Schroder$_a$	CRM300 WITec	Microscope	532 nm	15mW		600-1750 cm			
Schroder$_b$	CRM WITec	Microscope	532 nm	35mW				133	Multiple V-cups sampled
Tien	QEPro	Spectrometer	785 nm	20mV		400-2300 cm	5 s		
Yang	LabRam HR Horiba	Microscope	633 nm	0.14mW	2cm-1	50-2000 cm	10 s		

NS = Not stated

TABLE 3. 15 SPECTRAL PRE-PROCESSING OF STUDIES INCLUDED IN SYSTEMATIC REVIEW

Author	Smoothing Method	Background Subtraction	Normalization	Additional
Avci		Cubic spline interpolation (14 manual points)	sum of intensity values of each spectrum = 1	
Oliveira		Polynomial subtraction (7th order)	Peak intensity (1453cm^{-1})	
Goodacre				
Jarvis$_a$	Savitsky-Golay (first order, 9 point window)	subtraction of a linear baseline	min-max normalization	median of 36 of 50 spectra were summed
Jarvis $_b$	Savitsky-Golay (3rd order, 15 point window)			
Kastanos	"cosmic spikes removed, no filtering done"			Mean of 5 independent samples. Spectral band ratios with 76 even bands
Kloss		SNIP clipping	vector	Spike removal using upper bound spectrum algorithm truncation to 3100-2650 & 1750-450
Mircescu		background subtracted, method not stated	Normalised, method not stated	multiplicate scattering correction
Yogesha	Savitsky-Golay (second order, 11 point window)	asymmetric least squares	vector	truncated to 600-1750. Manual removal of cosmic spikes. Mean centred
Premasiri		polynomial fitting		barcode method defined by second derivative sign

Schroder$_a$		5th order polynomial fitting	vector	truncated to 600:1750cm
Schroder$_b$ (Suspensions)		5th order polynomial	vector	
Schroder$_b$ (Patients)		extended multiplicative		
Tien	AccuRam software, processing unclear.			
Yang		Polynomial subtraction (3rd order)		

Table 3.15 presents the digital pre-processing of spectra in the studies included in the systematic review. A range of digital pre-processing techniques were utilised. The variation in techniques reflects the need to tailor the pre-processing to the spectra generated. Reporting was frequently absent or missing information required for replication, such as *Premasiri et al.* reporting subtracting a fitted polynomial without stating the order, *or Mircescu et al.* reporting normalisation without reporting a normalising factor[101, 159]. Two studies utilised manual removal of cosmic spikes[156, 158].

TABLE 3. 16 FEATURE REDUCTION, CLASSIFICATION, AND VALIDATION METHODS IN SYSTEMATIC REVIEW

Author	**Feature Reduction**			**Classification**		**Validation**
	Method	**Features assessed**	**Feature Number Choice**	**Method**	**Other**	
Avci	PCA	NS	% of variance	ND		
Oliveira	PCA	NS	variance	Weight score (SC), Mahalanobis distance	Latent variable (LV)	
Goodacre	PCA			Discriminant function analysis (DFA) using Euclidean distance		
				ANN (1 hidden layer)		
Jarvis$_a$	PCA	varied: 8 in one group and 26 in another	Parsimony Principle (maximal discrimination with minimal number of PCs)	DFA (maximising fisher ratio)	HCA on DFA points	
Jarvis$_b$	PCA			DFA	HCA on DFA points	
Kastanos	PCA	58	99.99% of variance	LDA		LOO CV
Kloss$_a$	ND	NA	NA	SVM (with linear kernel & cost factor 2)		Independent test set & 10 patient samples

Mircescu	PCA	NA		No classification. Just a PCA plot. Not quantified		
Yogesha	PCA	6	LOO-CV	PLS-DA		Test set
	None			SVM (Radial Kernel function with cost function of 1.6 and gamma set to 4.6)		Test set
Premasiri	ND	24	lowest root mean squared error	PLS-DA		cross validation with 27 different random subsets and 21 iterations
Schroder$_a$	PCA	10	not stated	LDA		"independent" set (multiple spectra from each training and test samples)
Schroder$_b$				Not classified		Not quantified
Tien	NA			PCA only presented		
Yang	ND			Discriminant analysis with Mahalanobis distance		Training set (12 of 48 retained)

ND = Not Done, NA = Not Applicable

Table 3.16 presents the feature reduction, classification and validation methods presented in the articles included in the systematic review. PCA was frequently used for feature reduction of spectra[86, 96, 101, 102, 110, 117, 123, 124, 149, 156-158, 160]. The number of reduced features passed for classification varied widely. Similarly, the method for the number of features selected varied widely or was not stated. *Kastanos et al.* passed 58 reduced features despite having only 75 samples[156]. Not all articles undertook sample classification. Discriminant analysis was the most frequent classification technique used, with SVMs used in 2 studies[99, 158] and ANN used once[102].

TABLE 3. 17 TRAINING AND VALIDATION CLASSIFICATION PERFORMANCE OF STUDIES INCLUDED IN SYSTEMATIC REVIEW

Author	**Group**	**Training Set**			**Validation**		
		Accuracy	**Sensitivity**	**Specificity**	**Accuracy**	**Sensitivity**	**Overall Specificity**
Avci		Not quantified. PCA plots presented with excellent separation					
Oliveira		83.5% (152/182)	58-100%	87-100%			
Goodacre	**PC-LDA**	Not quantified plot of discriminants presented					
	ANN	74% (25/34)					
Jarvis$_a$		Not quantified					
Jarvis$_b$		Not quantified, Discriminant function plot presented with excellent separation					
Kastanos		94.7% (71/75)	88-100	94-100%	Not quantified, 3 of the LOOCV PCA plots presented		
Kloss	**Bacterial suspensions**	92.1% (2718/2952)			95.1% (489/514)		
	Patient samples				100% (10/10)	100 (10/10)	100% (10/20)
Mircescu **2014**		Not quantified					

Yogesha	**single species, PC-LDA**	Not quantified, but depicted graphically to show good separation of all bacteria except EC from Pmir on first order PC-LDA, which were subsequently well separated on second order PC-LDA			96%		
	single species, SVM	100%			Single species 98.7%		
	mixed samples, PC-LDA				90% & 93% for M2 and M3 infections respectively		
	mixed samples, SVM				95% for M2 (one misclassified as *K. pneumoniae*). 96% for M3 with 1 misclassified as K pneumoniae		
Premasiri					95.80%	99.30%	
Schroder[a]	**Suspensions**	Not quantified: LD plot shows perfect separation linear discriminant both on training and testing.					
	Patient samples				99.8% (899/900)		

Schroder$_b$		Not quantified					
Tien		Not quantified - PCA plots only presented. Table 1 reports a Raman SERS quantification but down not reports classification accuracy/ misclassification					
Yang	**Suspensions**	93.8% (45/48)			100% (12/12)	100% (12/12)	100% (12/12)
	From culture media	100% (48/48)			100% (12/12)	100% (12/12)	100% (12/12)

PCA = principal component analysis. PC-LDA = principal component – linear discriminant analysis. SVM = support vector machine. M2 = 2 pathogen mixed infection. M3 = 3 pathogen mixed infection.

Table 3.17 presents the results of classification performance. None of the studies included assessed diagnostic (infected versus uninfected) performance, and as such accuracies presented refer to pathogen classification accuracies. For this reason, sensitivities and specificities are infrequently presented as these would refer to pathogen classification rather than diagnostic performance. Training set accuracies range from 74% to 100%, although not all studies report classification performance (or alternatively present them graphically without quantification). Most studies did not present validation results, or on occasion, present these graphically without quantification. The reported validation accuracies range from 95.1% to 100%. Frequently validation performance exceeded those presented in training sets[99, 149].

TABLE 3. 18 SPECTRAL BAND ASSIGNMENTS FROM STUDIES INCLUDED IN SYSTEMATIC REVIEW

Spectral Band (cm^{-1})	Assignment	Reference
364-474	Carbohydrates	[101]
500-586	Carbohydrates, Glycosidic ring	[101]
518-519	Hypoxanthine, Guanine	[149]
538	COC glycosidic ring deformation (bacteria)	[110]
545	CCC Deformation (Agar)	[110]
562-567	Hypoxanthine, xanthine, Guanine	[149]
624	CC Twisting Tryptophan (Bacteria)	[110]
642-643	Tyrosine	[158]
643 - 688	COO deformation, Guanine	[101]
645	Tyrosine	[110]
655	carboxyl groups	[123]
656-657	Hypoxanthine, xanthine, guanine	[149]
667-668	Guanine	[158]
672	Valine	[110]
676	guanosine	[149]
721	Agar	[110]
721-749	Glycosidic ring, Adenine	[101]
723	CH2 rocking	[99]
724-725	Adenine	[158]
725-731	hypoxanthine, adenine, guanine AMP	[149]
726	Adenine ring stretch peptidoglycan	[110]
730	adenine	[123]
730	C-N stretching	[123]
730	ring breathing adenine	[123]
742	CC-skeletal deformation of galactose ring (Agar)	[110]
748	DNA	[99]

748	cytochrome c	[99]
756-757	Tryptophan	[158]
759	Tryptophan	[110]
774	CC-skeletal deformation of galactose ring (Agar)	[110]
780-781	Cytosine, Uracil	[158]
781	ring breathing mode of cytosine, uracil and thymine	[99]
781	OPO backbone of DNA	[99]
784	cytosine, uracil - ring stretching	[110]
788	PO2 stretching, cytosine and thiamine	[160]
801-819	Tyrosine v(CN)	[101]
808-809	Tyrosine	[158]
814	COPOC RNA binding	[110]
824-825	Tyrosine (Exposed)	[158]
829	Tyrosine	[110]
830	Breathing Phenylalanine	[123]
846	CC-deformation, OCO wagging, Ch Vibrations (Agar)	[110]
849-852	Tyrosine (Buried)	[158]
850	CH2 Scissoring	[123]
850	Breathing Phenylalanine	[123]
854-857	Guanine	[149]
857	COC-stretching of glycosidic linkages; C-C proline stretches, CCH deformation ring breathing of tyrosine, teichuronic acid of Gam positive cell wall	[110]
875-878	tryptophan ring deformation	[158]
887-896	C-O-C stretching	[158]
890	CCH deformation (Agar)	[110]
907	COC stretching of glycosidic linkages (saccharides) Teichuronic acid of Gram positive cell walls	[110]
921-953	Ring breathing vibration	[101]
926-933	C_C stretching, alpha helix, COC glycosidic bond	[158]

930	Saccharides (Agar)	[110]
935	protein extract (culture media)	[110]
935	CC-stretch of protein (culture media)	[110]
938	Amide III - CC stretching.	[110]
951	Phenylalanine, proline (Agar)	[110]
952-954	C-N stretching	[158]
957-960	hypoxanthine, adenine, guanine, guanosine	[149]
966	CCH deformation (Agar)	[110]
1000	phenylalanine	[158]
1001	CH2 Scissoring	[123]
1001	phenylalanine	[123]
1001	pyranose ring	[123]
1004	protein extract (culture media)	[110]
1004	haemoglobin (culture media)	[110]
1004	Phenylalanine -CC skeletal stretching of ring breathing (Agar)	[110]
1004	ring breathing mode of phenyl alanine	[99]
1004	phenylalanine	[160]
1007	Phenylalanine & tyrosine - CC stretching of aromatic ring	[110]
1023	AMP	[149]
1027-1028	C-H in plane	[158]
1030	CH2 Scissoring	[123]
1030-1130	Carbohydrates mainly CC, CO and COH stretching	[110]
1033	Phenylalanine & Proline CH deformation, CO and CC stretching of saccharides	[110]
1049	CO exocyclic stretching (Agar)	[110]
1077-1078	C_C chain stretching (lipids), CO. CC stretching (carbohydrates)	[158]
1084	COH deformation, CCO Stretching (Agar)	[110]
1091-1098	hypoxanthine	[149]
1093	po2 stretching	[160]

1093-1097	Carbohydrates (CC, CO, COH deformation)	[158]
1099	Nucleic acid PO2 symmetric stretching; CC and COC skeletal stretching of glycosidic linkage of saccharides	[110]
1099	phenylalanine	[99]
1099	CN stretching	[99]
1100-1130	carbohydrate (deformation C-C, CO, COH)	[101]
1121-1122	CN, CC & CO stretching	[158]
1127	cytochrome c	[99]
1130	lipid acyl CC skeletal stretching; CO and CC saccharide stretching	[110]
1132	COH sugar deformation (Agar)	[110]
1143-1147	guanosine	[149]
1149-1209	Lipid =C-C=	[101]
1151-1153	CC stretching vibration of polyene chain of carotenoids	[158]
1155	COH deformation (Agar)	[110]
1156	CC-CN protein stretching; CO & CC Saccharides	[110]
1160	Guanine	[149]
1162	Carotenoid CC conjugated stretching	[110]
1166-1168	CC stretching vibrations	[158]
1172	Tyrosine	[86]
1173	Tyrosine CH Wagging; Guanin and Cytosine; fatty acids(stearic acids)	[110]
1205-1206	C-C6H5 stretch, phenylalanine, tryptophan	[158]
1211	Amide III, Tyrosine CC Stretching; phenylalanine, tryptophan	[110]
1226	haemoglobin (culture media)	[110]
1226	Haemoglobin CH stretching (Agar)	[110]
1238-1239	amide III	[158]
1240-1300	Amide III	[123]
1241	amide III	[99]
1241	PO2 stretching asymmetric in DNA bases	[99]
1242-1445	Amide III	[101]

1247	Guanine, Adenine and Uracil	[86]
1253	Amide III	[160]
1261	amide II CN & NH stretching; thymine and adenine ring breathing; Lipid CH2 deformation; saccharides	[110]
1266-1287	Protein Deformation CH	[101]
1270	Lactose	[110]
1270	Lactose (Agar)	[110]
1274	hypoxanthine, Adenine	[149]
1285	CH2 twisting (Agar)	[110]
1293	Fatty Acid CH2 deformation; cytosine	[110]
1296-1297	CH2 twisting	[158]
1310	CH2-CH3 twisting, waggling and bending in lipids	[99]
1310	cytochrome c	[99]
1316-1319	Guanine, CH deformation	[158]
1320	Amide II CN and NH stretching; protein CH2 and CH3 deformation; Guanine Breathing ring	[110]
1324	Adenine, Guanine and Tyrosine	[86]
1326-1329	Xanthine, Adenine, AMP	[149]
1333	adenine	
1334	CH2 deformation of proteins	[99]
1334	ring vibrations of guanine and adenine	[99]
1334	tryptophan	[99]
1338-1339	Adenine, CH deformation	[158]
1340	Fatty acid and protein CH2 and CH3 deformation; amide III NH stretching; tryptophan CC stretching; adenine and guanine ring breathing	[110]
1341	CH2 deformation	[160]
1346-1368	protein (deformation CH), symmetric stretching COO	[101]
1350	CH2 wagging (Agar)	[110]
1376-1374	hypoxanthine, adenine, AMP	[149]
1382	peptidoglycan COO stretching	[110]

1413	CH deformation (Agar)	[110]
1421	Adenine; guanine; peptidoglycan CO vibration	[110]
1422-1465	Saturated lipids, deformation CH2	[101]
1425	Guanine, Adenine	[86]
1446	CH2 Scissoring	[123]
1446-1448	CH2 Bending	[158]
1450	protein extract (culture media)	[110]
1450	haemoglobin (culture media)	[110]
1450	protein CH2 & CH3 deformation (Agar)Lipid and protein	[110]
1451	CH2-CH3 deformation	[99]
1453	Lipid and Protein deformation	[110]
1453-1466	hypoxanthine, adenine, guanine	[149]
1469	CH2 deformation(Agar)	[110]
1480-1481	Guanin, Adenine CH deformation	[158]
1521	In phase C=C vibrations of polyene chain of carotenoids	[158]
1523-1543	Ring stretching Vibration	[101]
1524	cytosine	[86]
1525	Carotenoids CC conjugated stretching	[110]
1528-1533	hypoxanthine	[149]
1541	guanine, guanosine	[149]
1550	Amide II	[123]
1550-1551	Tryptophan	[158]
1557	tryptophan; exopolysaccharides	[110]
1562	haemoglobin (culture media)	[110]
1567	haemoglobin CH_2 Stretching	[110]
1567	Guanine, Adenine	[86]
1572-1573	exopolysaccharide associated band	[158]
1573	ring vibrations of guanine and adenine	[99]

1573	Cytochrome C	[99]
1575-1581	hypoxanthine, guanosine	[149]
1578	peptidoglycan CO vibration mode; adenine and guanine ring stretching	[110]
1578	ring stretching of guanine and adenine	[160]
1589-1668	stretching DNA	[101]
1602-1603	phenylalanine	[158]
1606	CC ring vibration of phenylalanine and tyrosine	[99]
1607	tyrosine and tryptophan	[86]
1611	phenylalanine; tyrosine and tryptophan CC ring stretching	[110]
1613-1615	Tyrosine	[158]
1624	haemoglobin (culture media)	[110]
1624	haemoglobin CC asymmetric stretching	[110]
1640-1659	AMP, Adenine	[149]
1644	Amide I CO stretching (Agar)	[110]
1656-1655	Amide I	[158]
1658	amide I	[86]
1660	Amide I Co stretching; lipid CC stretching	[110]
1665	Amide I	[99]
1665	CC alkene stretching	[99]
1665	nucleic acids	[99]
1670	Amide I	[123]
1690-1702	stretching C=C	[101]
1692	hypoxanthine, uric acid	[149]
2935	asymmetric CH2 stretching	[99]
2935	symmetric CH3 stretching	[99]
3059	Olefinic CH stretching	[99]

Table 3.18 presents the spectral band assignments from the studies included in the systematic review. The band assignments cover a broad range of Raman shift from 364cm^{-1} up to 3059 cm^{-1}[99, 101]. The high density of biochemical assignments represented across this range reflect the resolution and sensitivity provided by Raman spectroscopy. Biochemical assignments range from relatively generic origins such as C-C backbones likely to be

present in a range of proteins and carbohydrates, up to specific components such as teichuronic acid from Gram positive cell walls[110]. An array of potential biochemical origins are present including nuclear components such as DNA, cell membrane components such as cytochrome C, a plethora of cell wall components such as peptidoglycan, and extracellular excretions such as AMP. Similarly, a range of non-pathogen originating substances are presented by *Oliviera et al.*[110].

3.5.4 DISCUSSION

With classification accuracies ranging from 75% to 100% in the included studies, Raman spectroscopy demonstrates potential to act as an effective UTI diagnostic as defined in **Chapter 2**[99, 102, 110, 156, 158]. The accuracies attained in these studies are comparable with currently implemented diagnostics (such as chromogenic culture) as well as those under development (including mass biosensors, multiplex PCR). A significant potential advantage of Raman spectroscopy as an effective UTI diagnostic technology is the potential to provide classification without prior biomass amplification through culture, therein providing substantial improvements in turn-around time. Only a few of the studies included explicitly report the sample turnaround time, including *Mircescu et al.* (under 2 hours)[101], *Premasiri et al.* (under 1 hour)[159], *Schroder et al.* (approximately 1 hour)[160], *Schroder et al.* (a few minutes)[117] . Other studies allude to the time benefits gained through using Raman spectroscopy without explicitly quantifying the temporal advantage [99, 124, 149].

The ideal UTI diagnostic would answer a series of questions: firstly is the sample infected (diagnosis); secondly, what is the pathogen(s) (classification); thirdly what is the pathogen load (quantification); finally what is the antimicrobial sensitivity profile. None of the studies included in this systematic review included negative controls, and as such were unable to address the first question regarding diagnostic performance. Not attempting diagnosis is counterintuitive as many of the components identified in the spectral band assignments (**Table 3.18)** are likely to be absent or significantly different in uninfected urine. A potential explanation for this failure to address the primary goal of UTI diagnostics is an overreliance on Raman microscopy in Raman based UTI research. All but two of the included studies used Raman microscopes rather than spectrometers. Raman microscopes require user control to focus the illuminating laser onto the pathogens, and so are limited to samples already defined as positive[88, 100, 101, 156].

Despite the promise of Raman research achieving uropathogen recognition there is no clinically implemented Raman diagnostic nor large published diagnostic clinical trials[83]. Understanding the barriers toward larger clinical trials and clinical implementation are key toward planning successful Raman research. Most studies use Raman microscopes as the considerably smaller field of focus provides for much higher resolution Raman spectra. This benefit is contrasted against the substantial drawbacks of Raman microscopy. Raman microscopy relies upon the user locating the pathogen and focussing the Raman laser beam, which requires technical expertise and therefore has an inherent user variability. For example, *Mircescu et al.* had to discard 30% of collected spectra because of suboptimal focussing[101]. Raman microscopes are expensive and have a large physical footprint, therein limiting their implementation to research centres and potentially large, centralised labs only[88, 100, 101, 156].

Samples used in the majority of Raman research are not representative of the diversity present in clinical samples. Most studies included in the review used only a small number of, typically reference strain, species. Raman spectroscopy has demonstrated sensitivity to strain level, and so the multiple strains present in clinical samples presents a substantially greater classification challenge. Only one study diluted the pathogen load down to the clinically relevant concentration of 10^5 CFU/ml with all the other studies effectively approaching a simplified classification challenge[149]. Similarly, the controlled growth phase simplifies the classification challenge by reducing the effect of dynamic cell envelope changes as pathogen move between growth phases[123]. Clinical samples frequently contain mixed infections, while most of the studies included only assessed single species infections. While *Yogesha et al.* validated their results on mixed infection samples they counted identification of the included species as a correct classification, in effect doubling or tripling the probability of “correct” classification (as evidenced by improving classification performance with more species)[158]. *Tien et al.* attempted to classify mixed infections arising from 11 of their samples using a PCA approach, however their gold-standard culture was only able to provide classification for four of these, and as PCA is not a supervised approach they were unable to assess classification performance.

Classification was only assessed on clinical samples in three of the included studies [99, 117, 124]. *Schroder et al.* assessed 900 spectra acquired from 3 patient samples achieving 99.9% accuracy[117]. While this classification performance appears promising, originating from only 3 samples implies a high degree of uncertainty in the quoted number[117]. *Kloss et al.* validated their technology on 10 patient samples including 7 *Escherichia coli* and 3 *Enterococcus faecalis* infections with all ten correctly identified[99]. *Tien et al*. assessed 108 clinical samples presenting SERS spectra from processed and unprocessed spectra of a few pathogen species, as well as PCA plots which show separation of species according to antimicrobial sensitivity. However, supervised learning was not applied and so the classification performance could not be quantified[124].

SERS was used to improve Raman signal in many of the included studies with many of these using colloidal nanoparticles[86, 101, 123, 124, 149, 159]. The ability of SERS to provide massive signal enhancement makes this central to these studies, however this massive signal enhancement risks inducing massive variability if SERS is inconsistently applied particularly in view of the exponentially decreasing enhancement with increased distance. This, along with a tendency for nanoparticles to aggregate or corrode may explain why these nanoparticles are prepared immediately prior to use in SERS research[70, 125, 136, 161]. Similarly, these nanoparticles are produced under strict control to ensure consistency. As a result, technologies reliant on these nanoparticles may be challenging to implement clinically. A clinically implementable SERS technology for UTI diagnosis would require a stable SERS substrate, which incorporates a mechanism to ensure close and consistent apposition to pathogens.

Many of the studies included present spectra, unsupervised classification figures, or supervised classification figures without classification. Presenting results in this manner is susceptible to "cherry-picking" or selective interpretation. Spectra plotted without some representation of variation risks interpreting noise as contributory peaks. PCA plots and linear discriminant plots are similarly susceptible to overinterpretation. Where supervised learning was applied and quantified, discriminant analysis was the most frequently applied technique. However, discriminant analysis is prone to overfitting and therefore poor generalisation as compared to techniques such as SVMs[122]. *Yogesha et al.* applied both PC-LDA and SVMs to their dataset, with SVMs providing superior cross validation classification accuracies[158]. Similarly, *Kloss et al.* also used SVMs with excellent validation accuracies achieved. The only study to use an ANN was *Goodacre et al.* who also utilised PC-LDA on this dataset, the results of which were unfortunately not quantified. As such, drawing comparisons between PC-LDA and ANNs was not possible based on this study. It is likely, however, that the dataset of 34 samples is underpowered for an ANN.

This systematic review captures the vast number of parameters and techniques to be controlled in Raman experiments from the point of physical processing, through Raman capture, to digital pre-processing and classification. This poses a significant challenge to generalisability as a degree of overfitting or selection bias is possible through optimisation of these parameters. It poses a similar challenge to furtherment of Raman research as many of the studies in this systematic review contained insufficient data for replication. There is no current widely adopted standardised reporting or trial reporting for Raman laboratory-based research. Raman-based pathogen research would thus benefit from standardised reporting and trial registration.

Validation remains a valuable backstop to guard against overfitting, and to a lesser degree, selection bias. Independence of the test data is essential, with the greatest robustness provided by prospectively collected test data ranging down to leave one out cross validation. Most of the included studies did not perform any validation [86, 96, 101, 102, 110, 117, 123]. For example, *Kastanos et al.* performed LOOCV, however did not quantify their results, but rather presented three PCA plots generated from the LOOCV[156]. Independence of data is imperative for reliable validation, which was frequently not maintained. In this regard, *Schroder et al.* trained their classification algorithm on 600 spectra derived from only 5 culture batches and validated 600 spectra from only 3 samples[160]. While not explicitly stated, the massive number of data points included by *Kloss et al.* implies that these refer to spectra rather than independent samples which are therefore not independent[99].

This systematic review demonstrates that Raman spectroscopy has potential to be developed into an effective diagnostic technology for urinary tract infections. Numerous studies have achieved excellent classification performance in substantially reduced timeframes as compared to currently implemented technologies. Working toward a clinically implementable Raman-based UTI diagnostic should focus on rapidly implantable physical processing methods with spectra acquired using a handheld spectrometer. Research performed during development should focus on samples which adequately reflect clinical sample, with analysis that is both replicable and can be validated.

Numerous challenges arise when performing studies to assess the performance of diagnostics studies. Imperfect gold-standard reference tests may influence the published diagnostic performance. Selection bias may influence generalizability of results to clinical use. Inconsistent application of diagnostic cutoffs (in the index or reference test) may influence comparability of studies and limit generalizability[162].

Systematic reviews aim to aim to identify and combine all published information on a topic, and in so doing, work towards a more precise understanding thereof[163]. The methodologies employed to assess a topic may evolve as a greater scientific understanding is developed, or need to be varied to assess to answer aligned research questions. As such, heterogeneity is frequently encountered when performing systematic reviews.

Quality assessment is an important component of systematic reviews, as biases in the included works influence the final result of the review and metanalysis. Quality Assessment of Diagnostic Accuracy Studies (QUADAS) were developed in 2003 and revised in 2011 to facilitate systematic reviews of diagnostic technologies[163, 164]. QUADAS-2 assesses studies by 4 domains including patient selection, the index test, the reference test, as well as flow and timing.

In developing and tailoring a systematic review aimed at describing the diagnostic and classification performance of Raman spectroscopy for UTIs substantial heterogeneity was encountered across all four QUADAS-2 domains. Samples were prepared or acquired using widely differing methods. While Raman spectroscopy was the diagnostic technology for all studies, varying equipment, and parameters as well as the use of SERS means these cannot be considered a single type of index test. For most of the included studies, a reference or confirmatory test was not used as samples were derived from cultured pathogens. Finally, the multiple processing steps involved in these Raman studies indicates substantial flow and timing variability. While the QUADAS-2 guidelines were considered during the development of this systematic review, formal assessments of bias and applicability were not performed due to the obvious heterogeneity.

Wide heterogeneity present in this systematic review rendered metanalysis impossible. Nevertheless, a systematic review was warranted to demonstrate the successes of Raman spectroscopy in achieving uropathogen classification, as well as documenting the methods employed in these studies.

The field of Raman spectroscopy would undoubtedly benefit from agreed-upon standards for bacteriologic research. Reduced heterogeneity provided by standardized methodology would improve comparability of studies, and potentially allow for metanalysis. An additional benefit of standardized methodology would reduce the barriers faced in implementing Raman-based research, making this more accessible to a broader range or researchers.

3.6 CONCLUSION

The strengths provided by Raman spectroscopy position it as a potential effective technology for UTI diagnosis, most notably the ability to circumvent the need for biomass expansion allows for rapid recognition, and the high-resolution spectra providing for accurate and granular classification. These strengths are evidenced in the literature, both applying to UTI and general bacteriologic studies, with excellent classification accuracies provided with rapid turnaround times. Raman spectroscopy has the potential to be developed towards meeting the other characteristics of an ideal UTI diagnostic as defined in **Chapter 2**. Specifically, limited physical processing and small physical footprint underly the potential to develop a point of care device is which widely implementable and useable with minimal training.

The central challenges to developing a clinically implementable Raman technology for UTI are initially to optimise the broad number parameters to gain the greatest signal while minimising noise. This is achieved through strict experimental standardisation allowing for systematic interrogation of techniques and parameters under control. Core to this is an analytical framework that can address the hypergeometric and colinear data with as few samples as possible, therein allowing for rapid prototyping. Successful optimisation of a Raman based technology for UTI diagnostics will need to be followed by collection of an extensive dataset able to account for the broad variation expected in clinical samples. Additionally, a robust analytical technique that makes best use of the larger dataset to provide generalisability will be required.

CHAPTER 4: RAMAN SPECTROSCOPY FOR UTI DIAGNOSIS

4.1 INTRODUCTION

Research aiming to provide pathogen classification from urine samples and pathogen suspensions using Raman spectroscopy follows a broadly standardised approach of sample preparation, physical processing, Raman acquisition, spectral digital pre-processing and classification (**Figure 4.1**). Within each step multiple options each with varying parameters leading to a tremendous number of permutations potentially applied to Raman research methods. Published research in Raman spectroscopy frequently focuses on the physical processing steps, with the description of other methods limited to those necessary for replication. Adapting these methods requires an intricate evaluation of the strength and weaknesses of each permutation. **Chapter 4** will systematically isolate and interrogate each process so that methods may be optimised for further experimental work. **Section 4.2** describes methods for consistent preparation of bacterial suspensions. **Section 4.3** describes the optimisation of parameters during Raman acquisition. **Section 4.4** describes the analysis of Raman spectra, including methods for digital pre-processing, classification and identification of pertinent spectral bands.

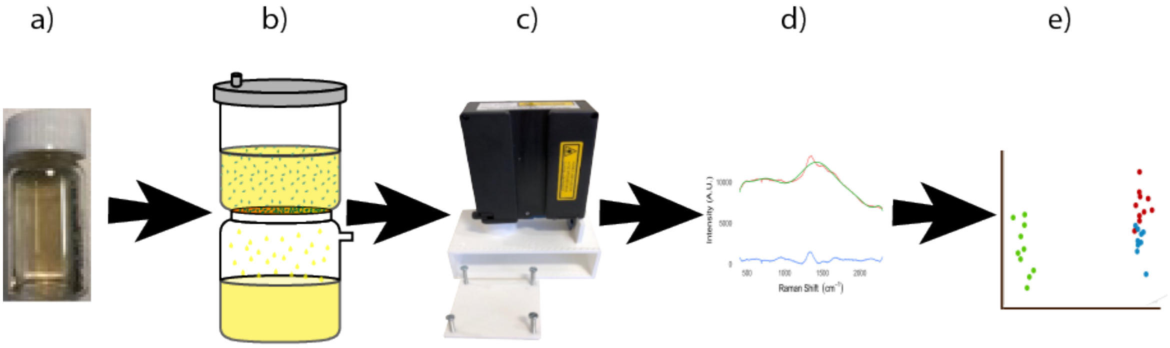

FIGURE 4. 1 SUMMARY METHOD FOR RAMAN RESEARCH ON UTI IDENTIFICATION AND CLASSIFICATION. (a)PREPARED SAMPLES ARE (b) PHYSICALLY PROCESSED BEFORE (c) RAMAN ACQUISITION, AFTER WHICH THEY ARE (d) DIGITALLY PRE-PROCESSED (e) BEFORE CLASSIFICATION

Aims:

- Develop methods for consistent production of samples representative of UTIs which are suitable for Raman spectroscopic assessment.
- Understand the parameters under control when acquiring Raman spectra, developing a standardised approach to spectral acquisition.
- Understand sources of noise in Raman spectra, understanding and applying methods for reducing noise.
- Identify and apply a classification technique suitable to rapid prototyping (low number of samples) on complex data (hypergeometric and colinear).
- Identify a quantitative method for identifying spectral bands contributing to classification.

4.2 BACTERIAL SUSPENSIONS

Early-stage Raman microbiology research requires samples whose bacterial type and load are representative of clinical samples, while controlling for the variation caused by diverse strains and loads. Representative samples are achieved using cultured reference strain pathogens suspended at controlled pathogen load. An additional step is required or Raman research to wash residual culture show strong Raman scattering may obscure the bacterial signal. **Section 4.2** describes the preparation of bacterial suspensions.

A reference bank of uropathogens was established and are presented in **Table 4.1**. Bacteria acquired from NWLH Microbiology Laboratory were cultured on Columbia blood Agar for 24 hours at 37 degrees. Bacterial colonies were harvested using a sterile disposable 10 μl loop and transferred to a Microbank cryopreservation vial. The vials were agitated for 1 minute before aspirating and discarding the supernatant. Microbank vials were stored at -70 degrees Celsius.

TABLE 4. 1 REFERENCE BANK OF UROPATHOGENS

Uropathogen
Escherichia coli ATCC25922
Enterococcus faecalis ATCC29212
Klebsiella pneumoniae ATCC13883
Pseudomonas aeruginosa ATCC27853
Proteus mirabilis NCTC10975
Streptococcus agalactiae NCTC8181
Staphylococcus aureus ATCC29213
Staphylococcus epidermidis ATCC12228

4.2.1 CULTURE MEDIA & WASHING

4.2.1.1 INTRODUCTION

Culture media are composed of a relatively small number of relatively strong Raman scattering components[123]. *Marotta et al.* postulated that classification of bacteria using Raman spectroscopy is dictated by Raman scattering from media components rather than that of signal arising from the bacteria[165]. *Premasiri et al.* refuted this claim by demonstrating that while bacterial spectra initially cluster according to the medium on which they were cultured, after 3 or more washes they clustered according to bacterial species[143]. Spectra from this work were acquired using a Raman microscope, which is able to focus more tightly upon bacteria, and has not been confirmed using a handheld spectrometer.

Hypothesis: Multiple wash and centrifuge cycles remove culture media from bacteria, with classification arising from bacterial components.

Objectives:

- Demonstrate centrifuge and washing of bacteria allows for classification of bacterial species according to Raman spectra acquired using a handheld spectrometer.

4.2.1.2 METHODS

Reference strain *Escherichia coli*, *Enterococcus faec*alis and *Klebsiella pneumoniae*, were cultured in 10ml brain heart infusion (BHI), Luria broth (LB) and Mueller Hinton Broth (MHB) for 24 hours at 37 degrees Celsius. The pathogens in culture media were centrifuged at 3350G for 10 minutes. The supernatant was discarded, and the pellet resuspended in 2 ml PBS, which was centrifuged for 1 minute at 8300G. This step was repeated to a total of 5 washes.

The resulting heavy suspensions were transferred to sterile borosilicate Raman vials. Raman spectra were acquired with IDRaman mini 2.0 handheld spectrometer. Spectra were acquired for 10 seconds with 50 mW laser power, with an average of 20 spectra for each sample.

The resulting spectra were smoothed with a Savitsky-Golay filter before baseline subtraction of a 7th order polynomial. The spectra were truncated from 500 to 2200cm^{-1} before vector normalisation. The resulting spectra underwent unsupervised classification by PCA.

4.2.1.3 RESULTS

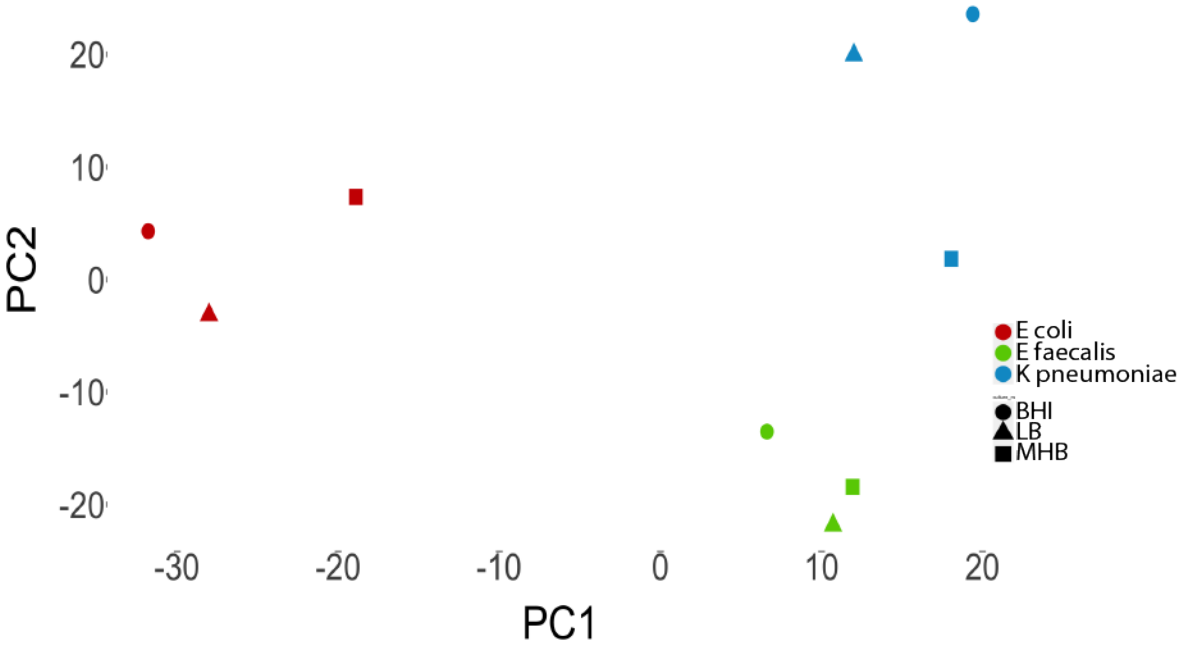

FIGURE 4. 2 PCA PLOT FOR UROPATHOGENS CULTURED IN DIFFERENT MEDIA AFTER 5 CYCLES OF CENTRIFUGE AND WASHING. THE RAMAN SPECTRA CLUSTER ACCORDING TO THE PATHOGENS (RED: *E. COLI*; GREEN: *E. FAECALIS*; BLUE: *K. PNEUMONIAE*), RATHER THAN ACCORDING TO THE CULTURE MEDIUM (CIRCLE: BHI; TRIANGLE: LB; SQUARE: MHB), WHICH DEMONSTRATES CLASSIFICATION OCCURS BASED ON THE PATHOGEN RATHER THAN THE CULTURE MEDIUM.

The PCA plot in **Figure 4.2** presents unsupervised classification of Raman spectra acquired from different uropathogens cultured in common non-selective media. The points are coloured by pathogen with point shape according to culture medium. The points can be seen to cluster according to uropathogen, rather than culture medium indicating the defining features of the Raman spectra arise from the pathogens.

4.2.1.4 DISCUSSION

The results presented here concur with the findings of *Premasiri et al.*, demonstrating multiple centrifuge and wash cycles provides for clustering according to pathogen rather than the medium used[143]. This is confirmed to be true using a handheld spectrometer rather than the microscope used in previous works. While 3 cycles were deemed sufficient by *Premasiri et al*., this work assessed 5 cycles to provide certainty media would not confound analysis.

4.2.4 OPTICAL DENSITOMETRY FOR PATHOGEN LOAD

4.2.4.1 INTRODUCTION

Early-stage bacteriologic research using Raman spectroscopy frequently relies on optimising and assessing technologies using suspensions finely controlled so as to minimise sample variability. Suspensions of reference strain pathogens must be consistently controlled to pathogen loads representative of clinical samples. Gold standard colony counting using the *Miles* and *Misra* method provides accurate colony counting, however it is time and resource intensive, requiring serial dilution and manual counting[152]. As this method requires microbial culture, it can only be used to establish the pathogen load, rather than control it. OD_{600} is an established method for control of pathogen load, with suspension turbidity correlating with pathogen load[153].

Hypothesis: Optical densitometry provides rapid and reliable pathogen load estimation.

Objectives:

- Correlate OD_{600} with pathogen load.
- Identify an optimal OD_{600} cut off for further experiments.

4.2.4.2 METHODS

Reference strains of *Escherichia coli, Enterococcus faecalis* and *Klebsiella pneumoniae* pathogen were used from an established reference bank. A single Microbank bead was cultured in 3ml of brain heart infusion at 37° Celsius for 24 hours. The cultured suspension was centrifuged at 8300 g, after which the supernatant was discarded and the pellet resuspended in 2ml PBS by Vortex mixing. This heavy suspension was diluted in PBS to OD_{600} ranging from 0.01 up to 0.12 measured using a Fisher Scientific Cell Density Meter. For each pathogen, 3 suspensions for each OD600 were created, totalling 108 samples.

For each sample, the pathogen load was established by the method as described by Miles and Misra[152]. Each sample underwent 6 serial dilutions. For each single Columbia Blood Agar plate was delineated into 6 sectors and 20μl of each serial dilution was pipetted into a sector. The plate was allowed to dry completely, before undergoing culture at 37° Celsius for 24 hours. Colonies were counted from the sector in which the largest number of non-overlapping colonies could be clearly identified and scaled up by the appropriate dilution factor.

The gold standard colony count was plotted against optical densitometry, and lines of best fit plotted for each pathogen. Linear regression was performed for colony count against OD_{600}, controlling for the pathogen.

4.2.4.3 RESULTS

Figure 4.3 presents the plot of gold standard colony counting against OD_{600} for the three reference pathogens, while the results of the linear regression are presented in **Table 4.2**. Significant correlation was observed between optical densitometry and colony count (Pearson's R = 0.68; p-value <0.001), while the reference pathogen had no effect on the correlation. At OD_{600} of 0.07 the colony count was approximately 10^8 CFU/ml (1.02×10^7 CFU/ml).

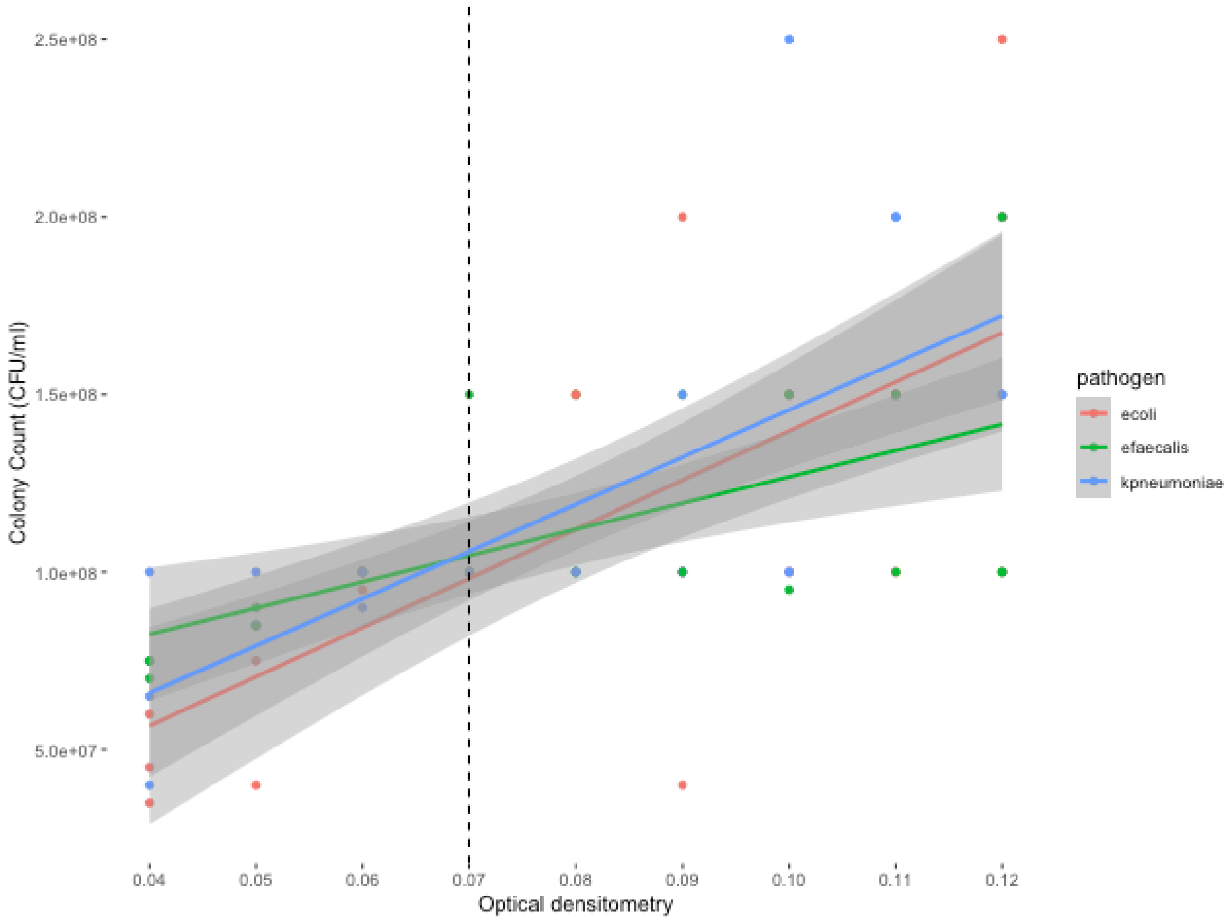

FIGURE 4. 3 COLONY COUNT VERSUS OPTICAL DENSITOMETRY AT 600NM FOR REFERENCE PATHOGENS. THE LEAST SQUARES FITTED LINE FOR THE *E. COLI* (RED), *E. FAECALIS* (GREEN) AND K. PNEUMONIAE (BLUE) WITH STANDARD ERROR PRESENTED AS SHADED REGIONS. THE VERTICAL DASHED LINE ILLUSTRATES A WELL SUITED FOR FURTHER RESEARCH WHERE AN OD_{600} OF 0.07 PROVIDES A CONSISTENT PATHOGEN LOAD OF 10^8 CFU/ML

TABLE 4. 2 REGRESSION TABLE FOR COLONY COUNT VERSUS OPTICAL DENSITOMTERY. OD_{600} IS DEMONSTRATED TO SIGNIFICANTLY CORRELATE WITH PATHOGEN LOAD WITH EACH UNIT INCREASE IN $O6_{600}$ LEADIN TO AN INCREASED PATHOGEN LOAD OF $1.15X10^9$ CFU/ML. THE TYPE OF PATHOGEN DID NOT SIGNIFCANTLY EFFECT THIS CORRELATION.

Variable		Coefficient	p-Value
Intercept		$2.04 *10^7$	0.127
OD_{600}		$1.15* 10^9$	<0.001
Pathogen	*E. coli* (ref)	-	-
	E. faecalis	$-4.39*10^{-10}$	1.00
	K. pneumoniae	$7.04*10^6$	0.434
Adjusted R^2 = 0.4516			

4.2.4.4 DISCUSSION

Optical densitometry at 600 nm is a suitable method for adjusting and controlling pathogen load in bacterial suspensions. Optical densitometry correlated well with gold-standard manual colony counting using the Miles and Misra method[152], with the pathogen type having no significant effect on this correlation. An OD_{600} of 0.07 approximated a colony count of 10^8 CFU/ml. Additionally, the plot demonstrated low variability at this OD_{600}. Therefore, an OD_{600} of 0.07 was used in further experiments with adjustment down to the target concentration by serial dilution.

4.3 RAMAN ACQUISITION

4.3.1 POWER AND ACQUISITION TIME

The effects of differing laser power and acquisition times on Raman spectra acquired from Rhodamine 6G are presented in **Figure 4.4**. A single sample was created by spotting 250µl of 1mM Rhodamine 6G onto aluminium foil and air dried. Spectra were acquired using the IDRaman mini 2.0 handheld spectrometer using the 5 power settings (corresponding to 10, 20, 30 40 and 50 mW), and acquisition times of 2, 4, 6, 8, and 10 seconds. Raster orbital scanning and reference scan settings were applied to all acquired spectra. The spectra were plotted without any digital pre-processing. Inset into each spectrum is a magnification of one of the Raman peaks arising from Rhodamine signal.

While the spectra all clearly demonstrate the same basic spectrum and baseline, there are notable differences arising from differing laser power and acquisition times. The absolute value of the baseline and spectral peaks increase proportionately to the laser power and acquisition time. The absolute value of the high frequency noise remains approximately constant across varying laser power and acquisition times. Therefore, higher laser power and acquisition times result in a relative reduction in high frequency noise. Excessively high laser power and acquisition lead to saturation of the device’s CCD, which is clearly visible in the spectrum with 10 s acquisition and 50mW, and to a lesser extent the spectrum with 10 s acquisition and 40mW power. A practical approach, provided photo destruction is not a concern, is to maximise laser power and acquisition. Optimal laser power and acquisition time settings are best identified during a pilot in which the maximal laser power is used and increasing the acquisition time to identify the point at which CCD saturation occurs.

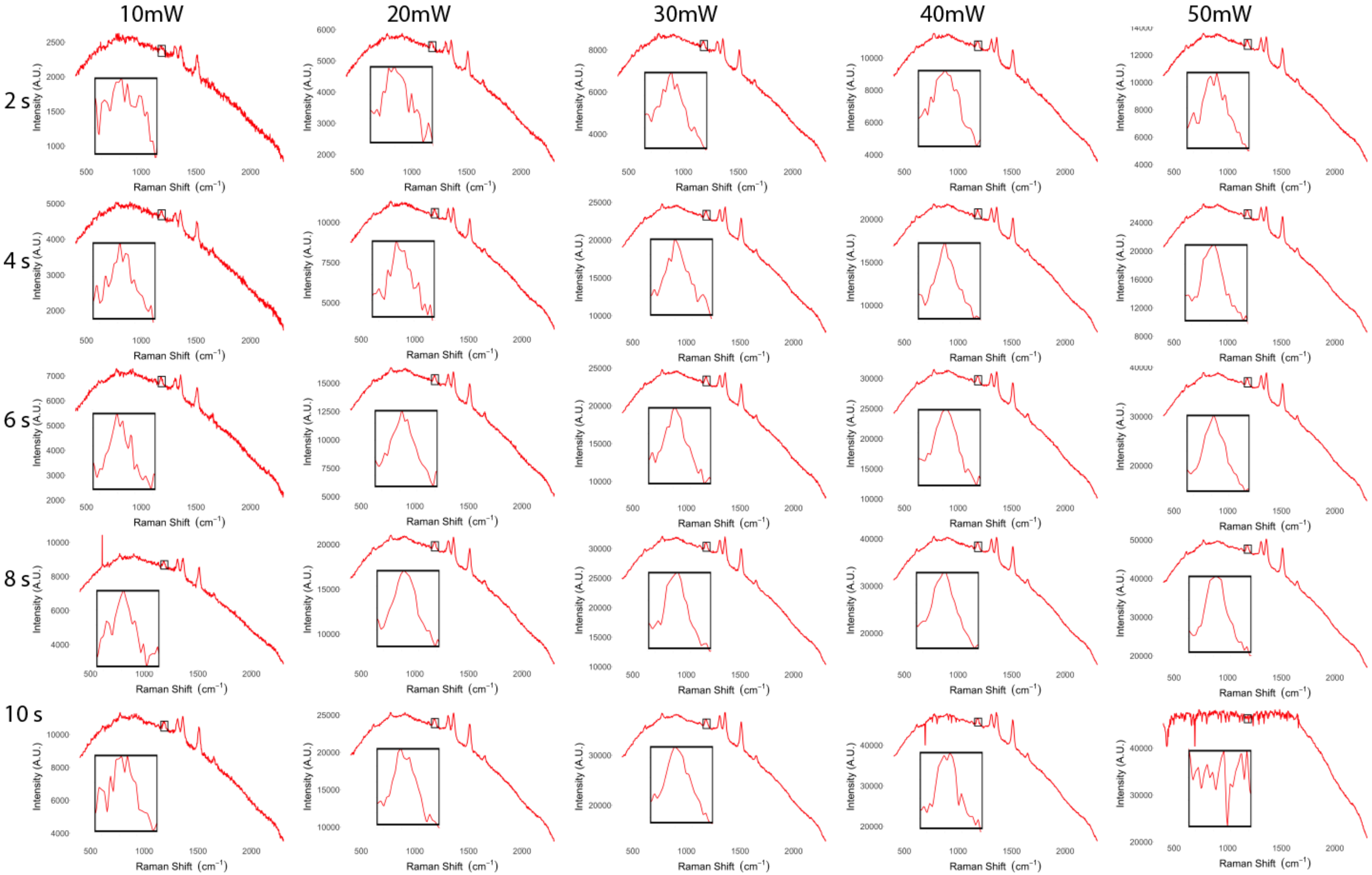

FIGURE 4. 4 RAMAN SPECTRA OF RHODAMINE 6G WITH DIFFERING LASER POWER AND ACQUISITION TIMES.

4.3.2 RASTER ORBITAL SCANNING

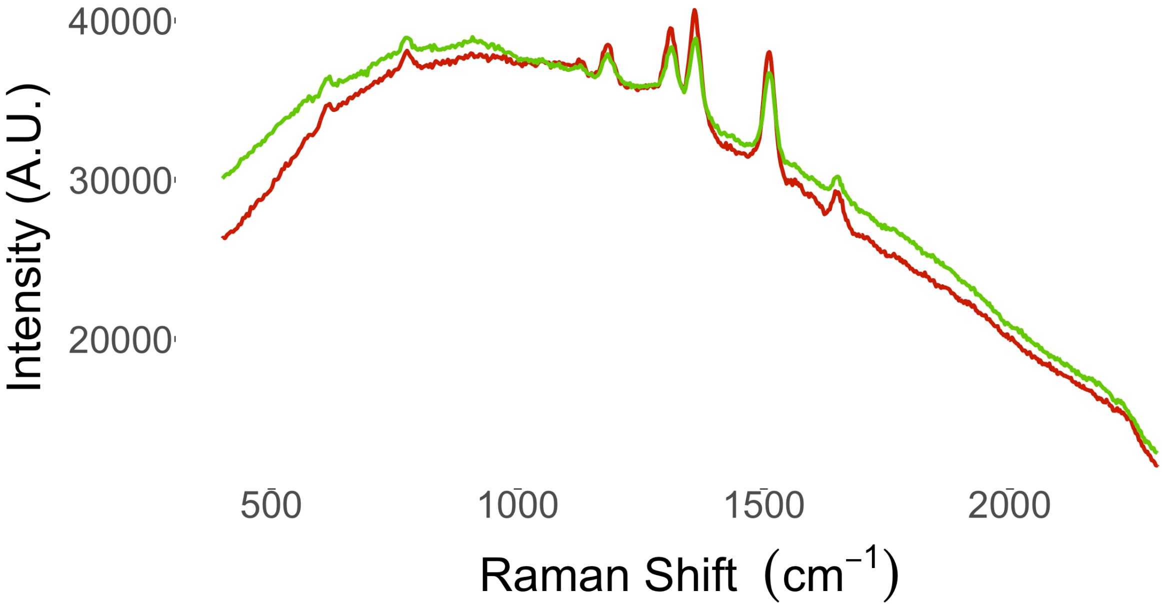

FIGURE 4. 5 RAMAN SPECTRUM FOR RHODAMINE 6G WITH RASTER ORBITAL SCANNING ON (RED) AND OFF (GREEN). THE SPECTRUM ACQUIRED WITH RASTER ORBITAL SCANNING DEMONSTRATES PEAKS OF GREATER AMPLITUDE AND RESOLUTION.

Raster orbital scanning (ROS) is a feature incorporated into handheld spectrometers, in which a narrowed focal volume is traversed across the sample, in contrast to holding a larger focal volume stationary[166]. This acts to provide higher resolution spectra while still sampling from a representative volume**. Figure 4.5** presents the Raman spectra of Rhodamine 6G acquired using the IDRaman mini 2.0 handheld spectrometer with the ROS function on and off. The spectrum with ROS engaged demonstrates taller and narrower peaks as compared to the spectrum without ROS engaged. The ROS feature was used for further works.

4.3.3 REFERENCE SPECTRUM

Reference spectrum is a feature incorporated into many Raman spectrometers, in which a background spectrum is acquired without the laser powered, and subtracted from the spectrum acquired with the laser engaged. Subtraction of a reference spectrum serves to reduce the noise arising from extraneous light and device electronics[166]. **Figure 4.6** presents Raman spectra acquired from Rhodamine 6G with the IDRaman mini 2.0 with reference spectrum setting engaged and without reference spectrum engaged. The spectrum without reference spectrum setting contains substantially greater noise. As such, the reference spectrum feature was used in further works

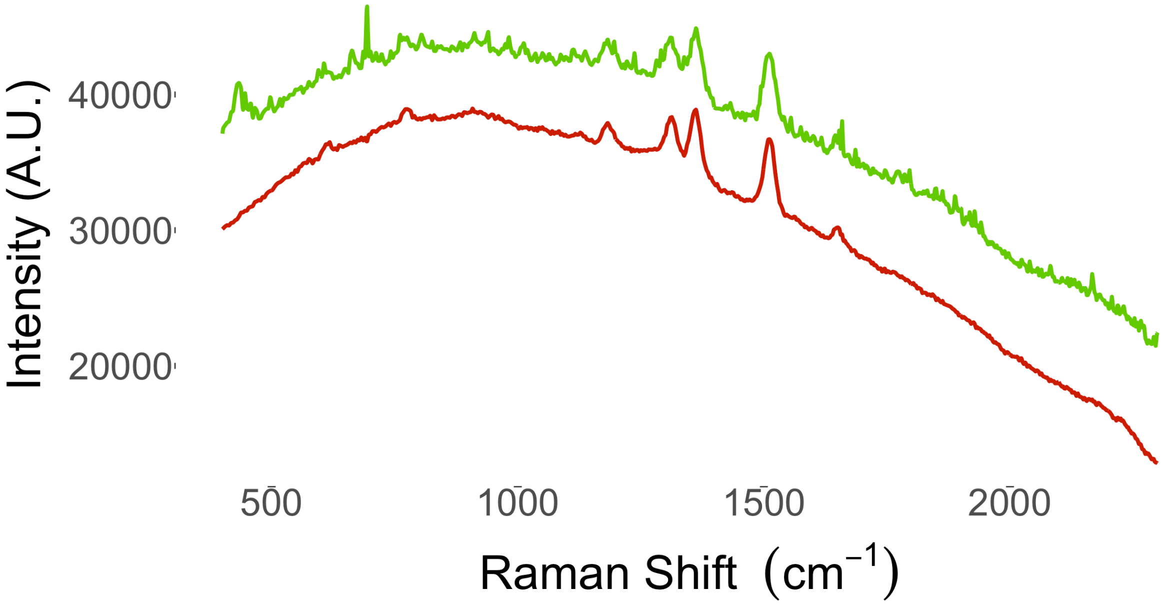

FIGURE 4. 6 RAMAN SPECTRUM FOR RHODAMINE 6G WITH REFERENCE SPECTRUM ON (RED) AND OFF (GREEN). THE SPECTRUM ACQUIRED WITH A REFERENCE SPECTRUM DEMONSTRATES LESS HIGH FREQUENCY NOISE.

4.3.4 Focal Length

4.3.4.1 Introduction

Raman spectra may be acquired from the IDRaman mini 2.0 handheld spectrometer using sample vials for liquid specimens, or in handheld mode for solid specimens. The spectrometer focuses the laser into a focal volume from which the inelastically scattered photons are captured and quantified. The spot size of the IDRaman mini 2.0 ranges from 0.2 to 2.5 mm dependent on the working distance[166].

Hypothesis: In handheld mode spectral amplitude and quality are dependent on focal length.

Objectives:

- Demonstrate the effect of focal distance on Raman spectra.
- Identify the optimal focal length for further experiments.
- Develop a method for providing consistent focal length.

4.2.4.2 Methods

To control focal distance, a support for the IDRaman mini 2.0 spectrometer was designed in Fusion360 and 3D-printed (**Figure 4.7**). Additionally, collars with lengths ranging from 26 to 30 mm in 0.5 mm increments were 3D-printed to allow for the spectrometer to be held at different focal lengths.

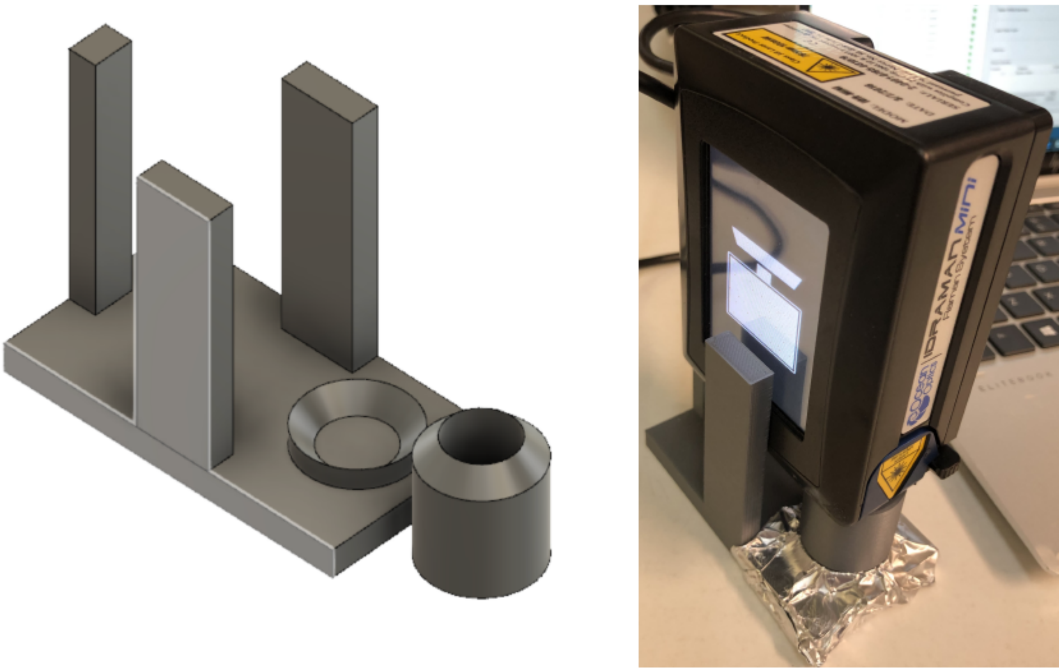

FIGURE 4. 7 CAD DESIGN (LEFT) AND 3D-PRINTED HOLDER WITH IDRAMAN (RIGHT)

Rhodamine 6G was spotted onto aluminium foil and air-dried. Raman spectra were acquired with the IDRaman at 785nm wavelength, 10mW laser-power and 5 second acquisition time. A total of 12 spectra were averaged for a total acquisition time of 1 minute. Using the 3D printed collars to create differing focal lengths, spectra were acquired for all lengths from 26.0mm to 30 mm in 0.5 mm increments. Spectra were plotted unprocessed for assessment.

4.3.4.3 RESULTS

The plots of the Raman spectra of Rhodamine 6G with increasing collar length are presented in **Figure 4.8**. The amplitude of the spectra is demonstrated to increase with collar length up to 29.5mm before reducing again. Additionally, Rhodamine 6G peaks are clearly visible on the spectrum acquired at 29.5 mm collar length, are reduced in the adjacent spectra while not discernible with collar lengths below 28.0 mm.

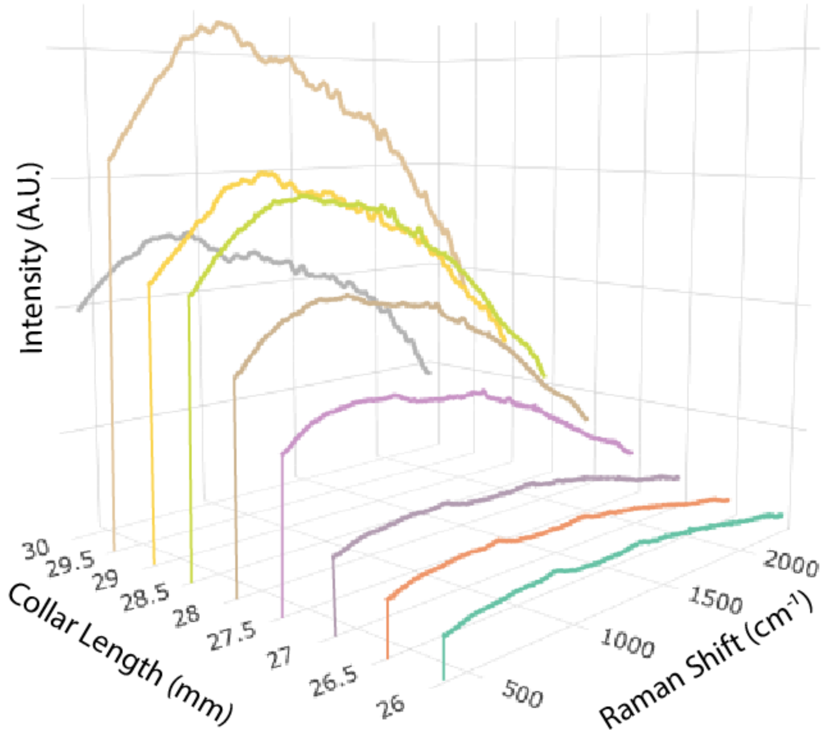

FIGURE 4. 8 RAMAN SPECTRA OF RHODAMINE 6G WITH ACQUIRED DIFFERENT COLLAR LENGTHS

4.3.4.4 DISCUSSION

The amplitude and quality of Raman spectra are extremely sensitive to focal length (controlled using collars), with visible differences seen with increments as small as 0.5mm. A collar length of 29.5mm provided the greatest amplitude spectra with clearly discernible peaks and so was selected for further experiments that required the handheld spectrometer in point and shoot mode. The 3D-printed spectroscope holder was used to ensure consistency of focal length.

4.4 RAMAN SPECTRAL ANALYSIS

The multistep process required to classify samples from Raman spectra is described in **Section 4.4.** Digital uses numerous methods to optimise SNR to improve classification. Feature reduction reduces spectra to a smaller number of descriptive predictors, before classification sing supervised learning algorithms. An additional step which, while not required for classification, is important for mechanistic understanding is identification of descriptive spectral bands.

4.4.1 DATA SET FOR SPECTRAL ANALYSIS

Datasets were required to demonstrate the effects of pre-processing as well as the outcomes of learning algorithms. Samples representing high, medium, and low SNR were pipetted in 2ml borosilicate Raman vials. Raman spectra were captured using the IDRaman mini 2.0 handheld spectrometer with laser power set to 50mW. Acquisition times used were 1, 2.5 and 10 seconds for the high, medium and low samples respectively with sufficient spectra acquired to total 200 seconds for each sample.

The high SNR samples comprised a single strong Raman scattering molecule at controlled concentrations. Ten samples each of Rhodamine 6G, crystal violet and 70% ethanol were used.

The medium SNR sample comprised three commonly used culture media, therein containing a small number of weaker scattering molecules in controlled concentrations.

The low SNR sample comprises heavy suspensions of three common uropathogens. Bacteria from the reference bank were cultured in BHI infusion for 24 hours at 37 degrees Celsius, and subsequently washed a total of 5 times in PBS. 2 ml of undiluted suspension was transferred to sterile borosilicate Raman vials for Raman acquisition.

4.4.2 DIGITAL PRE-PROCESSING

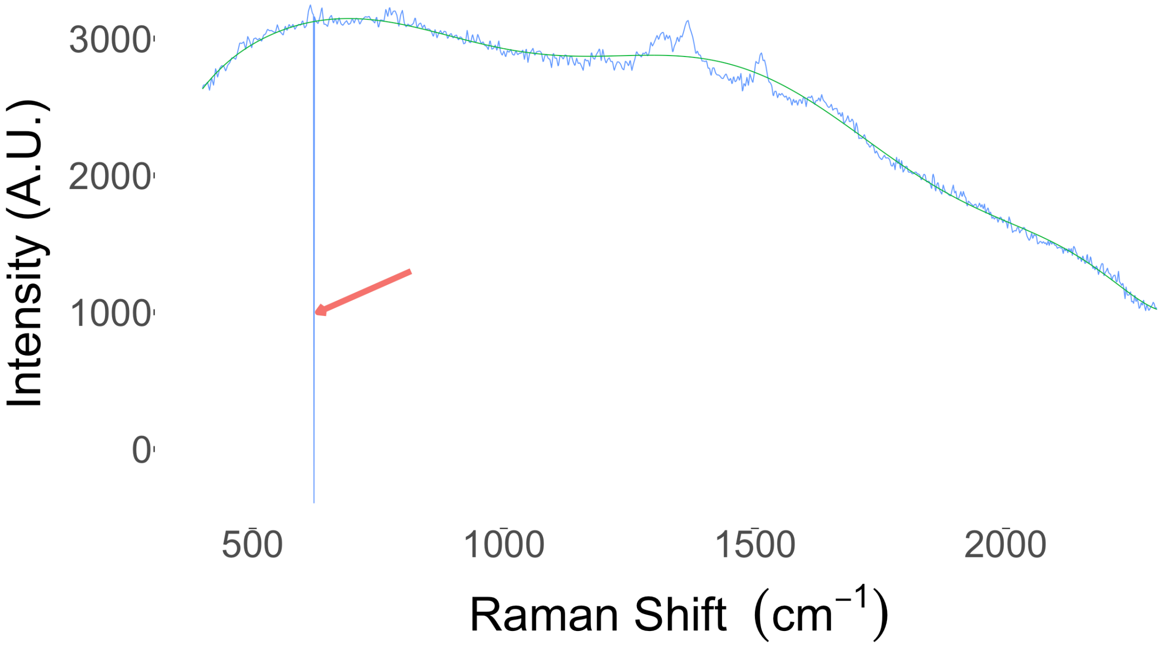

FIGURE 4. 9 UNPROCESSED RHODAMINE 6G RAMAN SPECTRA DEMONSTRATING DIFFERENT TYPES OF NOISE. THE ORIGINAL SPECTRUM IS PLOTTED IN BLUE AND DEMONSTRATES A HIGH DEGREE OF HIGH FREQUENCY NOISE VISIBLE AS A RANDOMLY DISPERSED FLUCTUATION ACROSS THE ENTIRE SPECTRUM. A SINGLE COSMIC SPIKE IS DEMONSTRATED BY THE RED ARROW. LOW FREQUENCY NOISE VISIBLE AS A SLOW UNDULATING BASELINE IS PRESENTED AS THE GREEN FITTED LINE.

Raman Spectra contain high resolution chemometric signals present as peaks in spectra, overlaid by competing noise arising from numerous sources. Signal is defined as variability in the data associated with the outcome of interest, while noise is variability in the data not associated with the outcome of interest. Gaining the greatest classification performance is contingent on maximising signal while minimising noise. Therefore, understanding the sources of noise and how best to remove them is required. The common types of noise present in Raman spectra are illustrated in **Figure 4.9.** Low frequency noise arises from extraneous light and sample fluorescence. High frequency noise arise from device electronics. Cosmic spikes present as massive point deviations from the spectrum arising cosmic ray events generated from atmospheric solar activity[103]. Additionally, an additive and multiplicative shift arises in spectra, such that successive spectra acquired from the same sample appear different. The same spectrum after digital pre-processing with the noise reduced is depicted in **Figure 4.10**.

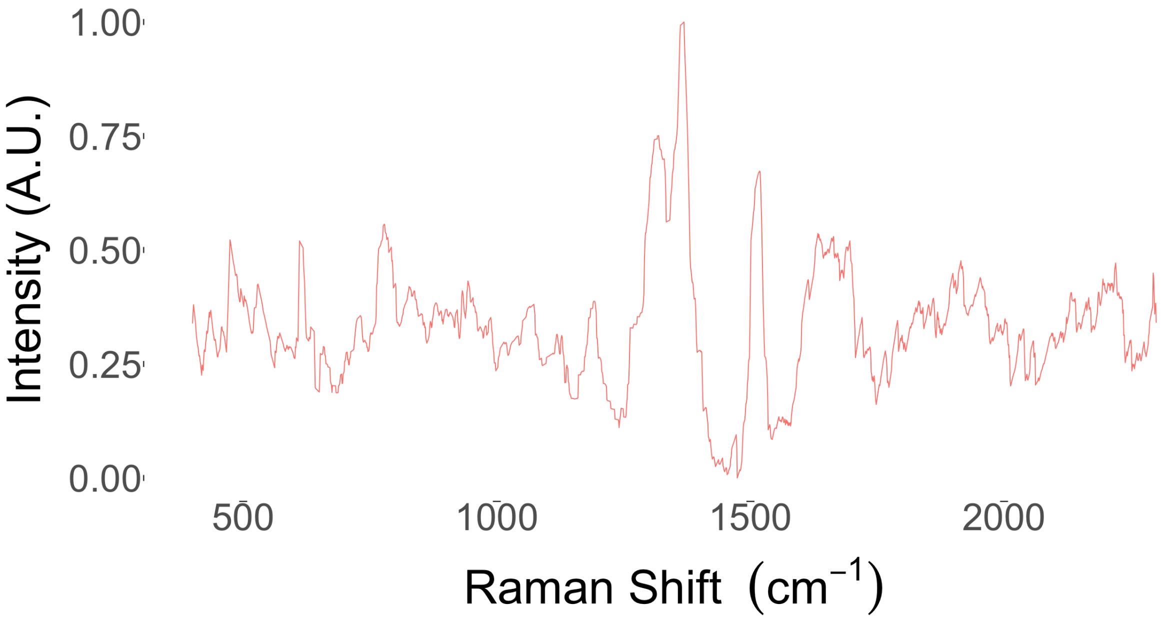

FIGURE 4. 10 PROCESSED RAMAN SPECTRA OF RHODAMINE 6G WITH NOISE REDUCED

The mean unprocessed spectra with standard error ribbons in addition to the PCA plots for the high, medium and low SNR datasets are illustrated in **Figure 4.11**. The spectra of the high SNR dataset show visible features without the need for further processing, although substantial variation is present in the spectra of the Rhodamine 6G (visible as a wide standard error ribbon). These features provide for excellent separation on the accompanying PCA plot.

The spectra of the medium SNR dataset are dominated by fluorescence with minimal spectral features visible. Different fluorescence profiles provide for good separation on the accompanying PCA plot. The spectra of the low SNR dataset are overwhelmed by a single cosmic spike arising from a *Klebsiella pneumoniae* sample. There is no separation visible on the accompanying PCA plot.

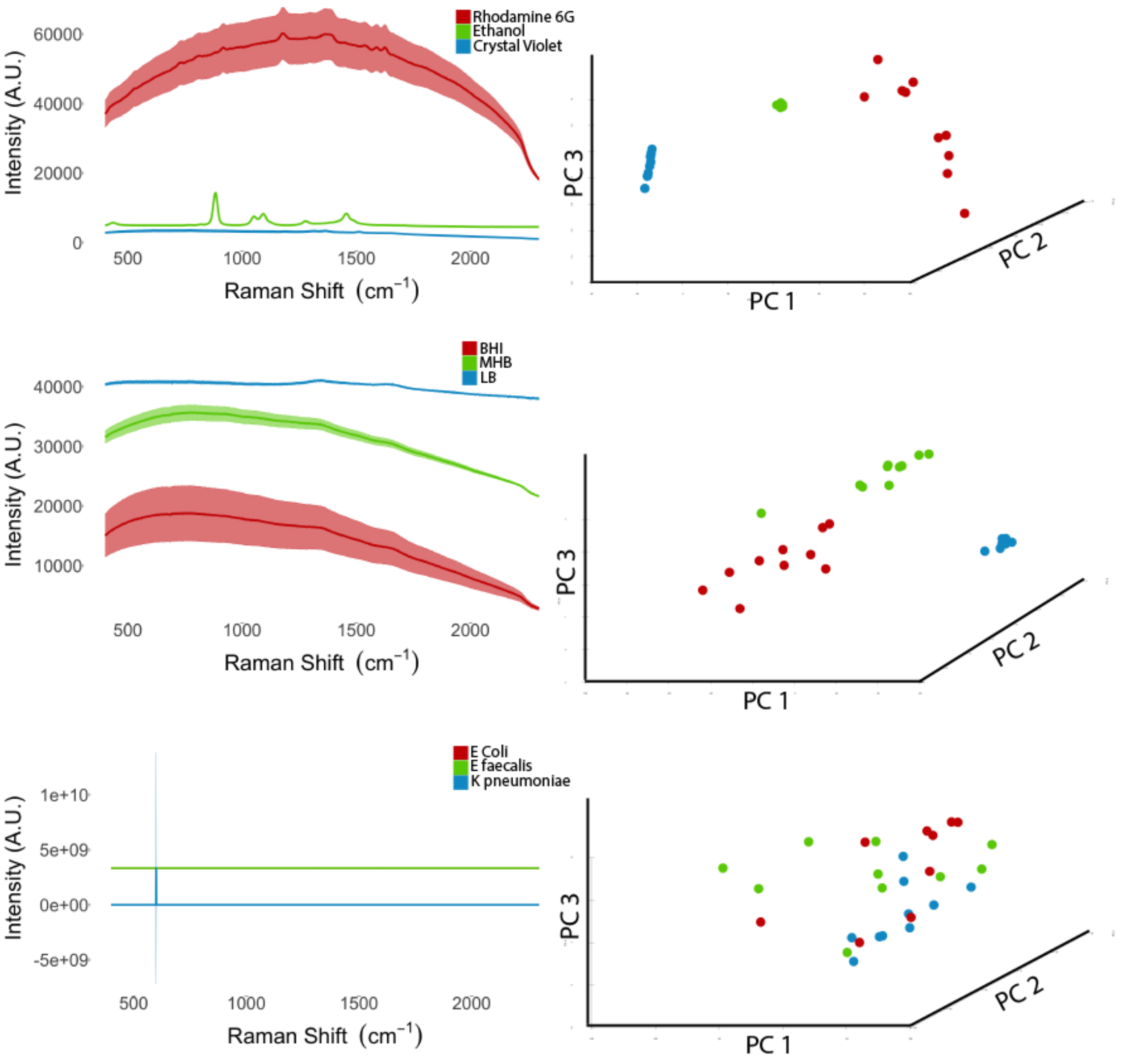

FIGURE 4. 11 MEAN SPECTRA, WITH STANDARD ERROR RIBBONS, (LEFT) AND PCA (RIGHT) PLOTS FOR HIGH, MEDIUM AND LOW SNR DATASETS WITHOUT PROCESSING (TOP TO BOTTOM). SPECTRA FROM THE HIGH SNR DATASET HAVE VISIBLE FEATURES WHICH PROVIDE CLUSTERING AND SEPARATION ON THE PCA PLOT, ALTHOUGH RETAINED BASELINE VARIABILITY IN THE RHODAMINE SPECTRUM IS PRESENT AS WIDE ERROR RIBBON. THE MEDIUM SNR SPECTRA ARE DOMINATED BY FLUORESCENCE WITH MINIMAL SPECTRAL FEATURES. THE LOW SNR SPECTRA ARE OVERWHELMED BY A COSMIC SPIKE THAT COMPLETELY OBFUSCATES ALL OTHER FLUORESCENCE AND SPECTRAL FEATURES.

4.4.2.1 AVERAGING SCANS

High frequency noise is present as low amplitude, high frequency disturbances in the spectrum, and cosmic spikes presents as infrequently occurring single high amplitude disturbances in the Raman spectrum. High frequency noise and cosmic spikes are both randomly distributes in the spectrum, and as such may be reduced by taking a mean of multiple spectra of multiple spectra acquired from the same sample. **Figure 4.12** presents the effects of averaging sequential spectra from a single Rhodamine 6G sample. A single spectrum (top panel) demonstrates a high degree of high frequency noise. An average of 10 spectra (middle panel) reduces the high frequency noise, however the occurrence of a cosmic spike leads to a substantial spectral abnormality at 625 cm^{-1}. An average of 50 spectra (bottom panel) demonstrates substantially reduced high frequency noise, with the reduction of the amplitude of the cosmic spike.

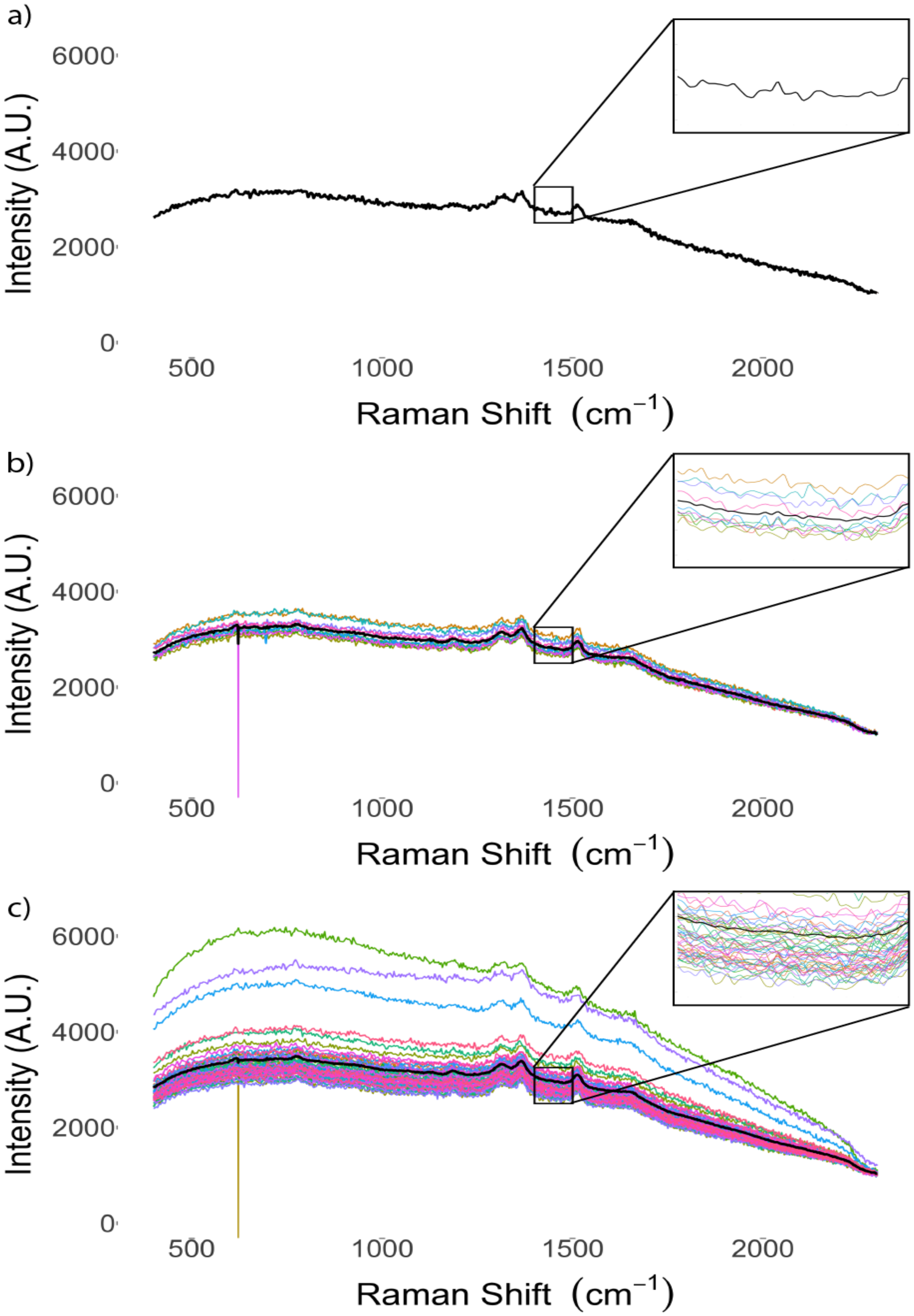

FIGURE 4. 12 EFFECT OF AVERAGING SPECTRA. MEAN (BLACK), AND INDIVIDUAL SPECTRA (MULTIPLE COLOURS) OF 1 (a), 10 (b) AND 50 (c) SEQUENTIAL SPECTRA ACQUIRED FROM A SINGLE SAMPLE OF RHODAMINE 6G (TOP TO BOTTOM). A SINGLE SPECTRUM DEMONSTRATES A LARGE DEGREE OF HIGH FREQUENCY NOISE. THIS HIGH FREQUENCY NOISE IS REDUCED WHEN 10 SPECTRA ARE AVERAGED, HOWEVER A COSMIC SPIKE IS INCLUDED. THE EFFECT OF THE COSMIC SPIKE IS REDUCED WITH THE AVERAGING OF 50 SPECTRA.

Averaging multiple spectra from an individual sample is an effective method for reducing high frequency noise and the effects of cosmic spikes. The benefits provided by averaging spectra are contrasted against the risk of photodestruction and practicality of prolonged acquisitions. Applied to Raman pathogen research, within the constraints of sample integrity, taking a mean of the highest feasible number of Raman spectra will best improve SNR.

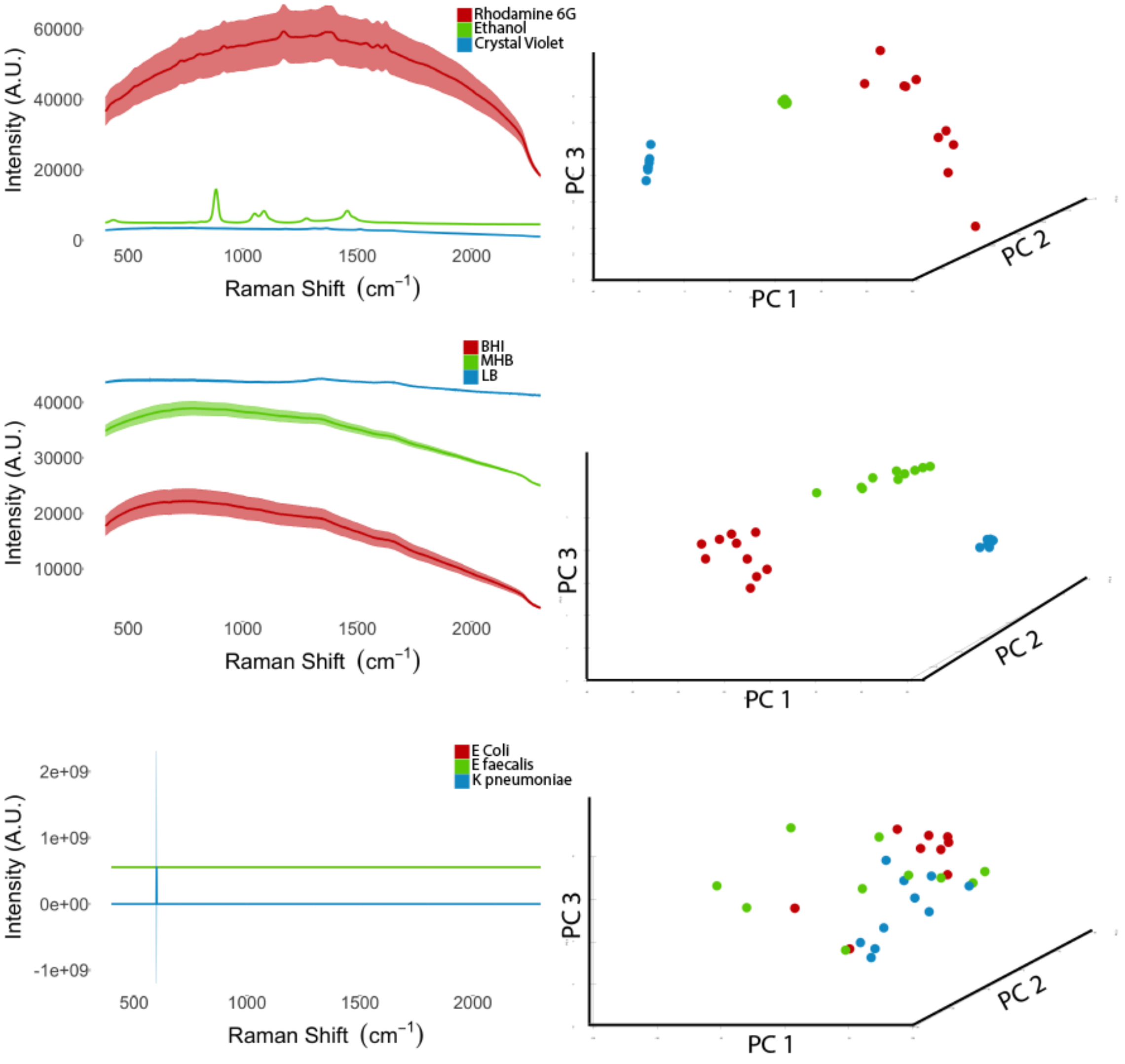

FIGURE 4. 13 MEAN SPECTRA, WITH STANDARD ERROR RIBBONS, AND PCA PLOTS FOR HIGH, MEDIUM AND LOW SNR DATASETS AFTER TAKING AN AVERAGE OF SPECTRA TOTALLING 1 MINUTE ACQUISITION.

The benefits of averaging spectra are demonstrated in **Figure 4.13** which plots the mean spectra with standard error ribbons for the high, medium, and low SNR datasets after taking an average of spectra. Averaging spectra has little effect on the spectra or dataset for the high SNR dataset. Averaging scans reduces the spectral variability in the medium SNR dataset, evidenced by narrower standard error ribbons, leading to an improvement in the separation on the accompanying PCA plot. Averaging scans substantially reduces, but does not remove the cosmic spike, in the low SNR dataset (evidenced by the reduction in magnitude of the y axis).

4.4.2.2 Smoothing Algorithms

Smoothing algorithms are used to reduce high frequency noise and cosmic spikes. Smoothing algorithms pass a moving window across the spectrum and apply a smoothing process, most commonly a median or Savitsky-Golay filter.

4.4.2.2.1 Median Filtering

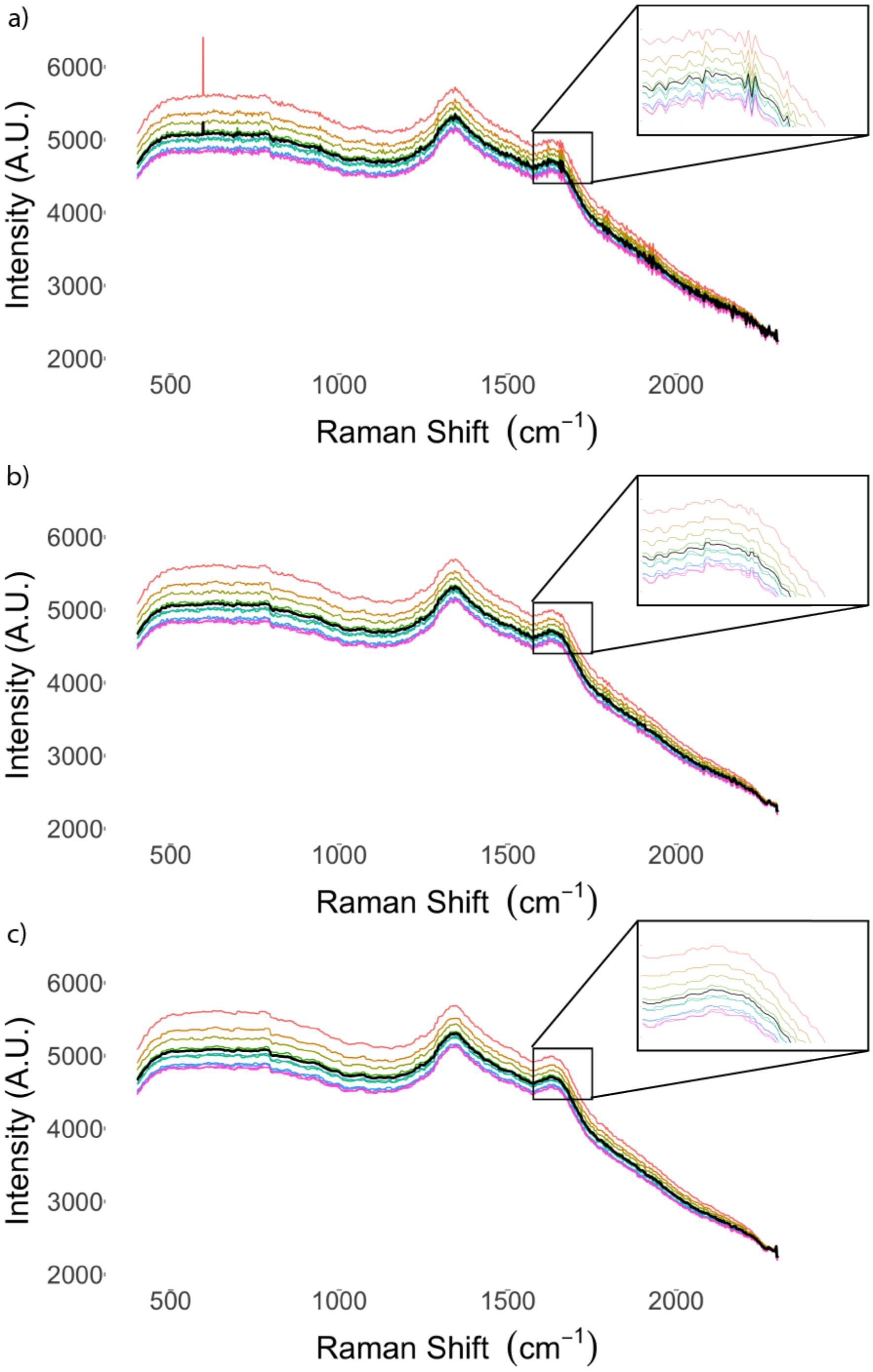

FIGURE 4. 14 SMOOTHING WITH MEDIAN FILTERS OF 1 (a), 7 (b), AND 13 CM^{-1} (c) WINDOWS APPLIED TO RAMAN SPECTRA ACQUIRED FROM MUELLER HINTON BROTH

The effects of application of a median filter with increasing window size to Raman spectra acquired from Mueller Hinton Broth are presented in **Figure 4.14**. The unfiltered (top panel) demonstrates residual cosmic spikes and high frequency noise. Application of a median filter of 7cm^{-1} window width (middle panel) removes the cosmic spikes and reduces high frequency noise. Further widening of filter window to 13 cm^{-1} shows improved smoothing, however with potential loss of signal (inset).

4.4.2.2.2 SAVITSKY-GOLAY FILTER

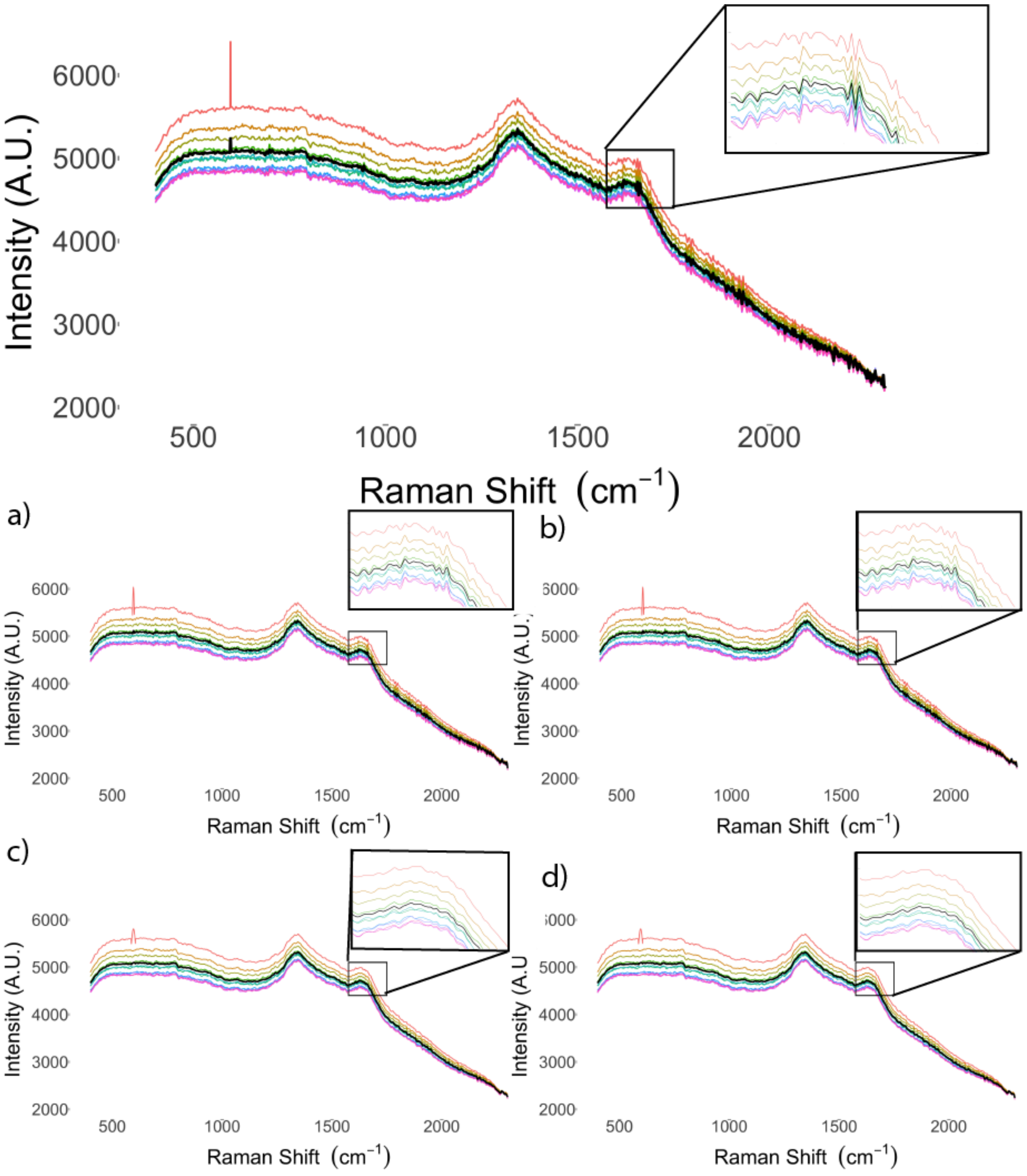

FIGURE 4. 15 SMOOTHING WITH SAVITSKY-GOLAY FILTERS OF 1, 9 (A&C), AND 10 (B&D) CM^{-1} WINDOWS AND 2ND (A&B) AND 3RD (C&D) ORDER POLYNOMIALS APPLIED TO RAMAN SPECTRA ACQUIRED FROM MUELLER HINTON BROTH. THE SPECTRA WITHOUT SMOOTHING ARE PRESENTED IN THE ENLARGED TOP PANEL.

The effects of applying a Savitsky-Golay filters of increasing window size and polynomial order to Raman spectra acquired from Mueller Hinton Broth samples is presented in **Figure 4.15**. Similar to median filters, Savitsky-Golay filters provide greater smoothing with widening windows reducing noise at the potential cost of signal. In contrast to median filters, control of the polynomial order maintains finer signal. Savitsky-Golay filters are sub-optimally suited to removal of cosmic spikes.

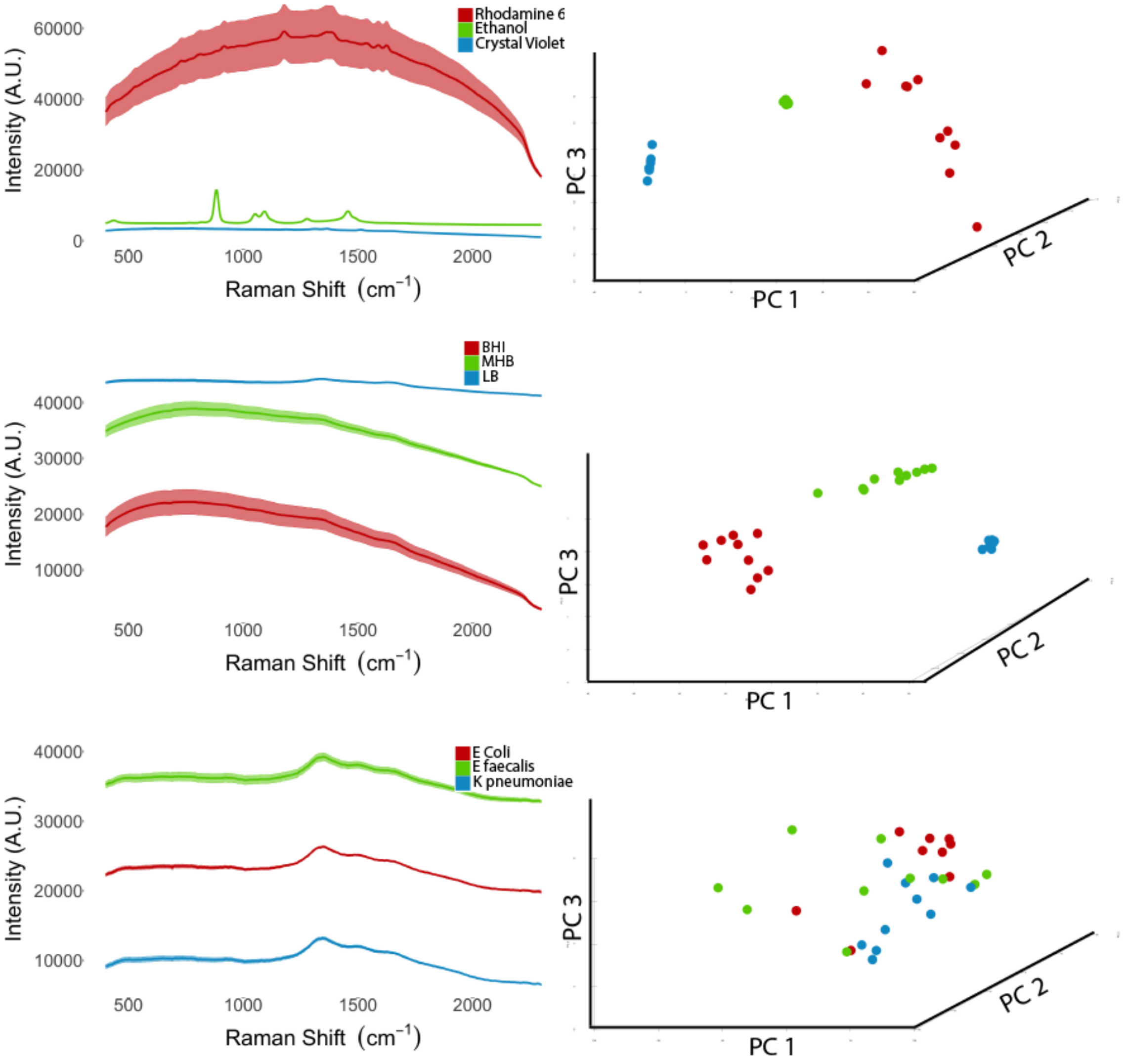

FIGURE 4. 16 MEAN SPECTRA, WITH STANDARD ERROR RIBBONS, AND PCA PLOTS FOR HIGH (TOP), MEDIUM (MIDDLE), AND LOW (BOTTOM) SNR DATASETS AFTER TAKING AN AVERAGE OF SPECTRA TOTALLING 1 MINUTE ACQUISITION AND SMOOTHING WITH A MEDIAN FILTER.

The means spectra with standard error ribbons and PCA plots for the high, medium and low SNR datasets after averaging of scans and smoothing with a median filter is presented in **Figure 4.16**. No substantial changes are visible in the high and medium SNR datasets. Effective removal of the cosmic spikes in the low SNR dataset provides for visualisation of the spectra, although no separation is seen in the PCA plot.

4.4.2.3 BACKGROUND SUBTRACTION

Baseline subtraction is used to remove low frequency noise, through fitting an approximation of the baseline and subtracting this from the original spectrum. The fitted baseline may be approximated by least squares fitting of a nth order polynomial, or by spline interpolation.

4.4.2.3.1 POLYNOMIAL FITTING

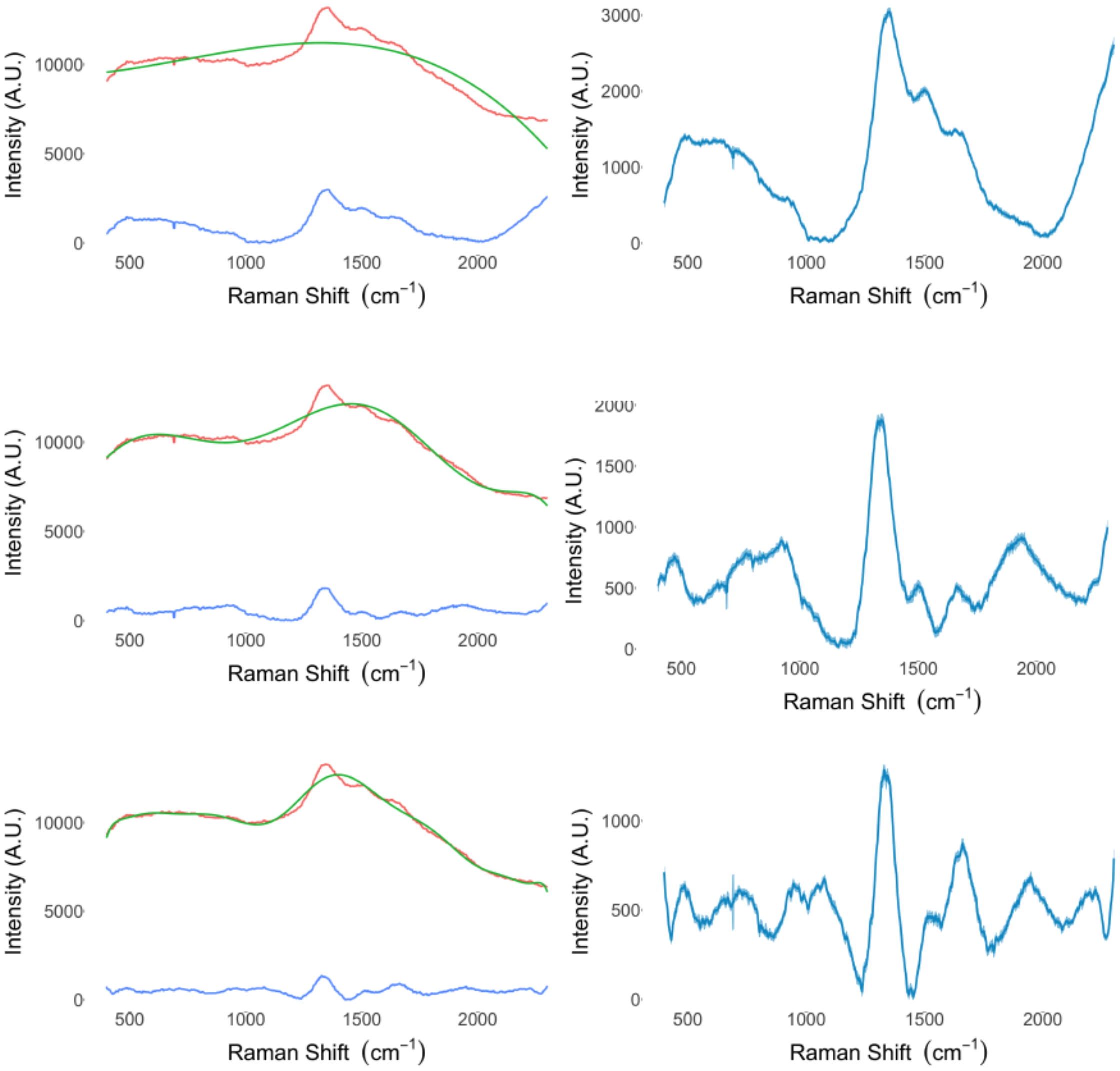

FIGURE 4. 17 BASELINE SUBTRACTION OF A FITTED 3^{RD} (TOP), 7^{TH}(MIDDLE) AND 19^{TH} (BOTTOM) ORDER POLYNOMIAL APPLIED TO RAMAN SPECTRA ACQUIRED FROM *ENTEROCOCCUS FAECALIS* SAMPLES. LEFT PRESENTS THE ORIGINAL SPECTRUM (RED), FITTED BASELINE (GREEN) AND CORRECTED SPECTRUM (BLUE). THE RIGHT PANELS PRESENT THE MEAN CORRECTED SPECTRUM WITH STANDARD ERROR RIBBON.

Figure 4.17 presents the effects of baseline subtraction of a 3^{rd} , 7^{th} and 19^{th} order polynomial, with the left panels presenting a single original spectrum (red) with fitted baseline (green) and corrected (blue), while the right shows the mean spectrum with standard error ribbons for all *Enterococcus faecalis* samples. The top demonstrates an underfitted baseline with a low order polynomial poorly approximating the baseline. The middle panel demonstrates a well fitted baseline with a 7^{th} order polynomial closely approximating the baseline. The bottom panel demonstrates an overfitted polynomial tightly fitted to the original spectrum. Runge's phenomenon is visible as oscillation induced either end of the spectrum in this panel.

4.4.2.3.2 CUBIC SPLINE INTERPOLATION

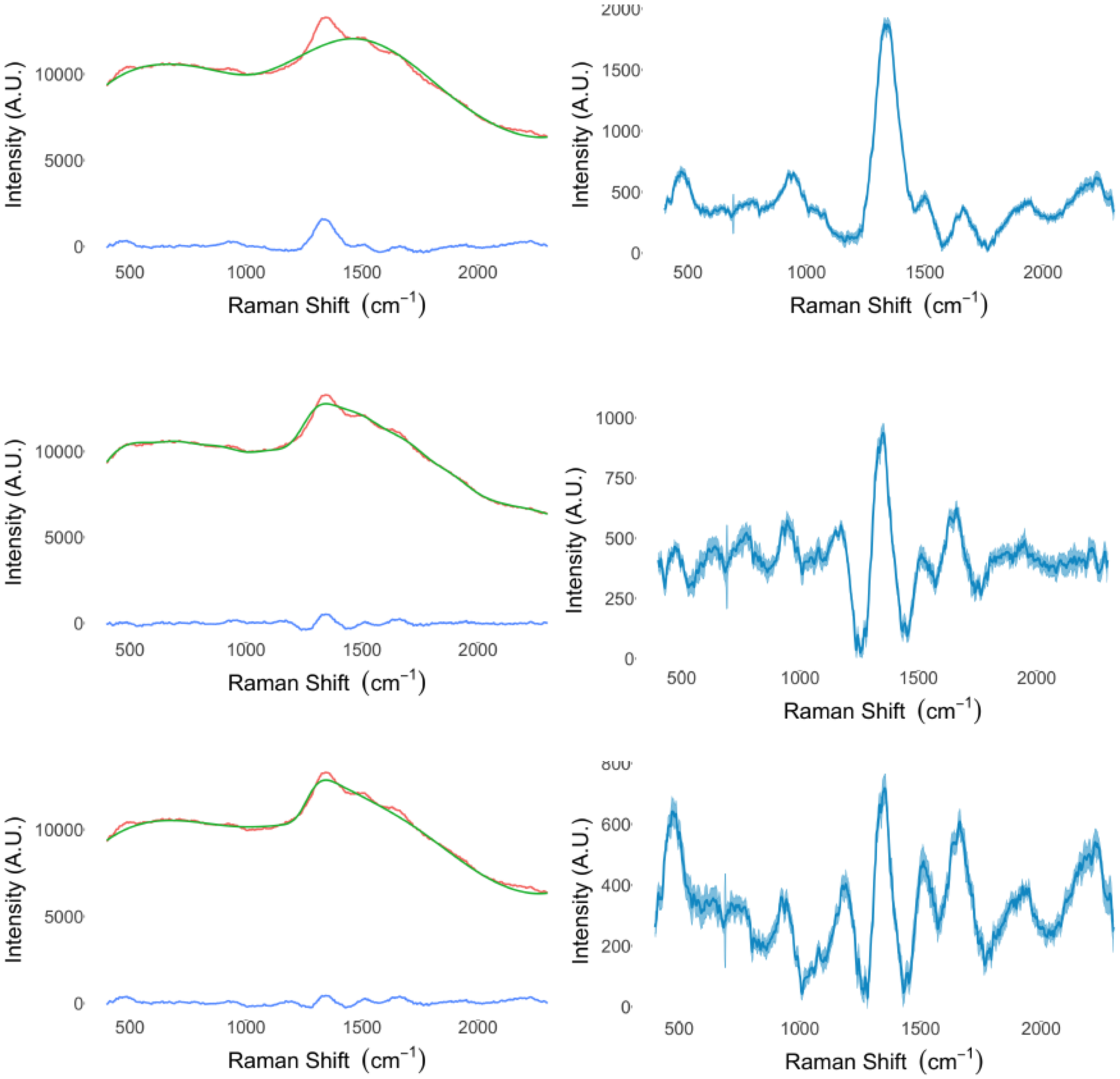

FIGURE 4. 18 BASELINE SUBTRACTION THROUGH CUBIC SPLINE INTERPOLATION WITH 10 (TOP) AND 20 (MIDDLE) EVENLY DISTRIBUTED INTERPOLANTS, AS WELL AS SELECTED (BOTTOM) INTERPOLANTS APPLIED TO RAMAN SPECTRA ACQUIRED FROM *ENTEROCOCCUS FAECALIS* SAMPLES. LEFT PRESENTS THE ORIGINAL SPECTRUM (RED), FITTED BASELINE (GREEN) AND CORRECTED (BLUE), WHILE THE RIGHT PANEL DEMONSTRATES THE MEAN SPECTRUM FOR *ENTEROCOCCUS FAECALIS* SAMPLES WITH STANDARD ERROR RIBBONS.

The effect of baseline using cubic spline interpolation applied to Raman spectra acquired from samples containing *Enterococcus faecalis* is presented in **Figure 4.18**. The spectra were an average of six 10 second acquisitions and had been smoothed with a median filter of 9 cm^{-1} window width. The left presents a single original spectrum (red) with fitted baseline (green) and corrected spectrum (blue), while the right presents the mean spectrum with standard error ribbons for the Raman spectra acquired from the 10 *Enterococcus faecalis* samples. The top panel demonstrates baseline correction with 10 evenly distributed cubic spline interpolants, providing a close baseline fit. The middle panel demonstrates baseline correction with 20 evenly distributed cubic spline interpolants, leading to an overfitted baseline. The bottom panel demonstrates baseline correction with cubic spline interpolants selected to optimise baseline subtraction, providing a close baseline fit and improvement of signal.

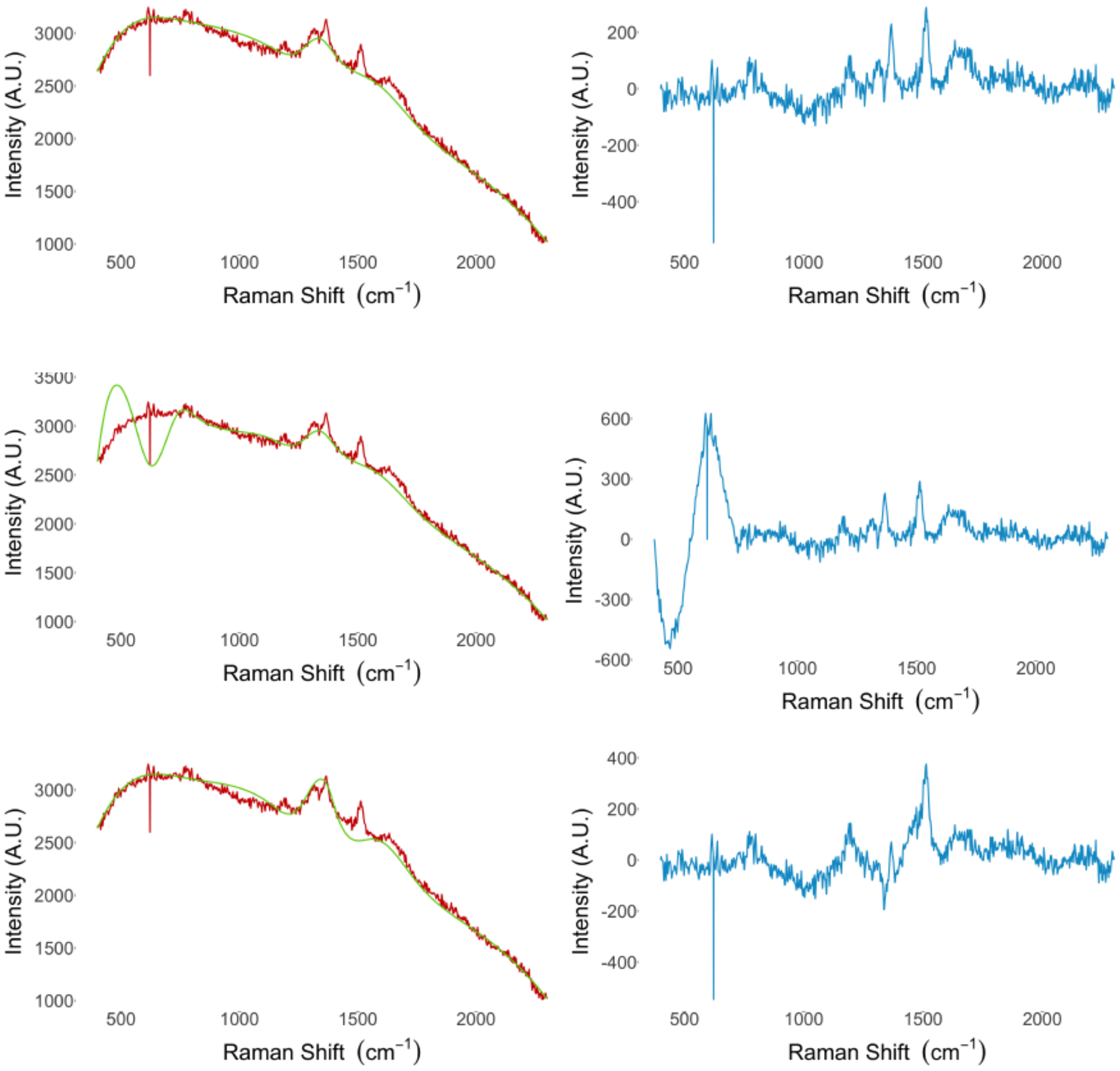

FIGURE 4. 19 CUBIC SPLINE INTERPOLANT ERRORS. THE TOP PANEL DEMONSTRATES AN UNPROCESSED RHODAMINE 6G WITH INTERPOLANTS PLACED TO PROVIDE A WELL FITTED BASELINE (GREEN) LEADING TO A REPRESENTATIVE CORRECTED SPECTRUM (RIGHT). IN THE MIDDLE PANEL PLACEMENT OF AN INTERPOLANT ON A COSMIC SPIKES SUBSTANTIALLY ALTERS THE FITTED BASELINE LEADING TO AN IMPROPERLY CORRECTED SPECTRUM. IN THE BOTTOM PANEL, PLACEMENT OF AN INTERPOLANT ON A PEAK FROM RHODAMINE SIGNAL SUBSTANTIALLY ALTERS THE FITTED BASELINE WHICH OBSCURES THE SIGNAL AND INDUCES LOW FREQUENCY NOISE.

Baselines fitted by cubic spline interpolation are defined by a small number of interpolants, and as such the resulting spectrum is exquisitely sensitive to the selected points. **Figure 4.19** demonstrates potential effects of poorly placed interpolants, using an unprocessed Raman spectrum acquired from a sample of Rhodamine 6G. The top left panel presents the original spectrum (red) with a well fitted cubic spline baseline (green) providing a representative corrected spectrum (blue) on the top left panel. The middle panels present the same spectrum with an interpolating point placed on a cosmic spike. The fitted baseline deviates substantially from the spectral baseline, inducing a large sinusoidal wave in the corrected spectrum. The bottom panels present the same spectrum with an interpolating point placed on a signal peak, which results in loss of the peak and induced low frequency noise in the surrounding spectral bands. Choice of interpolants needs to be made using pilot data, ideally placed at points representative of the baseline, while avoiding areas representing signal. It is imperative that high frequency noise and cosmic spikes are smoothed prior to baseline subtraction using spline interpolation.

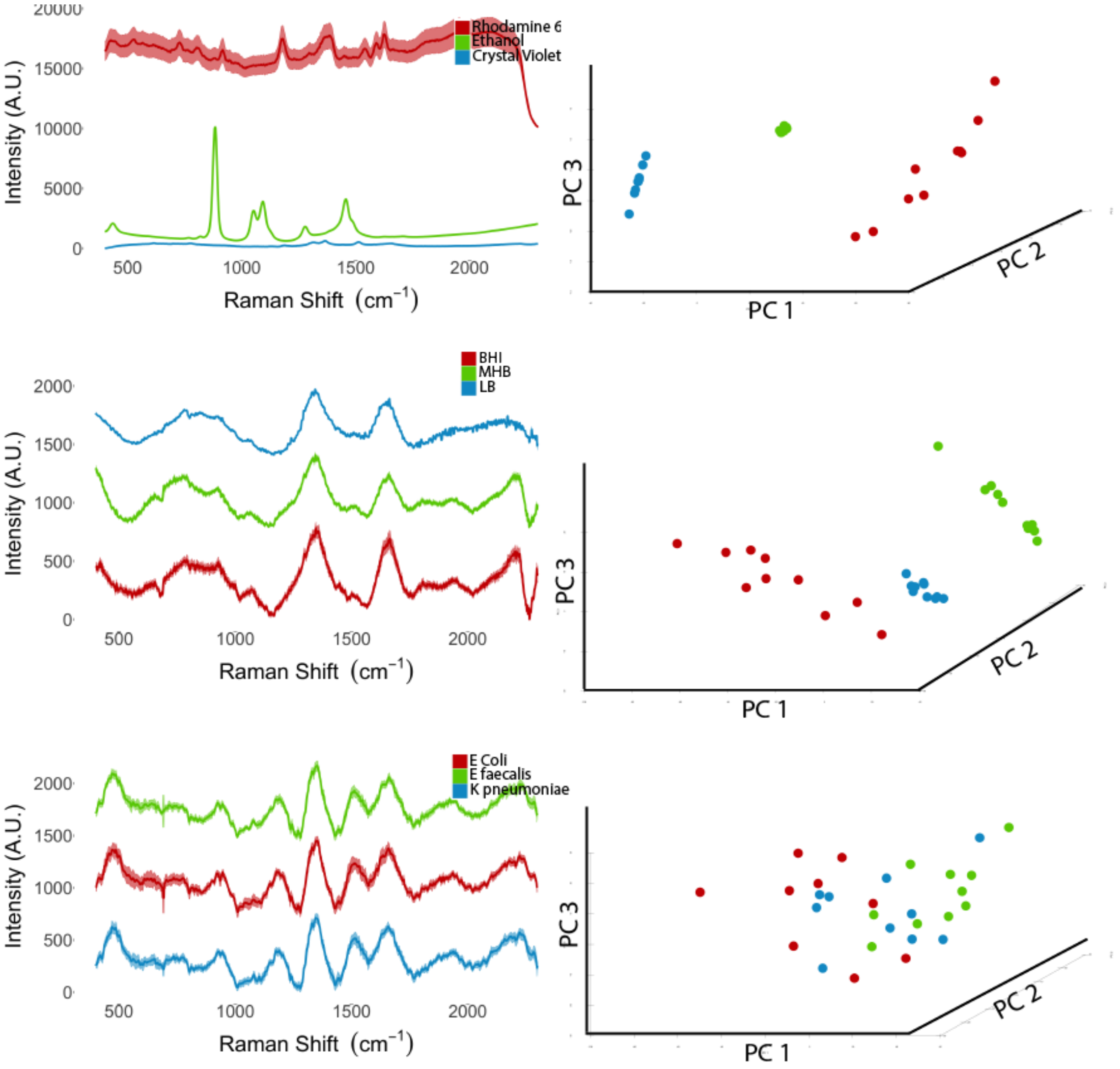

FIGURE 4. 20 MEAN SPECTRA, WITH STANDARD ERROR RIBBONS, AND PCA PLOTS FOR HIGH (TOP), MEDIUM (MIDDLE), AND LOW (BOTTOM) SNR DATASETS . THE SPECTRA ARE DIGITALLY PROCESSED BY TAKING AN AVERAGE TOTALLING 1 MINUTE ACQUISITION FOR EACH SPECTRUM, SMOOTHING WITH A MEDIAN FILTER, AND BASELINE SUBTRACTION OF A 2ND AND 6TH ORDER POLYNOMIAL FOR THE HIGH AND MEDIUM SNR DATASETS, AND CUBIC SPLINE INTERPOLATION FOR THE LOW SNR DATASET. THE ACCOMPANYING PCA PLOTS ARE PRESENTED ON THE RIGHT.

Figure 4.20 presents the means spectra with standard error ribbons and PCA plots for the high, medium, and low SNR datasets after averaging of scan, smoothing with a median filter and baseline correction. The Rhodamine 6G spectra demonstrate lower variation (as compared to the plots without baseline subtraction in **Figure 4.16)**, evidenced narrower standard error ribbons, leading to tighter clustering on the PCA plots. The medium SNR dataset present the spectra with fluorescence reduce, which in turn results in reduced clustering on the PCA plot. The low SNR dataset presents the Raman spectra with an incompletely removed baseline, without clustering visible on the PCA.

4.4.2.4 NORMALISATION

Sequentially captured Raman spectra from the same sample may vary due to an additive and multiplicative shift in the spectra. This may be corrected through normalisation, in which the spectrum is shifted to zero to account for the additive shift before dividing by a normalising factor to account for the multiplicative shift. Different normalising factors are available including: defined-peak, min-max, vector normalisation and area under the curve (AUC). As spectra are shifted to a zero baseline, normalisation is sensitive to the minimum point. As such, truncating the spectrum may improve spectral consistency if the spectrum minimum lies on a spectral extreme.

Figure 4.22 presents the Raman spectra (with a mean spectrum in black) acquired from samples containing crystal violet, pre-processed by averaging of spectra to a total of 60 seconds, smoothed by median filter and baseline subtraction of a second order polynomial. The top panel presents the Raman spectra prior to normalisation, demonstrating substantial additive and multiplicative shifts, in addition to a deep tail at 2200 – 2300 cm^{-1}. The middle panel presents the spectra after normalisation by the area AUC, demonstrating reduction in the variation caused by the additive and multiplicative shifts. The bottom panel presents the spectra if AUC normalisation is performed after truncating the spectrum to from 400 cm^{-1} to 2200 cm^{-1}, therein removing the tail, with further reduces the spectral variability. Truncation prior to baseline subtraction is demonstrated here to substantially improve replicability.

Figure 4.23 demonstrates the effect of applying different normalisation factors to the Raman spectra acquired from crystal violet samples. All methods substantially reduce the variation caused by additive and multiplicative shifts demonstrated in the top panel of **Figure 4.22**. The top panel presents min-max normalisation in which the normalisation factor is the intensity at the maximum point of the spectrum. This highlights a potential shortfall of this method in which the variation in the maximum peak may be normalised across the rest of the spectrum. The second panel present normalisation by the peak at 1625 cm^{-1}. This method performs well in these samples in which a low variation peak is available to normalise by, however may worsen noise any samples in which there is poor consistency at the chosen peak. The third and fourth panels present AUC and vector normalisation respectively. These methods normalise by the entire spectrum, avoiding the risk normalising by a point with high variation. Vector or AUC normalisation are more reliable on these grounds.

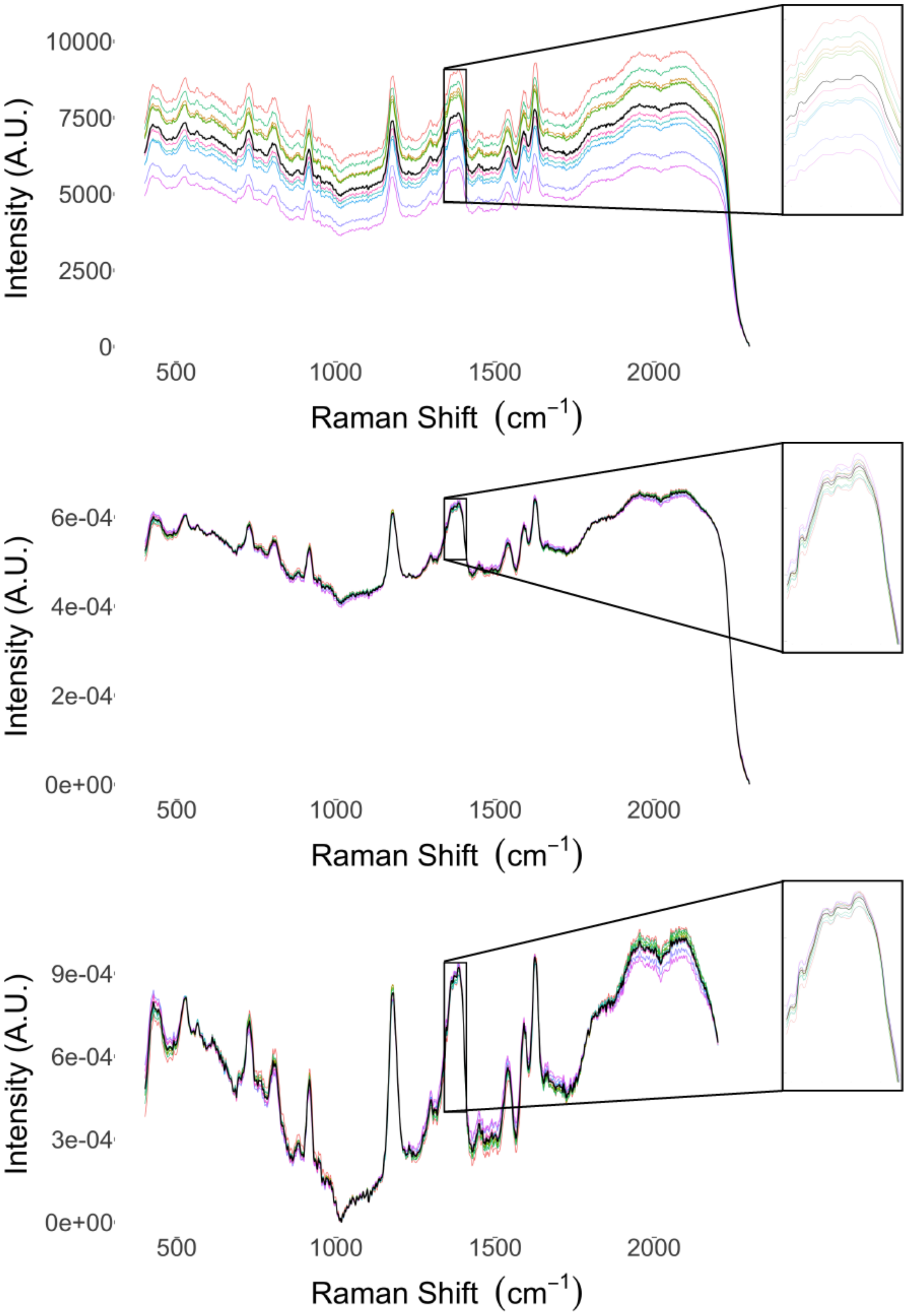

FIGURE 4. 21 THE BENEFIT OF TRUNCATION PRIOR TO NORMALISATION DEMONSTRATED BY PLOTS OF RAMAN SPECTRA ACQUIRED FROM CRYSTAL VIOLET SAMPLES. WITHOUT NORMALISATION (TOP PANEL) SUBSTANTIAL ADDITIVE AND MULTIPLICATIVE SHIFTS RESULT IN THE INDIVIDUAL SPECTRA DISPERSED AWAY FROM THE MEAN SPECTRUM (BLACK). THE SAME SPECTRA AFTER AUC NORMALISATION HAVE THESE SHIFTS SIGNIFICANTLY REDUCED (MIDDLE PANEL). THIS IS FURTHER IMPROVED BY TRUNCATION (BOTTOM PANEL) WHICH REMOVES THE DEEP TAIL SEEN AT THE RIGHT.

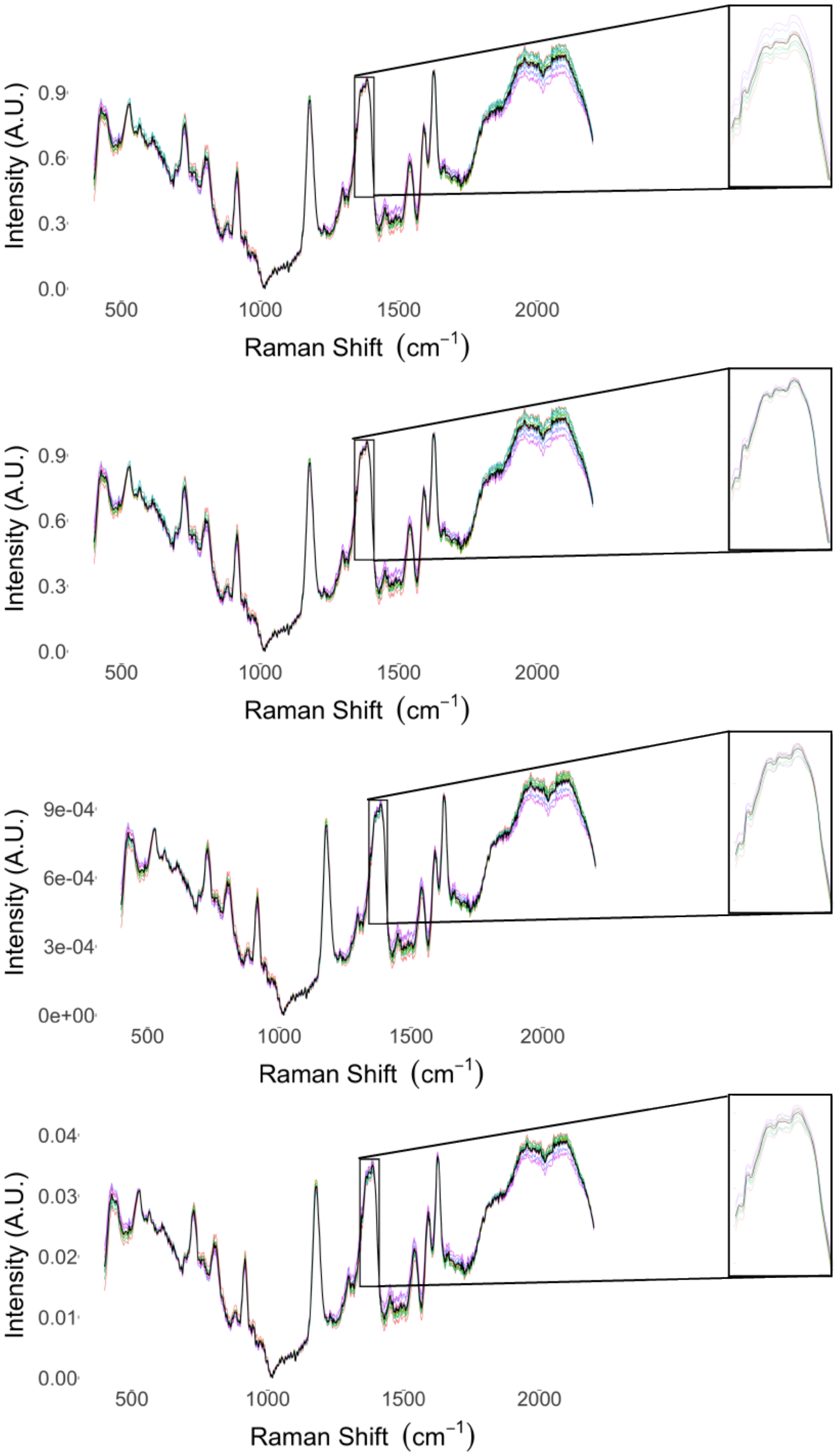

FIGURE 4. 22 NORMALISATION BY DIFFERENT NORMALISING FACTORS MIN-MAX, DEFINED PEAKS AT 1625CM^{-1}, AREA UNDER CURVE, AND VECTOR NORMALISATION (TOP TO BOTTOM). ALL FACTORS DEMONSTRATE SUBSTANTIAL REDUCTION ON THE SPREAD OF SPECTRA SEEN IN THE TOP PANEL OF FIGURE 4.21

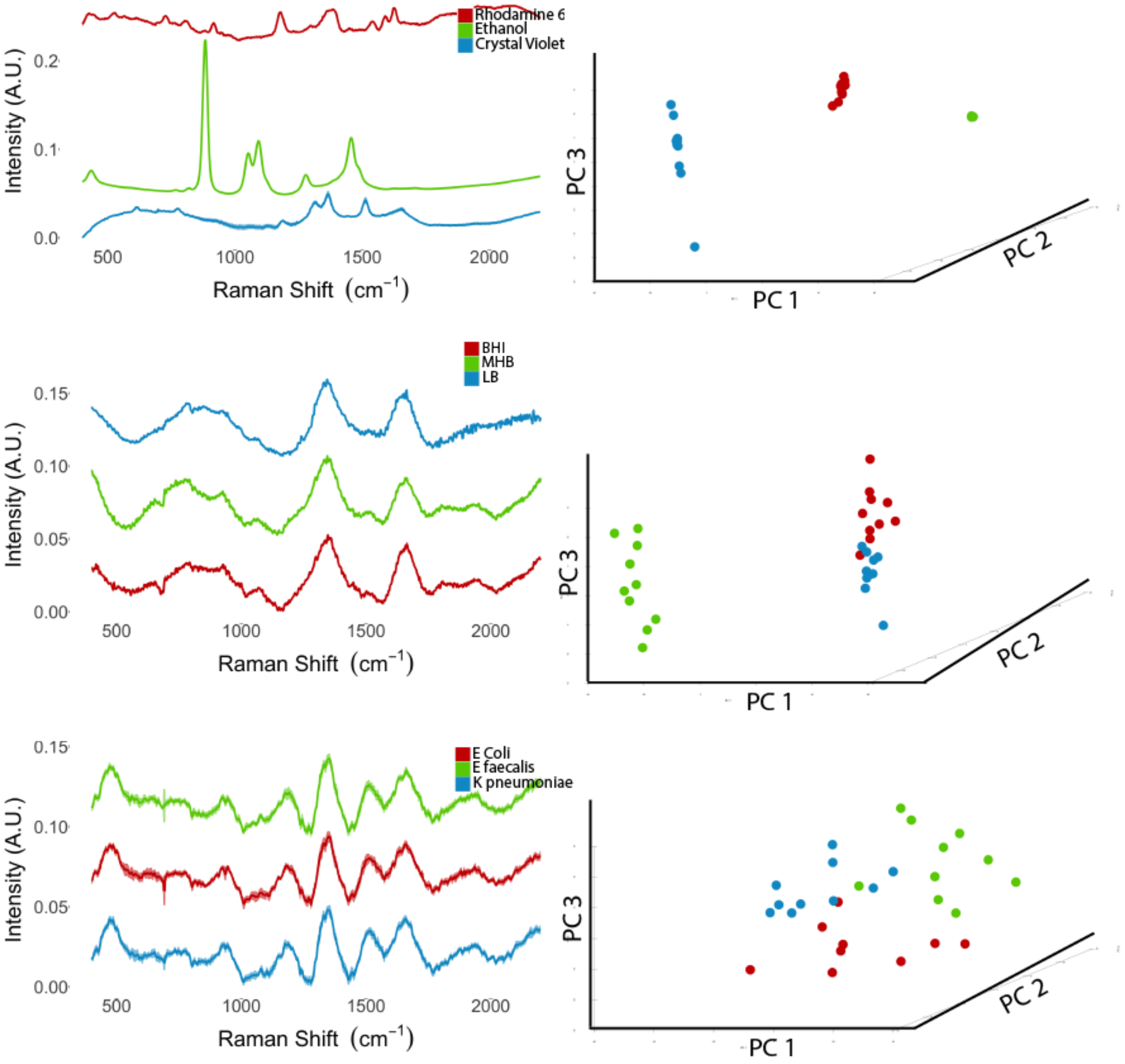

FIGURE 4. 23 MEAN SPECTRA, WITH STANDARD ERROR RIBBONS, AND PCA PLOTS FOR HIGH (TOP), MEDIUM (MIDDLE), AND LOW (BOTTOM) SNR DATASETS AFTER COMPLETE DIGITAL PRE-PROCESSING. PRE-PROCESSING WAS PERFORMED BY FIRST TAKING AN AVERAGE OF SPECTRA TOTALLING 1 MINUTE ACQUISITION AND SMOOTHING WITH A MEDIAN FILTER. THEREAFTER, BASELINE SUBTRACTION OF A 2ND AND 6TH ORDER POLYNOMIAL FOR THE HIGH AND MEDIUM SNR DATASETS, AND CUBIC SPLINE INTERPOLATION FOR THE LOW SNR DATASET WAS PERFORMED BEFORE VECTOR NORMALISATION OF ALL DATASETS.

Figure 4.23 presents the high, medium and low SNR datasets after completing pre-processing by vector normalisation. The spectra of the high SNR dataset demonstrate well defined peaks, and the variability previously seen in the Rhodamine spectra is substantially reduced. As such, the PCA plot demonstrates excellent clustering and separation. The medium SNR dataset demonstrates reduced variability of the spectra, allowing for better visualisation of the small defining peaks above the unresolved baseline. The PCA plot demonstrates good clustering and separation with the exception of the overlap of a single BHI sample. This apparent worsening of the separation after normalisation may be explained by further reduction in the fluorescence signal. The high SNR dataset demonstrates little visible differences on the spectra, however the PCA plot now demonstrates sufficient clustering for a reasonable degree of separation.

4.4.3 UNSUPERVISED LEARNING

Unsupervised learning refers to algorithms that identify clusters without prior knowledge of the classes of the spectra. These methods may be used to identify natural clustering of spectra. An additional benefit seen in PCA is that of feature reduction, in which each spectrum is reduced to a smaller number of descriptive principal components.

4.4.3.1 PRINCIPAL COMPONENT ANALYSIS

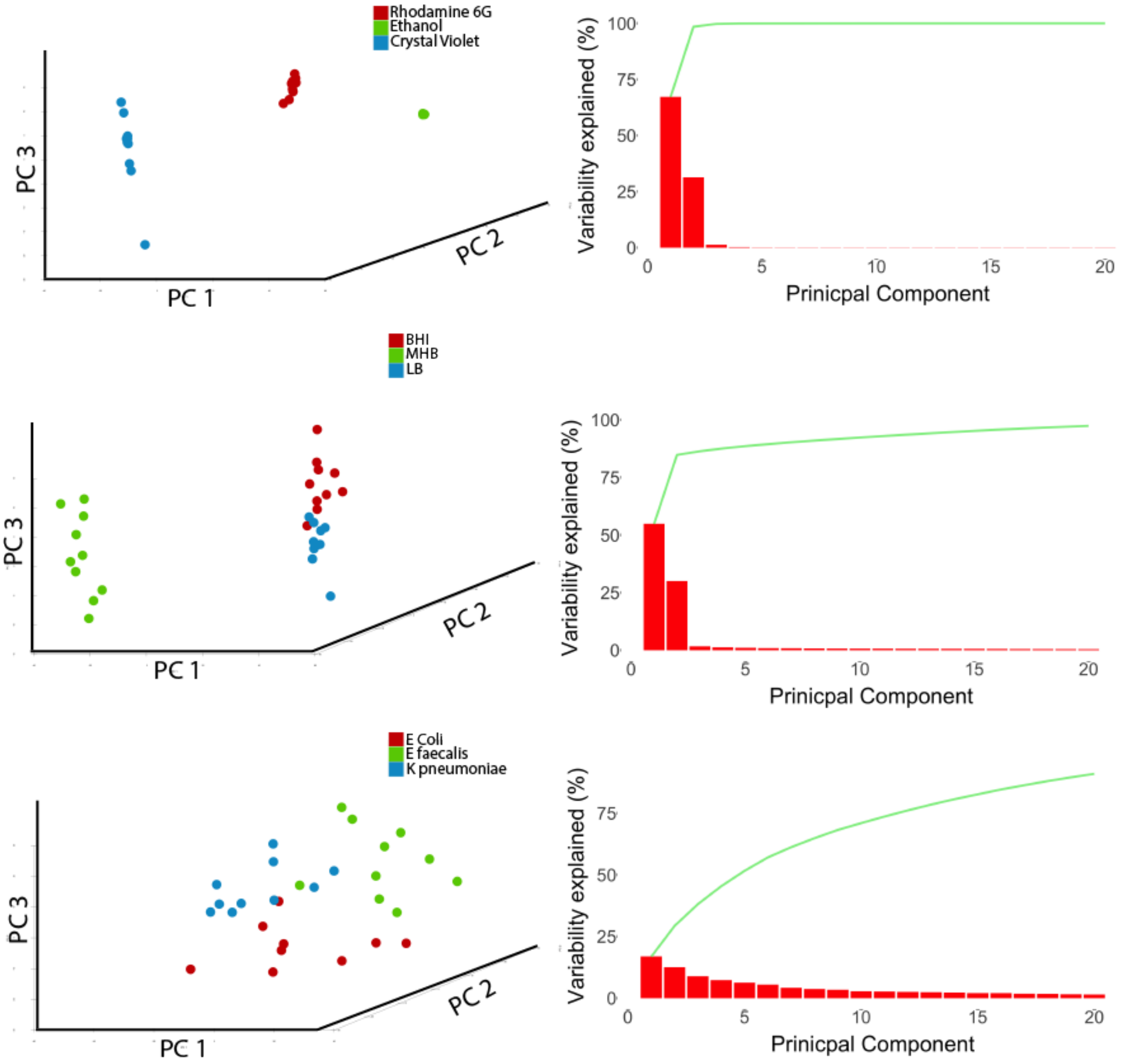

FIGURE 4. 24 UNSUPERVISED LEARNING BY PCA FOR THE PRE-PROCESSED HIGH (TOP), MEDIUM (MIDDLE) AND LOW (BOTTOM) DATASETS. COMPONENT PLOTS (LEFT) ARE USED TO VISUALISE CLUSTERING WHILE SCREE PLOTS (RIGHT) VISUALISE THE PROPORTION OF VARIABILTY EXPLAINED BY THE PRINICPAL COMPONENTS (RED BARS) AS WELL AS THE CUMMULATIVE VARIABILITY EXPLAINED (GREEN LINE).

Unsupervised learning by PCA for the high medium and low datasets are presented in **Figure 4.24**. Component plots (left) are used to visualise natural clustering of spectra, while scree plots (right) demonstrate the proportion of variability explained by each principal component and cumulatively proportion. The high SNR dataset demonstrates tight clustering with clear separation of groups on the component plot. A high proportion of variation is explained in a few components, with over 99% of variability explained by the first 3 components. The medium SNR dataset demonstrates good clustering and separation with minimal overlap. The scree plot is still loaded toward the early components with 86% of total variation explained by the first 3 components. The low SNR dataset demonstrates some natural clustering in the component plot, but significant overlap in the first three components. The scree plot demonstrates the explained variation is more widely disperse with only 38%

variation accounted for in the first 3 components. PCA has significant further advantages in that it may be used to for feature reduction, and the component loadings (see **Figure 4.28** below) may be used to gain a mechanist understanding of classification.

4.4.3.2 HIERARCHICAL CLUSTER ANALYSIS

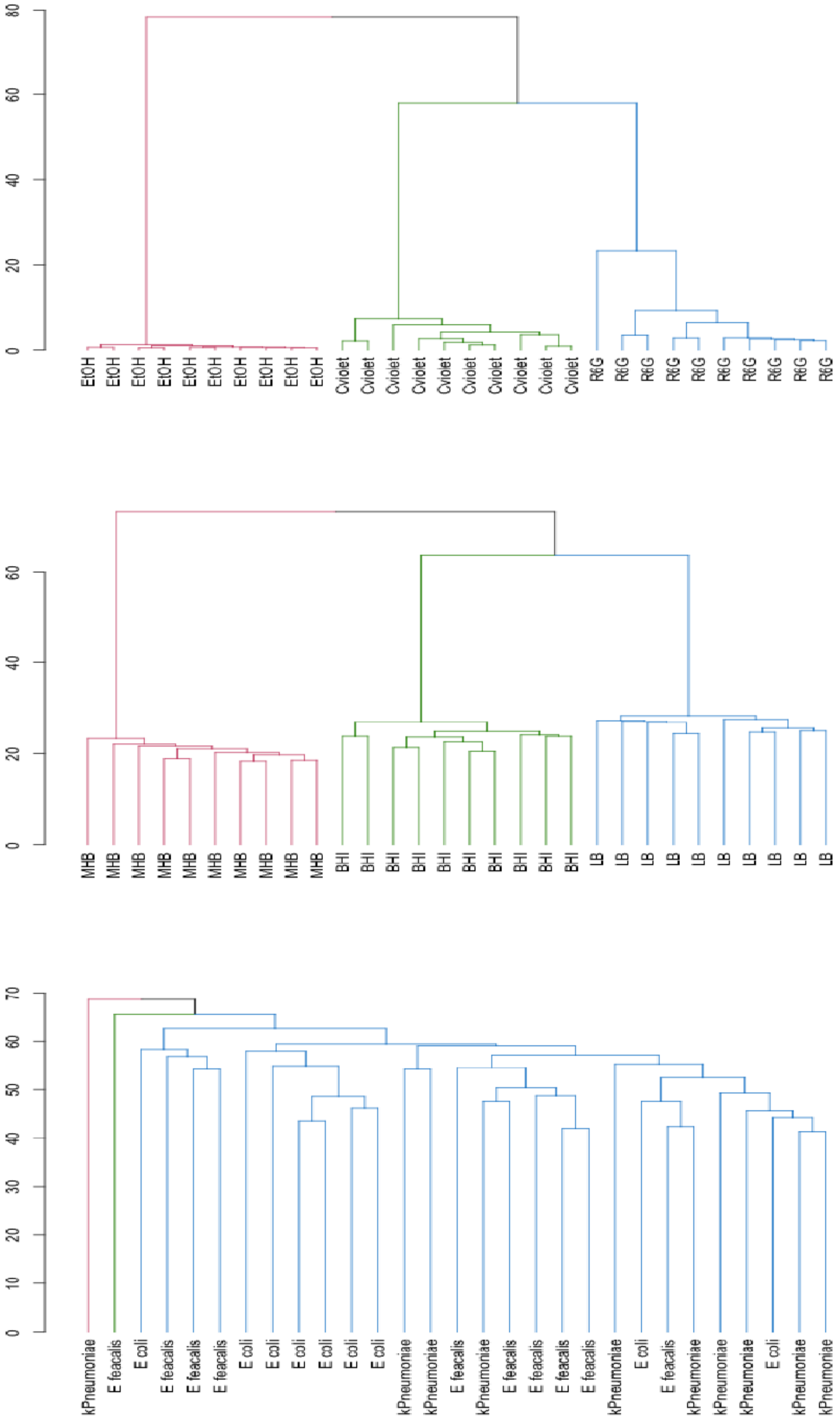

FIGURE 4. 25 UNSUPERVISED LEARNING BY HIERARCHICAL CLUSTER ANALYSIS

HCA achieves natural cluster by iteratively combining similar spectra, defined by the lowest distance between data points. Unsupervised learning though HCA applied to the high medium and low datasets is presented in **Figure 4.25**. Where natural clustering occurs (high and medium datasets) the dendrograms intuitively present natural clustering in addition to within and between group similarity (presented by branch length). However, where clustering is more complex (low SNR dataset), this is misrepresented on the dendrograms, and no mechanistic interpretation is provided. HCA does not reduce features. HCA, therefore provides limited value in analysis of Raman spectra.

4.4.4 SUPERVISED LEARNING

Supervised learning aims to identify the class from which spectra arise using prior knowledge. This entails training algorithms using labelled data, before using the trained algorithms to predict the class of spectra whose class is not known.

4.4.4.1 PC-LDA

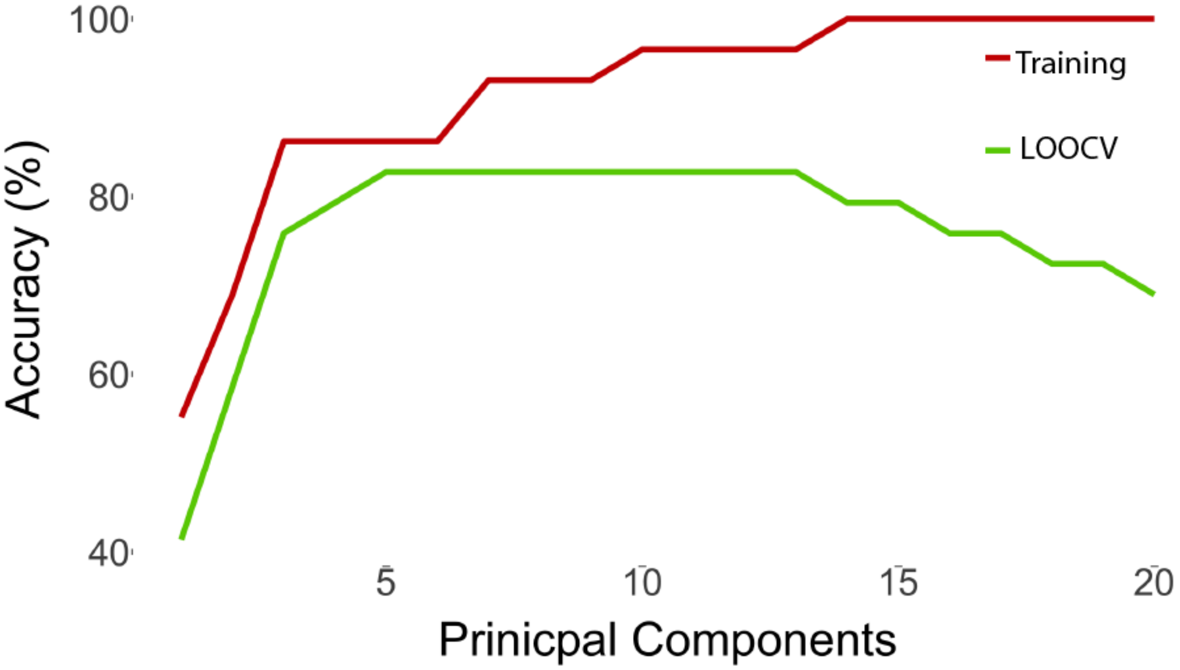

FIGURE 4. 26 PC-LDA TRAINING (RED) AND LOOCV (GREEN) ACCURACY WITH INCREASING NUMBER OF PRINCIPAL COMPONENTS FOR THE LOW SNR DATASET. TRAINING SET CLASSIFICATION ACCURACY CONTINUES TO IMPROVE WITH A GREATER NUMBER OF FEATURES. IN CONTRAST LOOCV ACCURACY INITIALLY IMPROVES WITH MORE FEATURES REDUCING, REFLECTING OVERFITTING OF THE DATA IF TOO MANY COMPONENTS ARE USED.

PC-LDA is a powerful supervised learning technique widely applied in Raman bacteriologic research in light of its ability to provide classification performance with relatively low number of samples. Initially principal component analysis is used to reduce spectra to a smaller number of descriptive variables, which are then used in linear discriminant analysis. Feature reduction is necessary as LDA requires fewer predictors than samples. PC-LDA performance is sensitive to the number of principal components passed to LDA. Training set accuracy will continue to improve with more PCs, however beyond a point this represents overfitting as demonstrated by the drop off in leave-one-out cross validation (LOOCV) accuracy beyond a certain number of PCs in **Figure 4.26**. The parsimony principal is advocated with least number of PCs providing the greatest LOOCV accuracy used (5 PCs for the low SNR dataset above).

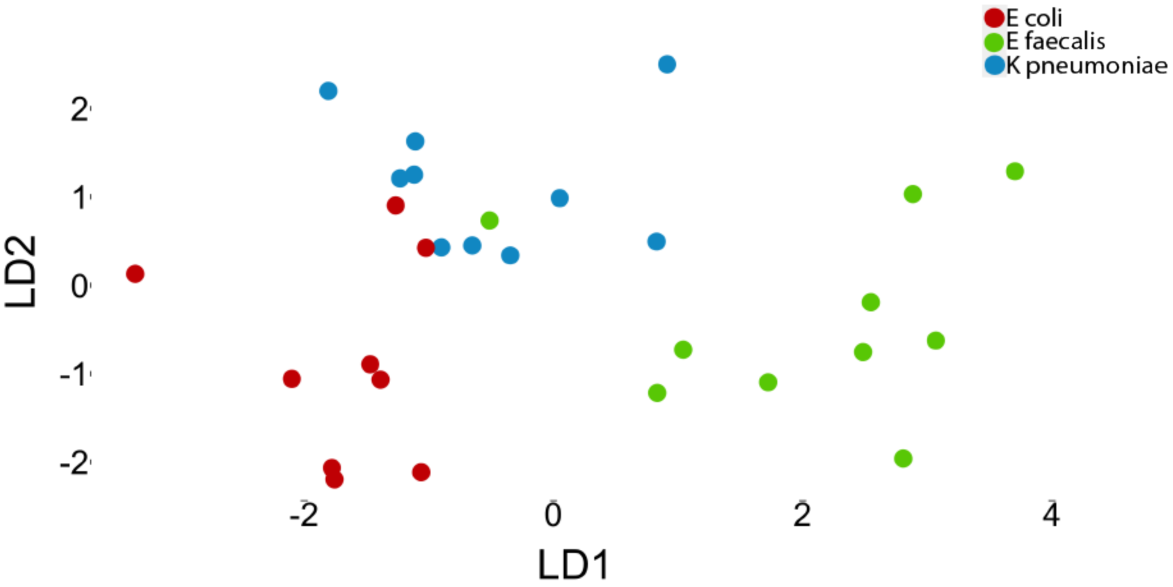

FIGURE 4. 27 SUPERVISED LEARNING BY PC-LDA FOR LOW SNR DATASET

Figure 4.27 presents the plot of the linear discriminants of the PC-LDA for the low SNR dataset. While the points are clustered, there remains a degree of overlap. This is reflected in the classification performance in **Table 4.3**. After complete pre-processing and supervised learning performed by PC-LDA spectra were classified with 86% accuracy (95% CI: 68.3;96.1%. p-value <0.05). Class sensitivities ranged from 84% to 100%, while specificities ranged from 78% to 100%.

TABLE 4. 3 PC-LDA CLASSIFICATION PERFORMANCE FOR THE LOW SNR DATASET

		Reference Pathogen		
		Escherichia coli	***Enterococcus faecalis***	***Klebsiella pneumoniae***
Predicted Pathogen	***Escherichia coli***	7	0	0
	Enterococcus faecalis	0	9	1
	Klebsiella pneumoniae	2	1	9
Classification performance				
Overall	Accuracy		86.2% (95% CI: 68.3;96.1. p-value<0.05)	
Escherichia coli	Sensitivity		100%	
	Specificity		78%	
Enterococcus faecalis	Sensitivity		95%	
	Specificity		90%	
Klebsiella pneumoniae	Sensitivity		84%	
	Specificity		90%	

4.4.5 SPECTRA BAND ASSIGNMENT

Identification of the spectral bands contributing to classification of Raman spectra, while not necessary for supervised learning, builds upon the scientific understanding of Raman research and provides a mechanistic validation of Raman technologies. **Figure 4.28** presents four techniques for identification of contributory spectral bands applied to the high, medium and low SNR datasets (left to right). Visual inspection (Top row) may be used where spectral features are clearly defined such as in the high SNR dataset, but is limited in more complex spectra. Without quantification and without accounting for variability, this method may overestimate the importance of features in areas of high variability, or miss small peaks lying in areas of low variation.

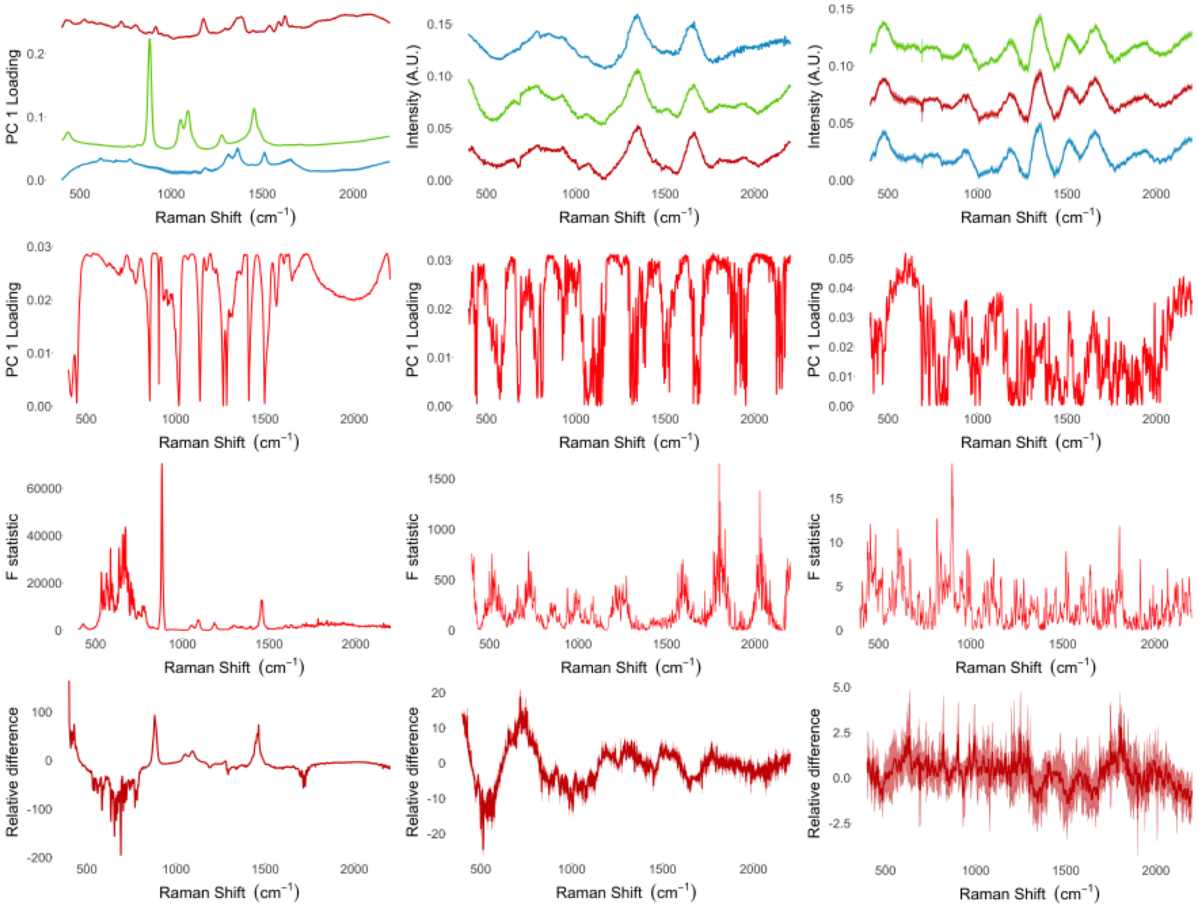

FIGURE 4. 28 METHODS FOR IDENTIFICATION OF CONTRIBUTORY SPECTRAL BANDS. VISUAL ASSESSMENT (TOP ROW), PRINCIPAL COMPONENT LOADING (SECOND ROW), F-STATISTIC PLOTS (THIRD ROW) AND RELATIVE DIFFERENCE (BOTTOM ROW) APPLIED TO HIGH (LEFT), MEDIUM (MIDDLE) AND LOW (RIGHT) SNR DATASETS

Principal component loading (second row) is frequently used for identification of contributory spectral bands, by assessing the eigenvectors used to transform the original data to create the principal components. This method assumes the classes had separated on PCA. This method suffers from poor interpretability, and plots may appear congested even where SNR is high.

$$F_{statistic} = \frac{\boldsymbol{Between\ group\ variation}}{\boldsymbol{Within\ group\ variation}}$$

EQUATION 4. 1 F-STATISTIC EQUATION

Signal is variability associated with the class of interest, while noise is variability not associated with the class of interest. As such a plot of the F statistic used in analysis of variance (ANOVA) (**Equation 4.1**) provides an approximation of the SNR (third row). Interpretation of the F-statistic is contingent on the sample size and number of classes, and as such there is no set threshold for a definitive peak. Despite this, F-statistic plots provide a rapid and simple method for identifying spectral bands with higher SNR across a study population. This may be augmented with pairwise comparisons achieved by centring and scaling each spectrum by spectra from a reference group (bottom row). This method provides an easily interpretable visual representation of relative difference of spectra accounting for variation.

4.5 DISCUSSION

Raman spectroscopy has demonstrated capability in bacteriologic research ranging from basic science to technologies that have potential to be clinically applied[45, 70, 77, 85, 128, 167-169]. Most importantly Raman spectroscopy rapidly delivers high resolution spectra, allowing for strain level classification with minimal physical processing. This sensitivity is similarly the greatest challenge in Raman spectroscopic research in that minor experimental and sample variation leads to disproportionate changes in the acquired spectra. Furthermore, pathogen classification using Raman spectroscopy is a multistep process, with each step having multiple parameters under control which may have non-linear effects on the Raman spectrum acquired and therefore the classification. This results in an extraordinary number of permutations to Raman research.

An approach to pathogen classification using Raman spectroscopy has therefore been developed to be relatively standardised. Samples are physically processed after which experimental technologies are applied typically with the intention of concentrating pathogens or reducing sample complexity. Raman spectra are acquired using Raman spectrometers, which may be augmented with optical microscopes. The acquired spectra need to be digitally pre-processed to optimise SNR. Classification is performed using supervised learning techniques, frequently on a reduced number of features. To understand and optimise the experimental controls in each of these steps, a strict approach of isolating the parameter and assessing the effects on the spectra has been employed in this work.

4.5.1 BACTERIAL SUSPENSIONS

As research into Raman spectroscopy evolves the samples assessed typically need to progress in complexity from samples containing a low number of reference strain pathogens at controlled concentrations suspended in a simple solution, to samples reflective of real-world clinical samples containing different pathogen strains in varying concentration suspended in complex media. Development of methods to consistently produce samples suitable for Raman assessment was achieved. Bacteria undergo dynamic changes while progressing through growth phases which reflect in dynamic changes to the Raman spectra. Dynamic spectra changes settle as pathogens enter the stable growth phase and as such uropathogens are cultured in a non-selective media[95, 123, 137, 170].

Culture media contain several strong Raman scatterers which may obfuscate bacterial signal, or if different media are used, provide classification not based on the pathogen Raman spectra[165]. Multiple cycles of centrifuge and washing has previously been demonstrated to remove residual culture medium Raman signal acquired using Raman microscope[143]. In this work, 5 centrifuge and wash cycles were demonstrated to culture medium signal from Raman spectra acquired using a handheld Raman spectrometer. **Figure 4.2** demonstrates that after 5 centrifuge and wash cycles pathogens clustered by pathogen rather than culture medium demonstrating the Raman signal arises from the pathogens.

Granular and consistent control of pathogen load in samples is required to contrive samples whose characteristic are consistent with clinical samples while still reducing variability. Gold-standard colony counting using the Miles and Misra method provides accurate pathogen load counts, but the need for culture limits this to confirmation of load rather allowing for control thereof[152]. Optical densitometry is demonstrated here **Figure 4.3 & Table 4.2**) to provide a reliable surrogate marker for pathogen load, with an OD_{600} of 0.07 approximating 10^8 CFU/ml. Subsequent serial dilution provides for clinically relevant cut-offs of 10^5 CFU/ml, while the choice of diluting fluid) provides for complexity ranging from simple suspensions (suspended in PBS or saline) up to phantom urine samples (suspended in sterile human urine).

4.5.2 RAMAN ACQUISITION

Numerous controls are available on spectrometers which may be tailored to optimise signal during spectral acquisition. Automated acquisition and subtraction of a reference spectrum substantially reduced high frequency noise. Activation of the Raster orbital scanning function provided superior Raman spectra with greater and more defined peaks. Despite providing superior spectra, these functions are rarely mentioned in Raman pathogen research, with only *Jarvis et al.* describing an analogous[86] feature of averaging multiple scans acquired from a grid layout.

Higher laser power and prolonged acquisition time provide a linear increase in Raman spectral intensity through provision of a greater number of photons available for non-elastic scatter. While low frequency noise demonstrated a similar linear increase, high frequency noise remained consistent. As such higher power and longer acquisition times provided an increase in signal relative to high frequency noise. Therefore, within limits of sample photodegradation and time constraints, laser power and acquisition time should be maximised.

This work demonstrates the exquisite sensitivity of Raman spectra to focal length, with 0.5mm differences substantially altering both the amplitude and resolution of acquired spectra. A similar challenge was highlighted by *Mircescu et al.* when 30% of acquired spectra were discarded due to poor focussing[101]. A spectroscope holder was thus designed and 3D printed to ensure optimal and consistent focussing at 29.5mm in all further work.

4.5.3 SPECTRAL DIGITAL PRE-PROCESSING

Noise in Raman spectra arising from several sources poses a significant challenge in Raman spectral analysis. Unresolved noise retains variation in data that reduces classification accuracy[104-106]. Noise in Raman spectra presents as cosmic spikes and high frequency noise arising from device electronics and low frequency noise arising from extraneous light and samples fluorescence. Additionally, an additive and multiplicative shift occurs with sequentially collected spectra appearing different while still containing the same signal. High, medium and low SNR datasets were created to illustrate the need for adequate digital pre-processing to gain classification performance in the low SNR set and similarly how overfitting can reduce classification performance in the high SNR set.

Taking a mean of multiple scans is a frequently employed first step in Raman pre-processing. This work demonstrates this is an effective means of reducing both high frequency noise and cosmic spikes. This is because both sources of noise are randomly distributed across the spectrum. Averaging spectra is also demonstrated here to reduce the additive and multiplicative shift. Averaging scans has another significant advantage in that it is unlikely to influence signal, as it is non-randomly distributed across the spectrum. A potential means of further augmenting this method was demonstrated by *Jarvis et al.*, in which the median 36 of the 50 collected spectra were averaged [82]. In this way outliers, notably those including cosmic spikes or substantial shifts are excluded.

Smoothing of spectra is performed to reduce high frequency noise and cosmic spikes. Two frequently utilised methods include median filtering and Savitsky-Golay filters[105]. Both are demonstrated here to substantially reduce high frequency noise. Median filters were demonstrated to be highly effective at cosmic spike removal, however rapidly reduced signal with widening windows. In contrast, Savitsky-Golay filters retained better signal however demonstrated suboptimal spike removal. Given the pathogen signal in Raman spectra are typically relatively low intensity and densely situated within the fingerprint region, superior signal retention by Savitsky-Golay filters make these the smoothing modality of choice[108].

A significant challenge in digital processing of biologic Raman spectra is complex baselines arising from competing signal from background. Complex baselines are particularly challenging when using a handheld spectrometer rather than a Raman microscope as the larger focal volume incorporates a greater proportion of background material. Both the medium and low SNR datasets demonstrate complex baselines. Interestingly classification performance of the medium SNR dataset deteriorated following baseline subtraction in the medium SNR dataset, indicating that the baseline from fluorescence of the culture media was providing for classification. Two frequently employed methods, polynomial subtraction and cubic spline interpolation were assessed.

Subtraction of a fitted polynomial is the most frequently employed method for baseline correction, likely due to its relative simplicity[110, 117, 149, 160]. This method is demonstrated to here to perform well in simple baselines which may be approximated with low order polynomials. It does not, however, perform well with complex baselines where higher order polynomials are required, as these induce artefacts and suffer from Runge's phenomenon (oscillation at the ends of the fitted polynomial).

Cubic spline interpolation provides for better estimation of complex baselines through user defined interpolants. As the baseline is defined by a small number of points, it is extremely sensitive to the selection of these points, as demonstrated in **Figure 4.18** where interpolants were intentionally placed in areas of signal and noise. Cubic spline interpolation is also particularly susceptible to overfitting, in which interpolant may be selected to maximise signal in the dataset[105]. Therefore, interpolants need to be selected *a priori* on pilot data.

Normalisation is required to account for the additive and multiplicative shift present in Raman spectra, by shifting to zero prior to dividing by a normalising factor. Options for normalising factor assessed included min-max, defined peak, AUC and vector normalisation. Where normalising factors are based on a single band (min-max, and defined peak) a risk of extending variability (either in amplitude or extent) across the entire spectrum is a possibility[171]. **Figure 4.22** demonstrated this risk where min-max normalisation led to greater spread of spectra acquired form crystal violet samples. Both vector and AUC normalisation normalise by a factor generated by the entire spectrum and so perform superiorly[85, 171]. One potential advantage to defined peak normalisation not demonstrated here, is where an internal standard may allow for estimation of concentration or load. The benefit of truncation to the area of interest prior to normalisation was demonstrated. This is particularly valuable when using polynomial subtraction where spectral extremes are likely to have higher variability dure to poorer fits in these regions[172].

The above digital pre-processing steps are crucial to optimising SNR, and therefore, to gain the greatest performance out of further analysis. Each processing step has resounding influence on the final spectrum passed forward to analysis, which explains the great diversity in processing approaches. The large number of available pre-processing methods available, each with many tuning parameters, generate a massive number of permutations to pre-processing. This massive number of permutations risks both overfitting processing to the acquired dataset, or over-processing with signal loss. Therefore, a minimalist approach utilising the simplest pre-processing techniques that works on a pilot dataset should be used[116].

4.5.4 UNSUPERVISED LEARNING

PCA is the most widely used method for unsupervised learning, feature reduction and spectral band assignment[114]. The technique has numerous advantages that make it well suited to analysis of Raman spectra. PCA is performed in a mathematically closed form, without user defined inputs, leading to good interpretability and replicability, as well as providing computational efficiency. PCA is well suited to hypergeometric data, substantially reducing a massive number of features to a few descriptive components. Plots of components provide an easily interpretable demonstration of natural cluster (or lack thereof). Scree plots are a good reflection of SNR in datasets (see Figure **4.23**)[115]. Reduction of features is required for, or may improve performance of, supervised learning algorithms such as LDA[113]. Assessment of PCA eigenvectors (loading) may be used for identification of contributory spectral bands. These many benefits must be tempered by a recognition that PCA is designed to maximise variation in earlier components, drawing attention to the importance of careful pre-processing.

HCA is presented as an alternative unsupervised learning approach, but is demonstrated to perform poorly on the low SNR dataset. Many other reasons deem HCA poorly suited to Raman analysis: user defined inputs (agglomerative vs distributive & distance method) reduce interpretability and replicability; HCA is computationally cumbersome, particularly with hypergeometric data; HCA does not reduce features, and so does not aid in further analysis; and finally where clustering occurs, HCA does not provide insight into which spectral bands provide for clustering.

4.5.5 Supervised Learning

PC-LDA is presented as a suitable method for supervised learning applied to Raman research. Crucial benefits to PC-LDA are the ability to efficiently work with hypergeometric data (provided by PCA feature reduction), as well as the ability to assess classification performance with a relatively small sample size. PC-LDA further benefits from good visual interpretability of discriminant plots[113, 173]. The performance of PC-LDA, both in training and validation, is highly sensitive to the number of components passed to LDA. As such a systematic approach applying the parsimony principal to LOOCV should be used to select the number of PCs used[116].

A potential disadvantage to PC-LDA is inferior generalisability as compared to methods such as SVMs and ANNs[121]. These methods require considerably larger training datasets as compared to LDA, and so are unsuitable for early-stage Raman research which relies upon refinement of techniques with as few samples as possible. Furthermore, these methods are susceptible to a black box effect in which little understanding of how classification is achieved, and so are poorly suited to further development of early-stage technologies. An additional shortcoming of SVMs in particularly is that these are binary classifiers, and while workarounds (one-vs-one & one-vs-all) are available these are likely to worsen classification performance when applied to multiple class problems (such as pathogen classification)[119].

4.5.6 Spectral band assignment

Assignment of the spectral bands providing classification is an integral part of early-stage Raman research, providing both a mechanistic validation as well deeper understanding of the technology used. Visual assessment and principal component loading plots are frequently used to identify bands, despite being poorly suited. A challenge arises when using visual assessments to account for variability at the band. Specifically, the importance of small peaks arising in bands of low variability may be underestimated, and conversely the importance of large peaks on bands with high variability may be overestimated

Plots of principal component eigenvectors (loadings) provide a visual representation of the contribution of spectral bands in each principal component. Given PCA is unsupervised, assigning bands by this method is therefore contingent on class separation within the component. A further challenge is that PC loadings are not naturally interpretable. Furthermore, **Figure 4.28** demonstrates that even in high SNR datasets the PC loadings can be widely dispersed.

Plots of the F-statistic are proposed here as an intuitive display of the SNR across the dataset. The provide an easily interpretable quantitative assessment of the discriminatory value of each band. This may be augmented with pairwise comparisons.

4.6 CONCLUSION

Pathogen research, and indeed clinical diagnostics research, using Raman spectroscopy follow a similar broad approach of sample preparation, physical processing, Raman acquisition, digital pre-processing, feature extraction and classification, with spectral band assignments as an additional step applied to research studies. Each step is systematically interrogated here to define a suitable method for Raman research and understand the importance of each aspect in achieving the best classification performance.

A method for producing samples of consistent pathogen type and load is demonstrated. Additionally, control of the suspending fluid allows for a simplified challenge using suspensions while developing Raman techniques, which may then be progressed to more representative phantom urine samples needed for validation.

The importance of pre-processing is demonstrated in the series of pre-processing applied to high, medium and low SNR datasets. Strengths and weaknesses of frequently used techniques and control parameters are demonstrated in applied examples drawn from the datasets. Attention is drawn to the massive number of permutations possible during pre-processing, highlighting the value in deciding these *a priori* using prior or preliminary data, to both avoid both overfitting and signal loss.

PCA is demonstrated to perform multiple important roles is Raman analysis as it is used in unsupervised learning as well as for feature reduction prior to supervised learning. It may also play a role in spectral band assignment.

PC-LDA is identified as the ideal method for early-stage Raman research considering its strength in working with low sample numbers in the setting of hypergeometric data. The importance of parsimony in the selection of components passed to LDA is highlighted.

Overall, the work presented in this chapter demonstrates the important parameters to optimise in Raman research, particularly in the case of pathogen identification. The experiments performed here were used to identify an optimal experimental procedure, which was taken forward to the experiments presented in the following chapters.

CHAPTER 5: UNENHANCED RAMAN SPECTROSCOPY

5.1 INTRO

UTI leads to significant patient morbidity, mortality, and societal costs. Core to this burden of disease is the pervasiveness of the condition, affecting 150 million people annually[1, 2]. The staggering number of UTIs, translates to a considerable health burden as any sequelae of the conditions is amplified millions of times over. This amplification of disease sequelae is extended to the shortcomings of the existing diagnostic paradigm, with inaccuracies and diagnostic delays similarly being extended to a multitude of people. The UTI diagnostic paradigm is plagued by inaccuracy and delay, with screening tests suffering from poor sensitivity leading to delay or overtreatment respectively, while definitive diagnosis incurs such delays that diagnostic value is lost[5].

These disease characteristics define the ideal diagnostic for UTIs, specifically that substantially improved accuracy is required to reduce both delayed recognitions risking progression to pyelonephritis or sepsis, and overtreatment leading to AMR. Additionally, rapid pathogen classification is required to limit the use of broad-spectrum antimicrobials, therein reducing development of AMR[174, 175].

Raman spectroscopy possesses many of the characteristics required to act as the ideal diagnostic. Most notably, Raman spectroscopy can provide instantaneous biochemical phenotyping on a single cell, negating the need for prior biomass expansion[89, 176]. Numerous physical and digital techniques may be employed to optimise diagnostic and classification performance[104, 107, 171, 172].

A major limitation of Raman spectroscopy is weak biologic Raman scattering. SERS is frequently employed to overcome this weakness in light of its ability to provide massive signal enhancement. SERS has a limitations that warrant interrogating whether pathogen classification may be achieved without requiring SERS, specifically: the enhancement provide by SERS is extremely sensitive to the probe characteristics and so strict technical production is required to gain consistent enhancement, and SERS enhancement declines exponentially with distance requiring close apposition to ensure enhancement but more importantly consistent apposition to avoid inducing variation[45].

Pathogen recognition has been successfully achieved using Raman spectroscopy without surface enhancement[89, 90, 95, 96, 99, 102, 110, 117, 142, 151, 156, 160, 176-178]. While this has frequently entailed pre-culture, pathogen classification has been achieved without the need for pre-culture[99, 117, 142, 160].

Hypothesis: Raman spectroscopy can provide rapid UTI diagnosis and bacterial classification without complex physical processing or surface enhancement.

Objectives:

- Measure and observe the Raman spectra of common uropathogens, identifying descriptive peaks and areas of variability.
- Define the limit of detection for unenhanced Raman spectroscopy to identify uropathogens.
- Assess the Raman spectrum of urine, with significant peaks and spectral variability.

5.2 RAMAN SPECTROSCOPY OF CLINICAL URINE SPECIMENS

5.2.1 INTRODUCTION

Raman spectroscopy is a powerful chemometric technique which utilises the inelastic scattering of light to provide immediate chemical analysis. Raman spectroscopy has been applied to urine samples to provide rapid chemometric urinalysis with success in quantifying common urinary metabolites without the need for complex physical processing or surface enhancement [179-182]. *McMurdy et al.* demonstrated Raman spectroscopy could accurately quantify urinary creatinine levels without physical processing of urine[183]. *Moreira et al.* quantified urinary concentrations of urea, creatinine, ketone bodies, phosphate and other nitrogenous in healthy volunteers, successfully differentiating levels in physically active participants as compared to sedentary participants[180]. Raman urinalysis was extended to clinical assessments by *Cassiano et al.* who quantified urea and creatinine concentrations as a method for chronic kidney disease (CKD) screening, although these measurements were acquired from healthy controls only[182]. *De Sousa et al.* performed Raman urinalysis on a patient population at risk of CKD due to concomitant hypertension and diabetes mellitus, quantifying urinary urea, creatinine and glucose[179]. The urinary metabolites in these studies provide for relatively simple Raman identification as they are strong Raman scatterers and are present in high concentrations.

Raman urinalysis has similar potential to identify urinary metabolites present in lower concentrations and with weaker Raman signal. *Guimarães et al.* demonstrated a role for Raman spectroscopy to identify performance enhancing drugs in athletes by detecting trace level of ephedrine in urine from healthy controls[184]. *Huttanus et al.* classified urine samples from healthy control, patients with CKD and sufferers of bladder cancer using Raman spectroscopy, identifying bladder cancer with 80.4% accuracy[185]. This work also highlighted that sensitivity and specificity can be optimised according to clinical need by varying the number of PCs passed to the classification algorithm.

Raman spectroscopy has similarly been used to identify bacteria without the need for surface enhancement, complicated pathogen capture methods, or Raman microscopes[95, 96, 102, 110, 176, 177]. Earlier Raman work made use of ultraviolet Raman resonance (UVRR) to enhance signal without the SERS or bacterial isolation[95, 96, 177]. This technique fell out of favour due to superior enhancement provided by SERS. *Kastanos et al.* classified three common uropathogens using a handheld Raman spectrometer with 94% accuracy[156]. *Oliviera et al.* identified successfully classified uropathogens with 83% accuracy[110]. Notably, these successes were attained from pathogens suspended in simple fluids and not in urine

The potential of Raman spectroscopy to identify uropathogens directly from unprocessed urine without SERS has not been investigated.

Hypothesis: Raman spectroscopy can differentiate infected from uninfected clinical samples without physical processing.

5.2.2 METHODS

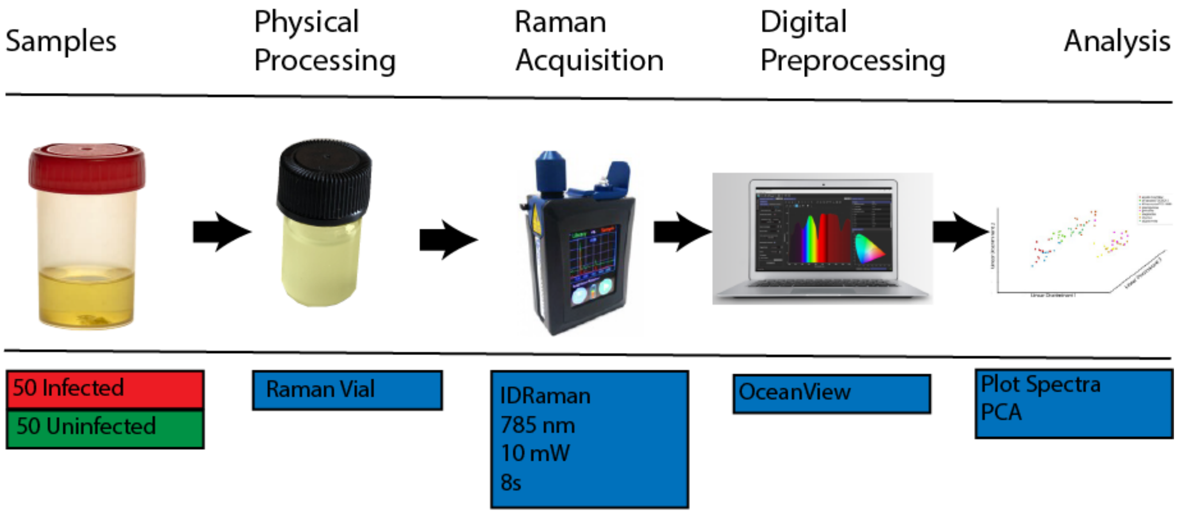

FIGURE 5. 1 METHODS FOR RAMAN SPECTROSCOPY OF CLINICAL SAMPLES. ONE HUNDRED CLINICAL SAMPLES WERE TRANSFERRED TO RAMAN VIALS FOR RAMAN ACQUISITION WITH THE IDRAMAN SPECTROSCOPE. DIGITAL PRE-PROCESSING WAS PERFORMED WITH THE OCEANVIEW DEFAULTS BEFORE ANALYSIS USING SPECTRAL PLOTS AND PCA PLOTS

5.2.2.1 SAMPLE PREPARATION

The methods used are summarised in **Figure 5.1**. One hundred clinical samples were acquired from North West London Pathology (NWLP) Microbiology Laboratory. An augmented convenience sample including 100 consecutive samples with a 1:1 ratio of infected to uninfected controls was used. Samples were processed according to NWLP standard operating procedures, initially screened with a Sysmex flow cytometer before plating all cells on chromogenic agar. After plating the samples were stored at 4 degrees Celsius, with all samples submitted for Raman analysis within 48 hours. Infected samples were defined as those with greater than 10^5 CFU/ml of one or more pathogens.

For Raman spectral capture urine samples were vortex mixed before pipetting 2ml into sterile borosilicate Raman vials. Raman spectra were captured using the IDRaman mini 2.0 handheld spectrometer with laser wavelength of 785 nm and power set 10 mW and a single acquisition of 8 seconds.

5.2.2.2 SPECTRAL ACQUISITION AND ANALYSIS

Spectra were captured and pre-processed using Oceanview software[166]. Analysis of processed spectra was performed using scripts developed in R programming language. Mean spectra with standard deviation ribbons were plotted for infected and uninfected controls. Unsupervised learning was performed using hierarchical cluster analysis and principal component analysis.

5.2.3 RESULTS

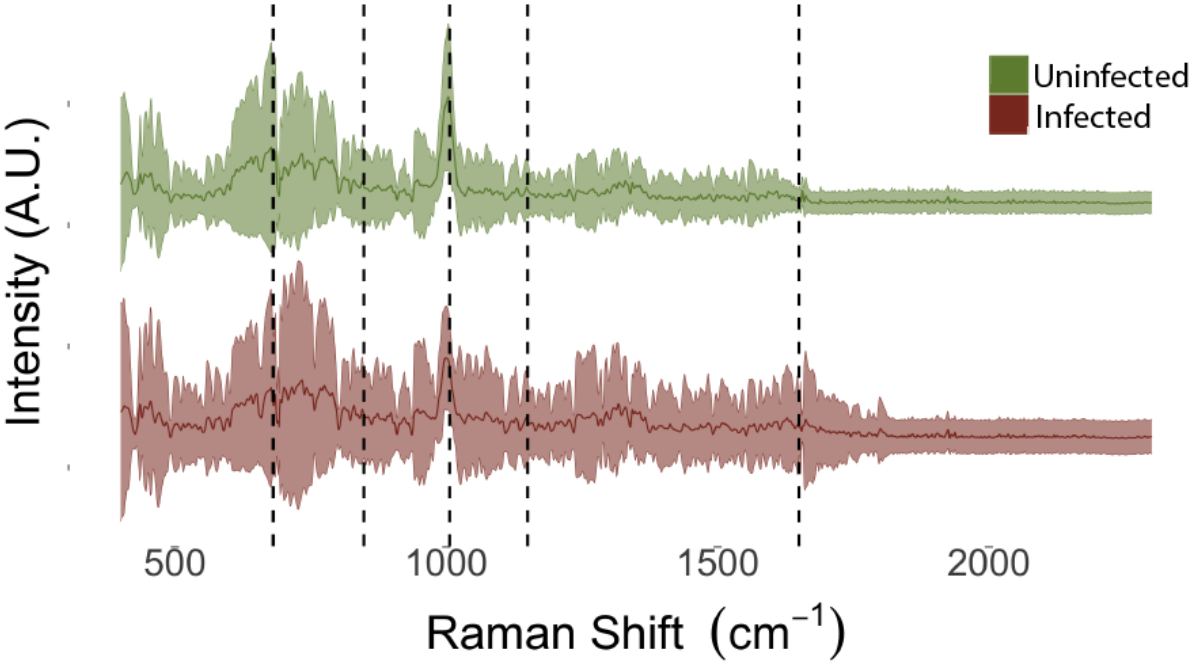

FIGURE 5. 2 MEAN SPECTRA WITH STANDARD ERROR RIBBONS FOR INFECTED (RED) AND UNINFECTED (GREEN) CLINICAL URINE SAMPLES. PEAKS ARISING FROM COMMON URINARY METABOLITES ARE EMPHASISED WITH VERTICAL DASHED LINES. THE SPECTRA DEMONSTRATE A HIGH DEGREE OF VARIABILITY DEPICTED BY WIDE STANDARD ERROR RIBBON PLOTS.

The unenhanced Raman spectra were acquired from 100 clinical comprised evenly of infected and uninfected samples. The mean spectra for infected and uninfected clinical urine samples are presented in **Figure 5.2**. Spectral variability is demonstrated by the standard error ribbon plots overlaid on the mean spectra for infected and uninfected samples. Notable peaks were identified by visual inspection and are assigned to likely origins in T**able 5.1**.

TABLE 5. 1 SPECTRAL BAND ASSIGNMENT FOR RAMAN PEAKS IN CLINICAL URINE SAMPLES

Raman Shift (cm^{-1})	**Band assignment**	**Reference**
681	Creatinine	[180]
848	Creatinine	[180, 182]
1006	Urea (NCN Stretching)	[180, 182]
1159	Urea (NH_2 Rocking)	[180, 182]
1650	Water (HOH bending)	[180]

Natural clustering of infected and uninfected samples was assessed with unsupervised learning through principal component analysis. The biplot of the first two principal components is presented in **Figure 5.3**.

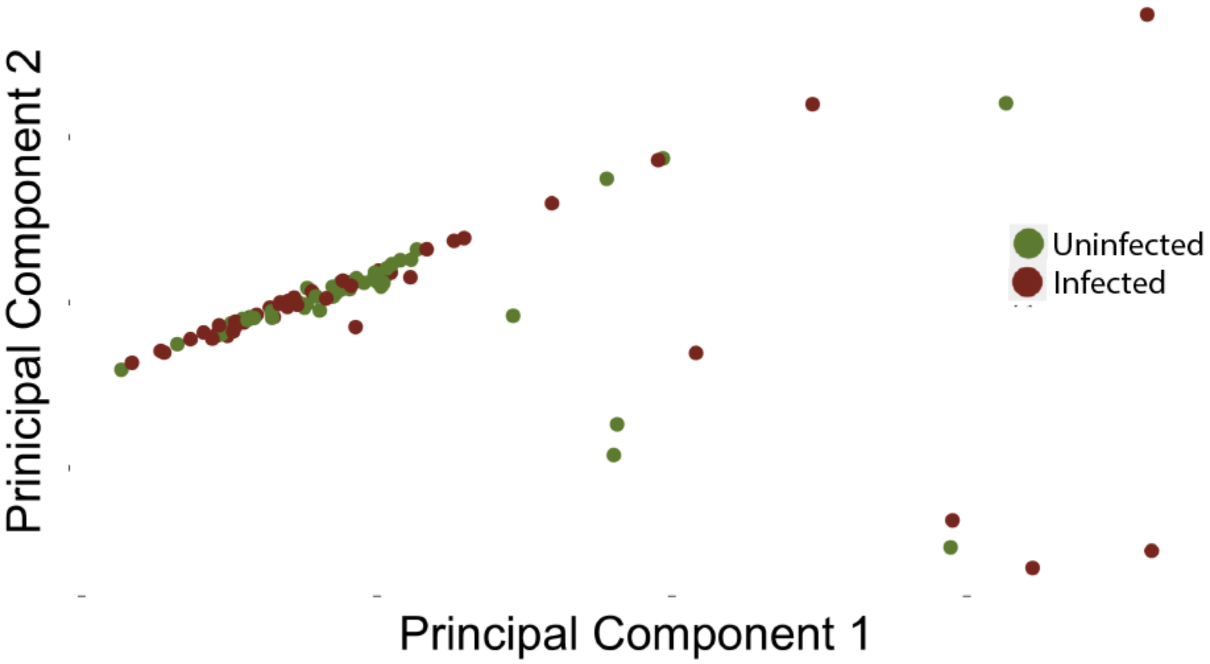

FIGURE 5. 3 PCA BIPLOT OF FIRST TWO PRINCIPAL COMPONENTS FOR CLINICAL URINE SAMPLES

5.2.3 DISCUSSION

In this work Raman spectroscopy was unable to differentiate infected clinical samples from uninfected clinical samples. This work demonstrates the substantial challenge of identifying uropathogens in clinical urine samples.

The spectra of both infected and uninfected samples (**Figure 5.2**) are dominated by 681, 848, 1006 and 1159 cm^{-1}, consistent with creatine and urea peaks demonstrated in other works. Smaller peaks reported in other works including 527 cm^{-1} (urea), 587 cm^{-1} (urea), 605 cm^{-1} (creatinine), 880 cm^{-1} (nitrogenous compounds), 907 cm^{-1} (creatinine, hydroxybutyrate, and acetoacetate), 983 cm^{-1} (phosphate), 1050 cm^{-1} (hydroxybutyrate and ketone bodies), 1079 cm^{-1} (amines), 1344 cm^{-1} (hydroxybutyrate), 1420 cm^{-1} (creatinine, acetoacetate, and 1456 cm^{-1} (hydroxybutyrate)[180]. It is likely these contribute to the substantial variation seen in both plots (ribbons).

This extreme variation is also likely to have completely obfuscated the weaker Raman signal from uropathogens, providing an explanation for the poor separation in the PCA plot (**Figure 5.3**). In addition to this, clinical samples are likely to have a range of uropathogen species and strains in varying concentrations[8], although certain cell components such as peptidoglycan would be expected to be present in all uropathogens[46].

Impaired classification using these spectra may potentially be attributed to suboptimal digital pre-processing and analysis. This is visible as retained high frequency noise across both sets of spectra **Figure 5.2**. A limitation of this study is that pre-processing was performed using the OceanView software accompanying the handheld spectrometer. Where successful discrimination of uropathogens have been achieved without SERS or complex physical processing, this has been done with careful pre-processing[96, 102, 110, 156, 176, 177].

This work emphasises the need for physical processing steps, not only to capture and aggregate pathogens, but importantly to separate these from urine to avoid fluorescence and competing signal. Numerous techniques including differential centrifugation, filtration and evaporation may be used for pathogen aggregation and separation from urine[186].

5.3 BACTERIAL RAMAN SPECTRA

5.3.1 INTRODUCTION

Raman spectroscopy has considerable benefits as a technique for pathogen identification and classification, notably the ability to provide classification without the need for biomass expansion provides for rapid pathogen identification[7, 76]. Numerous studies have performed bacterial identification and classification using Raman spectroscopy however most of these studies are augmented using SERS[69, 80, 82-84, 86, 88, 90, 96, 97, 102, 110, 123, 124, 149, 156, 157, 159-161, 169, 176-178, 187, 188]. The tremendous signal enhancement provided by SERS offset by some challenges that need to be accounted for: SERS substrates may be technically challenging to produce; the stability of SERS substrates needs to be considered; and importantly the strong distance relationship of enhancement necessitates close apposition, failing which massive variation is induced[7, 72, 80]. Pathogen classification in these studies is mediated by a number of cell components **(Table 5.2)**

Achieving pathogen classification without requiring surface enhancement may therefore may counterintuitively provide less complexity in Raman mediated pathogen classification. Raman spectroscopic pathogen classification without SERS has been achieved or the need for complex aggregation methods ([90, 96, 99, 102, 110, 117, 156, 160, 176-178, 189]. Many of these studies did however work with cultured pathogens.

UVRR was used to provide signal enhancement in earlier studies[96, 176, 177]. UVRR provides for enhancement of chemical components whose vibrational frequency is similar to the excitation frequency, typically nucleosides and aromatic amines[177]. Additionally, less fluorescence is seen with UVRR[96, 177]. UVRR has certain limitations, including a higher cost for the lasers[82]. Photons of ultraviolet wavelengths have higher energy, and so methods are required to reduce photodestruction, such as a revolving samples stage[96]. A potential further drawback of UVRR is that the narrow region of enhancement means learning is based on relatively few chemical components and so may not generalise well. *Dalterio et al.* used a 242 nm wavelength laser and achieved high resolution spectra with visible difference for multiple pathogens. Classification performance was not quantified.[177]. *Jarvis et al.* acquired Raman spectra from 20 clinical isolates of four different uropathogens. Similarly high-resolution spectra which provided excellent clustering and separation on PC-DFA.[96]

Harz et al. achieved classification accuracy of 95.7% for 5 common meningitis pathogens using a Raman microscope, both from culture suspension and clinical samples with physical pre-processing limited to simple airdrying after spotting on a silica chip[178]. While the work did not involve complex physical processing or preculture, it did use a Raman microscope rather than a handheld spectrometer. Raman microscopes significantly improve spectral quality as a result of the narrow focal volume (down to 1 μm), effectively excluding background signal. Raman microscopes are however expensive, and require technical expertise to focus on pathogens[69, 88, 100].

Oliviera et al. achieved 83.5% accuracy classifying of 7 different reference strain uropathogens, with physical processing limited to spotting and airdrying on aluminium foil[110]. *Kastanos et al.* achieved 94% classification accuracy for 3 common uropathogens from clinical isolates using a handheld spectrometer[69, 156]. The isolates were suspended in PBS in Raman vials, with no further physical processing performed[156]. The pathogen load is, however, not stated in this work, and so may not be reflective of clinical samples. These two papers demonstrate pathogens can be accurately classified without complex physical processing, SERS or Raman microscopes.

TABLE 5. 2 SPECTRAL BAND ASSIGNMENTS FROM PUBLISHED WORKS ATTEMPTING PATHOGEN CLASSIFICATION WITHOUT PHYSICAL PROCESSING, SERS OR RAMAN MICROSCOPY

Paper	**Band (cm^{-1})**	**Assignment**	**reference**
Jarvis et al.	1172	Tyrosine	[96]
Jarvis et al.	1247	Guanine, adenine uracil	[96]
Jarvis et al.	1324	Adenine, guanine Tyrosine	[96]
Jarvis et al.	1475	Guanine, adenine	[96]
Jarvis et al.	1524	cytosine	[96]
Jarvis et al.	1567	Guanine and adenine	[96]
Jarvis et al.	1607	Tyrosine, Tryptophan	[96]
Oliviera et al.	538	Glycosidic ring deformation	[110]
Oliviera et al.	624	Tryptophan	[110]
Oliviera et al.	645	Tyrosine	[110]
Oliviera et al.	672	Valine	[110]
Oliviera et al.	726	Adenine, peptidoglycan	[110]
Oliviera et al.	759	Tryptophan	[110]
Oliviera et al.	784	Cytosine	[110]
Oliviera et al.	814	RNA binding	[110]
Oliviera et al.	829	Tyrosine	[110]
Oliviera et al.	857	Saccharides, protein, teichuronic acid	[110]

Hypothesis: Uropathogens have distinct Raman spectra that may be used for bacterial classification.

Objectives:

- Capture the Raman spectra for common uropathogens using reference strain bacteria.
- Describe the contributory peaks of uropathogen Raman spectra.
- Assess the classification performance of unenhanced Raman spectroscopy on uropathogens.

5.3.2 METHODS

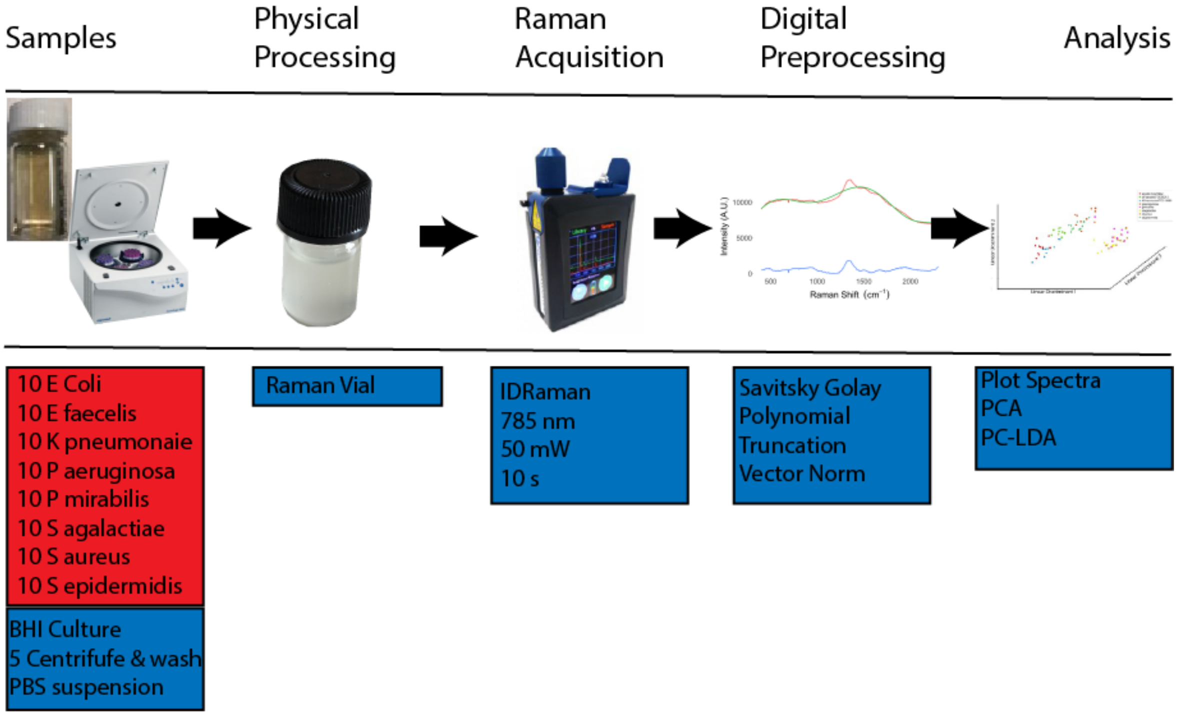

FIGURE 5. 4 METHODS FOR RAMAN ASSESSMENT OF CONCENTRATED SUSPENSIONS. SAMPLE WERE PREPARED BY CULTURE OF REFERENCE STRAIN PATHOGENS SUBSEQUENTLY CENTRIFUGED AND WASHED 5 TIMES. THE SUSPENSIONS WERE TRANSFERRED UNPROCESSED TO RAMAN VIALS FOR RAMAN ACQUISITION USING THE IDRAMAN SPECTROMETER. THE SPECTRA WERE PRE-PROCESSED BY SAVITSKY-GOLAY FILTERING, POLYNOMIAL SUBTRACTION AND VECTOR NORMALISATION. SPECTRA WERE PLOTTED AND ANALYSED USING PC-LDA

5.3.2.1 SAMPLE PREPARATION

The methods employed are summarised in **Figure 5.4.** For each uropathogen 10 samples were prepared for Raman assessment. To prepare a sample, a single bead from the established reference bank was transferred from a Microbank cryopreservation vial into 10 ml of brain-hart infusion broth and cultured for 24 hours at 37 degrees Celsius. The culture broth was then vortex mixed and subsequently centrifuged at 3350 g for 10 minutes. The supernatant was discarded, and the bacterial pellet resuspended in 2 ml of PBS by Vortex mixing. This suspension was then centrifuged at 8300 g for 1 minute. The supernatant was discarded, and the bacterial pellet resuspended in 2ml PBS by Vortex mixing. This centrifuge and washing process was repeated a total of 5 times. The resulting heavy suspension was not further diluted.

5.3.2.2 SPECTRAL ACQUISITION AND ANALYSIS

The suspension was transferred to a sterile borosilicate Raman vial for spectral acquisition. Spectra were captured using the IDRaman mini 2.0 handheld Raman spectrometer with a laser wavelength of 785 nm and power of 50mW with acquisition time of 10 seconds. An average of 18 spectra, totalling 3 minutes acquisition, was captured for each sample.

Pre-processing and spectral analysis were performed using scripts developed in R programming language. Spectra were smoothed with a 3rd order Savitsky-Golay filter over 19 cm^{-1} moving window. Baseline correction was achieved by subtraction of a 9th order polynomial before truncation to 600-2000cm^{-1}. The spectra were vector normalised. Mean spectra with standard deviations were plotted for each pathogen. PC-LDA was used for supervised learning, with the number of components selected by parsimonious LOOCV. For assessment of spectral peaks contributing to bacterial classification all spectra were centred and scaled using all other species, with plots of the mean and standard deviation.

5.3.3 RESULTS

5.3.3.1 RAMAN SPECTRA OF UROPATHOGENS

The mean Raman spectra of the reference strain uropathogens are plotted in **Figure 5.5**, with spectral variability demonstrated by standard error ribbon plots. The spectra demonstrate a significant baseline incompletely accounted during pre-processing, as evidenced by consistent broad peaks. Despite incomplete baseline removal during pre-processing, the spectra demonstrate clear narrow deviations from the baseline which vary between uropathogen species. Notably, the very narrow standard error ribbons indicate consistency of Raman spectra within species.

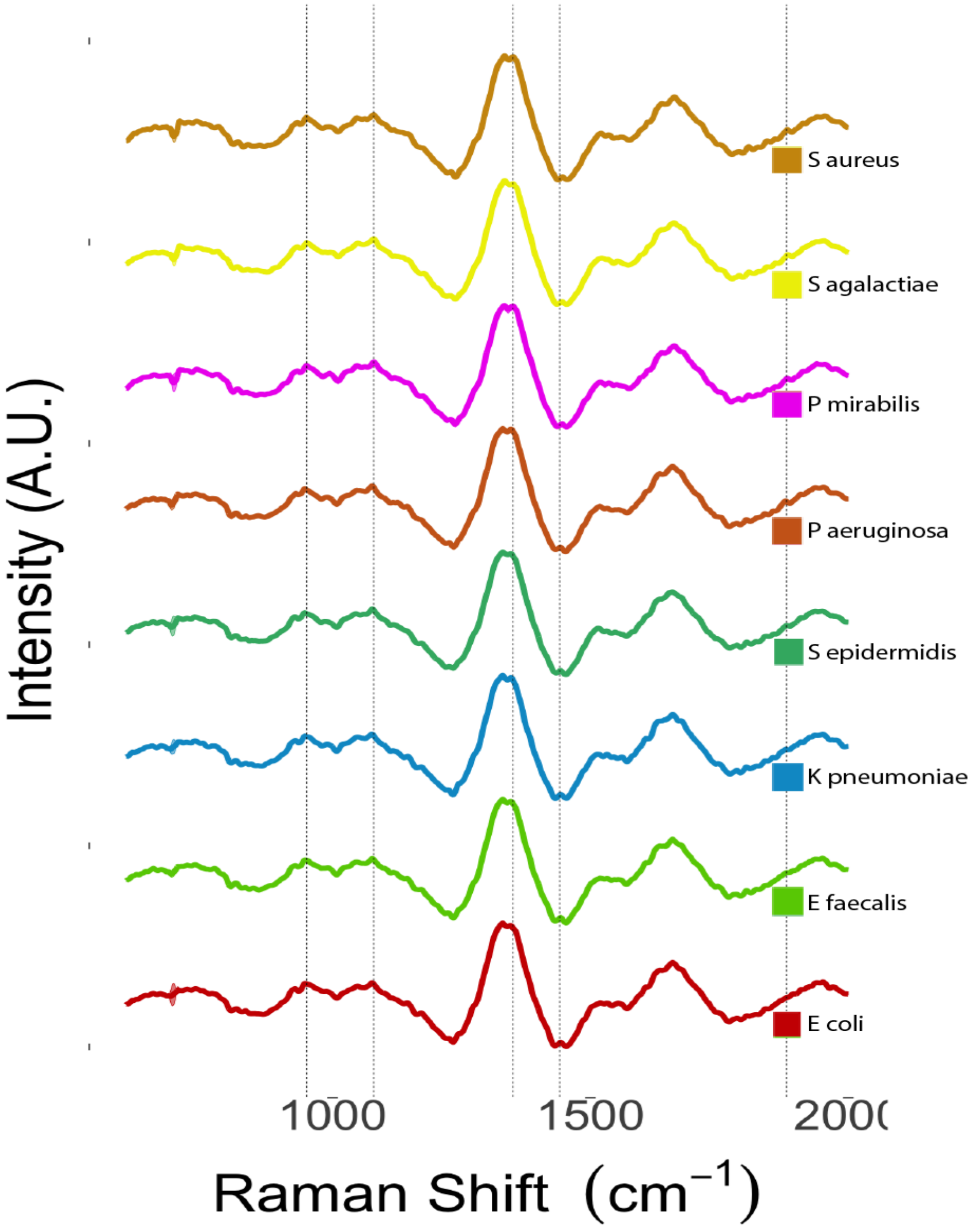

FIGURE 5. 5 RAMAN SPECTRA OF REFERENCE STRAIN PATHOGENS IN SUSPENSION

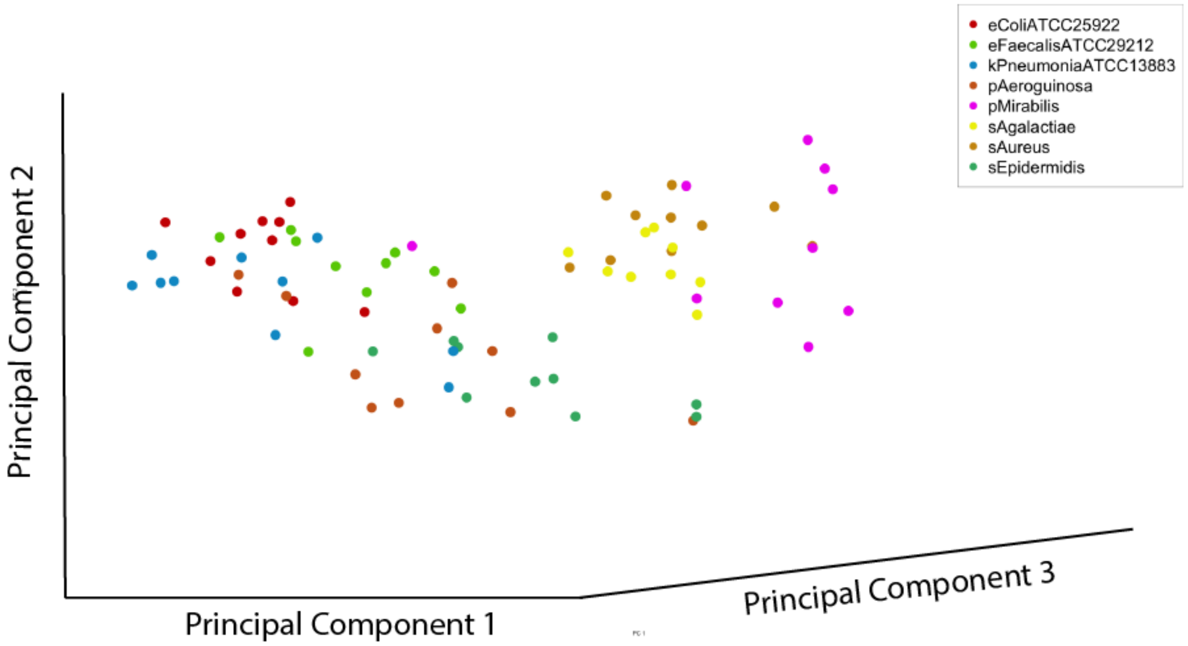

FIGURE 5. 6 PCA PLOT OF ALL BACTERIAL SUSPENSIONS

5.3.3.2 SPECTRAL CLASSIFICATION

Unsupervised learning was performed using PCA. **Figure 5.6** presents the PCA plot of the first 3 principal components with all suspensions included. This PCA plot demonstrates a degree of clustering of the Raman spectra by uropathogen. However, the relatively high number of different uropathogens included results in cluster overlap. Limiting the number different uropathogens included in PCA assessment (**Figure 5.7**) allows for easier visualisation of clusters.

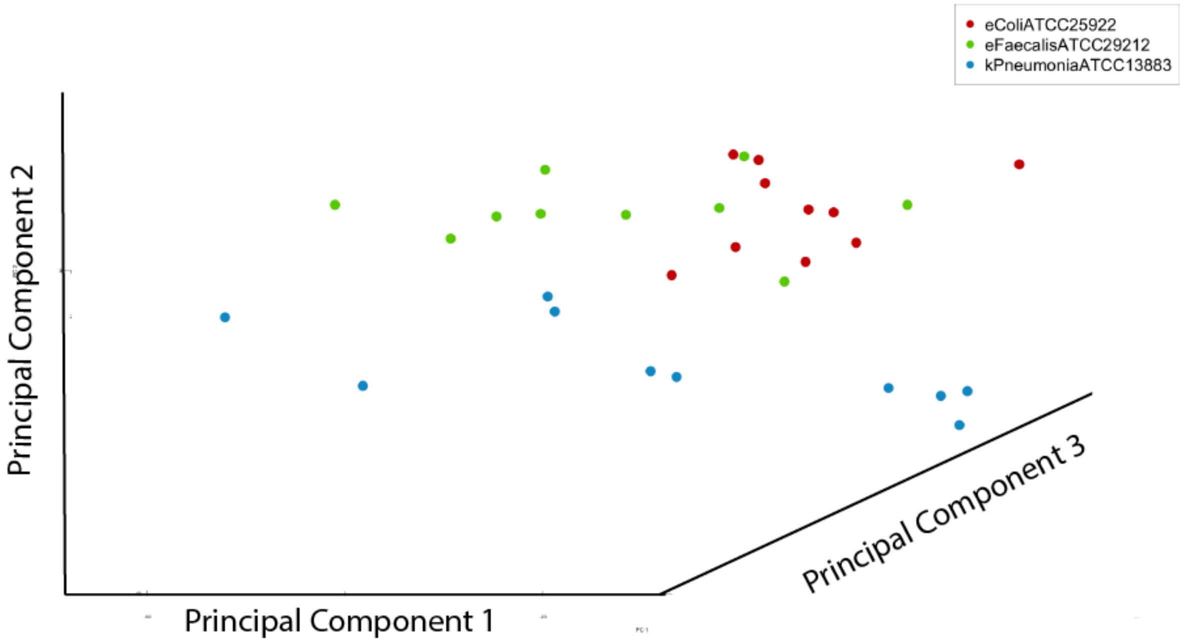

FIGURE 5. 7 PCA PLOT INCLUDING A LIMITED NUMBER OF PATHOGENS

Supervised learning was performed through PC-LDA. **Figure 5.8** plots the first 3 linear discriminants for the Raman spectra of the reference pathogen suspensions. **Table 5.3** demonstrates the classification of the suspensions, while T**able 5.4** summarises the classification performance.

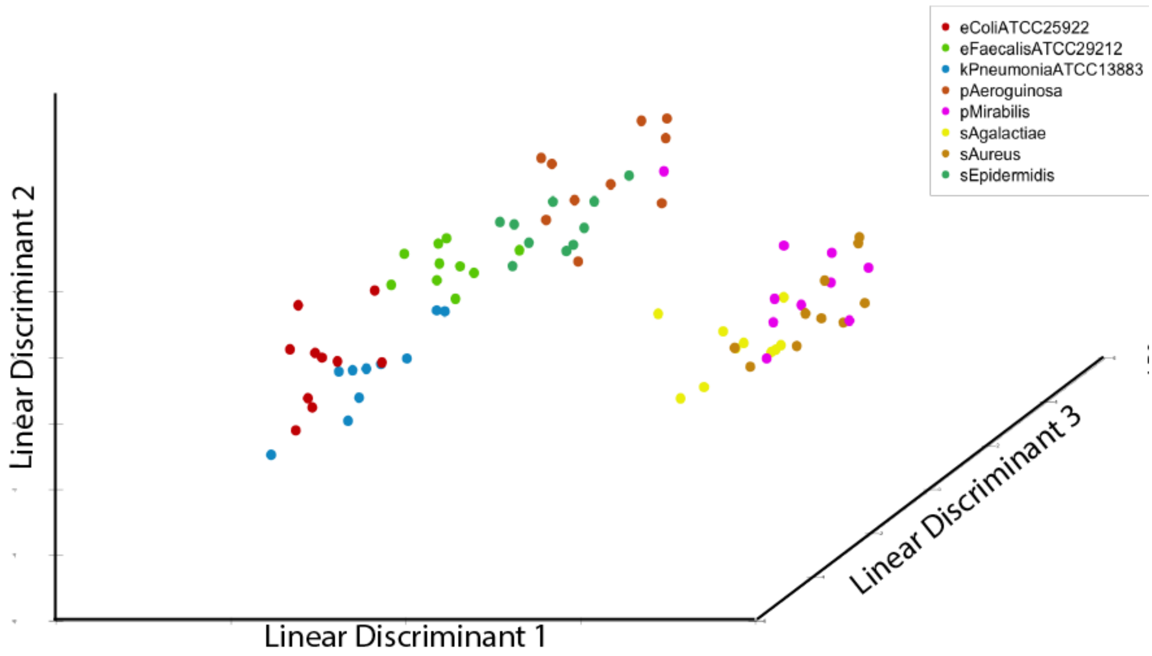

FIGURE 5. 8 PC-LDA PLOT FOR BACTERIAL SUSPENSIONS

TABLE 5. 3 SUSPENSION PC-LDA CLASSIFICATION

	Predicted								
Actual		***E. coli***	***E. faecalis***	***K. pneumoniae***	***P. aeruginosa***	***P. mirabilis***	***S. agalactiae***	***S. aureus***	***S. epidermidis***
	E. coli	10	0	0	0	0	0	0	0
	E. faecalis	0	10	0	0	0	0	0	0
	K. pneumoniae	0	0	10	0	0	0	0	0
	P. aeruginosa	0	0	0	9	0	0	0	1
	P. mirabilis	0	0	0	0	8	0	0	0
	S. agalactiae	0	0	0	0	0	10	0	0
	S. aureus	0	0	0	0	1	0	10	0
	S. epidermidis	0	0	0	1	1	0	0	9

The PC-LDA plot demonstrates clustering of the pathogens by their Raman spectra, however similarly to the PCA plot, the relatively high number of different pathogens included leads to some apparent overlap of the clusters. Quantitatively, the pathogen spectra are classified with 95.0% (95% CI: 87.7-96.6%; p-value <0.001) overall accuracy, with no pathogen having less than 80% classification accuracy.

TABLE 5. 4 PERFORMANCE OF PC-LDA CLASSIFICATION

	Accuracy	**Sensitivity**	**Specificity**
Total	95.0% (95%CI: 87.7-96.6%; p-value <0.001)		
E. coli	100%	100%	100%
E. faecalis	100%	100%	100%
K. pneumoniae	100%	100%	100%
P. aeruginosa	90%	98.6%	95.0%
P. mirabilis	80%	100%	80%
S. agalactiae	100%	100%	100%
S. aureus	100%	98.6%	100%
S. epidermidis	90%	97.1%	90%

5.3.3.3 SPECTRAL BAND ASSIGNMENT

Pairwise comparison, by centring and scaling each uropathogen strain referenced against all other strains, was used to assess spectra differences. These centred and scaled spectra are plotted in **Figure 5.9** with standard error ribbons. Dashed lines indicate where individual bands are significantly different with 95% confidence. These plots demonstrate that within this set, all pairwise comparisons can be differentiated by one or more peaks. The point of greatest relative difference for each comparison is presented in **Table 5.5**, with putative band assignments.

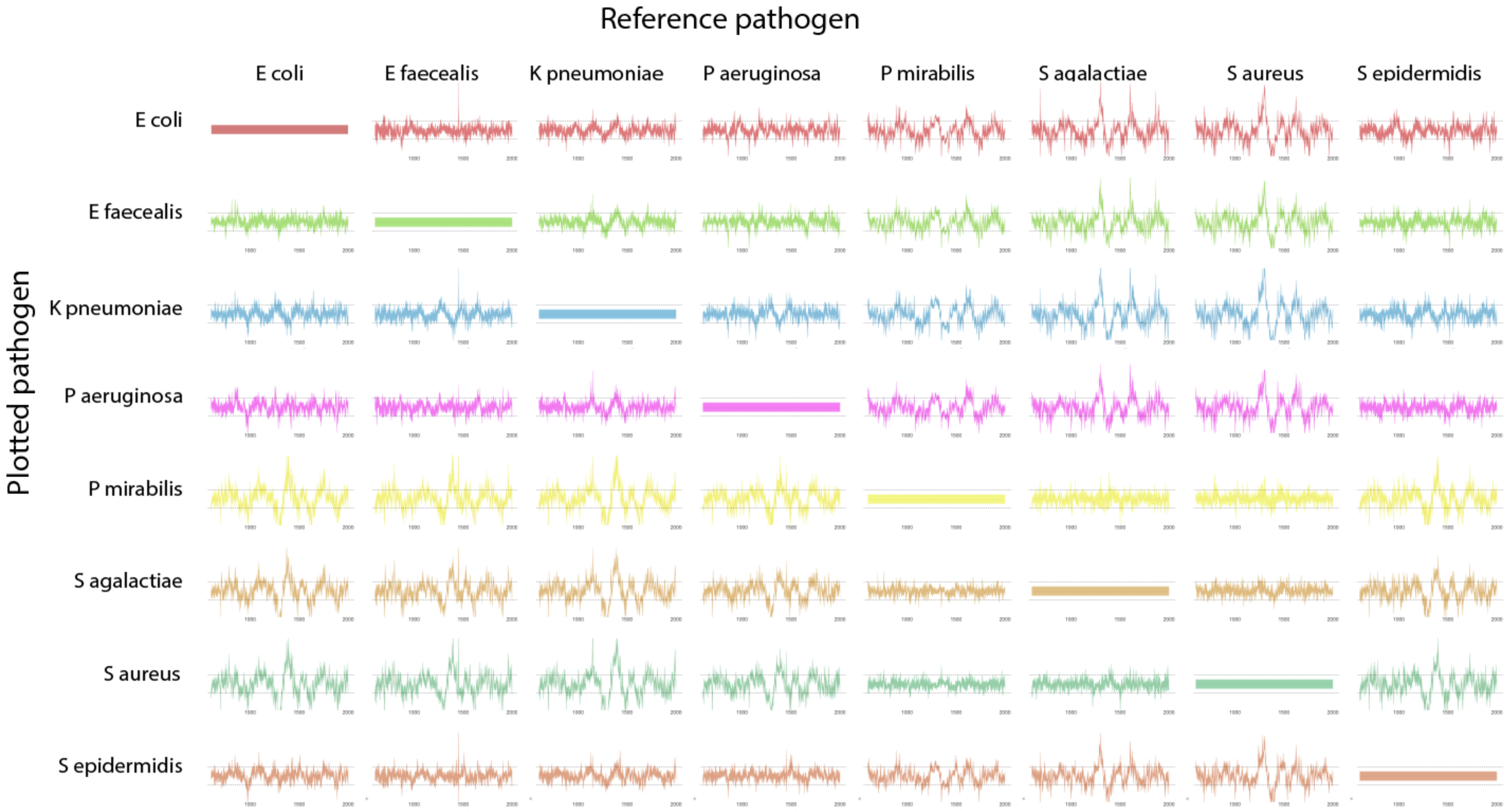

FIGURE 5. 9 PAIRWISE COMPARISON OF UROPATHOGEN SPECTRA PERFORMED BY CENTRING AND SCALING SPECTRA

TABLE 5. 5 SPECTRAL BAND ASSIGNMENT FOR PEAKS OF MAXIMAL DIFFERENCE IDENTIFIED IN REFERENCE STRAIN PATHOGENS

Reference Bacteria	**Bacteria**	**Raman Peak**	**Relative difference**	**Band assignment**	**Reference**
E. coli	*A faecalis*	812	3.1	RNA Binding	[110]
	K. pneumoniae	1253	3.2	Amide III	[117]
	S epidermidis	974	5.1	Protein backbone	[190]
	P. aeruginosa	974	4.7	Protein backbone	[190]
	P. mirabilis	1288	14.1	Cytosine, Nucleic acids	[190]
	S. agalactiae	1288	13.7	Cytosine, Nucleic acids	[190]
	S. aureus	1288	15.3	Cytosine, Nucleic acids	[190]
E. faecalis	*E. coli*	1453	4.5	Lipid and Protein - CH2 &CH3 deformation	[99, 110]
	K. pneumoniae	1453	6.5	Lipid and Protein - CH2 &CH3 deformation	[99, 110]
	S. epidermidis	1453	4.4	Lipid and Protein - CH2 &CH3 deformation	[99, 110]
	P. aeruginosa	1666	3	Amide I, Alkene stretching, Nucleic acids	[99, 190]
	P. mirabilis	1453	13.1	Lipid and Protein - CH2 &CH3 deformation	[99, 110]
	S. agalactiae	1453	8.2	Lipid and Protein - CH2 &CH3 deformation	[99, 110]
	S. aureus	1396	9.5	C=O stretching	[190]
K. pneumoniae	*E. coli*	1400	2.2	Amino acids (Glutamic and aspartic acid)	[190]
	E. faecalis	1400	2.8	Amino acids (Glutamic and aspartic acid)	[190]
	S. epidermidis	1126	3.1	Cytochrome C, Disaccharides	[99, 190]
	P. aeruginosa	1147	4.9	Guanosine, carotenoids	[149, 190]
	P. mirabilis	1385	9	CH3	[149, 190]
	S. agalactiae	1293	8.6	Cytosine, Nucleic acids	[110, 190]
	S. aureus	1148	10.6	Guanosine, carotenoids	[149, 190]
S. epidermidis	*E. coli*	1516	5.3	Cytosine, Carotenoids	[158, 190]
	E. faecalis	1516	4.2	Cytosine, Carotenoids	[158, 190]
	K. pneumoniae	1133	3.7	Lipids, Saccharides, phospholipid, cytochrome C	[110, 158, 190]
	P. aeruginosa	1515	2.9	Cytosine, Carotenoids	[158, 190]
	P. mirabilis	1401	7.7	Amino acids (Glutamic and aspartic acid)	[190]
	S. agalactiae	1291	7.4	Cytosine, Nucleic acids	[110, 190]
	S. aureus	1401	8.9	Amino acids (Glutamic and aspartic acid)	[190]
P. aeruginosa	*E. coli*	859	4.3	Proline, Tyrosine, phosphate	[110, 190]
	E. faecalis	859	4.4	Proline, Tyrosine, phosphate	[110, 190]
	K. pneumoniae	859	4	Proline, Tyrosine, phosphate	[110, 190]

	S. epidermidis	1508	3.2	Cytosine, Adenine	[190]
	P. mirabilis	1293	7.6	Cytosine, Nucleic acids	[110, 190]
	S. agalactiae	1294	8	Cytosine, Nucleic acids	[110, 190]
	S. aureus	1294	8.4	Cytosine, Nucleic acids	[110, 190]
P. mirabilis	*E. coli*	1350	5.2	Protein deformation	[101]
	E. faecalis	1734	5	Lipids	[190]
	K. pneumoniae	1734	5.8	Lipids	[190]
	S. epidermidis	1351	4.7	Protein deformation	[101]
	P. aeruginosa	1734	4.9	Lipids	[190]
	S. agalactiae	1119	2.1	Ribose, carbohydrates	[101, 190]
	S. aureus	763	2	Tryptophan	[110, 190]
S. agalactiae	*E. coli*	1301	10.6	Lipids	[99, 190]
	E. faecalis	1604	8.6	Phenylalanine, Tyrosine, Tryptophan	[96, 99, 158]
	K. pneumoniae	1301	12.1	Lipids	[99, 190]
	S. epidermidis	1301	8.3	Lipids	[99, 190]
	P. aeruginosa	1301	7.7	Lipids	[99, 190]
	P. mirabilis	1503	2.9	Cytosine, Adenine	[190]
	S. aureus	1503	3.8	Cytosine, Adenine	[190]
S. aureus	*E. coli*	1301	9	Lipids	[99, 190]
	E. faecalis	1305	7.7	Lipids	[99, 190]
	K. pneumoniae	1301	10.1	Lipids	[99, 190]
	S. epidermidis	1298	7.4	Lipids	[99, 190]
	P. aeruginosa	1305	7.4	Lipids	[99, 190]
	P. mirabilis	793	2.7	Cytosine, Thiamine	[117]
	S. agalactiae	1400	2.5	Amino acids (Glutamic and aspartic acid)	[190]

5.3.4 DISCUSSION

Uropathogens are demonstrated in this work to have unique Raman spectra which may be used for pathogen identification and classification. The 7 reference strain uropathogens were classified with 95.0% accuracy. This is comparable with other published work that attempted pathogen classification using Raman spectroscopy without complex physical processing, SERS enhancement or the use of Raman microscopy[96, 110, 156].

Kastanos et al. achieved 94% classification of 3 common uropathogens, and with a similar sized dataset (75 samples as compared to 70 in this work)[156]. Given the fewer number of classes it would have been expected their work may have delivered superior accuracy. Their work used a novel, and not widely adopted, method of spectra band ratios to process the spectra, which may explain the classification performance. Unfortunately, this method does not generate spectra or spectral band assignments, limiting comparability[156].

Oliviera et al. achieved 83.5% classification accuracy from 7 different uropathogens[110]. The sample set was considerably smaller (38 samples) and used clinical isolates which may explain the lower classification accuracy seen here. Despite the use of clinical isolates in their study, many of the spectral bands used for classification were the same here and in their work, therein providing a mechanistic validation[110].

Notably, the contributory spectral bands seen in the work by *Jarvis et a*l. played little role in the classification seen in this work[96]. This is explained by enhancing effect of UVRR, leading to the dominance in their spectra of bands associated with nucleosides and aromatic amino acids. Without enhancement through UVRR, the spectra in this work arise indiscriminately from the entire pathogen (and surrounding solution), and so the descriptive peaks arise from a broader range of components[96].

This demonstrates a challenge of spectral band assignment for pathogens, particularly when using handheld spectrometers and without the benefit of enhancement through SERS or UVRR. Raman spectroscopy is a high-resolution technique, and while each biologic component will have a unique Raman spectrum, the final spectrum is the sum of these overlapping spectra. This may explain the many components identified to have contributed to pathogen classification. This challenge is amplified by the used of spectrometers which have lower spectral resolution (IDRaman has a resolution of 12cm^{-1} as compared to many microscopes that have a resolution of 2cm^{-1} [166]). Similarly, enhancement through SERS or UVRR is likely to allow classification to be based on few, more descriptive chemical components (such as cell envelope components). The dispersion of significant bands seen in this work, explains both the lack of grossly visible spectral peaks on the mean Raman spectra, as well as the need for supervised learning methods to gain classification.

The use of heavy suspensions in this experimental work, and in other published works, provide for a relatively simplified classification challenge as the weak biologic signal is overcome by the increased pathogen load. Nonetheless, demonstrating the descriptive potential of these Raman spectra is relevant, for multiple reasons: It confirms Raman spectroscopy is technology that may be applied to pathogen classification and identification; the considerably lower pathogen load of clinical samples may be circumvented by methods to capture and aggregate them, ranging from simple methods such as centrifugation or evaporation to considerably more complex approaches including optical tweezer or dielectrophoresis; and finally understanding the descriptive bands here may allow for more targeted analysis of bands with higher SNR, to improve classification performance.

5.4 PROLONGED ACQUISITION TIME RAMAN SPECTRA FOR CLASSIFICATION

5.4.1 INTRODUCTION

Uropathogens are demonstrated to have unique Raman spectra that allows for classification. Demonstrating this, however, has most frequently been achieved through preculture to massively expand biomass, therein delivering considerable signal enhancement relative to that expected in unprocessed clinical samples. A crucial strength of Raman spectroscopy however lies in its ability to acquire definitive spectra without then need for prior biomass expansion[7, 76]. Multiple studies have achieved uropathogen classification using technologies not reliant on preculture. Gaining this accurate classification in these studies was contingent on employing a diverse set of technologies to capture and aggregate the uropathogens.

Schroder et al. achieved 100% classification accuracy in training set of *Escherichia coli* and *Enterococcus faecalis* spectra and over 99% accuracy on spectra from 3 patients [117]. While limit of detection is not interrogated, the technology was validated on clinical samples. Pathogen aggregation was achieved using a dielectrophoresis chip that used the electrostatic forces to aggregate the negatively charged pathogens in the centre. Raman spectra were acquired with a Raman microscope[117].

In other work, *Schroder et al.* captured *Escherichia coli* and *Enterococcus faecalis* from suspension and captured spectra similar to those acquired using their dielectrophoresis chip[160] . Supervised learning was not performed and so classification and limit of detection were not interrogated. Aggregation was achieved with a microfluidic chip that used centrifugal force to capture pathogens ahead of Raman acquisition using a Raman microscope. The authors report these chips can simultaneously process 4 samples and are amenable to mass production[160].

Pahlow et al. achieved 90% classification of amongst 5 different bacterial species which are known to cause UTIs [142]. A limit of detection of $5x10^3$ CFU/ml was achieved. Pathogen aggregation was achieved through immunocapture: antibodies against lipopolysaccharide and lipoteichoic acid (for Gram negative and positive bacteria) were immobilised onto specialised aluminium chips [142]. Pathogen suspensions were incubated on the chip for 10 minutes before washing with PBS. Raman spectra were captured with a Raman microscope[142].

Kloss et al. achieved 92% classification accuracy amongst 11 different reference uropathogen species, and correctly identified 10 out of 10 clinical isolates of *Escherichia coli* and *Enterococcus faecalis* [99]. A limit of detection of 10^3 CFU/ml was reported. Pathogen aggregation was performed, without specialized equipment, by centrifuge and washing in PBS before air drying on nickel foil [99]. Raman spectra were acquired using a Raman microscope[99].

While the earlier work performed by *Schroder et al.* may appear too complex for mass adoption, these other works use physical processing technologies that are either widely available or amenable to mass production[99, 117, 142, 160]. Central to all these technologies, however, is the use of a Raman microscope for spectral acquisition. Raman microscopes have a significant benefit in that focal volumes as low as 1 cubic μm may be used, effectively excluding competing and background signal. However, their cost and large physical footprint limit their feasibility for clinical use[88, 100].

None of the published work has assessed the potential of Raman spectrometry to identify and classify uropathogens without the aid of microscopy or SERS at clinically relevant concentrations. Attempting pathogen recognition under these constraints requires cognisance that considerably lower pathogen loads will provide significantly lower SNR, and so further physical processing may be required to increase concentrations or improve pathogen signal. Increased acquisition time was demonstrated in **Section 4.2** to improve SNR by reducing cosmic spikes and high frequency noise.

Hypothesis: Prolonged acquisition during Raman spectra acquisition of uropathogen suspensions will allow for diagnosis and classification at clinically relevant concentrations.

Objectives:

- Describe the diagnostic and classification performance of unenhanced Raman spectroscopy on pathogens in suspension at clinically relevant concentrations (10^5CFU/ml).
- Identify if prolonged acquisition of Raman spectra from uropathogens at clinically relevant concentrations improved diagnostic and classification accuracy.
- Identify if augmentation through higher pathogen loads or targeted analysis can improve diagnostic performance.

5.4.2 METHODS

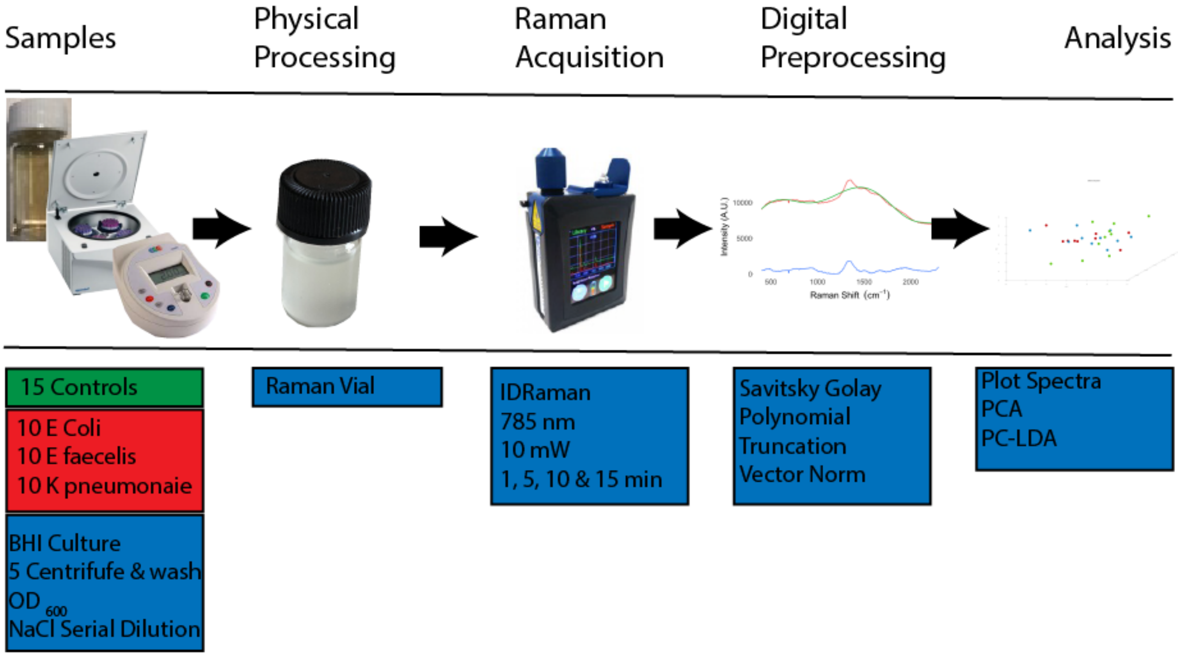

FIGURE 5. 10 METHODS FOR PROLONGED RAMAN ACQUISITION STUDY. 45 SAMPLES INCLUDED 30 REFERENCE STRAIN PATHOGENS AND 15 NEGATIVE CONTROLS. PATHOGENS WERE CULTURED IN BHI, THEN CENTRIFUGED AND WASHED 5 TIMES, BEFORE DILUTION BY OD_{600} AND SERIAL DILUTION IN SALINE TO VARYING PATHOGEN LOADS. SAMPLES WERE TRANSFERRED TO RAMAN VIALS. SPECTRA WERE ACQUIRED WITH THE IDRAMAN IN 30 SECOND INCREMENTS UP TO 15 MINUTES. SPECTRA WERE PRE-PROCESSED BY SAVITSKY-GOLAY FILTERING, POLYNOMIAL SUBTRACTION AND VECTOR NORMALISATION. ANALYSIS FOR ALL COMBINATIONS OF PATHOGEN LOADS AND ACQUISITION TIMES INCLUDED SPECTRAL PLOTS, PCA AND PC-LDA.

5.4.2.1 SAMPLE PREPARATION

The methods employed are summarised in **Figure 5.10.** The study population consisted of 10 samples each of 3 reference strain uropathogens in addition to 15 negative controls. For each sample, a single Microbank bead from the reference bank was cultured in 3ml of brain-heart infusion broth for 24 hours at 37 degrees. The culture broth with uropathogens was vortex mixed and 2 ml transferred to a sterile centrifuge tube. The resulting suspension was centrifuged at 8300 g for 5 minutes, after which the supernatant was discarded, and the remaining pellet resuspended in 0.85% saline by Vortex mixing. The centrifuge and washing process was repeated a total of 5 times. The resulting suspension was diluted by OD_{600} to a concentration of 10^8 CFU/ml, and then serially diluted such that each sample yielded suspensions of 10^7, 10^5 and 10^3 CFU/ml.

5.4.2.2 SPECTRAL ACQUISITION AND ANALYSIS

Raman spectra were acquired from each bacterial load of all samples. Two millilitres of the suspension were transferred to a sterile borosilicate Raman vial for spectral capture. Raman acquisition with the IDRaman mini 2.0 handheld Raman spectrometer with 10mW power and acquisition time of 20 seconds. A total of 45 spectra were acquired from each bacterial load of each sample for a total of 15 minutes acquisition (i.e., sum of 45 spectra of 20 second acquisition time for each spectrum). To assess the effect of prolonged acquisition time, each had a sum of 3, 15, 30 and 45 spectra representing 1 minute, 5 minute, 10 minute and 15 minute acquisitions.

Pre-processing and analysis of spectra was performed using scripts developed in R programming language. Spectra were smoothed using a 3rd order Savitsky-Golay filter across 19 cm^{-1} windows. The smoothed window was baseline corrected through the subtraction of a 5th order polynomial and truncated to 600-2000 cm^{-1}. Mean spectra, with standard deviations, for infected and uninfected controls were plotted as well as for each species. Supervised learning was performed using PC-LDA allowing for assessment of diagnostic and classification performance. In order assess the spectral peaks contributing to diagnosis, infected samples were centred and scaled on uninfected controls and the mean plotted along with standard deviation. Similarly, for pairwise comparison, each uropathogen species was centred and scaled by each other uropathogen species and the mean plotted along with the standard deviation.

5.4.3 RESULTS

5.4.3.1 SPECTRA AND PCA PLOTS

The average spectra, with standard error ribbons, for infected (bacterial load 10^5CFU/ml) and uninfected, in addition to the plots when PCA is applied to these spectra are presented in **Figure 5.11**. Similarly, the mean spectra with standard error ribbon for pathogens in infected (10^5 CFU/ml) in addition to the PCA plots applied to these spectra are presented in **Figure 5.12**. The spectra demonstrate a consistent high noise background with consistent peaks. No peaks differentiating infected from uninfected samples are visible, leading to near complete overlap of the PCA points irrespective of acquisition time in **Figure 5.12**. The width of the standard error ribbons are substantially narrower for 60 and 300 second acquisition times as compared to 600 and 900 seconds acquisition times. Less variation, as evidenced by the narrower error ribbons, leads to tighter clustering of the PCA points for longer acquisition times, but does not provide for separation of infected from uninfected samples.

Similar features are seen in **Figure 5.12**, in which the Raman spectra for pathogens demonstrate a consistent high noise background across pathogens, with no differentiating peaks visible. The PCA plots provide no clustering and substantial overlap according to pathogen irrespective of acquisition time.

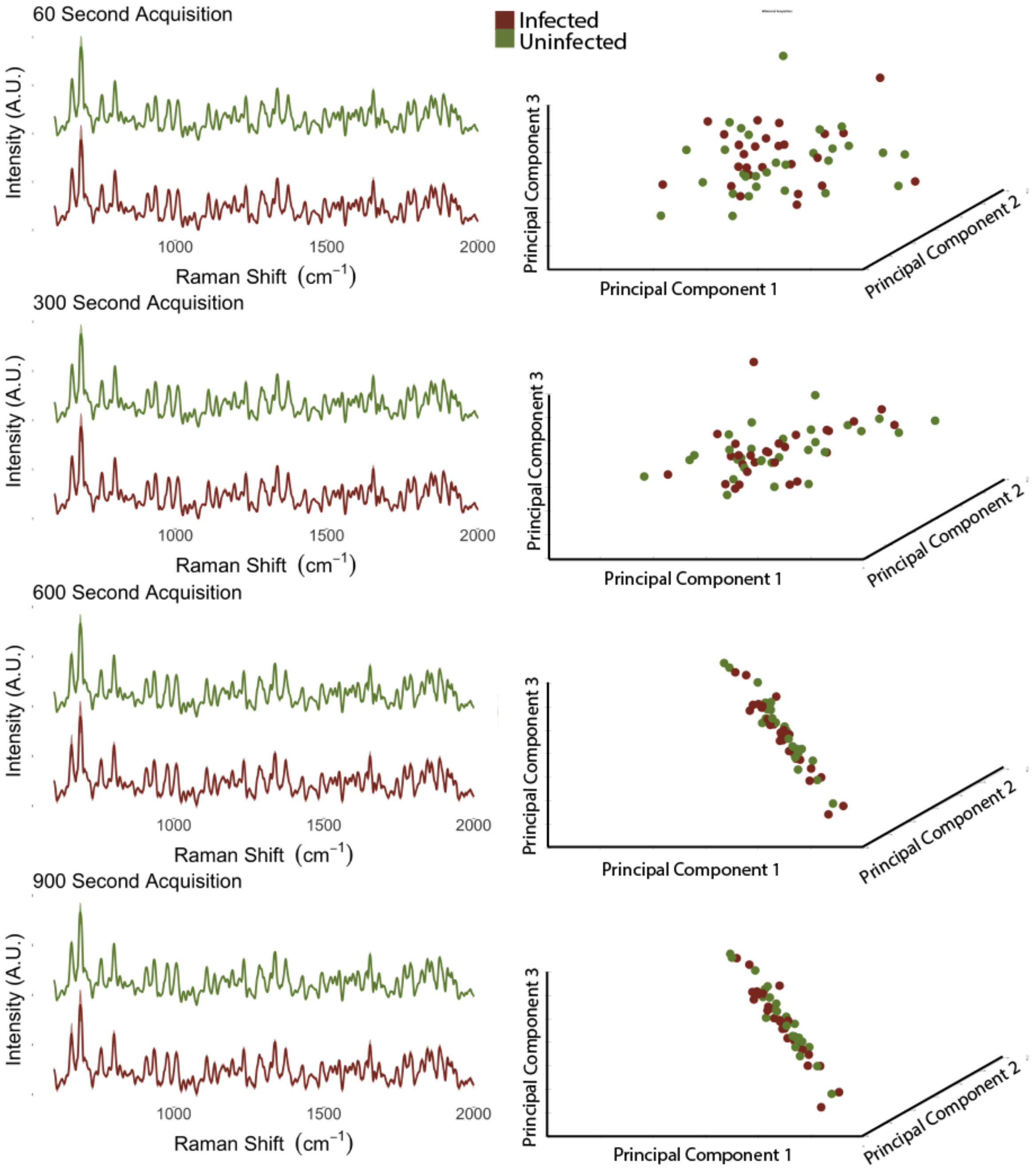

FIGURE 5. 11 MEAN SPECTRA WITH STANDARD ERROR RIBBONS FOR INFECTED AND UNINFECTED SAMPLES (LEFT), AND PCA PLOTS WHEN APPLIED INFECTED AND UNINFECTED SPECTRA (RIGHT) WITH INCREASING ACQUISITION TIME.

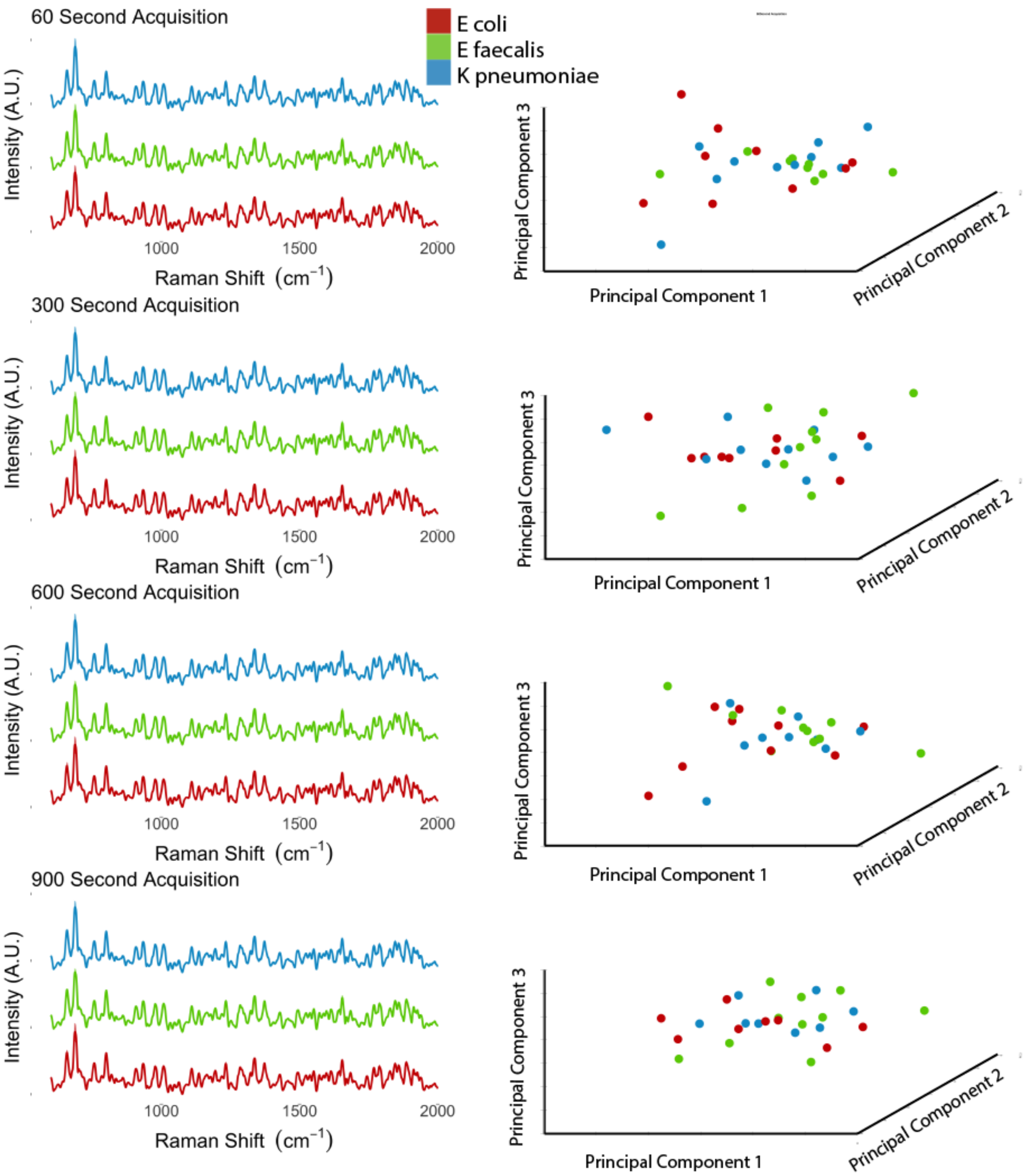

FIGURE 5. 12 MEAN SPECTRA, WITH STANDARD ERROR RIBBONS (LEFT), AND PCA PLOTS (RIGHT) FOR INFECTED (10^5 CFU/ML) WITH INCREASING ACQUISITION TIME.

5.4.3.2 Diagnostic and classification performance

The diagnostic and classification performance achieved though PC-LDA are quantified in **Table 5.6** and depicted in **Figure 5.13**. The number of components passed to LDA was selected by LOOCV for diagnostic accuracy. The diagnostic and classification accuracy improved as acquisition time was extended from 1 minute to 5 minutes, with no further improvement thereafter. With a 5-minute acquisition diagnostic accuracy was 74.1%, with classification accuracy of 86.2%. While these values may appear higher, the diagnostic accuracy was, in fact, only marginally better than random assignment.

TABLE 5. 6 PC-LDA DIAGNOSTIC AND CLASSIFICATION ACCURACY BY ACQUISITION TIME

Acquisition time	Diagnostic accuracy (%)	Classification accuracy (%)	Principal components	Variability explained
60	55.2 (41.5; 68.3)	58.6 (38.9; 76.5)	3	83.1%
300	74.1 (61.0; 84.7)	86.2 (68.3; 96.1)	19	99.7%
600	62.1 (48.4; 74.5)	86.2 (68.3; 96.1)	13	99.4%
900	62.5 (48.6; 75.8)	89.3 (71.8; 97.3)	13	99.5%

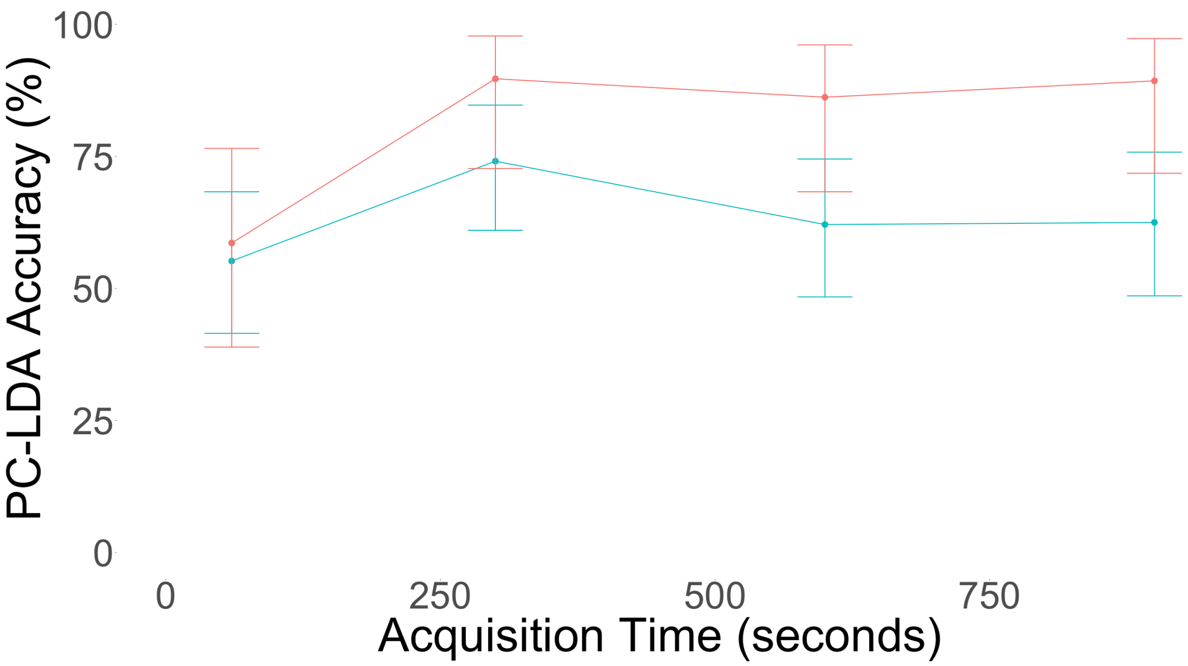

FIGURE 5. 13 PC-LDA DIAGNOSTIC (RED) AND CLASSIFICATION (BLUE) ACCURACY PLOTTED AGAINST ACQUISITION TIME.

5.4.3.3 POST HOC ANALYSIS: INCREASED PATHOGEN LOAD AND TARGETED ANALYSIS.

Pathogen load could feasibly be improved in a clinical setting with widely implemented methods. Analysis was performed with a pathogen load of 10^7 CFU/ml to assess if unenhanced Raman spectroscopy can identify pathogens at this level with the optimal acquisition time of 5 minutes. This diagnostic and classification performance are presented in **Table 5.7**, with the PC-LDA plot for classification depicted in **Figure 5.14**. Diagnostic and classification accuracy improve marginally with a higher pathogen load; however, this improvement is non-significant and does not provide meaningful identification of infected samples nor pathogen classification.

TABLE 5. 7 PC-LDA DIAGNOSTIC AND CLASSIFICATION PERFORMANCE WITH RAISED PATHOGEN LOAD (10^7 CFU/ML)

Diagnostic	**Accuracy**	63.4 (50.1; 76.0)
	Sensitivity	58.6%
	Specificity	69.0%
Classification	**Accuracy**	69.2% (48.2; 85.7%)

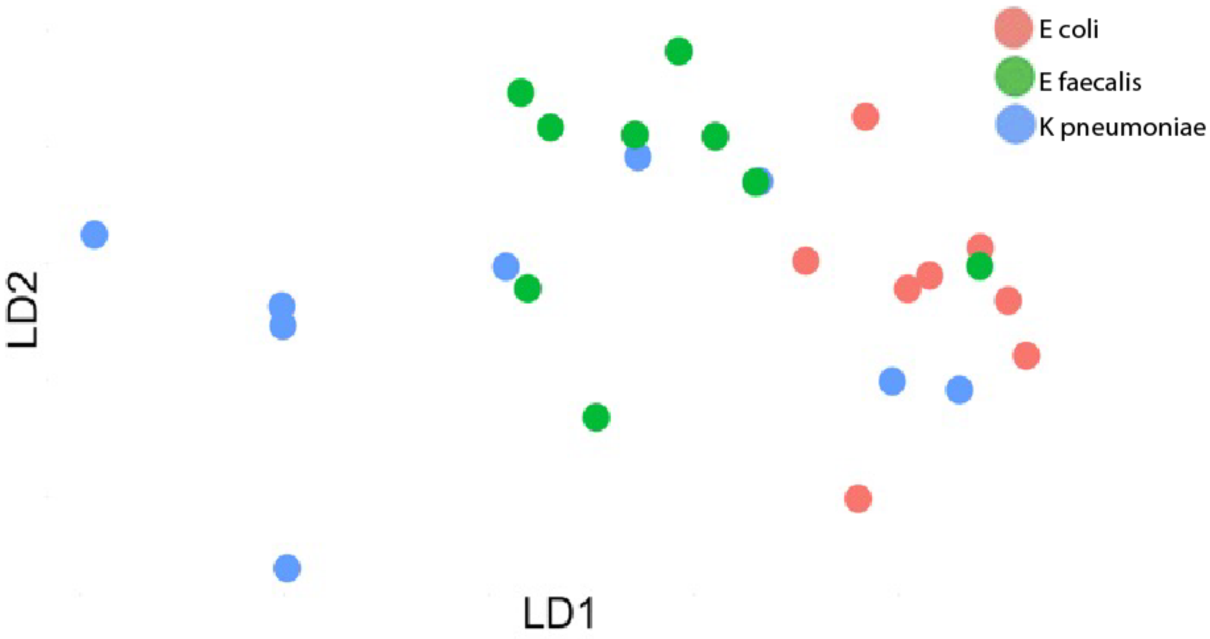

FIGURE 5. 14 PC-LDA PLOT FOR UROPATHOGEN CLASSIFICATION USING UNENHANCED RMAN SPECTROSCOPY ON UROPATHOGEN LOAD OF 10^7 CFU/ML

Additional techniques, both physical and digital are available to target analysis at spectral bands expected to have higher SNR, therein avoiding the noise arising from other area of the spectrum. A final step of analysis limited PC-LDA to spectral bands identified in **Section 5.3** as descriptive for the three uropathogens. Significance is defined here as an F-statistic value below a threshold with α =0.05. Result of this analysis are presented in **Table 5.8**.

TABLE 5. 8 PC-LDA DIAGNOSTIC AND CLASSIFICATION ACCURACY WITH ANALYSIS TARGETED AT SPECTRAL BANDS IDENTIFIED AS SIGNIFICANT IN SECTION 5.3.

Diagnostic	**Accuracy**	53.5 (39.9; 67.7)
	Sensitivity	51.8%
	Specificity	55.2%
Classification	**Accuracy**	51.7% (32.5; 70.6%)

5.4.4 DISCUSSION

Raman spectroscopy with prolonged acquisition times did not provide adequate diagnostic or classification performance at clinically relevant concentrations. Diagnostic accuracy was limited to 74.1%, only marginally better than random assignments. This diagnostic performance is inferior to currently implemented diagnostics such as urinalysis or flow cytometry[191, 192]. Prolonging acquisition time did improve diagnostic and classification accuracy when increased from 1 to 5 minutes, but no further improvements in accuracy were observed. This was in keeping with methods **section 4.3** whish had demonstrated a reduction in high frequency noise and cosmic spikes initially, but with diminishing gains.

This contrasts with published works by *Kloss et al., Schroder et al.* and *Pahlow et al.*[99, 117, 142, 160]. These authors all demonstrated high resolution spectra with visible differences leading to excellent classification performance up to 92%. The crucial difference differentiating these studies is the use of Raman microscopes for spectra acquisition. A Raman microscope was not used in this study as it defies the aim of this thesis, to deliver a technology with potential to provide rapid, cost-effective UTI diagnosis with pathogen classification at the point of care. The advantage of Raman microscopes provided by a significantly smaller focal volume is offset by numerous limitations: firstly, the cost and physical footprint of these would limit use to central laboratories at best; secondly, focussing on pathogens requires technical expertise and methods to capture and aggregate pathogens; finally, as spectral acquisition is contingent on user-defined focussing on pathogens microscopes are limited to classification and not diagnosis[88, 100].

Furthermore, the classification performance of these works may be overstated. The reported datasets indicate that numerous spectra were acquired from each sample and treated as independent data points in analysis. This is particularly stark in *Schroder et al*., where 600 spectra were acquired from each sample[117]. The supervised learning techniques applied to these spectra assume the data points are independent[111]. Therefore, the classification seen may arise from idiosyncrasies in the samples, rather than from pathogen Raman signal.

To firmly interrogate the hypothesis that Raman spectroscopy without SERS can achieve uropathogen classification, two further *post hoc* analyses were reported in this chapter. Classification performance was assessed with higher pathogen loads of 10^7 CFU/ml, a 100 times greater pathogen load than established cut-off. This analysis was performed under the assumption that, if successful, samples may be concentrated using widely implemented techniques including centrifugation, evaporation, or filtration[186]. Diagnostic accuracy with higher pathogen loads of 64.1% did not differ significantly from those of standard pathogen loads, nor random assignment. This would indicate, at these pathogen loads, the Raman signal from the pathogen is too weak to provide meaningful diagnosis.

The second post-hoc analysis was predicated on the premise that any bacterial Raman signal is overwhelmed by noise arising across the spectrum. Targeting identified in **Section 5.3** to have higher signal levels. Should this method have been successful it could have been extended to other work digitally, or preferably be performed using optical band-pass filters or liquid crystal tuneable filters. Diagnostic accuracy in this analysis was 53.5%, a reduction as compared to assessment of the entire spectrum. This would indicate this Raman signal in these areas was too weak with the lower pathogen load.

A limitation of this work is that no efforts were made to aggregate pathogens to increase signal. Aggregation methods including dielectrophoresis, optical tweezers and immunocapture were used in the published works as these are Raman microscopy requires this aggregation and capture for proper focussing[117, 142]. While many of these methods are unlikely to be cost-effective and feasible in a clinical setting, more implementable methods for pathogen capture such as centrifugation or filtration have been studied[124, 144-147]. These methods may be sufficient to concentrate pathogen to a level above the limit of detection for unenhanced Raman spectroscopy without microscopy.

5.5 CONCLUSION

Uropathogens are demonstrated to have unique Raman spectra allowing for accurate classification. When applied to concentrated suspensions Raman spectroscopy classification accuracy of 7 common reference uropathogenic strains approaches 95%. Spectral bands contributing to classification were attributed to a wide range of cellular components, in keeping with previous published work.

Extending the diagnostic challenge to suspensions with a clinically relevant pathogen load of 10^5 CFU/ml emphasises the challenge of weak biologic Raman signal. Diagnostic accuracy was little better than random assignment, even failing to improve with post hoc analysis to assess whether increasing the pathogen load 100 fold or targeting analysis to spectral bands demonstrated to be significant.

Raman spectra of clinical urine samples was interrogated, demonstrating a large degree of variability across the entire spectrum with large peaks associated with common urine constituents such urea and creatinine.

When combined these findings indicate that while uropathogens have unique Raman spectra with the potential for rapid identification and classification, additional techniques are required to achieve this at clinically relevant concentrations. Achieving classification at clinically relevant concentrations may possibly be achieved through SERS or physical pre-processing to capture and aggregate uropathogens. Similarly, physical pre-processing is required to separate pathogens from urine to avoid the overwhelming fluorescence and competing signal.

CHAPTER 6: SURFACE ENHANCED RAMAN SPECTROSCOPY USING NANOPARTICLES

6.1 INTRODUCTION

UTIs contribute a substantial burden of disease which is primarily mediated by the massive rate at which UTIs occur[1, 2, 8, 10]. This burden of disease is exacerbated by an outdated diagnostic approach characterised by inaccuracy and delay[5]. A new UTI diagnostic paradigm built upon a novel diagnostic technology can substantially reduce the burden of disease by delivering accurate diagnostic information when and where it has the greatest impact: at the bedside. Therefore, the ideal diagnostic technology for UTIs would aim to deliver accurate diagnosis with precise pathogen classification at the point of care.

Raman spectroscopy is uniquely suited to form the basis of an ideal UTI diagnostic in light of its ability to identify pathogens without prior biomass expansion[7, 76]. This is achieved through rapid biochemical fingerprinting provided by the detection and analysis of inelastically scattered light[71]. While uropathogens are demonstrated to have unique Raman spectra that provide classification, weak biologic Raman scattering from pathogens is overwhelmed by background noise. As such, methods to physically aggregate and capture pathogens while separating them from urine are required prior to Raman acquisition[186]. Similarly, techniques to enhance the pathogen signal to allow for precise pathogen recognition at clinically relevant concentrations.

SERS may overcome the challenge of weak biologic Raman scattering by providing signal enhancement of up to 10^{14} times[72]. SERS has additional benefits when applied to pathogen recognition in that the signal enhancement is fluorescence quenching[70, 72, 82, 88, 123, 167]. Importantly, enhancement is selective, mediated an inverse and exponential relationship with the distance between the target and SERS substrate[7, 69, 72, 80, 85, 123]. The practical implication of this relationship is that biochemical entities held within a few nanometres of the substrate are massively enhanced, while those outside 20 nm have negligible enhancement. This is of tremendous value when applied to pathogens, in which the bulk of the descriptive biomass is incorporated in the cell envelope which comprises the most superficial few nanometres of the cell. As such closely and consistently applied SERS substrates will selectively and massively enhance the most descriptive components of pathogens.

SERS substrates may be applied to pathogens using one of three methods. Firstly, the SERS substrate may be formed directly on, or in, the cell envelope by reducing a noble metal salt in the pathogen suspension. While delivering highly resolved spectra, this method is limited to laboratory-based research owing to the need for reagents and technical processes. In the second approach, pathogens may be applied directly to a SERS surface. A challenge exists in getting close apposition of pathogens to these SERS surfaces. In the final approach, suspended pathogens may be mixed with colloidal nanoparticles[72, 97, 167].

SERS using colloidal nanoparticles has a substantial advantage in that silver and gold naturally interact with the pathogen cell envelope, and as such the SERS enhancement is selectively targeted to the cell envelope. This occurs in a time dependent fashion which is dependent on numerous nanoparticle characteristics including the noble metal, size, shape and presence of capping agents[70, 88, 136]. Hence, a great deal of versatility is provided by the control of the nanoparticle characteristics, which may then be optimised to acquire the best SERS spectra. This may be further optimised using physical methods to concentrate the pathogens and therefore increase the interaction of pathogens with the SERS substrates[186].

Hypothesis: Colloidal nanoparticles provide sufficient Raman signal enhancement to allow for identification and classification of uropathogens at clinically relevant concentrations.

Objectives:

- Investigate the SERS spectra of common uropathogens enhanced with colloidal nanoparticles.
- Identify the optimal nanoparticle metal and size for uropathogens SERS acquisition.
- Identify a rapid method for pathogen aggregation and capture to improve pathogen–nanoparticle interaction.
- Describe the performance of colloidal nanoparticle mediated SERS for uropathogen identification and classification.

6.2 SERS SPECTRA OF COMMON UROPATHOGENS USING VARYING NANOPARTICLES

6.2.1 INTRODUCTION

Overcoming the challenges posed by weak biologic Raman scattering is best achieved using SERS[82, 88, 123, 156]. The tremendous surface enhancement provided by SERS is additionally benefited by a strong selectivity mediated by an inversely and exponential distance relationship[7, 69, 72, 80, 85, 123]. As such, SERS substrates consistently to pathogens will massively enhance signal arising from the cell envelope where many of the defining chemical features arrive.

Compared to other methods, SERS using colloidal nanoparticles has an important benefit in the ability to work directly with solutions without pathogen aggregation or capture (although these are frequently performed). Cognizance must however be given to the fact that without methods to achieve pathogen apposition the nanoparticles are randomly distributed throughout the suspension and so the benefit is selective enhancement is lost[193]. Apposition to pathogens is most frequently achieved through the intrinsic interaction of metals with bacterial cell envelopes. This nanoparticle – envelope interaction is time dependent and so making use of this incurs a delay. Similarly, the time dependent spectral changes necessitate special attention to avoid inducing variation. This interaction is also dependent on multiple factors notably nanoparticle characteristics including metal, size, shape, and capping agents amongst others[70, 88]. Additional caution needs to be exercised as the cell envelope interaction is bactericidal, and so prolonged mixing will lead to cell death inducing spectral variability. For these reasons, where nanoparticles are used in Raman bacterial experiments they are commonly freshly produced and evaluated.

Colloidal SERS nanoparticles have been assessed in a number of published works: *Nordstrom et al.* attempted a simple method of classification by mixing of colloidal nanoparticles with bacterial suspensions at a range of pathogen loads [157].Three different strains of *Escherichia coli, Klebsiella pneumoniae* and *Proteus Mirabilis* were assessed. Nanoparticles were produced by the method of *Lee and Meisel*, combined with the bacterial suspension and airdried before acquisition with a Raman spectrometer [134, 157].The authors claim the bacterial load quantification and antimicrobial sensitivity identification [157]. While supervised learning using PC-LDA is reported in the methods section the classification performance is not reported in the results[157].

Kahraman et al. assessed the SERS spectra of bacteria after simple mixing with nanoparticles [88]. Silver nanoparticles were produced by the methods of *Lee and Meisel* as well as *Creighton* before mixing with suspensions of *Escherichia coli.* The differing methods of nanoparticles result in nanoparticles with different charge characteristics. The resulting mixture was spotted onto slides before airdrying over 15-30 minutes, before Raman acquisition with a Raman microscope. While the nanoparticles produced by the method of *Creighton* [194] appeared to interact more with the cell envelope, the reproducibility of those produced by the method of *Lee* and *Meisel* produced more repeatable spectra. The results demonstrates that the strong enhancement provided by SERS can negatively affect spectra by inducing variation when inconsistently applied[88].

Sengupta et al. acquired SERS spectra from bacterial suspensions mixed with silver colloidal nanoparticles. While successful classification of suspensions of *Escherichia coli, Pseudomonas aeruginosa* and *Salmonella Typhimurium*, the authors demonstrated the sensitivity of nanoparticle interaction to a number of colloidal and environmental factors including pH, pathogen load, colloidal concertation[195].

Avci et al. assessed the SERS spectra of common uropathogens enhanced with nanoparticles attempting to identify the minimum incubation time at which SERS can reliably identify pathogens [123]. Silver nanoparticles were created using the method described by Leopold and Lendl. Seven common uropathogens were cultivated for times ranging from 1 to 24 hours before suspension and mixing with nanoparticles. The bacteria-nanoparticles mixtures were spotted on slides and airdried prior to Raman acquisition with a Raman microscope. Uropathogens were accurately identified after only on hour of cultivation, although extremely dynamic changes were noted for all pathogens which settled as the stationary growth phase was achieved[123].

While pathogen apposition may be achieved using time dependent interaction of nanoparticles with the cell envelope the delay required may be unfeasible for clinical application. *Naja et al.* utilised antibody mediated immunocapture to achieve rapid apposition of nanoparticles to bacteria[139]. Nanoparticles were produced by the method of *Lee and Meisel[134]* before binding to protein A (a cell surface protein of *Staphylococcus aureus*) and then to antibodies to *Escherichia coli*. The antibody nanoparticles ensured rapid apposition to *E. coli* and good selectivity against a comparator bacterium. A limitation of immunocaptured nanoparticles in this work when applied to bacterial classification arises in that the specificity makes this unfeasible to broader classification challenges. This limitation may be avoided by the use of less specific antibodies such as those against teichuronic acid or lipopolysaccharide[139].

The challenges of random distribution of nanoparticles or time dependent variability of colloidal mixing may be circumvented by prior capture before addition of nanoparticles. *Mircescu et al.* used positively charged pegylated slides to electrostatically capture uropathogens, which are negatively charged, prior to washing and addition of nanoparticles[101]. The nanoparticles were produced by the method of Leopold and Lendl. Spectra were captured using a Raman microscope. Strain level uropathogen recognition was achieved. The sensitivity of their method was demonstrated by the ability to differentiate strains with and without O-antigen present[101]. A practicality overlooked by these researchers which may limit further translation is the plethora of competing negatively charged urinary components which would compete for slide apposition.

In all these works, SERS enhancement was achieved using laboratory produced nanoparticles. While well developed and standardise methods are available for nanoparticle production, these methods are time consuming, technically challenging and may lead to variability on nanoparticle characteristics. Using commercially available nanoparticles will reduce these challenges.

Hypothesis: Addition of colloidal metal nanoparticles to uropathogen suspensions provides Raman spectral enhancement, therein improving classification performance.

Objectives:

- Assess the classification performance achieved from SERS spectra of common uropathogens using commercially available colloidal nanoparticles.
- Demonstrate the effects of varying the nanoparticle size and noble metal on the SERS spectra.
- Assess if delayed acquisition improves classification performance through time mediated nanoparticle interaction with pathogens.

6.2.2 METHODS

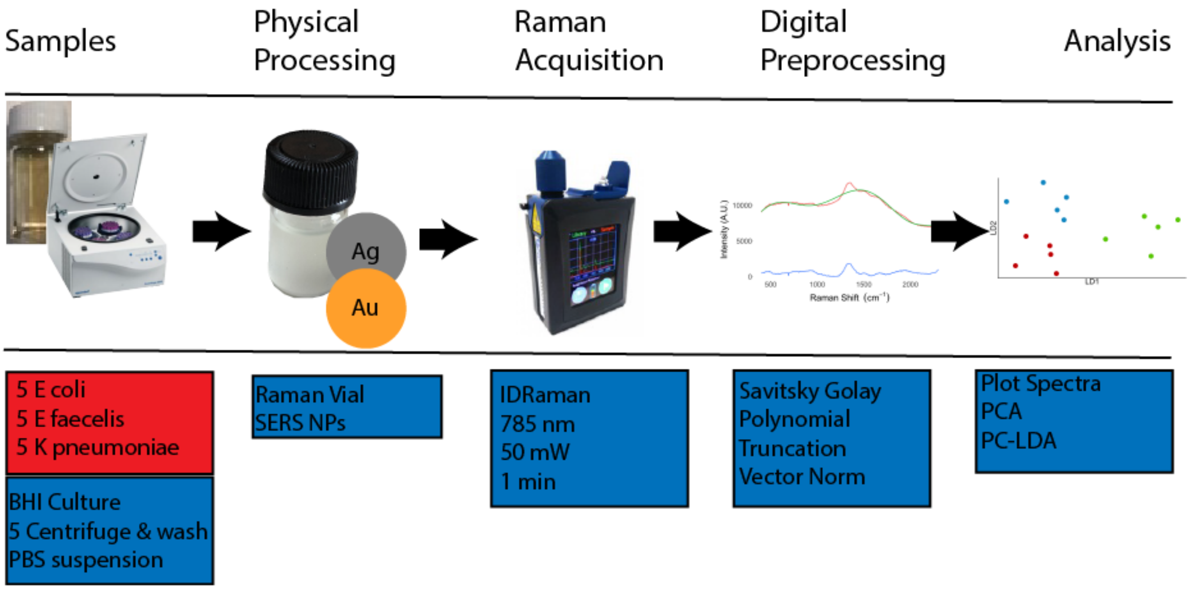

FIGURE 6. 1 METHODS FOR SERS SUSPENSIONS. SAMPLES WERE PREPARED BY CULTURE OF 3 REFERENCE STRAIN PATHOGENS WHICH UNDERWENT 5 CENTRIFUGE AND WASH CYCLES. THE SUSPENSIONS WERE TRANSFERRED TO RAMAN VIALS BEFORE ADDITION OF SERS NANOPARTICLES (10, 40 AND 100NM GOLD AND SILVER). SPECTRA WERE ACQUIRED WITH IDRAMAN SPECTROSCOPE. THESE SPECTRA WERE PRE-PROCESSED BY SAVITSKY-GOLAY FILTERING, POLYNOMIAL SUBTRACTION AND VECTOR NORMALISATION. SPECTRA WERE ANALYSED WITH SPECTRAL PLOTS, PCA AND PC-LDA

The methods employed are summarised in **Figure 6.1.** This study consisted of assessment 6 different colloidal nanoparticles on 3 differing reference strain pathogen suspensions, with 5 replicates of each.

6.2.2.1 SAMPLE PREPARATION AND SERS

Suspensions of *Escherichia coli ATCC25922, Enterococcus faecalis ATCC29212* and *Klebsiella pneumoniae ATCC13883* were created using the established reference bank (**Section 4.2)**. For each sample, a single microbank bead was inoculated into 10 ml of brain-heart infusion broth and cultured at 37 degrees Celsius for 24 hours. Thereafter, the broth-pathogen suspension was vortex mixed and centrifuged at 3350 g for 10 minutes. The supernatant was discarded, and the bacterial pellet resuspended in 2 ml of PBS by vortex mixing. The suspension was centrifuged at 8300 g for 1 minute, after which the supernatant was discarded, and the pellet resuspended. This centrifuge and wash process was repeated a total of 5 times to remove residual culture media.

On the final resuspension 750 µl of colloidal nanoparticle in addition to 1.5 ml of PBS before resuspension by Vortex mixing. Colloidal nanoparticles were purchased from Sigma-Aldrich and included 10 nm, 40 nm, and 100 nm nanoparticles of both gold and silver. The pathogen-colloid suspension was transferred to sterile borosilicate Raman vial for spectral acquisition.

6.2.2.2 SPECTRAL ACQUISITION AND ANALYSIS

Raman spectra were acquired immediately, and again after 30 minutes and 1-hour. Raman spectra were acquired with the IDRaman mini 2.0 handheld Raman spectrometer, with laser wavelength of 785 nm, power set to 50 mW and acquisition time of 10 seconds. A mean of 6 spectra were averaged for a total acquisition time of 1 minute.

All processing and analysis were performed using scripts developed in R programming language. Spectra were smoothed using a Savitsky-Golay filter with a 3rd order polynomial over a 19 cm^{-1} moving window. The baseline was corrected through subtraction of a fitted 9th order polynomial. Spectra were truncated from 600 cm^{-1} to 2000 cm^{-1} to include the fingerprint region before vector normalisation.

Mean spectra with standard deviations were plotted for the uropathogens with all 6 different nanoparticle types demonstrating the signal provided by different nanoparticles. Spectral differences between uropathogens were highlighted by plotting individual pathogens centred and scaled on other uropathogen spectra. PCA biplots were created for unsupervised classification of pathogen spectra for each nanoparticle and delay combination. PC-LDA was used for supervised classification of pathogen spectra for each combination of colloidal nanoparticles and acquisition delay.

6.2.3 RESULTS

Figure 6.2 depicts the mean SERS spectra with standard error ribbons of the reference strain spectra enhanced by different nanoparticles, and with increasing delay before spectral acquisition. The spectra are dominated by a residual baseline incompletely removed during pre-processing. Despite the prominent baseline, differentiating spectral peaks are visible as smaller deviations from the baseline. These differentiating peaks are highlighted in **Figures 6.3-6.5**, in which uropathogen spectra are centred and scaled by spectra from another uropathogen species as a reference. These spectra demonstrate where uropathogen spectra differ greatest relative to the local variability. These plots present all combinations of colloidal nanoparticles and acquisition delays. Horizontal dashed lines indicate boundaries where differences are significant at $\alpha = 0.05$. The point with greatest relative difference for each mean spectrum is emphasised by the dashed vertical line and listed in the accompanying tables (**Tables 6.1 – 6.3).** All plots demonstrate several significantly differing peaks with the potential to contribute toward bacterial classification. These peaks vary dependent on the colloidal nanoparticle and acquisition delay.

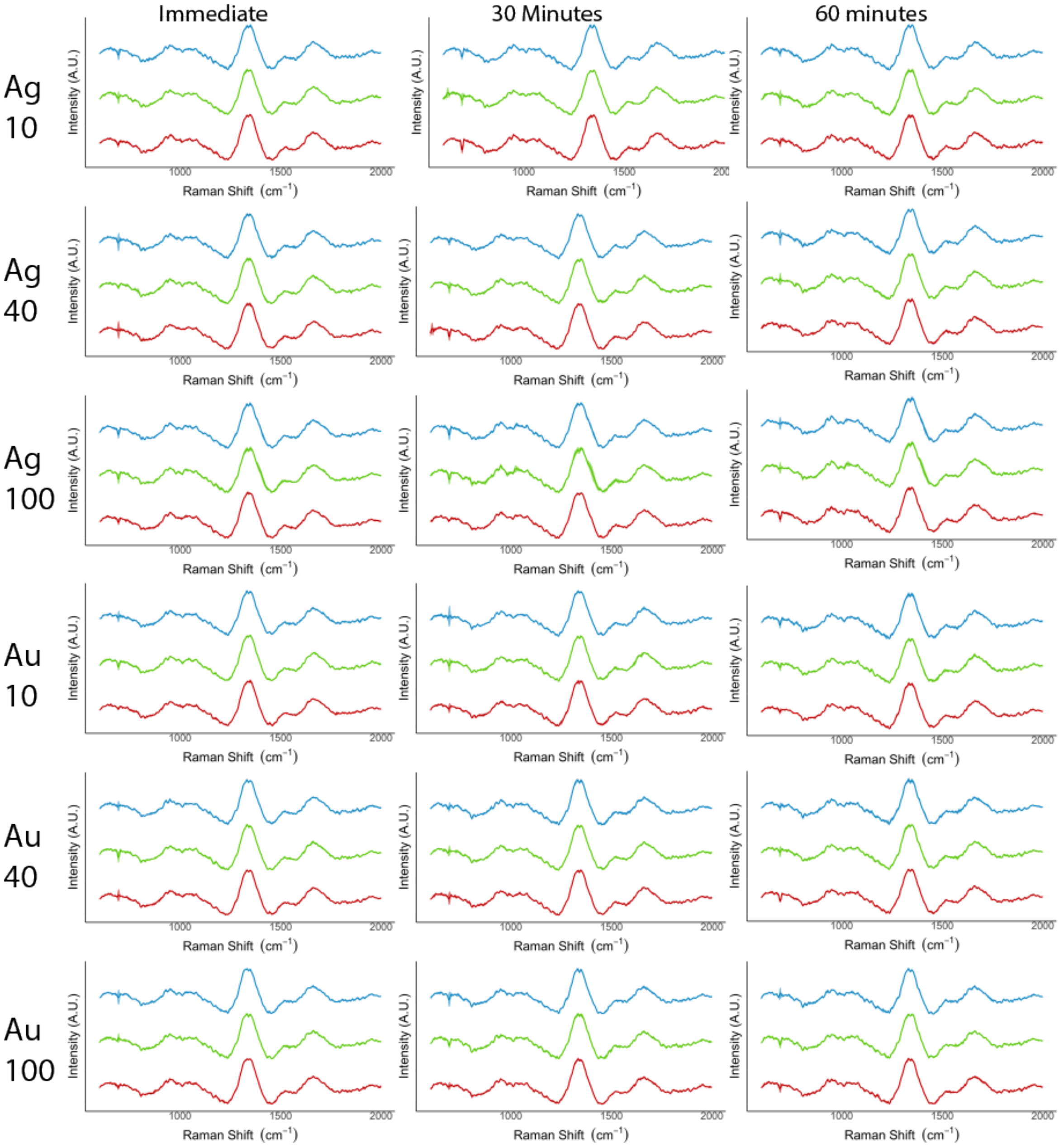

FIGURE 6. 2 MEAN SPECTRA WITH STANDARD ERROR RIBBONS FOR REFERENCE UROPATHOGENS (RED: *ESCHERICHIA COLI*; GREEN: *ENTEROCOCCUS FAECALIS*; BLUE: *KLEBSIELLA PNEUMONIAE*) ENHANCED WITH DIFFERENT COLLOIDAL NANOPARTICLES AND WITH DELAYED ACQUISITION.

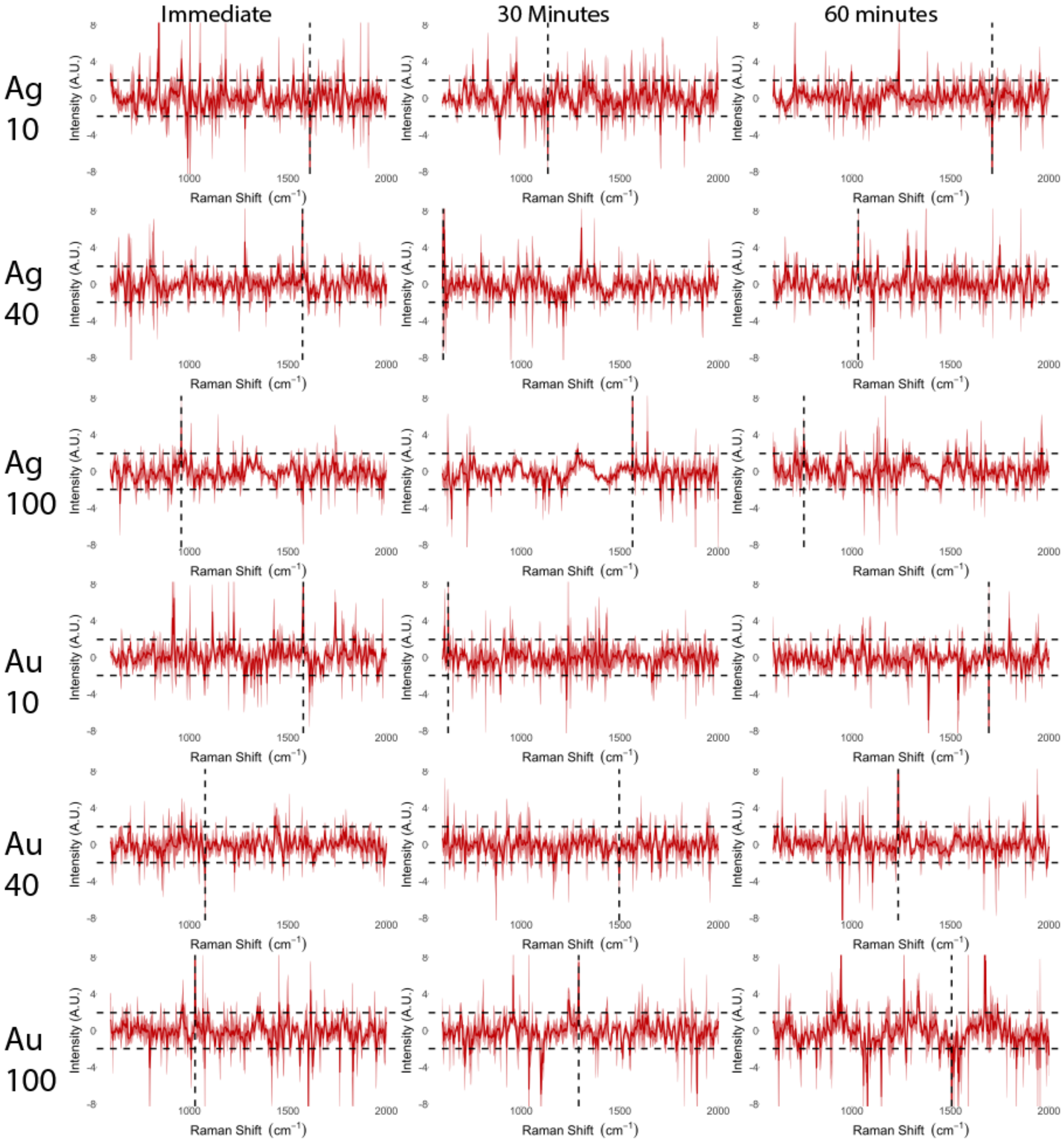

FIGURE 6. 3 *ESCHERICHIA COLI* SPECTRA CENTRED AND SCALED ON *ENTEROCOCCUS FAECALIS* SPECTRA ENHANCED BY DIFFERENT COLLOIDAL NANOPARTICLES WITH INCREASING DELAY BEFORE SPECTRAL ACQUISITION. HORIZONTAL DASHED LINES DELINEATE THE BORDERS AT WHICH DIFFERENCE ARE STATISTICALLY SIGNIFICANT AT α = 0.05. VERTICAL DASHED LINES INDICATE THE POINT OF MAXIMAL RELATIVE DIFFERENCE, ALTHOUGH ALL PLOTS DEMONSTRATE MULTIPLE SIGNIFICANT BANDS

Figure 6.3 demonstrates plots of mean spectra (with standard error ribbons) from *Escherichia coli* suspensions, centred and scaled by spectra acquired from *Enterococcus faecalis* suspensions. The band at which the greatest relative difference between *Escherichia coli* samples and *Enterococcus faecalis* samples are emphasised by the vertical dashed line and listed in **Table 6.1** along with potential band assignments.

TABLE 6. 1 SPECTRAL BAND ASSIGNMENTS FOR *ESCHERICHIA COLI* SAMPLE CENTRED AND SCALED ON *ENTEROCOCCUS FAECALIS* SAMPLES

Colloidal nanoparticles	Acquisition Delay (minutes)	Maximal difference peak (cm^{-1})	Band assignment	Reference
Silver 10 nm	0	1612	Tyrosine, phenylalanine, and tryptophan	[110, 158]
	30	1135	Cytochrome C, saccharides	[99, 110]
	60	1712	Aspartic and glutamic acid	[190]
Silver 40 nm	0	1574	Exopolysaccharides, cytochrome C, peptidoglycan	[99, 110, 158]
	30	604	Cholesterol	[190]
	60	1032	Phenylalanine and proline	[110]
Silver 100 nm	0	959	Carotenoid	[190]
	30	1565	Exopolysaccharide	[110]
	60	759	Tryptophan	[110]
Gold 10 nm	0	1578	Peptidoglycan	[110]
	30	629	Tryptophan	[110]
	60	1695	C=C stretching	[101]
Gold 40 nm	0	1080	Carbohydrates	[158]
	30	1497	C=C stretching	[190]
	60	1235	Amide III	[123, 158]
Gold 100 nm	0	1029	Carbohydrates, Saccharides	[110]
	30	1292	CH2 Twisting	[158]
	60	1506	Carotenoids	[158]

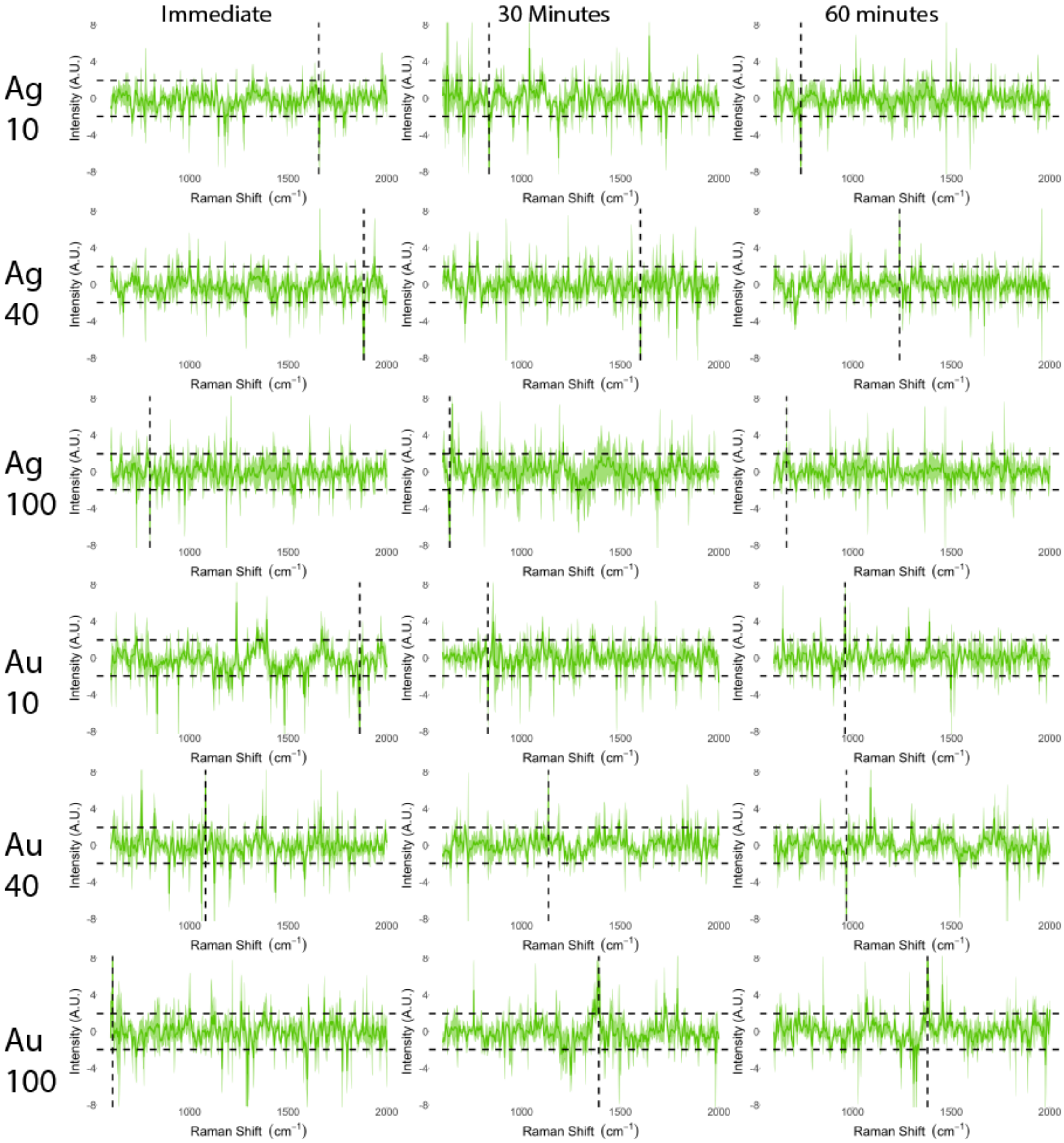

FIGURE 6. 4 *ENTEROCOCCUS FAECALIS* SPECTRA CENTRED AND SCALED ON *KLEBSIELLA PNEUMONIAE* SPECTRA ENHANCED BY DIFFERENT COLLOIDAL NANOPARTICLES WITH INCREASING DELAY BEFORE SPECTRAL ACQUISITION. HORIZONTAL DASHED LINES DELINEATE THE BORDERS AT WHICH DIFFERENCE ARE STATISTICALLY SIGNIFICANT AT α = 0.05. VERTICAL DASHED LINES INDICATE THE POINT OF MAXIMAL RELATIVE DIFFERENCE, ALTHOUGH ALL PLOTS DEMONSTRATE MULTIPLE AREAS SIGNIFICANT BANDS

Figure 6.4 demonstrates plots of mean spectra (with standard error ribbons) from *Enterococcus faecalis* suspensions, centred and scaled by spectra acquired from *Klebsiella pneumoniae* suspensions. The bands at which the greatest relative difference between *Enterococcus faecalis* and *Klebsiella pneumoniae* samples are emphasised by the vertical dashed line and listed in **Table 6.2** along with potential band assignments.

TABLE 6. 2 SPECTRAL BAND ASSIGNMENTS FOR *ENTEROCOCCUS FAECALIS* SPECTRA CENTRED AND SCALED ON *KLEBSIELLA PNEUMONIAE* SAMPLES.

Colloidal nanoparticles	Acquisition Delay (minutes)	Maximal difference peak (cm^{-1})	Band Assignment	Reference
Silver 10 nm	0	1656	Amide I	[110, 117, 158]
	30	835	Phenylalanine	[123]
	60	737	C-C stretch, DNA, AMP	[149, 161, 190]
Silver 40 nm	0	1884	C=C stretching	[101]
	30	1602	Phenylalanine	[99, 158]
	60	1238	Amide III	[158]
Silver 100 nm	0	799	Tyrosine	[101, 158]
	30	635	Tyrosine	[158]
	60	635	Tyrosine	[158]
Gold 10 nm	0	1863	C=C stretching	[101]
	30	829	Tyrosine	[110]
	60	961	Hypoxanthine, guanine, adenine	[149]
Gold 40 nm	0	1081	Carbohydrates	[158]
	30	1135	Saccharides, AMP	[110, 149]
	60	968	Lipids	[190]
Gold 100 nm	0	610	Tryptophan	[110]
	30	1391	CH Rocking	[190]
	60	1380	Peptidoglycan	[110]

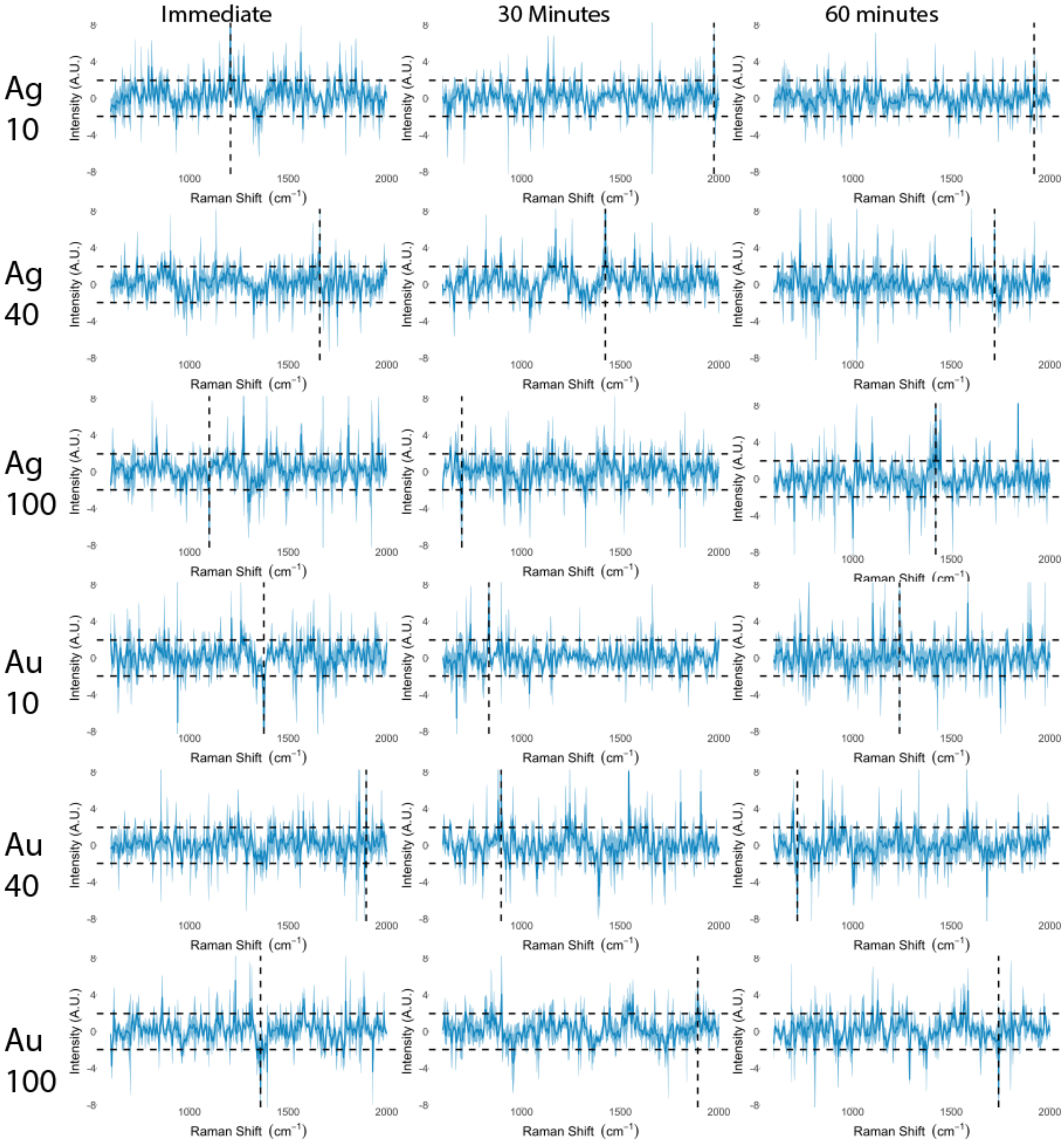

FIGURE 6. 5 *KLEBSIELLA PNEUMONIAE* SPECTRA CENTRED AND SCALED ON *ESCHERICHIA COLI* SPECTRA, ENHANCED BY DIFFERENT COLLOIDAL NANOPARTICLES WITH INCREASING DELAY BEFORE SPECTRAL ACQUISITION. HORIZONTAL DASHED LINES DELINEATE THE BORDERS AT WHICH DIFFERENCE ARE STATISTICALLY SIGNIFICANT AT $\alpha = 0.05$. VERTICAL DASHED LINES INDICATE THE POINT OF MAXIMAL RELATIVE DIFFERENCE, ALTHOUGH ALL PLOTS DEMONSTRATE MULTIPLE AREAS SIGNIFICANT BANDS

Figure 6.5 demonstrates plots of mean spectra (with standard error ribbons) from *Klebsiella pneumoniae* suspensions, centred and scaled by spectra acquired from *Escherichia coli* suspensions. The band at which the greatest relative difference between *Klebsiella pneumoniae* and *Escherichia coli* are emphasised by the vertical dashed line and listed in **Table 6.3** along with potential band assignments.

TABLE 6. 3 SPECTRAL BAND ASSIGNMENT FOR *KLEBSIELLA PNEUMONIAE* SAMPLES CENTRED AND SCALED ON *ESCEHRICHIA COLI* SAMPLES

Colloidal nanoparticles	**Acquisition Delay (minutes)**	**Maximal difference peak (cm^{-1})**	**Band Assignment**	**Reference**
Silver 10 nm	0	1208	Tyrosine, Phenylalanine, tryptophan, amide III	[110, 158]
	30	1975	C=C stretching	[101]
	60	1920	C=C stretching	[101]
Silver 40 nm	0	1661	Amide I, Lipids	[99, 110]
	30	1424	Lipids	[110]
	60	1720	Esters	[190]
Silver 100 nm	0	1100	Carbohydrates	[101]
	30	696	Cholesterol	[190]
	60	1421	Lipids	[101]
Gold 10 nm	0	1377	Hypoxanthine, adenine	[149]
	30	834	Phenylalanine	[123]
	60	1238	Amide III	[123, 158]
Gold 40 nm	0	1896	Esters	[190]
	30	896	Glycosidic ring of saccharides	[110]
	60	719	Glycosidic ring	[101]
Gold 100 nm	0	1600	Phenylalanine, tyrosine, tryptophan	[96, 99, 158]
	30	1893	Esters	[190]
	60	1740	Esters	[190]

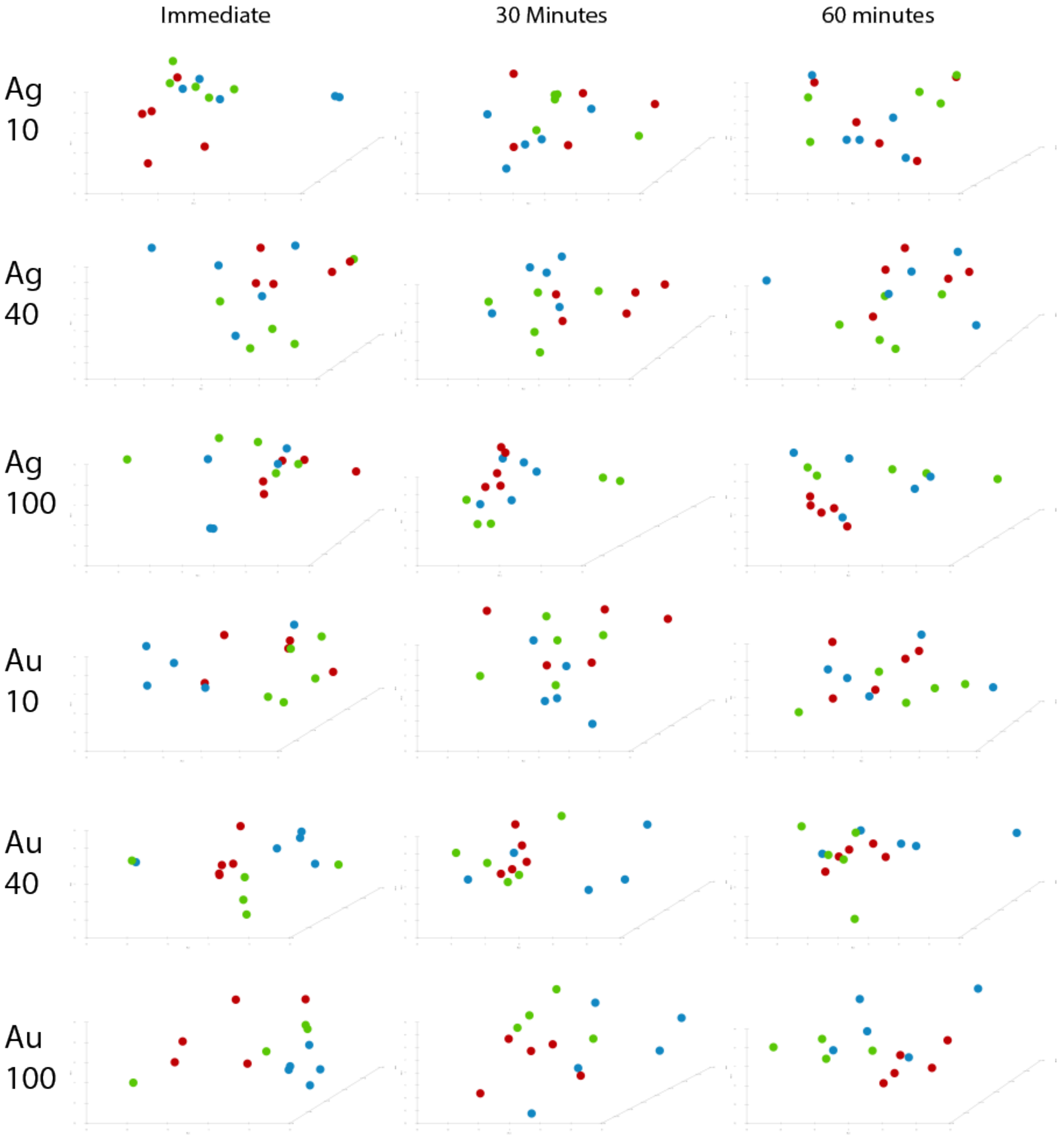

FIGURE 6. 6 PCA PLOTS FOR UNSUPERVISED CLASSIFICATION OF UROPATHOGEN SERS SPECTRA (RED: *ESCHERICHIA COLI*; GREEN: *ENTEROCOCCUS FAECALIS*; BLUE: *KLEBSIELLA PNEUMONIAE*) WITH DIFFERENT COLLOIDAL NANOPARTICLES AND INCREASING DELAY BEFORE SPECTRAL ACQUISITION

Figure 6.6 depicts the first 3 principal components of the uropathogen spectra for each combination. All plots demonstrate overlap of component points, likely reflective of the incompletely resolved baseline. Varying degrees of clustering by pathogen are seen reflecting differences in the within class variability.

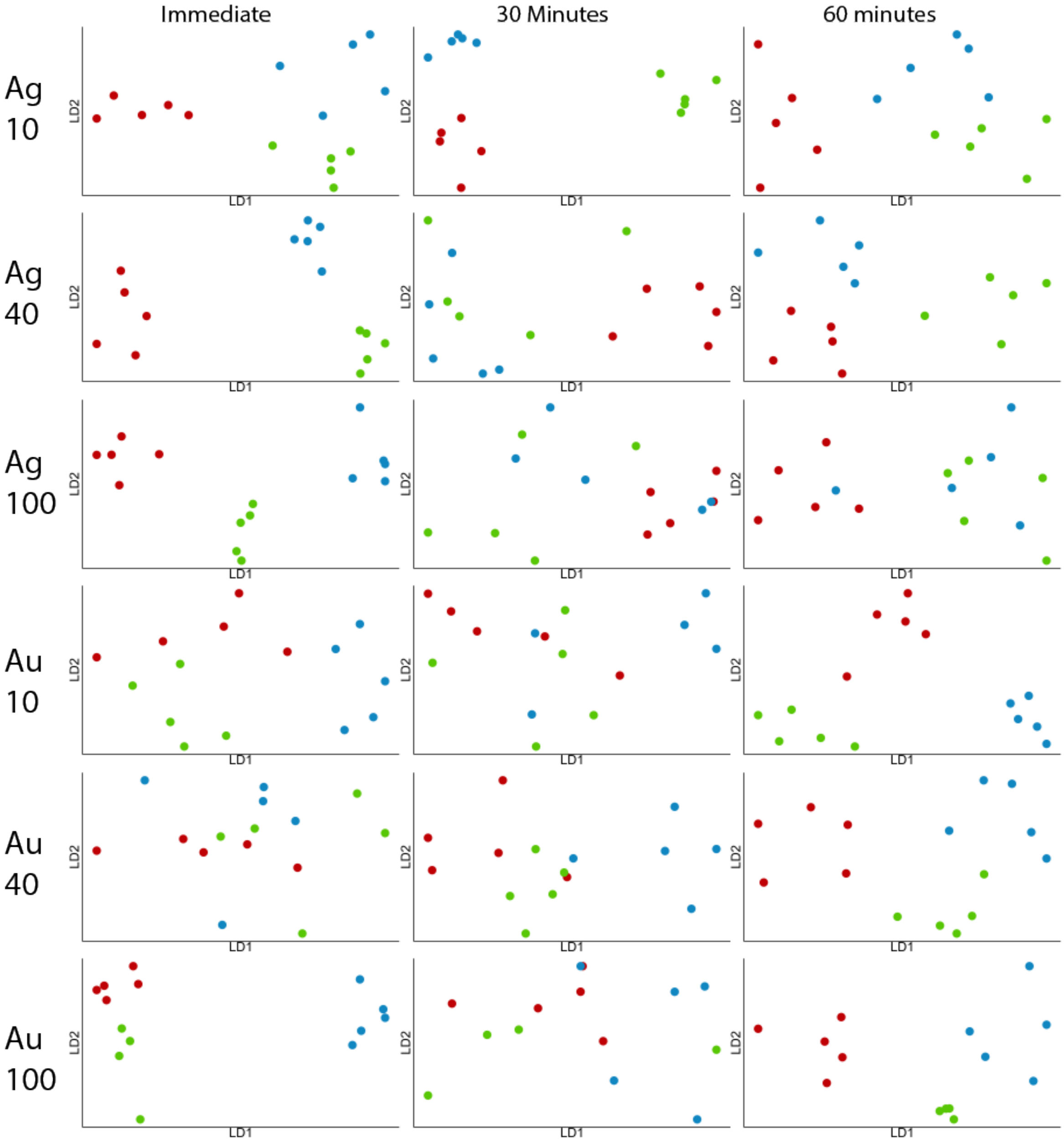

FIGURE 6. 7 PC-LDA PLOTS FOR SUPERVISED CLASSIFICATION OF SERS SPECTRA WITH DIFFERENT COLLOIDAL NANOPARTICLES AND INCREASING DELAY BEFORE SPECTRAL ACQUISITION

Figure 6.7 present plots of the first two linear discriminants from the PC-LDA classification. The spectra differences highlighted in F**igures 6.3-6.5** provide for clustering and separation of spectra allowing for classification. Classification accuracies are presented **in Table 6.4**. The classification accuracies in **Table 6.4** are reflected in the degree of clustering and separation in the LDA plots of **Figure 6.7.**

TABLE 6. 4 PC-LDA PATHOGEN CLASSIFICATION PERFORMANCE FOR DIFFERENT COMBINATION OF COLLOIDAL NANOPARTICLE AND DELAYS

Colloidal Nanoparticle	**Delay (minutes)**		
	0	**30**	**60**
Silver 10 nm	100%	100%	93.3%
Silver 40 nm	100%	66.7%	100%
Silver 100 nm	100%	73.3%	73.3%
Gold 10 nm	80.0%	66.7%	100%
Gold 40 nm	60.0%	80.0%	100%
Gold 100 nm	100.0%	71.4%	100%

6.2.4 DISCUSSION

SERS enhancement using commercially available nanoparticles achieved excellent classification performance of uropathogens. In these small samples perfect classification was achieved with many combinations of nanoparticles and delays.

These results appear to favour some nanoparticle size and metal combinations, with silver generally performing better than gold nanoparticles. This is unsurprising given the greater enhancement provided by silver as compared to gold[45]. With 10 nm nanoparticles appearing to provide the most consistent classification across time. The small individual sample sizes however do not allow for definitive identification nanoparticle type providing the greatest enhancement.

Time dependent interaction of nanoparticles with pathogens was assessed through repeated acquisition over multiple time points for each sample. An interesting phenomenon is that the best performance for most colloidal nanoparticles were achieved immediately or after an hour delay, with performance impaired at 30 minutes. This is also reflected in the scaled spectral plots which are flattened with wider uncertainty ribbons at 30 minutes compared to 0 and 60 minutes. A likely explanation is that variation is induced by dynamic interaction of nanoparticles with the pathogens at 30 minutes which stabilises at 60 minutes. The use of heavy suspensions in this work may have limited the benefit provided to delayed acquisition.

While good classification performance was achieved with the majority of combinations of nanoparticles and delays, there are some instances of poor classification as low as 60%. While this may be reflective of the small sample size, other factors may play a role in misclassification. *Sengupta et al.* noted the interaction of nanoparticles is affected by environment conditions such as pH, pathogen load and even the pathogen[195]. These potential limitations of SERS using nanoparticles require either investigation and strict control or methods to nullify their effects. Aggregation and capture of pathogens is likely to limit the effects that suspension characteristics is likely to have[70, 88].

A number of descriptive spectral bands are present for all nanoparticle and delay combinations, with all the difference plots (**Figures 6.3 to 6.5**) showing statistically significant peaks which are aligned with other published works[96, 99, 101, 110, 117, 123, 149, 158, 190]. When contrasting the spectral band assignments here against those produced by unenhanced Raman spectroscopy (**Section 5.3**) some notable differences are evident. A greater preponderance of chemical entities arising from the cell envelope, including peptidoglycan, amino acids and saccharides, as compared to a more dispersed array of chemical entities seen with unenhanced Raman spectroscopy, which included nucleotides and non-specific entities such as carbon backbones. Given these entities, assignments are present both at the 0 minute and 60-minute acquisition delays, which indicates these assignments are not a result of the time dependent reaction but more likely the SERS distance mediated selectivity[7, 69, 72, 80, 85, 123].

A substantial limitation of this work is the small sample size in each pathogenic sub-population assessed. This highlights one of the broader challenges of Raman research, in that multiple experimental parameters combine to from large experimental permutations. To assess 5 samples each of three uropathogens for enhanced with six different colloidal nanoparticles produces 90 permutations. Given each sample preparation and Raman acquisition required hours, these small individual sample groups require a disproportionately large amount of time.

In conclusion, this work demonstrates that compared to unenhanced Raman spectroscopy, there are substantial benefits provided by SERS for pathogen classification. Despite small sample sizes the enhancement provided for superior classification as compared to the earlier study using unenhanced Raman spectroscopy (**Section 5.3)**. While no nanoparticle type was demonstrated to be significantly more enhancing than another, these results did favour silver nanoparticles. Finally, while this work is in line with published work that increased time provides for improved classification accuracy, the initial dynamism while this occurs can induce variability leading to worse performance. As such, it may be of more value to immediately acquire spectra than to wait for this interaction to settle.

6.3 PATHOGEN CAPTURE AND IDENTIFICATION THROUGH A COMBINATION OF VACUUM FILTRATION AND SILVER NANOPARTICLES.

6.3.1 INTRODUCTION

SERS using nanoparticles is demonstrated in **Section 6.2** to provide significant enhancement of uropathogens potentially overcoming weak biologic Raman scattering allowing for pathogen identification at clinically relevant concentrations. With sufficiently concentrated pathogen loads SERS enhancement is achieved without requiring an acquisition delay to allow for nanoparticles to interact with pathogens. A range of methods for pathogen aggregation and capture may be employed in conjunction colloidal nanoparticle mediated SERS[186].

Kahraman et al. developed a convective assembly which created a monolayer of cells from bacterial suspensions mixed with colloidal nanoparticles [161]. Nanoparticles were prepared by the method of Lee and Meisel before mixing with pathogens suspended to pathogen loads in the order of 10^{10} CFU/ml. The mixed suspension was spotted on a slide, over which an additional held slide at a 24° angle was run to create the monolayer. The slide was rapidly airdried before Raman acquisition with a Raman microscope[161]. While valuable when combined with Raman microscopy, this method will be disadvantageous when using a spectrometer due to dispersion of pathogens.

Yang et al. utilised a specially developed, positively-charged slide to electrostatically capture negatively charged uropathogens prior to SERS acquisition [149]. Nanoparticles were produced by the method of Leopold and Lendl [196]. Colloidal nanoparticles were incubated with uropathogens before pipetting onto the pegylated slides and washing before Raman spectra were acquired with a Raman microscope. The authors investigated multiple experimental variations including mixing rate, incubation time and incubation temperature on the resulting SERS intensity demonstrating the nanoparticle varied substantially with these parameters. Using the optimised setting strain level discrimination was achieved[149].

Vacuum filtration is a rapid means of bacterial capture that may be implemented with widely available equipment. *Gao et al.* used membrane filters to capture bacteria before adding a Raman reporter, mercaptophenylboronic acid, known to interact with peptidoglycan from Gram positive cell walls[140]. Gold nanoparticles were applied to the membrane filter. Both Polyvinylidene fluoride (PVDF) and nitrocellulose membrane filters were assessed, with nitrocellulose preferred due to lower retained mercaptophenylboronic acid. Raman spectra were acquired by Raman mapping[140].

Nylon membrane filters were used by *Cho et al.* in a multistep method for bacterial aggregation and capture prior to spectral acquisition [144]. Rather than using conventional SERS spectra, a Raman reporter, mercaptobenzoic acid was used to identify a limited range of pathogens, without classification. A limit of detection of 10CFU/ml was achieved[144].

Chen et al. embedded gold nanoparticles into nylon membrane filters to produce a hotspot rich surface for acquisition of SERS spectra of protein complexes [197]. The filters are intended to produce an extensive SERS surface with multiple hotspots rather than to preform vacuum filtration, and as such, the authors do not interrogate whether this SERS substrate would withstand the physical forces caused by vacuum, filtration. The authors highlight the sensitivity of the substrate to particle size and assembly time and the resulting effect on SERS enhancement[197].

Filters created through electrospinning were investigated by *Szymborski et al.* as a method for bacterial capture while acting as a SERS substrate [147]. A range of filter materials were used including polylactic acid (PLA), PVDF, and nylon, with no preferred material reported. The authors report being able to detect a range of bacteria using Raman microscopy without quantifying classification performance[198]. The authors also report being able to identify circulating tumour cells with the same methods[199].

Applying SERS spectroscopy to pathogen using nanoparticles is a feasible method for pathogen identification. Physical methods to aggregate and capture pathogens improves pathogen-nanoparticle apposition leading improved SERS signal. While a number of physical capture methods exist, membrane filtration offers advantages of rapidity and ease of implementation. SERS with nanoparticles combined with vacuum filtration has not been applied to UTI diagnosis, and the optimal material for such an application has not been established.

Hypothesis: Vacuum filtration can be used to capture pathogens from suspension, therein aggregating pathogens and allowing for close application of SERS nanoparticles.

Objectives:

- Assess the diagnosis and classification performance provided by combining vacuum filtration with nanoparticle-based SERS.
- Identify the filter material with the lowest background Raman signal to be used for further SERS filtration-based experiments.
- Investigate the SERS spectra of uropathogens captured on vacuum filters, and enhanced with silver nanoparticles.

6.3.2 Methods

6.3.2.1 Preliminary work - ESTABLISHING the optimal filter material

Four different materials commonly used for membrane filtration were assessed, including polysulphone, nylon, mixed cellulose and polyvinylidene fluoride (PVDF). Five samples of each filter material were prepared by vacuum filtering 30ml of sterile 0.85% saline before airdrying. Raman spectra were acquired from the filters using the IDRaman mini 2.0 handheld spectrometer, mounted in a 3D printed custom designed stand to provide consistent focal length. The laser power was set to 10 mW with spectra acquired over 10 seconds. A mean of 30 spectra were acquired from each sample for a total acquisition time of 5 minutes.

Spectra were smoothed using a Savitsky-Golay filter with a 3^{rd} order polynomial across moving 25 cm^{-1} windows. The baseline subtraction of a 2^{nd} order polynomial before vector normalisation. Mean spectra, with standard error ribbons of each filter material was plotted for visual assessment.

6.3.2.2 Sample preparation, Vacuum filtration and SERS

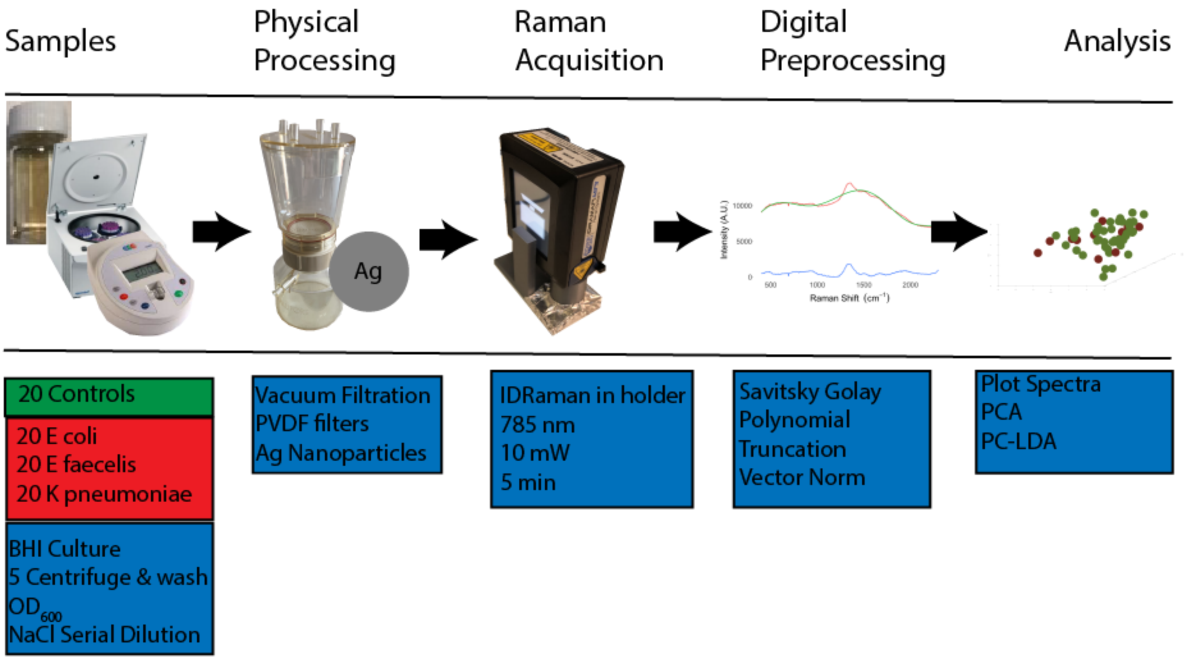

FIGURE 6. 8 METHODS FOR SERS WITH PVDF MEMBRANE FILTERS. SAMPLES WERE PREPARED BY CULTURING REFERENCE STRAIN PATHOGENS WHICH WERE CENTRIFUGED AND WASHED 5 TIMES BEFORE CONTROLLING PATHOGEN LOAD BY OD_{600} AND SERIAL DILUTION IN SALINE. THE SAMPLES WERE VACUUM FILTERED USING PVDF MEMBRANE FILTERS BEFORE PIPETTING ON SILVER NANOPARTICLES. SERS SPECTRA WERE ACQUIRED WITH THE IDRAMAN IN THE 3D-PRINTED HOLDER. SPECTRA WERE DIGITALLY PRE-PROCESSED BY SAVITSKY-GOLAY FILTERING, POLYNOMIAL SUBTRACTION AND VECTOR NORMALISATION. THESE WERE ANALYSED BY PLOTTING SPECTRA, PCA AND PC-LDA.

The methods utilised are summarised in **Figure 6.8**. 60 bacterial suspensions were created for SERS assessment in addition to 20 negative controls consisting of uninoculated 0.85% saline solution. Suspensions of *Escherichia coli* ATCC25922, *Enterococcus faecalis* ATCC29212 and *Klebsiella pneumoniae* ATCC13883 were created using the established research bank. A single microbead was cultured in 3 ml brain heart infusion for 24 hours at 37 degrees. After Vortex mixing, the suspension was transferred to a 2ml centrifuge cuvette and centrifuged at 8300 g for 1 minute. The supernatant was discarded, and the bacterial pellet resuspended in 0.85% saline. This centrifuge and wash process was repeated a total of 5 times. The concentration of the bacterial suspension was adjusted by OD_{600} and serial dilution to a final concentration of 10^5 CFU/ml.

The resulting suspension was vacuum filtered through a 47 mm diameter, 0.45 µm pore size sterile PVDF membrane filter. The membrane filter was removed from the vacuum filter, and 200 µl of 40 nm silver nanoparticle colloid pipetted on the centre of the membrane filter. Filters were then airdried, before transfer for Raman spectral capture.

6.3.2.3 SPECTRAL ACQUISITION AND ANALYSIS

Raman spectra were acquired using the IDRaman mini 2.0 spectrometer mounted in the 3D-printed mount. Spectra were acquired with 10 mW laser power and 10 second acquisition time. A total of 30 spectra were collected from each sample for 5 minutes total acquisition time.

Spectra were pre-processed and analysed using scripts developed in R programming language. Spectra were smoothed using a Savitsky-Golay filter with a 3rd order polynomial over a moving 19 cm^{-1} window. The baseline was corrected by subtraction of a 13th order polynomial. Spectra were truncated from 600 am^{-1} to 2000 cm^{-1} before vector normalisation.

Mean spectra with standard deviation were plotted for infected suspensions as well as uninfected control in addition to those of the uropathogens. To facilitate identification of spectral bands differentiating samples, infected samples were centred and scaled using uninfected controls as a reference. Similarly, pairwise comparison of uropathogens was facilitated by centring and scaling each uropathogen referenced by each other uropathogen. Assessment of diagnostic and classification performance was achieved using PC-LDA for supervised learning.

6.3.4 RESULTS

6.3.4.1 OPTIMAL FILTER MATERIAL

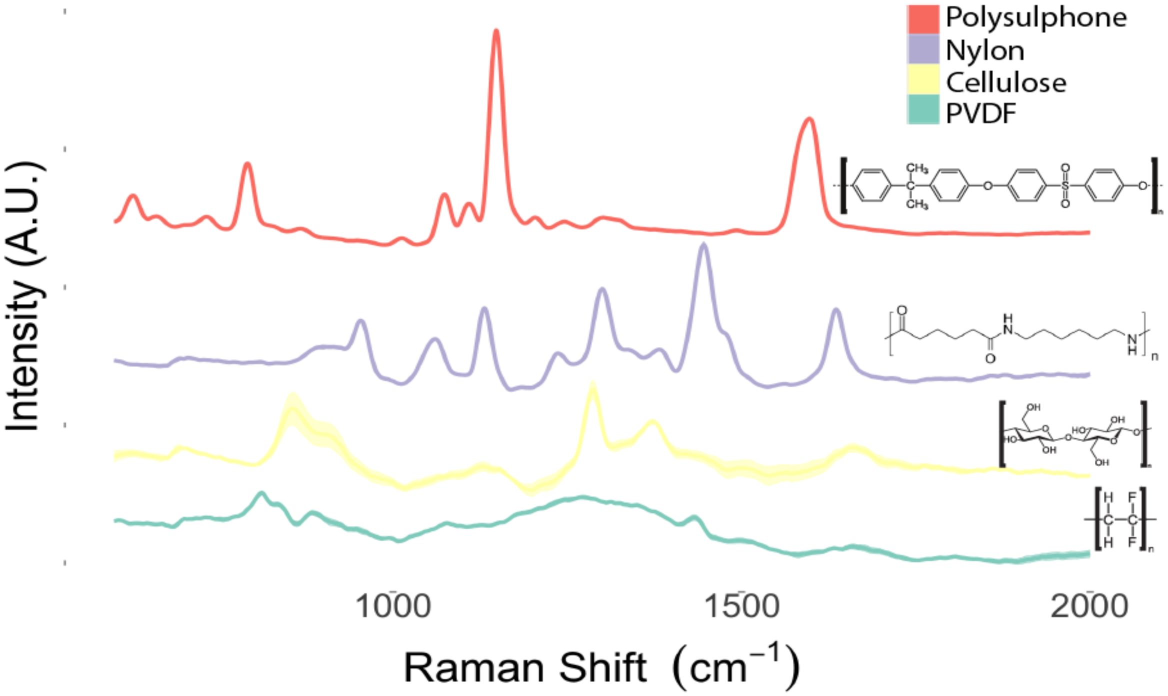

FIGURE 6. 9 MEAN SPECTRA WITH STANDARD ERROR RIBBONS FOR FOUR COMMONLY USED MEMBRANE MATERIALS.

Figure 6.9 presents the mean Raman spectra of four common material used as laboratory membrane filters. The chemical structures of the material monomers are inset for reference. The Raman spectra for polysulphone, nylon and mixed cellulose all demonstrate complex baselines dominated by well-defined peaks arising from the complex chemical structures. In contrast, the PVDF spectrum has a relatively simple baseline with small peaks at 750 cm^{-1} and 1430 cm^{-1} arising from the polymer carbon backbone. PVDF filters were, therefore, used for future experiments.

6.3.4.2 SPECTRAL PLOTS, PCA AND DIAGNOSIS OF INFECTED VERSUS UNINFECTED SAMPLES

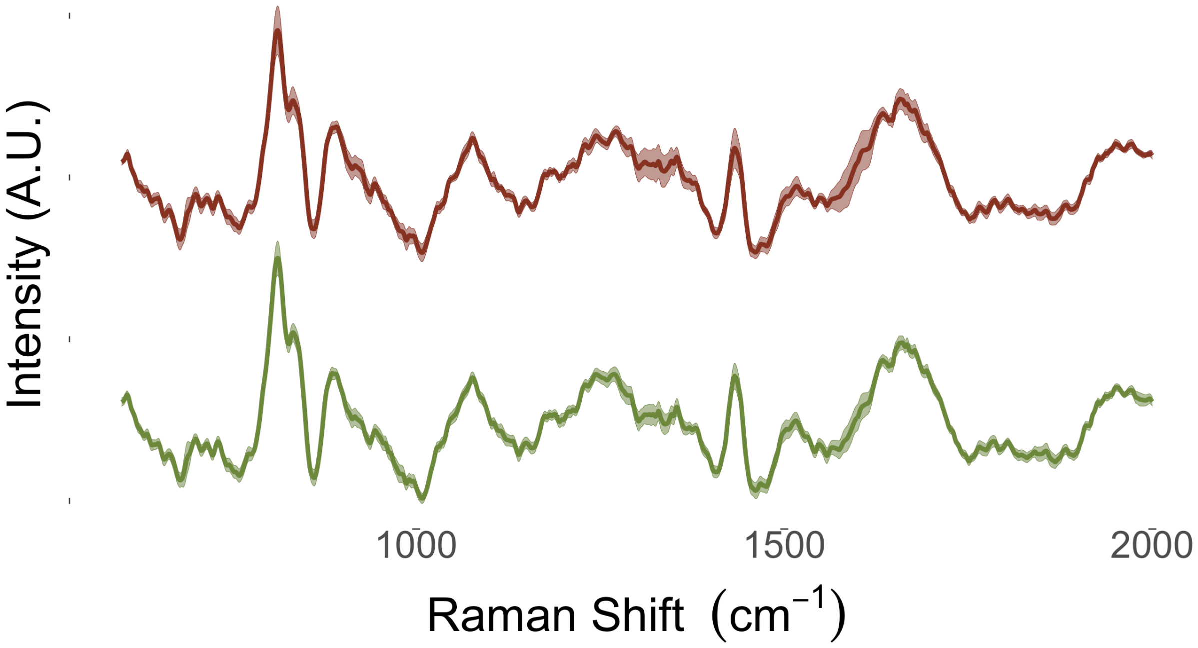

FIGURE 6. 10 MEAN SPECTRA WITH STANDARD ERROR RIBBONS FOR INFECTED (RED) AND UNINFECTED CONTROL SAMPLES (GREEN). FILTERS WITH CAPTURED UROPATHOGENS HAD SPECTRA ACQUIRED USING THE IDRAMAN MINI 2.0 HANDHELD SPECTROMETER WITH 10MW LASER POWER AND 10 SECOND ACQUISITION TIME. THE RESULTING SPECTRA WERE DIGITALLY PRE-PROCESSED USING A SAVITSKY-GOLAY FILTER BEFORE SUBTRACTION OF A 3RD ORDER POLYNOMIAL AND VECTOR NORMALISATION.

Figure 6.10 presents the mean Raman spectra with standard error ribbons for samples vacuum filtered through PVDF membrane filters and enhanced using 40 nm silver colloidal nanoparticles. The spectra retain the two large peaks arising from the PVDF membrane filter at 750cm^{-1} and 1430 cm^{-1}, in addition to a residual baseline incompletely removed during pre-processing. A number of discriminatory peaks, visible as deviations from the baseline are visible in the spectra. The wider standard error ribbon of infected samples as compared to uninfected controls indicates a higher degree of variability in these samples, potentially arising from difference in pathogen contributions to spectra. The differences are emphasised in **Figure 6.11** in which infected samples are centred and scaled using uninfected controls as a reference.

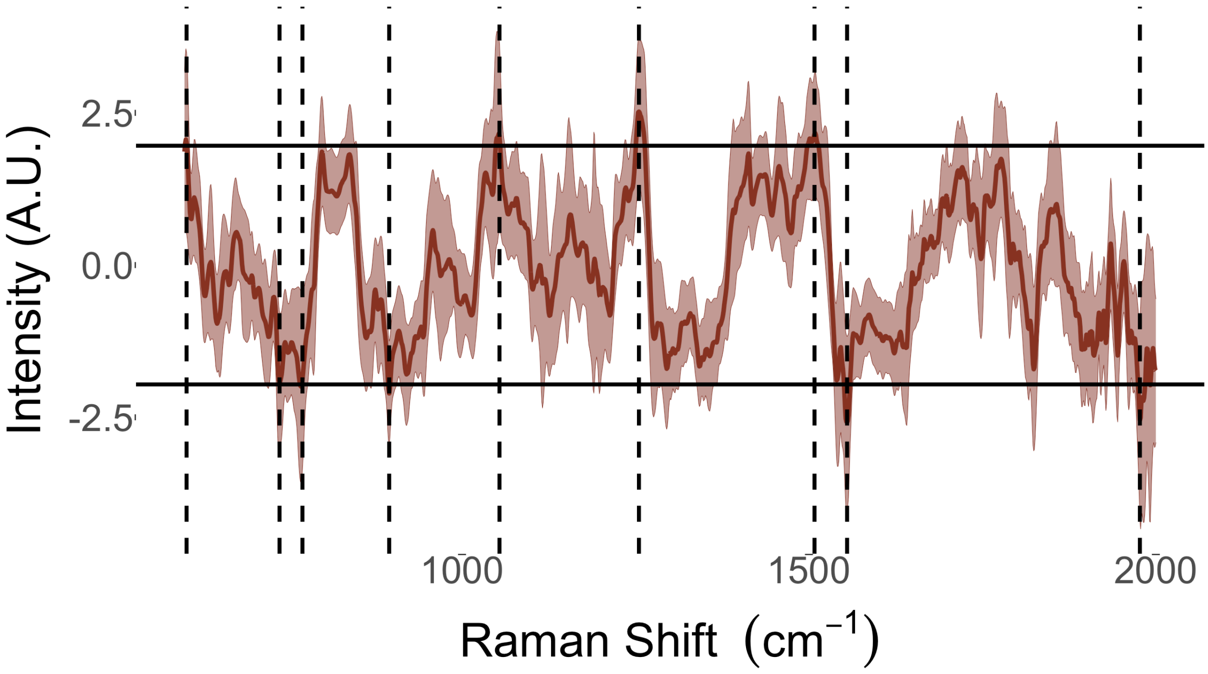

FIGURE 6. 11 MEAN RAMAN SPECTRUM WITH STANDARD ERROR RIBBONS FOR INFECTED SAMPLES, CENTRED AND SCALED ON NEGATIVE CONTROLS. HORIZONTAL DASHED LINED DELINEATE THE BORDER AT WHICH DIFFERENCES ARE STATISTICALLY SIGNIFICANT AT $\alpha = 0.05$. VERTICAL DASHED LINES DEPICT THE PEAKS OF MAXIMUM DIFFERENCE.

Figure 6.11 presents the mean Raman spectrum, with standard error ribbons for infected samples centred and scaled on negative control spectra. Horizontal lines delineate the boundary where differences are significant at $\alpha = 0.05$. Discriminatory bands at which infected spectra differ significantly from those of uninfected controls are indicated by vertical dashed lines and listed in **Table 6.5**.

TABLE 6. 5 SPECTRAL BAND ASSIGNMENTS FOR INFECTED SAMPLES.

Spectral band	Band assignment	References
737 cm^{-1}	C-N Stretching, Ring breathing adenine	[123]
770 cm^{-1}	Tryptophan	[158]
895 cm^{-1}	C-C backbone	[190]
1054 cm^{-1}	Protein C-O and C-N stretching	[190]
1255 cm^{-1}	Amide III	[117]
1508 cm^{-1}	Adenosine, cytosine, N-H bending	[190]
1555 cm^{-1}	Tryptophan, exopolysaccharides	[110]

6.3.4.3 DIAGNOSTIC AND CLASSIFICATION PERFORMANCE

Table 6.6 quantifies the diagnostic performance provided by Raman spectroscopy of samples vacuum filtered onto PVDF membrane filters and enhanced with 40 nm silver colloidal nanoparticles. Infected samples were diagnosed with 85% accuracy (95% CI 73.4% ; 92.9%, p-value: 0.045), while sensitivity and specificity were 93.3% and 60% respectively.

TABLE 6. 6 DIAGNOSTIC PERFORMANCE OF PC-LDA CLASSIFICATION FOR OF INFECTED VERSUS UNINFECTED CONTROLS.

		Reference class	
		Uninfected control	**Infected**
Predicted class	**Uninfected controls**	9	3
	Infected	6	42
Diagnostic performance			
Accuracy		85% (95% CI: 73.4-92.9%; p-value: 0.045)	
Sensitivity		93.3%	
Specificity		60.0%	

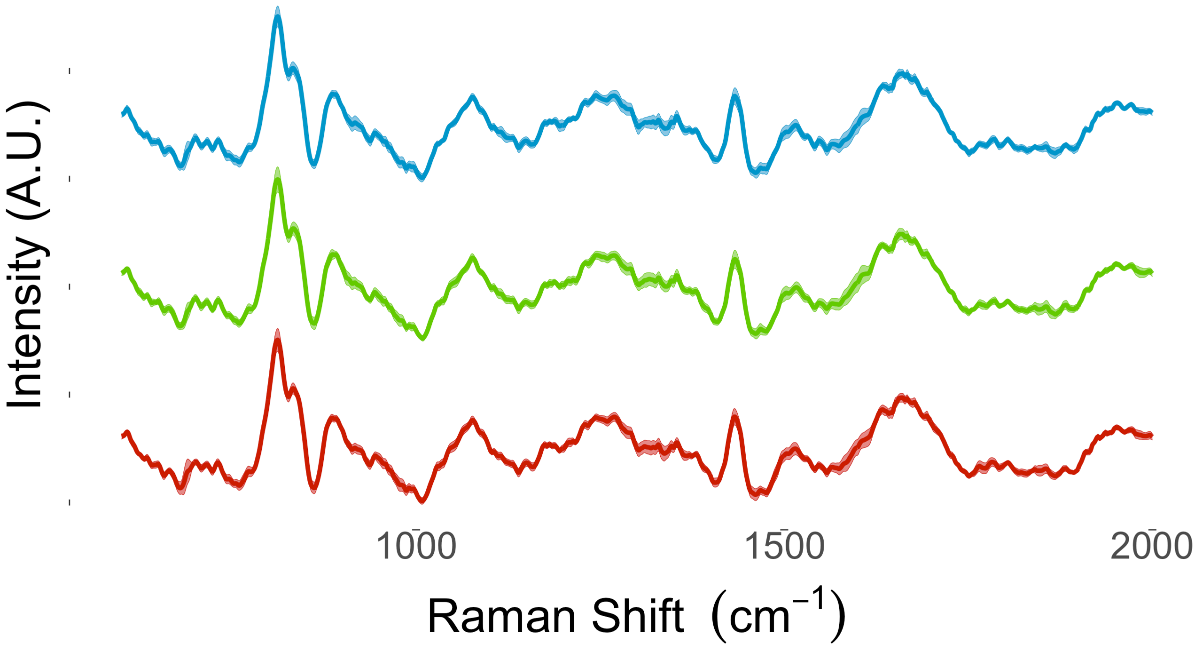

FIGURE 6. 12 MEAN SPECTRA WITH STANDARD ERROR RIBBONS FOR REFERENCE PATHOGENS (RED: *ESCHERICHIA COLI*; GREEN: *ENTEROCOCCUS FAECALIS*; BLUE: *KLEBSIELLA PNEUMONIAE*) CAPTURED ON PVDF MEMBRANE FILTERS AND ENHANCED WITH 40 NM SILVER COLLOIDAL NANOPARTICLES

6.3.4.3 SPECTRAL PLOTS, PCA AND CLASSIFICATION OF UROPATHOGENS

Figure 6.12 presents the mean spectra with standard error ribbons for pathogens captured on PVDF membrane filters and enhanced with 40 nm colloidal silver nanoparticles. There are no visible differences in the spectra which may provide for pathogen classification.

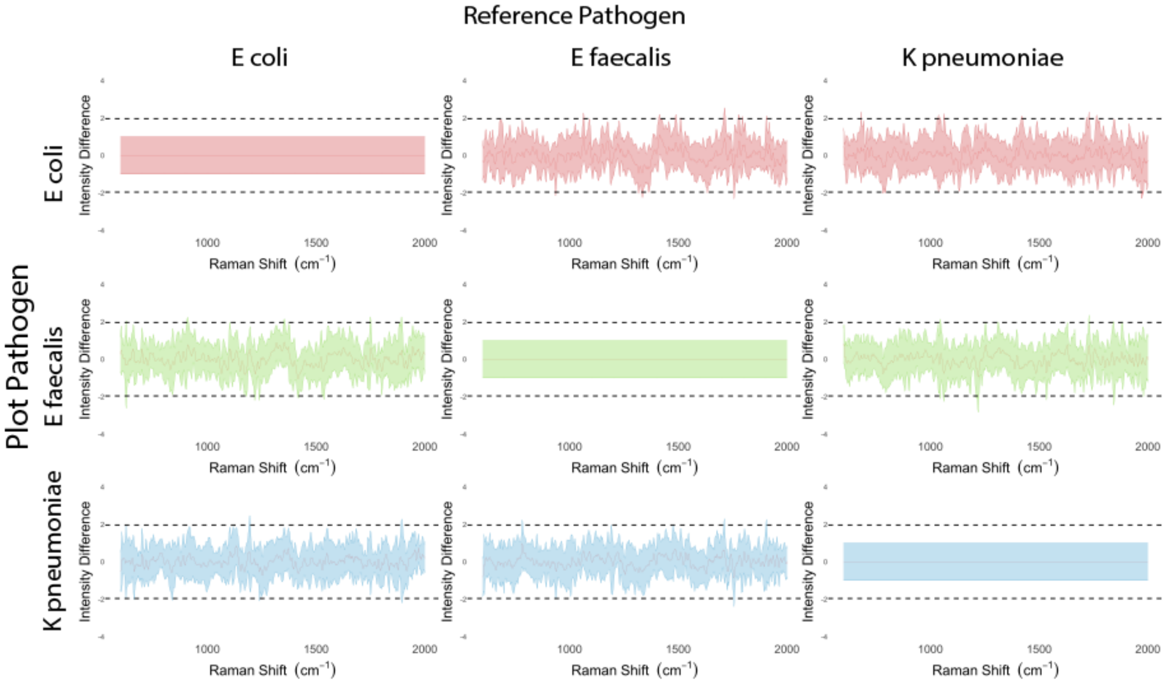

FIGURE 6. 13 MEAN SPECTRA WITH STANDARD ERROR RIBBONS FOR UROPATHOGENS CENTRED AND SCALED BY OTHER UROPATHOGEN SPECTRA. HORIZONTAL DASHED LINED DELINEATE THE BORDER AT WHICH DIFFERENCES ARE STATISTICALLY SIGNIFICANT AT α = 0.05.

Figure 6.13 depicts pairwise comparison of pathogen spectra by centring and scaling each pathogen group by all other individual pathogen groups. Boundaries at which bands will differ significantly at α = 0.05 are indicated by dashed horizontal lines. These plots confirm that within these study samples, there are no individual bands which exhibit statistically significant differences between species.

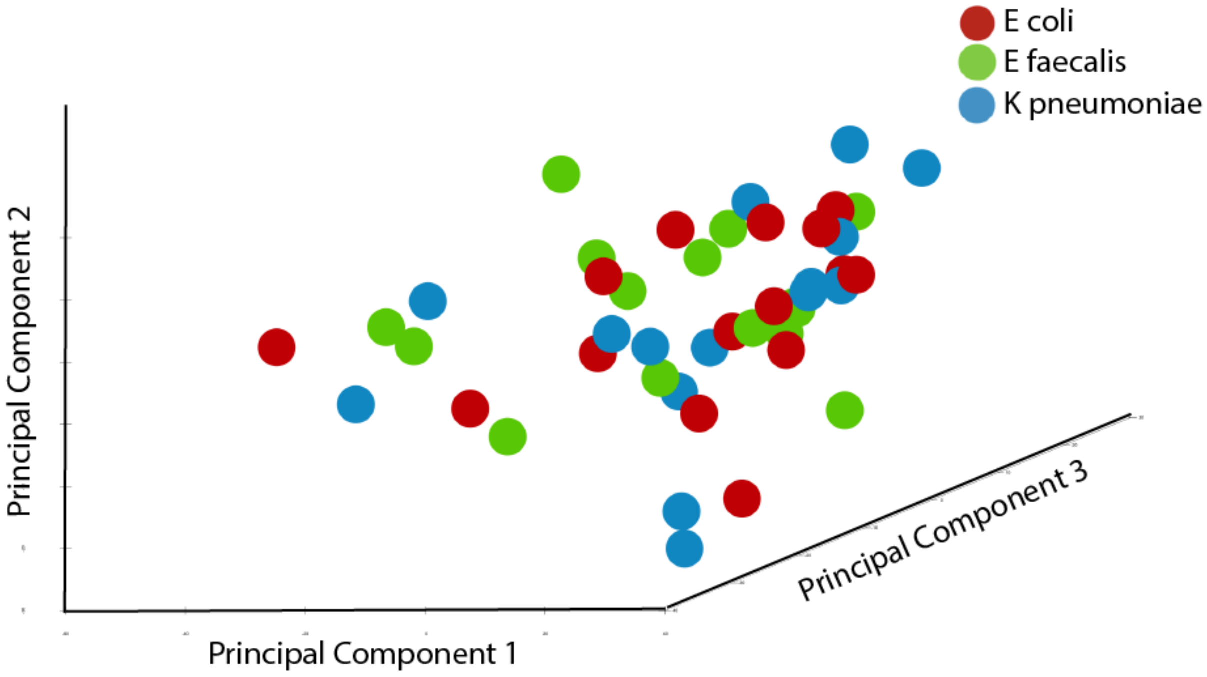

FIGURE 6. 14 PLOT OF THE FIRST 3 PRINCIPAL COMPONENTS FOR SPECTRA OF UROPATHOGENS (RED: *ESCHERICHIA COLI*; GREEN: *ENTEROCOCCUS FAECALIS*; BLUE: *KLEBSIELLA PNEUMONIAE*) CAPTURED ON PVDF MEMBRANE FILTERS AND ENHANCED THROUGH WITH 40 NM SILVER COLLOIDAL NANOPARTICLES

Figure 6.14 presents unsupervised classification of pathogen spectra using PCA. This plot of the first 3 principal components demonstrates no natural grouping by uropathogen spectra, with near complete overlap of the component groups.

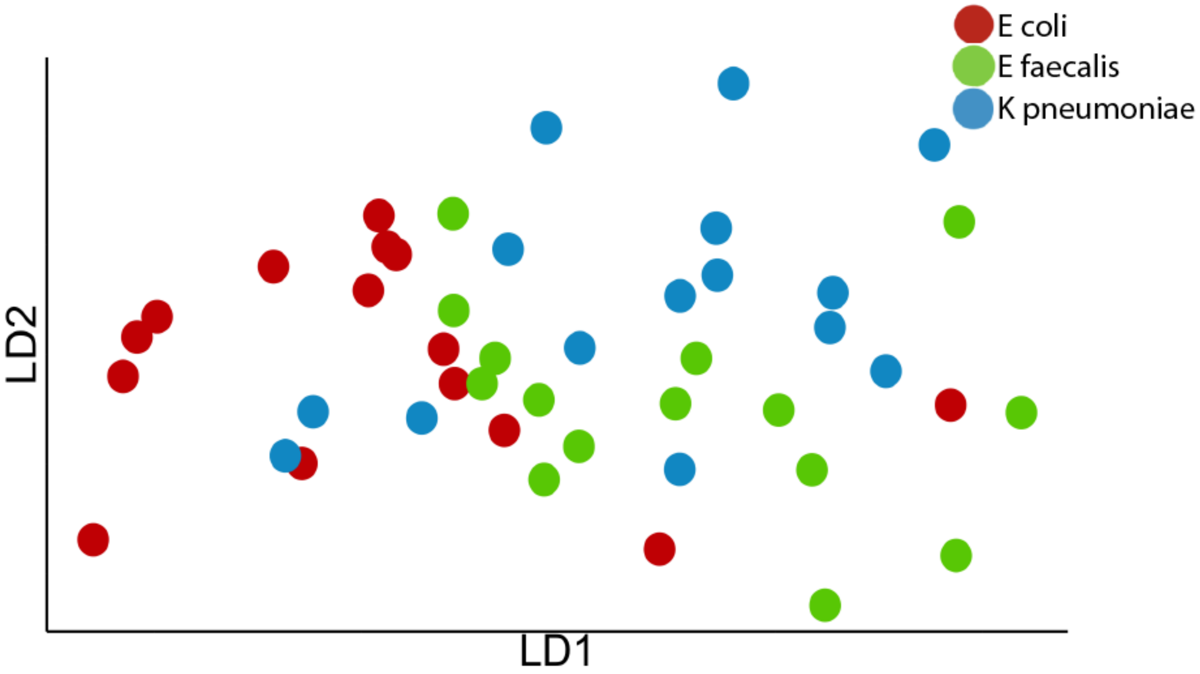

FIGURE 6. 15 PC-LDA PLOT FOR SUPERVISED CLASSIFICATION OF UROPATHOGEN SPECTRA (RED: *ESCHERICHIA COLI*; GREEN: *ENTEROCOCCUS FAECALIS*; BLUE: *KLEBSIELLA PNEUMONIAE*).

Figure 6.15 presents a plot of supervised learning through PC-LDA classification and is quantified in **Table 6.7**. The PC-LDA plot demonstrates poor clustering and minimal separation of spectra. Pathogen species were classified with 73.3% (95% CI: 58.0; 85.4%, p-Value >0.05) accuracy. This low classification performance is reflective of the plots in **Figure 6.13**, in which no spectral bands differed significantly between species.

TABLE 6. 7 PC-LDA CLASSIFICATION OF UROPATHOGEN SPECIES

		Reference		
		Escherichia coli	***Enterococcus faecalis***	***Klebsiella pneumoniae***
Predicted	***Escherichia coli***	13	3	3
	Enterococcus faecalis	2	10	2
	Klebsiella pneumoniae	0	2	10
Classification performance				
Accuracy		73.3% (95% CI:58.0% - 85.4%; p-value >0.05)		

6.3.5 DISCUSSION

SERS using colloidal nanoparticles is a suitable method for improving pathogen Raman signal therein allowing for pathogen identification and classification. This is best paired with physical methods to aggregate and capture pathogens to aid apposition of pathogens to nanoparticles[186]. In this work, combining vacuum filtration with colloidal nanoparticle-mediated SERS provides for sufficient signal enhancement to allow for diagnosis of infected samples, although insufficient to provide reliable classification.

Vacuum filtration has been combined with SERS in numerous published research works attempting to identify a range of biologic and chemical entities[126, 144-147, 197, 199-201]. In these works, the filters appear to have fulfilled the dual role of physical separation as well as increasing the surface area on which surface enhancement can take place. Filter materials including cellulose, polylactic acid, nylon and PVDF have been employed without reviewing the Raman spectra of the materials, and therefore providing an understanding of which material is best suited to the intended purpose[126, 144, 145, 147, 198]. When applied to pathogen detection, the ideal filter will provide for physical capture of pathogens without contributing competing Raman signal. In this work, the Raman spectra of four commonly utilised membrane filter materials was assessed, including methylcellulose, polysulphone, nylon and PVDF. The Raman spectrum of PVDF contributed significantly less Raman signal as compared to spectra acquired from other filter materials.

The chemical structure of PVDF consists of carbon backbone with alternating hydrogenation and fluorination. As such, the only Raman contribution is that of the carbon backbone, which is common to many biologic compounds and so is unlikely to contribute significantly to differentiation of pathogens. In contrast, the chemical structures of the other materials assessed were consisted of complex monomers composed of benzene rings, ester, and amide bonds amongst others. Therefore, these demonstrated complex Raman spectra, with large peaks likely to obfuscate pathogen Raman signal. PVDF was therefore selected as the optimal material for vacuum filtration prior for SERS acquisition in further experiments.

Diagnosis of infected samples was achieved with 85% accuracy (95% CI: 73.4-92.9%; p-value: 0.045), which exceeds that of currently implemented screening technologies such as urinalysis[4, 51, 191, 202]. Drawing on comparisons with other published Raman based pathogen detection draws a similar challenge to that seen in earlier experimental work in that an overreliance on Raman microscopy means many of these works do not include negative controls. While the works by *Cho et al.[145]* as well as *Gao et al.[145]* did contain negative controls, identification was based on labelled SERS, in which a strong Raman scatterer was bound to the pathogen of interest. This technique is well suited to their intended application of food contamination detection which requires identification of infected sample, with less emphasis on pathogen identification. Classification performance was not quantified in these works, with results presented as spectra only[144, 145]. Nevertheless, both works confirm vacuum filtration can be used for physically aggregate and capture pathogens and present these for Raman acquisition.

In this chapter, classification of uropathogens in infected samples was performed with 73.3% accuracy (95% CI: 58.0% - 85.4%; p-value >0.05), which is inferior to other classification technologies such as PCR and mass spectrometry. This performance is similarly inferior to other attempts at pathogen classification using colloidal SERS. *Yang et al.* had only a single misclassification amongst 48 spectra acquired from uropathogens electrostatically captured from and enhanced with silver nanoparticles[149]. This excellent classification performance must be tempered by the fact that spectra were acquired with a Raman microscope, and an unaddressed limitation that the physical capture using electrostatics forces is unlikely to work in urine given the myriad of competing negatively charged components. While not quantified, *Kahraman et al.* achieved clear excellent quality spectra from two pathogens captured from suspension and enhanced with colloidal silver nanoparticles[161]. The excellent performance of their technology once again must be tempered by the fact that spectra were acquired using a Raman microscope, and the high pathogen load of 10^{10} CFU/ml. Nevertheless, the diagnostic performance in this work is in agreement with the classification performance in these published works in that enhancement using colloidal nanoparticles can substantially improve pathogen Raman signal.

While the combination of SERS and vacuum filtration achieved diagnosis of infected samples, it did not provide pathogen classification comparable with other published work. This is likely because spectra were acquired in this experimental work using a handheld spectrometer in contrast to the Raman microscopes used in other published work. The decision to use a handheld spectrometer was made in light of the minimal scope for development of a microscope-based technology towards a clinically implementable technology.

Additionally, surface enhancement provided by colloidal nanoparticles, while important improving the signal for pathogen detection may inadvertently induced noise that worsens classification performance. The SERS effect is inversely and exponentially proportional to the distance between the target and SERS substrate, and as such any variation in nanoparticle apposition while induce a disproportionate amount of spectral noise. Nanoparticles are prone to variable apposition because pathogens are nonuniformly distributed in solution, and because nanoparticles are prone to agglomerate when physical conditions vary (such as in bacterial suspensions)[70, 136].

This phenomenon may explain the relatively generic nature of the contributing components identified in the spectral band analysis in **Table 6.5,** with the chemical components not being specific to any cellular structure or particular pathogen. As such, these widely existing chemical entities may be sufficient to differentiate infected from uninfected samples, but not to differentiate between pathogens.

Combined, these results demonstrate that combing vacuum filtration with SERS using colloidal nanoparticles provides sufficient signal enhancement for diagnosis of infected samples at clinically relevant concentrations of 10^5 cfu/ml without identifying the causative uropathogen. Improving the SERS signal stability is likely to further improve classification performance to allow for classification of pathogens at clinically relevant concentrations.

6.4 CONCLUSION

Uropathogens have unique SERS spectra acquired using colloidal nanoparticles providing for accurate classification. The signal enhancement provided by colloidal nanoparticles, when augmented by pathogen aggregation through vacuum filtration, allows for identification of infected samples with accuracy greater than that of currently implemented screening technologies such as urinalysis.

The experimental work in **Chapter 6** extends the current understanding of SERS using colloidal nanoparticles by demonstrating that classification may be achieved using a low-cost handheld spectrometer rather than the Raman microscopes used in published literature. Furthermore, while vacuum filtration has been proposed in the published literature as a means of pathogen capture, this work presents the first robust assessment of filter materials tailored to Raman analysis[144-147, 198, 201].

Analysis of SERS spectra of uropathogen suspensions enhanced using a variety of commercially acquired colloidal nanoparticles demonstrates the substantial signal enhancement provides for classification with accuracy up to 100%. Analysis of the spectral bands indicates classification arises from recognition of the cell envelope components identified in other published works on SERS mediated uropathogen identification[128, 137]. While no specific nanoparticle size was demonstrated to provide superior classification in this work, silver outperformed gold nanoparticles which is in keeping with previous works[45]. The inability to demonstrate a preferred nanoparticle size is likely reflective of the small group sample sizes dictated by the large number of experimental permutations assessed. These small group sample sizes along with the excellent classification performance may also explain the failure to demonstrate a trend of improved classification performance with longer acquisition delays.

The assessment of diagnostic and classification performance of SERS using colloidal nanoparticles was extended to suspensions of clinically relevant concentrations. Vacuum filtration was identified as a means of rapidly aggregating and capturing uropathogens direct from suspension prior to SERS acquisition. While filters have been paired SERS acquisition in the published literature, this has typically been as a means of providing a large SERS area, rather than a means of pathogen capture. As such, no robust assessment of filter material as applied to Raman analysis of captured pathogens is available in the published literature. An assessment of four common filter materials here demonstrates PVDF contributes minimal competing Raman signal due to its simple chemical structure.

Combining vacuum filtration for pathogen capture with enhancement using silver nanoparticles achieved identification of infected samples with 85% accuracy. This is greater than published accuracy of widely adopted screening technologies such as urinalysis[4, 51]. Assessment of the contributing spectra bands demonstrated enhancement of nonspecific biochemical entities likely to be widely present in bacteria rather than those likely to be species specific. This is reflected by the failure to provide pathogen classification. This indicates that while the enhancement is sufficient to allow for identification of infected samples, it is insufficient to provide for classification of the causative pathogen.

The suboptimal enhancement provided by SERS nanoparticles may be explained by variability in the proximity of the SERS substrate to the pathogens. Colloidal nanoparticles may agglomerate in response to environmental factors including solution ionicity, pH and temperature, with greater agglomeration seen with smaller nanoparticle size[203, 204]. In addition to the risk of agglomeration affecting uniform dispersion of nanoparticles, environmental factors similarly alter the interaction of these nanoparticles with pathogens. Higher agglomeration seen with increased ionicity, lower pH and larger particles is demonstrated to reduce the interaction of nanoparticles with *Escherichia coli*[205]. While these risks may be mitigated through careful environmental control, the highly variable nature of urine and ability of pathogens to influence their environment warrants investigation of alternative SERS methods.

In summation combining vacuum filtration with SERS provides Raman signal enhancement allowing for detection of infected samples at clinically relevant concentrations. Attaining greater SERS stability is required to deliver classification performance required for clinical application. As such, **Chapter 7** will apply a SERS substrate directly to PVDF filters to achieve greater stability of the pathogen SERS.

CHAPTER 7: GOLD NANOCOATED SERS-ACTIVE FILTERS

7.1 INTRODUCTION

UTIs are demonstrated in **Chapter 2** to be one of the most common bacterial infections leading to a substantial patient morbidity and mortality in addition to massive societal costs[1, 2, 8, 10, 206]. The current diagnostic approach, characterised by inaccuracy and delay, exacerbates this burden disease[5, 51]. A new diagnostic paradigm underpinned by a novel technology could reduce the burden of disease caused by UTIs. The ideal technology for this purpose would deliver rapid and accurate diagnosis with pathogen classification, therein allowing for precision antimicrobial management from the outset.

As described in **Chapter 3,** Raman spectroscopy is uniquely suited to performing this role, specifically through its ability to deliver info highly resolved information rich spectra without requiring prior biomass expansion[7, 76, 82, 88, 123, 156]. Uropathogens are demonstrated in **Chapter 5** to have unique Raman spectra allowing for strain level classification, however, a significant challenge arises in that weak biologic Raman scattering is overwhelmed by urine fluorescence. As such, methods are required to physically aggregate and capture pathogens as well as separate these from urine[186]. Additionally, techniques to enhance pathogen Raman signal such as SERS are required.

Vacuum filtration is a microbiologic technique employed to rapidly concentrate pathogens using low-cost and widely available equipment. PVDF filters are demonstrated in **Chapter 6** to contribute minimal competing Raman signal[207]. A potential challenge arises in applying vacuum filtration to capture pathogens, in that urine contains other particulate matter such as cells and casts. Fortunately, eukaryotic cells are an order of magnitude larger than pathogens (greater than 10 μm as compared to 1μm), and as such dual filtration can be used to separate them, therein ensuring only the targeted pathogen are on the final filter[55].

SERS may be used to overcome weak biologic Raman scattering through delivery of massive signal enhancement[82, 88, 123, 156]. Additionally, SERS enhancement is strongly dependent on the distance between the SERS substrate and target, and as such enhancement can be targeted[7, 69, 72, 80, 85, 123]. This is of particular benefit when applied to pathogen detection as the majority of pathogen's definitive biomass is incorporated into the cell envelope which makes up the most superficial aspect of the cell, and so a close and consistently applied SERS substrate will massively and selectively enhance this biomass.

While the application of SERS using colloidal nanoparticles has the potential advantage in that these naturally interact with the pathogen cell envelope, the sensitivity of nanoparticles to environmental conditions may result in variability in this interaction.[70, 88, 136]. Alternatively, applying pathogens to a SERS-active surface may avoid the challenges of variable nanoparticle interaction[70]. At its simplest, pathogen suspensions may be applied to glass slides with roughened noble metal surfaces[141]. Improved enhancement, or greater functionality, may however be gained through application to a surface tailored to a specific purpose. This provides great versatility in the material and structure of the surface, as well as the method of application of the SERS substrate. Gold and silver have been applied to materials such as glass slides, silicon wafers, mesoporous silica and filters using methods including thermal evaporation, electrodeposition, and physical vapour deposition (PVD)[78, 98, 136, 208-212].

Application of a SERS surface to membrane filters may improve the performance SERS stability as compared to the nanoparticles used in **Chapter 6.** These SERS-active filters will perform as a multifunctional component capable of capturing and aggregating pathogens, separating them from urine, and providing a SERS-active surface.

Hypothesis: SERS-active filter membranes can provide UTI diagnosis with pathogen classification, through aggregation and capture of pathogens, separation of urine and enhancement of Raman signal.

Objectives:

- Identify and optimise a method for applying a SERS surface to PVDF membrane filters.
- Develop a dual filtration method capable of rapid pathogen capture with separation from urine.
- Investigate the SERS spectra of uropathogens captured on SES active filters.
- Assess the diagnostic and classification performance of SERS -active filters.

7.2 DIAGNOSIS OF PHANTOM URINE INFECTIONS USING SERS-ACTIVE FILTERS

7.2.1 INTRODUCTION

The central challenge to developing a Raman-based technology for UTI diagnosis with uropathogen classification arises in that weak biologic scattering from pathogens is overwhelmed by competing signal and fluorescence from urine. A SERS-active filter can overcome these challenges by simultaneously performing multiple roles: firstly, the filter can rapidly concentrate and capture pathogens from a large volume of urine; secondly, pathogens can be separated from urine by subsequently passing a washing solvent over the filter; finally, the filter can act as a SERS surface, therein providing signal enhancement.

Filters have been used as used as SERS substrates in a number of published works. *Lin et al.* created custom-made filters by embedding gold nanoparticles in mesoporous silica, which was then compressed into a filter structure using a stainless-steel mould[136]. These filters were used primarily as a SERS surface rather than a filter, as pathogen suspensions were simply spotted instead of filtered through. Nevertheless, highly resolved spectra from *Staphylococcus aureus* suspensions on the filters were acquired using a Raman microscope. The authors highlight the signal enhancement was strongly dependent on the interparticle spacing of the gold particles[136].

Wigginton et al. applied a gold coating to polycarbonate membrane filters as a method of fluorescence quenching, prior to SERS using immunobound gold nanoparticles for the detection of *Giardia* cysts[146]. Raman mapping was used to identify and quantify cysts with 95% recovery[146].

Kaminska et al. created SERS-active filters creating electrospun polylactic acid mats onto which a 40 nm gold and silver nanolayer was applied by sputtered PVD[199]. These SERS-active filters were used to directly capture circulating tumour cells from blood phantoms prior to Raman acquisition using a Raman microscope. The authors identified circulating cervical cancer, prostatic cancer and leucocytes (control) with 98% sensitivity[199].

Szymborski et al. produced similar electrospun mats with a 90 nm gold nanocoating for capture of pathogens from biofluids prior to Raman acquisition with a Raman microscope[147]. Differing filter materials along with 3 gold nanocoating thicknesses were assessed, with the authors not identifying a superior material type but did report greatest enhancement with 90 and 200 nm thickness. The authors report highly resolved spectra for *Escherichia coli* and *Staphylococcus aureus* captured from various fluids including saline, apple juice and urine. Classification performance in these fluids was not quantified. Similarly, the processing of the urine is not described with regards to separation of other particulates (cells and casts), nor washing of fluorescent urine components [147].

PVD is a widely employed technique for application of thin films. The process of PVD entails vaporisation of a target, such as gold, by bombarding it with a plasma. The vapourised gold is directed onto a substrate by a high voltage electric field. PVD has numerous advantages including the ability to closely control an evenly applied and high purity nanolayer down to a few nanometres thickness. The process does not require the high temperatures used in chemical vapour deposition avoiding destruction of the substrate. Furthermore, the need to establish a vacuum provides an additional benefit in the removal of impurities[213, 214].

Prior to this work, no published works have developed a SERS-active filter through application of a gold nanolayer to commercially acquired membrane filters[148]. Where gold has been applied to electrospun fibres, the gold thickness is inadequately optimised. Where SERS-active filters have been assessed, spectra were acquired with a Raman microscope, which limits further translation, and is not amenable to assessment of negative controls. Diagnostic and classification performance had not been quantified.

Hypothesis: Application of a SERS nanostructure to membrane filters will provide a rapid means of pathogen capture and separation from urine, while providing Raman signal enhancement. SERS-active membrane filters, therefore, can provide rapid pathogen identification and classification directly from phantom urine samples.

Objectives:

- Identify the gold nano-thickness providing optimal Enhancement of SERS signal from membrane filters.
- Develop a system for rapid urine sample processing, allowing for rapid pathogen capture and segregation from urine, in addition to Raman spectral capture.
- Describe the SERS spectra of reference strain uropathogens captured from phantom urine on SERS-active filters.
- Describe the diagnostic and classification performance of SERS-active filters for infected phantom UTI samples.

7.2.2 METHODS

7.2.2.1 OPTIMISATION OF GOLD NANOCOATING THICKNESS

To fabricate SERS-active filters a gold nanocoating were applied to PVDF membrane filters by PVD using a Korvus Hex thin film deposition system. PVDF filters were selected as they were demonstrated in **Chapter** 6 to have simple Raman background with minimal variability. The PVDF filters were loaded onto the 4-inch rotating stage, and a vacuum of 10^{-5} Bar established in the chamber. A DC magnetron source with potential difference of 600 V, and current of 0.15 mA established a plasma using argon with flow rate of 20 standard cubic centimetres per minute (sccm). The plasma bombarded a 2-inch gold target, leading to sputtered physical deposition at a rate of approximately 30 Angstroms per second. The exact gold nanocoating thickness applied was controlled using quartz crystal monitoring (QCM). In addition to unsputtered controls, gold nanocoatings of 2.5, 5.0, 7.5, 10.0, 12.5, 15.0, 20.0, 25.0, 50.0, 100.0 and 150.0 nm were applied to PVDF membranes for assessment.

Rhodamine 6G (R6G), a Raman dye with a well described Raman spectrum was used to assess enhancement provided by filters with different gold thicknesses. A 1 μM solution was created by dissolving R6G in sterile deionised water and 100 μl was pipetted onto the centre of each filter and allowed to air dry before Raman acquisition. For each filter sputter thickness, 12 replicates for were assessed.

Raman spectra were acquired using the IDRaman mini 2.0 handheld spectrometer loaded into the 3D-printed mount (designed in **Section 4.3.4)**. The laser power was set to 10 mW at 785 nm. Acquisition time was set to 5 seconds, with 5 averages taken for each sample.

Spectra were pre-processed and analysed using scripts developed in R programming language. Spectra were smoothed using a Savitsky-Golay filter of 3rd order polynomial over moving 19cm^{-1} windows, and baseline corrected through subtraction of 7th order polynomial. Mean spectra of the R6G on each filter were plotted.

Intensities for important R6G peaks were plotted against gold nanocoating thickness. Enhancement factors at the common R6G peaks were calculated as the ratio of the Raman intensity at the defined peak in the coated filters as compared to uncoated controls.

7.2.2.2 Development of a High Throughput dual filtration system

Development and assessment of a Raman-based technology for UTI diagnosis requires assessment of many samples to train learning algorithms and overcome spectral variability. Major bottlenecks were encountered which make standard laboratory vacuum filtration equipment unsuitable for further evaluation. Firstly, the stage of the Korvus Hex deposition has sufficient surface area to hold only four 47 mm diameter membrane filters (which is the diameter of the commercially available filters used in these experiments). The total time taken for a single thin film deposition was approximately an hour. Therefore, smaller diameter filters were required so that single thin film deposition could prepare a reasonable number of filters. Secondly, vacuum filtration equipment needs to be autoclaved between samples to avoid contamination. As such, a large number of vacuum filtration sets would be required to process and assess a reasonable number of samples. The size and cost of the vacuum filtration sets however, meant this approach would have been impractical. Finally, dual filtration was required for clinical samples to remove larger particulate matter such as epithelial cells and urinary casts. This dual filtration would require two vacuum filtration sets to process a single sample.

As such, an insert was developed for the vacuum filtration apparatus that met the following constraints:

1. Compatible with existing vacuum filtration equipment, so as to make use of the existing vacuum pump and waste collection available in the laboratory.
2. Reduce the membrane filter diameter from 47 mm to 10mm or less.
3. Be compatible with standard steam autoclave (121 degrees Celsius, at 15 psi pressure).
4. Allow for dual filtration, with a 5 μm filter for removal of large particles before capture of pathogens onto a 0.45 μm pore size, SERS-active filter.

7.2.2.3 Preparation of phantom UTI samples

The methods employed are summarised in **Figure 7.1.** Phantom urine samples were created by inoculating cultured reference strain uropathogens into sterile human volunteer urine. Ninety samples were prepared including 30 uninfected controls and 60 infected samples including 20 each of *Escherichia coli* ATCC25922, *Enterococcus faecalis* ATCC29212 and *Klebsiella pneumoniae* ATCC13883. To create an infected phantom urine a single bead from the Microbank reference bank was inoculated into 3 ml brain heart infusion and cultured for 24 hours at 37 degrees Celsius. The pathogen laden culture medium was Vortex mixed and transferred to a 2 ml centrifuge tube. After centrifuging at 8300 g for 1 minute the supernatant was discarded and the bacteria resuspended in 2 ml of PBS by Vortex mixing. This centrifuge and wash process was repeated a total of 5 times to remove all culture medium. The resulting heavy suspension was diluted in PBS to an OD_{600} of 0.07 (equivalent of 10^8 CFU/ml) and subsequently underwent serial dilution in urine from healthy volunteers to a final concentration of 10^5 CFU/ml. Prior to inoculation, urine from healthy volunteers had been sterilised by vacuum filtration through 0.22 μm pore size filter to avoid contamination. This sample preparation process culminated in 30 ml of urine with 10^5 CFU/ml of reference strain uropathogen, equivalent to a standard infected urine sample.

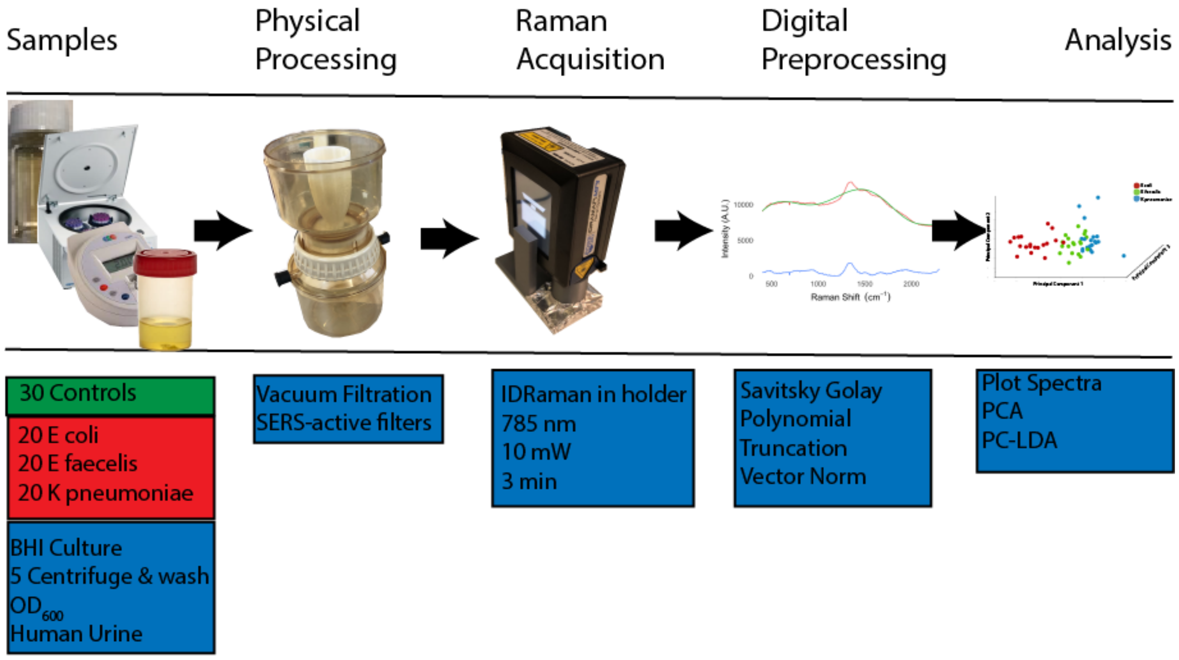

FIGURE 7. 1 METHODS FOR PHANTOM URINE SERS STUDY. PHANTOM URINE SAMPLES WERE PREPARED BY CULTURING REFERENCE STRAIN PATHOGENS WHICH THEN UNDERWENT 5 CENTRIFUGE AND WASHES. THE PATHOGEN LOAD WAS CONTROLLED BY OD_{600} BEFORE SERIAL DILUTION IN STERILE HUMAN URINE. THE SAMPLES WERE VACUUM FILTERED ONTO SERS-ACTIVE MEMBRANE FILTERS. SERS SPECTRA WERE ACQUIRED WITH THE IDRAMAN IN THE 3D-PRINTED HOLDER. THE SPECTRA WERE DIGITALLY PRE-PROCESSED WITH SAVITSKY-GOLAY FILTERING, POLYNOMIAL SUBTRACTION AND VECTOR NORMALISATION. SPECTRA WERE ANALYSED WITH SPECTRAL PLOTS, PCA AND PC-LDA.

7.2.2.4 Physical processing and SERS spectral acquisition

Samples were physically processed by vacuum filtration of 30 ml of phantom urine onto SERS-active membranes. Excess urine was removed by subsequent vacuum filtration of 10 ml of PBS through the SERS-active membrane. The SERS-active membrane was removed from the vacuum filter and air-dried prior to Raman capture.

Raman spectra were captured from the SERS-active filters using the IDRaman mini 2.0 handheld spectrometer mounted in the 3D printed holder. Spectra were acquired with a 785 nm laser set to 50 mW power with an acquisition time of 3 seconds per spectrum. Each sample had an average of 60 spectra, for a total acquisition time of 3 minutes.

7.2.2.5 Spectral digital pre-processing and analysis

Spectra were pre-processed and analysed using scripts developed in R programming language. High frequency noise and cosmic spikes are removed by smoothing using a Savitsky-Golay filter with 3rd order polynomial across a moving 19 cm^{-1} window. Baseline correction was achieved through cubic spline interpolation, using interpolant points selected *a priori*. Spectra were truncated to 500 to 2200 cm^{-1} to capture signal from the fingerprint region while avoiding excessive noise. Spectra were vector normalised.

Mean spectra with standard error ribbons were plotted for infected and uninfected phantom urine samples, and additionally mean spectra with standard error plots were prepared for the reference uropathogens. In order to highlight spectra differences leading to diagnosis, infected samples were centred and scaled using negative sample spectra. Similarly, pairwise comparison of spectral differences providing classification was achieved by centring and scaling each pathogen, using each other pathogen as a reference. Diagnostic and classification performance was assessed using PC-LDA.

7.2.3 RESULTS

7.2.3.1 OPTIMISATION OF GOLD NANOCOATING THICKNESS

Figure 7.2 presents photos and scanning electron micrographs (SEMs) of PVDF filters with different sputter thicknesses applied. The photographs demonstrate visibly increasing gold as the sputter thickness increases. The SEMs show increasing number and size of gold deposits on the PVDF filters with increasing sputter thicknesses, ultimately coalescing to form gold coated fibres in the membrane filters.

Figure 7.3 presents the mean spectra of R6G on PVDF filters with different gold sputter thicknesses. Substantial enhancement of the R6G spectrum is demonstrated on all gold coated filters with the sharp well-defined peaks well above the baseline. The spectrum for 50 nm sputter thickness demonstrates the tallest, most well-defined peaks. The characteristic peaks for R6G are emphasised by vertical dashed lines. The intensity at these points are plotted against increasing sputter thickness in **Figure 7.4** and tabulated in **Table 7.1. Figure 7.4** demonstrates all gold coating thicknesses provide significantly higher peaks than unsputtered controls. This enhancement increases with sputter thickness to a maximum at 50 nm before a slight reduction in enhancement thereafter. Given the greatest signal enhancement, 50 nm gold coated PVDF filter were used for further experiments.

TABLE 7. 1 INTENSITY OF R6G PEAKS FOR DIFFERENT GOLD NANOLAYER THICKNESSES

Sputter thickness (nm)	Intensity at peaks			
	1188 cm^{-1}	1311 cm^{-1}	1360 cm^{-1}	1511 cm^{-1}
	Xanthene ring deformation, C-H Bending, N-H Bending.	Xanthene Ring Bending, N-H Bend CH_2 Wagging.	Xanthene ring stretching, C-H Bending	Xanthene ring stretching, C-N stretching
2.5	538	662	870	867
5	1130	1307	1787	2052
7.5	1569	1853	2492	2750
10	1438	1670	2240	2530
12.5	1713	2047	2756	2910
15	1532	1842	2445	2630
20	1532	1859	2473	2648
25	1496	1839	2443	2633
50	1961	2487	3358	3658
100	1274	1718	2370	2598
150	1060	1543	206	2168

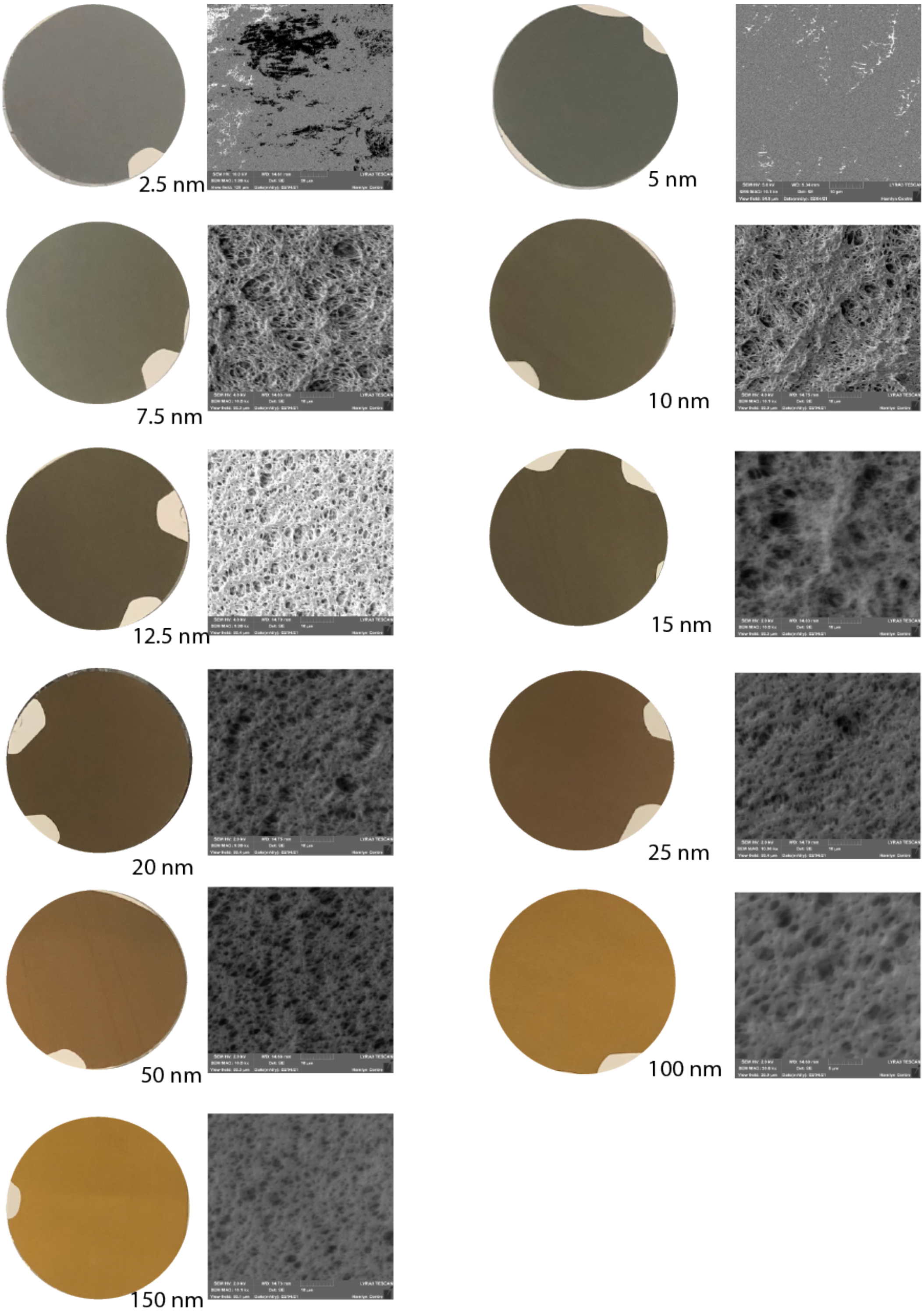

FIGURE 7. 2 PHOTOGRAPHS AND SCANNING ELECTRON MICROGRAPHS OF PVDF FILTERS WITH DIFFERING SPUTTER THICKNESSES

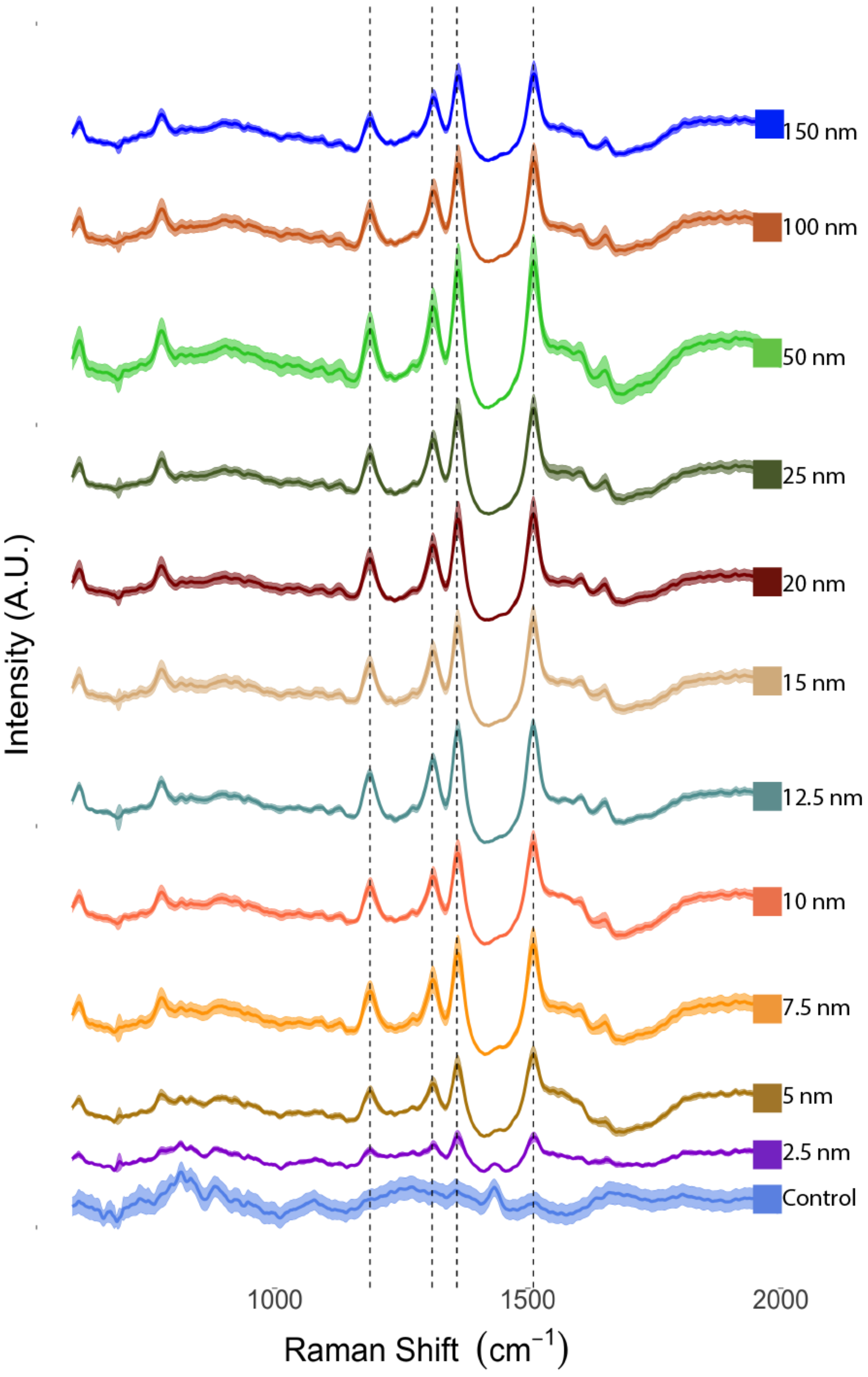

FIGURE 7. 3 MEAN SERS SPECTRA FOR R6G ON PVDF FILTERS WITH DIFFERENT GOLD THICKNESS LAYERS.

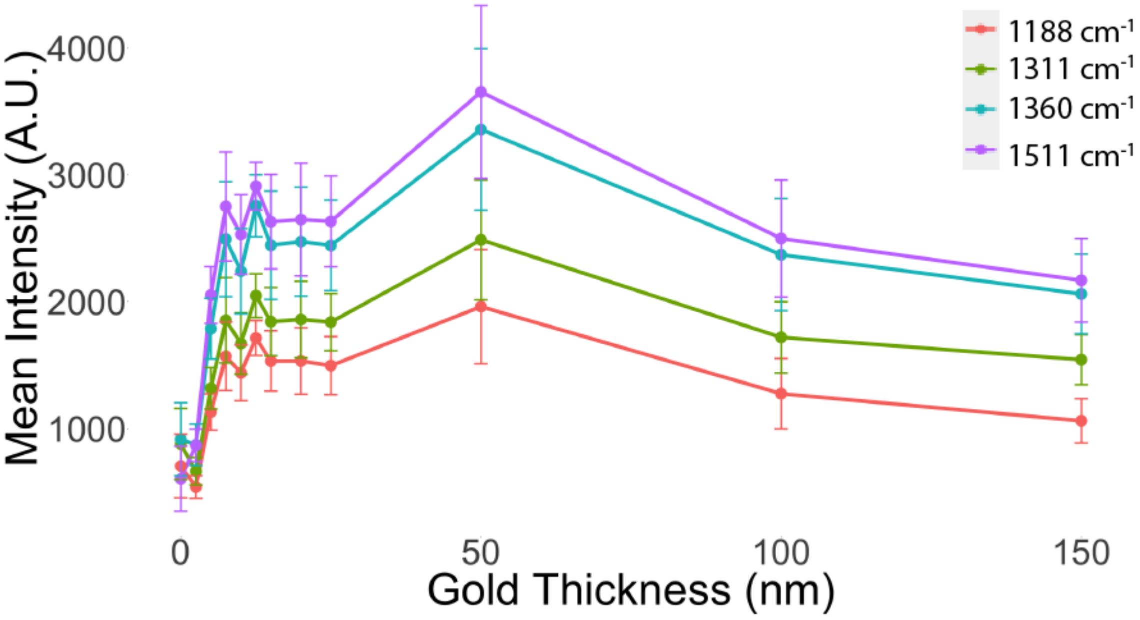

FIGURE 7. 4 PLOT OF MEAN INTENSITY AGAINST GOLD SPUTTER THICKNESS FOR PROMINENT R6G PEAKS

7.2.3.2 DESIGN AND PRODUCTION OF A DUAL FILTRATION SYSTEM

The dual filtration system was parametrically designed in Fusion360 (**Figure 7.5**) design software. The design consists of 2 levels to hold the differing pore size filters. Each level consists of two parts, the lower part housing the filter and interfacing with the container below, while the upper part acts as receiving container for the urine. Between each layer a slot is available for a high temperature nitrile O-ring to create an airtight seal.

The dual filtration insert was 3D printed on a Formlabs 2, stereolithography printer using high temperature resin. The 3D printed parts were washed for 15 minutes in isopropyl alcohol to remove excess resin, before curing the printed parts under UV light at 60 degrees Celsius for one hour. The build supports were removed and the completed parts smoothed. The parts were rinsed in deionised water and sterilised in a benchtop autoclave prior to use. In comparison, parts printed with fused deposition printer materials such as polylactic acid and polyethylene terephthalate warped when undergoing steam sterilisation.

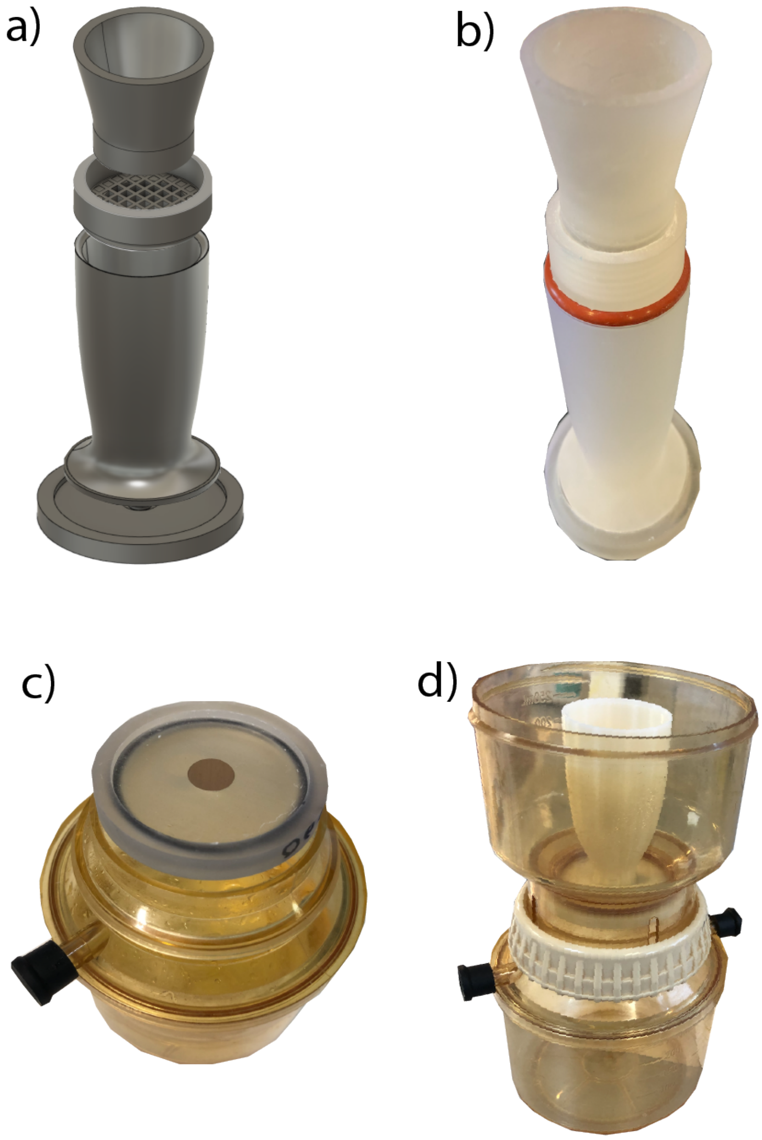

FIGURE 7. 5 THE DUAL FILTRATION VACUUM FILTER INSERT. A) RENDERING OF THE PARAMETRICALLY DESIGNED FUSION360 MODEL. B) INSERT 3D PRINTED WITH FORMLABS STL PRINTER USING HIGH TEMPERATURE RESIN. C) INSERT BASEPLATE FITTED ONTO A COMMERCIALLY AVAILABLE VACUUM FILTRATION SET WITH A 10 MM SERS-ACITVE FILTER IN PLACE. D) FILTRATION INSERT ENCLOSED IN COMMERCIALLY AVAILLABLE VACUUM FILTER SET.

7.2.2.3 Diagnosis of infected vs uninfected samples

Figure 7.6 presents the mean spectra with standard error ribbons for spectra from infected phantom urine and uninfected controls vacuum filtered onto SERS-active filters. Even with the low, clinically relevant concentrations used here, the spectra are visibly different in a number of areas, indicated by vertical dashed lines. These differences are emphasised in **Figure 7.7** which presents the mean spectrum with standard error ribbons for infected samples centred and scaled on the spectra of uninfected controls. The same spectra bands are indicated by the vertical dashed lines. **Table 7.2** provides biochemical assignments for these bands.

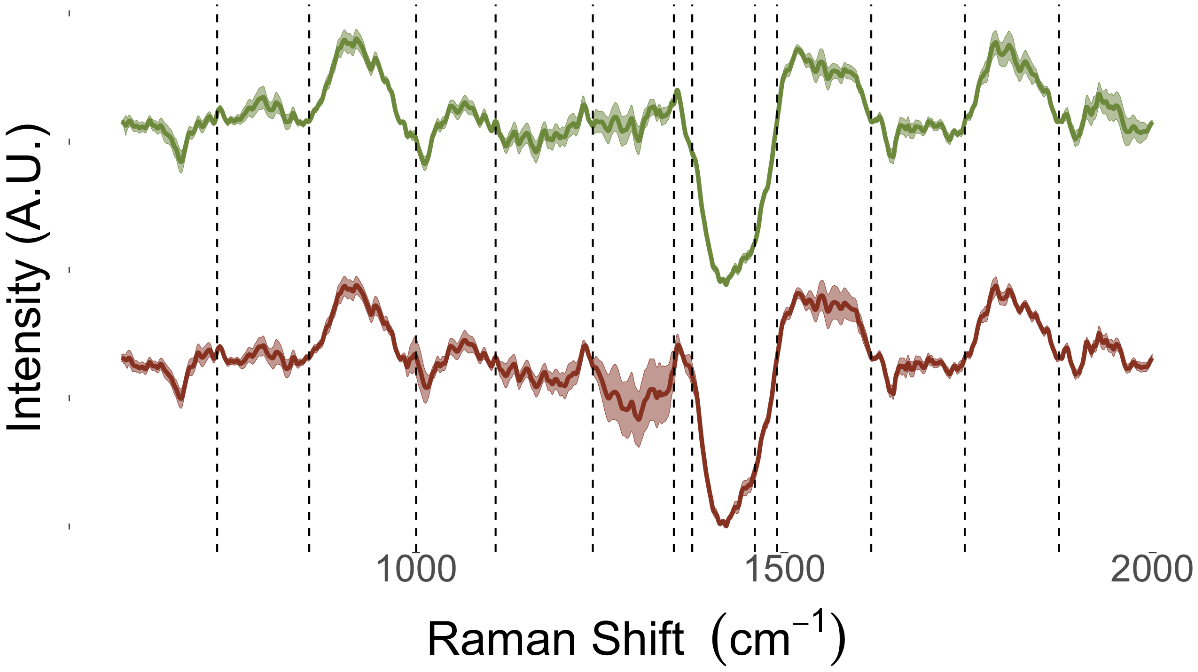

FIGURE 7. 6 MEAN SPECTRA WITH STANDARD ERROR RIBBONS FOR INFECTED (RED) AND UNINFECTED (GREEN) CONTROLS OF PHANTOM URINE SAMPLES VACUUM FILTERED THROUGH SERS-ACTIVE MEMBRANE FILTERS. VERTICAL DASHED LINES DELINEATE BANDS AT WHICH SPECTRA DIFFER SIGNIFICANTLY (SEE FIGURE 7.7 AND TABLE 7.2)

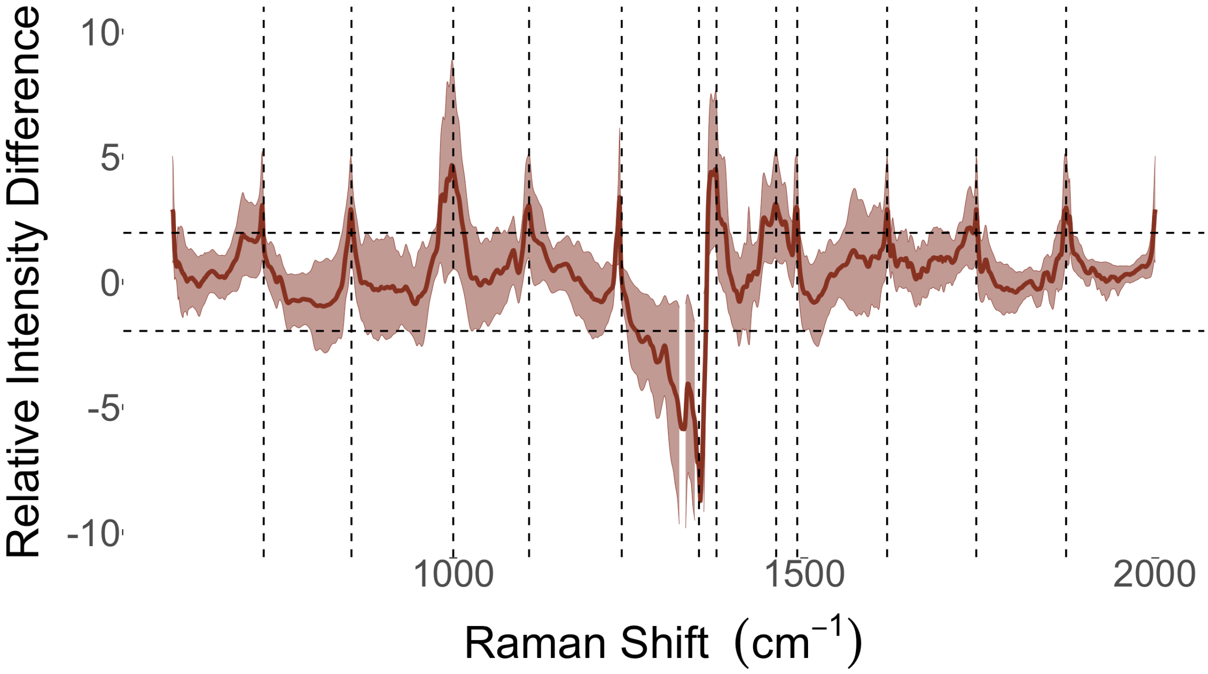

FIGURE 7. 7 MEAN SPECTRUM WITH STANDARD ERROR RIBBONS FOR INFECTED SPECTRA CENTRED AND SCALED ON UNINFECTED SPECTRA FOR SAMPLES VACUUM FILTERED THROUGH SERS-ACTIVE MEMBRANE FILTERS. VERTICAL DASHED LINES DELINEATE SPECTRAL BANDS WHERE PEAKS DIFFER SIGNIFICANTLY (SEE TABLE 7.2 FOR BIOCHEMICAL ASSIGNMENTS)

TABLE 7. 2 SPECTRAL BAND ASSIGNMENT FOR PEAKS DIFFERENTIATING INFECTED SAMPLES FROM UNINFECTED CONTROLS

Raman shift (cm^{-1})	Band assignment	Reference
730	Adenine, peptidoglycan	[110, 123]
855	Tyrosine, Phenylalanine, glycosidic linkages	[110, 123, 158]
1000	Phenylalanine, carotene	[99, 110, 117, 123, 136]
1235	Amide III	[123, 158]
1350	Protein	[101]
1375	Hypoxanthine, Adenine, AMP, peptidoglycan	[110, 149]
1460	Hypoxanthine, adenine, guanine	[149]
1490	Guanine, Adenine	[158]
1618	Tyrosine	[158]
1745	Phospholipid, triglycerides	[190]

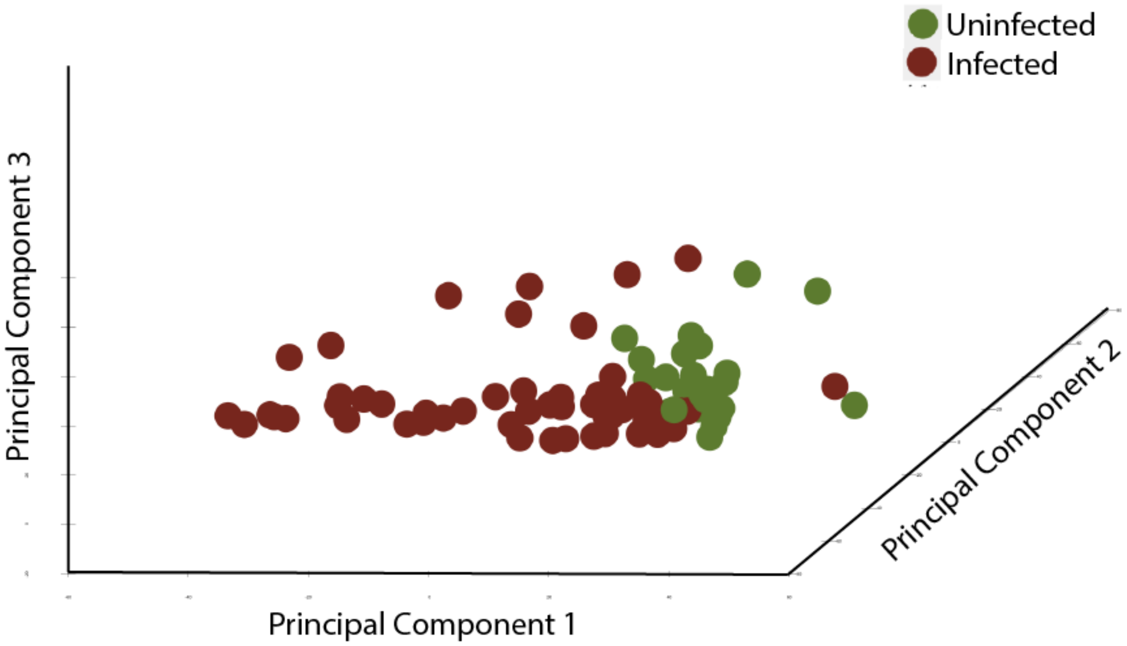

FIGURE 7. 8 PCA PLOT FOR INFECTED (RED) AND UNINFECTED CONTROL (GREEN) SPECTRA OF SAMPLES VACUUM FILTERED THROUGH SERS-ACTIVE MEMBRANES

Figure 7.8 presents unsupervised classification through PCA. Visualisation of the first three principal components demonstrates the infected and uninfected samples naturally cluster together. A greater degree of spread is notable within the infected samples, representative of the higher degree of variability seen when capturing spectra from different species. Application of supervised learning through PC-LDA provides diagnostic accuracy of 93.2% (95%CI: 85.9%; 97.5%. p-value <0.05) for identification of infected and uninfected samples (**Table 7.3)**. Sensitivity and specificity were 94.9% and 90.0% respectively (**Table 7.3)**.

TABLE 7. 3 PC-LDA DIAGNOSTIC PERFORMANCE FOR RAMAN SPECTRA FROM SAMPLES VACUUM FILTERED ONTO SERS-MEMBRANES

		Reference Pathogen	
		Uninfected control	**Infected**
Predicted pathogen	**Uninfected control**	27	3
	Infected	3	56
Diagnostic performance			
Accuracy		93.2% (95% CI: 85.9; 97.5%. p-value: <0.05)	
Cohen's kappa		0.85	
Sensitivity		94.9%	
Specificity		90%	

7.2.3.4 CLASSIFICATION OF PATHOGEN SPECIES WITHIN INFECTED SAMPLES

Figure 7.9 presents the mean spectra with standard error ribbons for the three reference pathogen spectra vacuum filtered onto SERS-active membranes. A number of the peaks contributing to differentiating infected from uninfected controls remain visibly different between uropathogen. Differences between pathogen spectra are emphasised in **Figure 7.10**, with the same peaks highlighted by vertical dashed lines. All pathogens demonstrate bands significantly different from other pathogens providing for classification of uropathogens using the SERS spectra.

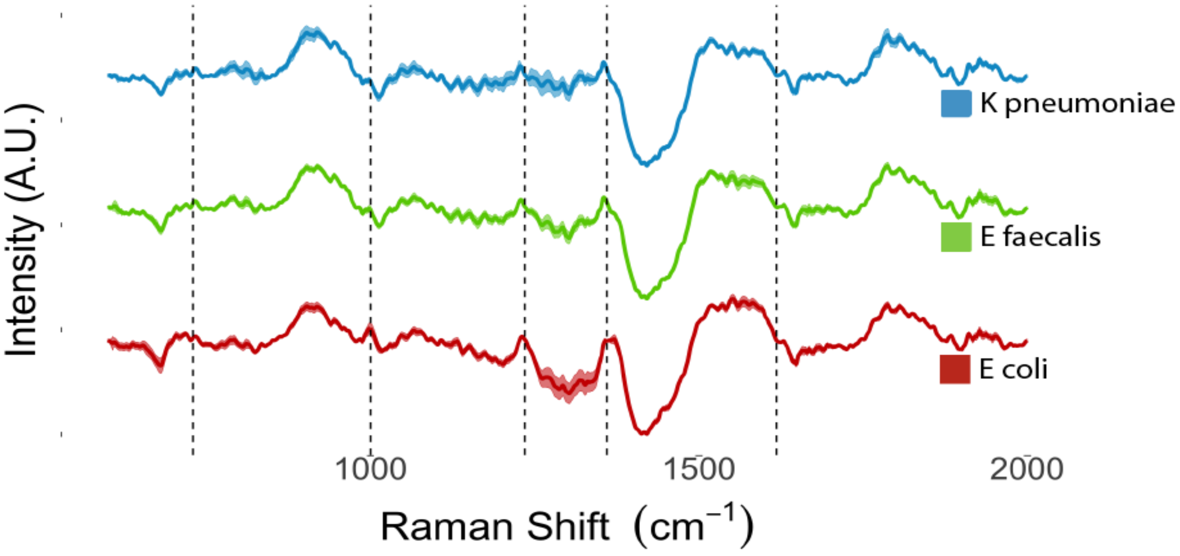

FIGURE 7. 9 MEAN SPECTRA WITH STANDARD ERROR RIBBONS FOR THREE REFERENCE STRAIN PATHOGENS VACUUM FILTERED ONTO SERS-ACTIVE MEMBRANE FILTERS. VERTICAL DASHED LINES DELINEATE BANDS WHERE SPECTRA DIFFER (SEE FIGURE 7.10)

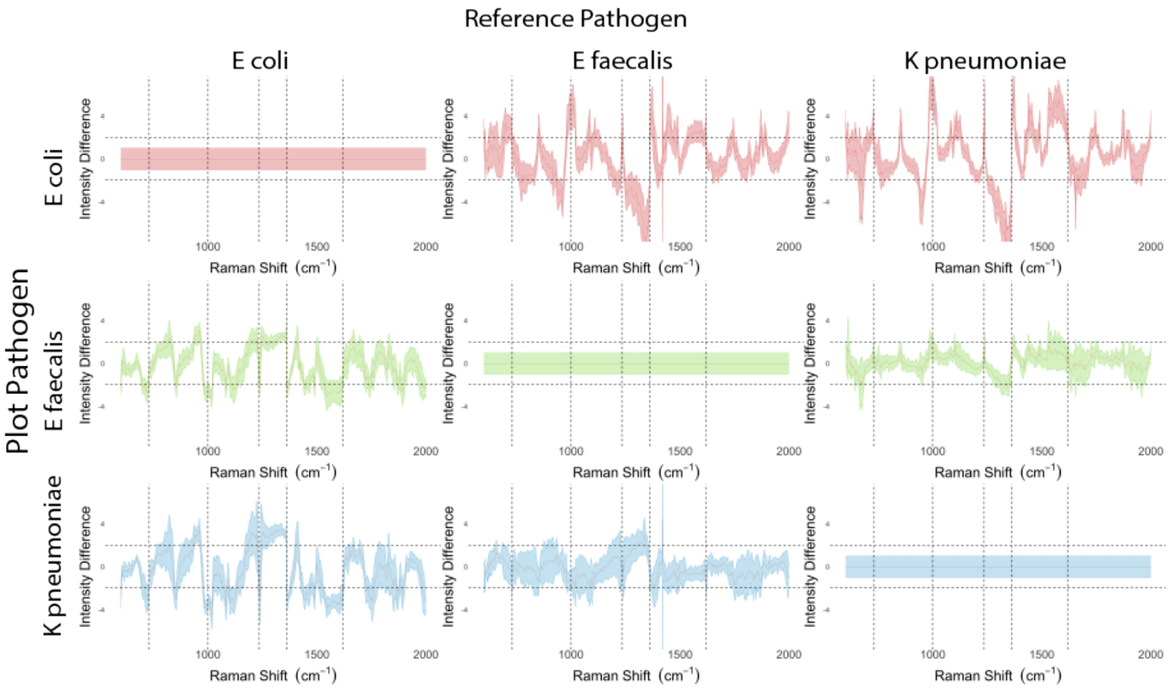

FIGURE 7. 10 MEAN SPECTRA WITH STANDARD ERROR RIBBONS FOR REFERENCE UROPATHOGENS CENTRED AND SCALED BY ALL OTHER REFERENCE UROPATHOGENS. HORIZONTAL DASHED LINES DELINEATE THE BORDER AT WHICH DIFFERENCES ARE SIGNIFICANT AT α = 0.05). VERTICAL DASHED LINES IDENTIFY BANDS AT WHICH SPECTRA DIFFER.

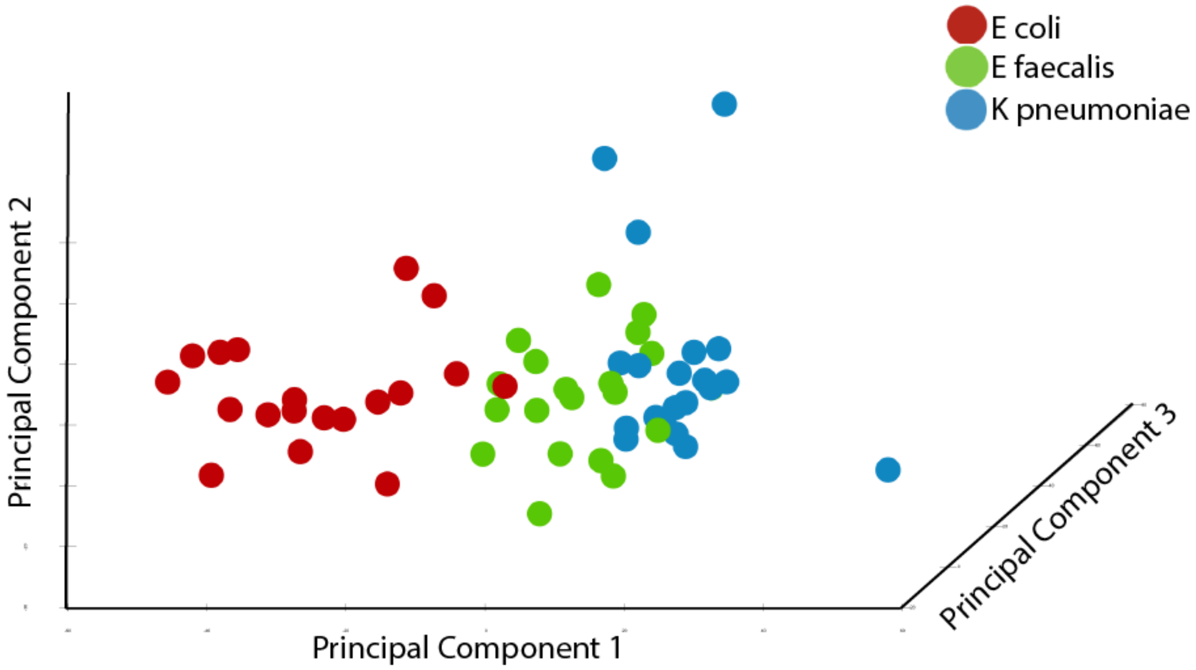

FIGURE 7. 11 PCA PLOT FOR SERS SPECTRA OF UROPATHOGENS (RED: *E. COLI*, GREEN: *E . FAECALIS* AND BLUE: *K. PNEUMONIAE*) VACUUM FILTERED ONTO SERS-ACTIVE MEMBRANE FILTERS

Figure 7.11 presents unsupervised classification of pathogens through PCA. Visualisation of the first three principal components demonstrates the spectra naturally cluster according to pathogen species, although some overlap is visible in the first three principal components.

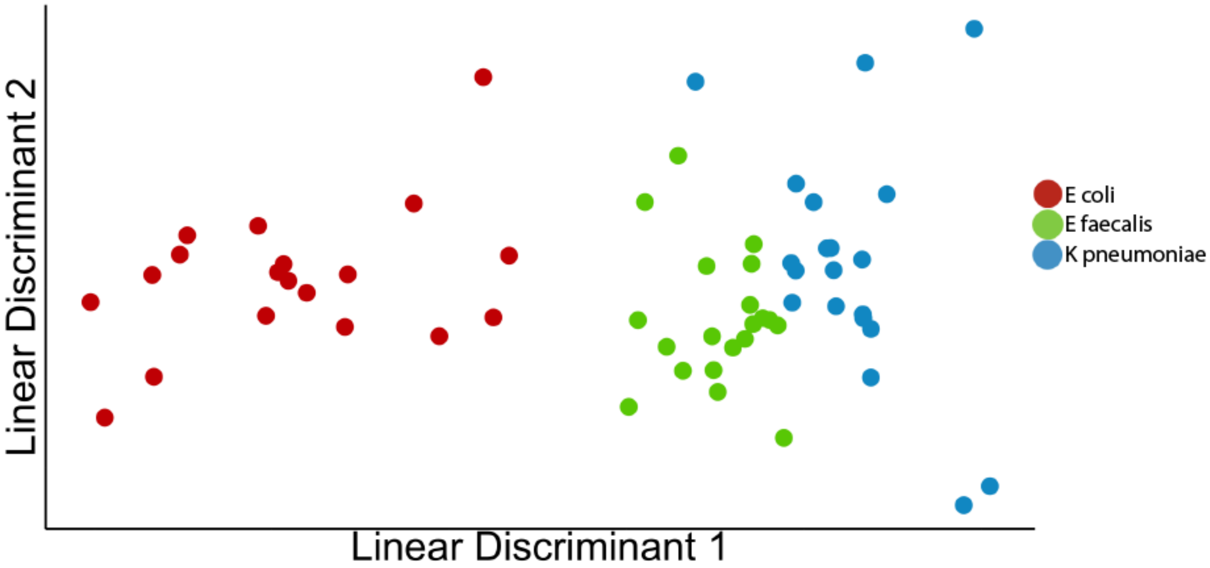

FIGURE 7. 12 PC-LDA PLOT FOR CLASSIFICATION OFSPECTRA FROM UROPATHOGENS (RED: *E. COLI,* GREEN: *E. FAECALIS* AND BLUE*: K. PNEUMONIAE*) VACCUM FILTERED ONTO SERS-ACTIVE FILTERS

PC-LDA was applied for supervised classification of pathogens using Raman spectra acquired after vacuum filtration through SERS-active filters (**Figure 7.12**). Pathogen classification performance is summarised in **Table 7.4**. Spectra were classified with 91.7% accuracy (95% CI: 83.5;98.1. p-value<0.05). Sensitivity and specificity for pathogen groups were all above 90%.

TABLE 7. 4 CLASSIFICATION OF UROPATHOGENS VACUUM FILTERED ONTO SERS-ACTIVE-MEMBRANE FILTERS

		Reference Pathogen		
		Escherichia coli	***Enterococcus faecalis***	***Klebsiella pneumoniae***
Predicted Pathogen	***Escherichia coli***	17	0	0
	Enterococcus faecalis	2	19	1
	Klebsiella pneumoniae	0	1	19
Classification performance				
Overall	**Accuracy**		91.7% (95% CI: 83.5;98.1. p-value<0.05)	
	Cohen's Kappa		0.90	
Escherichia coli	**Sensitivity**		90%	
	Specificity		100%	
Enterococcus faecalis	**Sensitivity**		95%	
	Specificity		95%	
Klebsiella pneumoniae	**Sensitivity**		95%	
	Specificity		97%	

7.2.5 DISCUSSION

SERS-active filters created by applying a 50 nm gold nanolayer to PVDF membrane filters rapidly captured pathogens from phantom urine samples and provided signal enhancement, therein achieving accurate diagnosis of infected samples, and simultaneously providing accurate pathogen classification. The time taken from sample to classification, including physical processing, Raman acquisition and analysis, was less than 15 minutes per sample.

Assessing the diagnostic and classification performance of SERS-active filters was contingent on two pieces of preliminary work. Firstly, the optimal sputter thickness was identified, with 50 nm thickness providing greater enhancement of the main Rhodamine 6G peaks than both thicker and thinner gold nanocoatings. These results are in contrast to the work by *Szymborski et al*., in which assessment of 3 thicknesses demonstrated 90 and 200 nm nanolayer thicknesses to provide enhancement equal to each other, and superior to 30 nm thickness[147]. The considerably larger number of thicknesses assessed in this work provides a greater granularity, and therefore more robust assessment of enhancement provided. Therefore, 50 nm thickness was used in further works rather than the 90 nm recommended by *Szymborski et al.*[147].

The second piece of preliminary work developed an insert for the vacuum flask used to pass urine samples through SERS-active filters. Assessing classification performance is contingent on assessing a representative number of samples. A challenge arises in that applying a 50 nm gold nanolayer through PVD takes approximately

1 hour, primarily resulting from the time taken to establish a vacuum in the Korvus Hex deposition system. As the 4-inch stage of the Korvus can hold a maximum of 4 filters (with 47 mm diameter), this would translate into an excessively long time to produce a sufficient number of SERS-active filters to perform this study. An insert was designed in Fusion360 CAD software and 3D oriented with high temperature resistant resin, which reduced the filter diameters from 47mm to 10 mm. This allowed over 40 filters to be produced during a single nanocoating application. The insert provided multiple other advantages: reducing the filter diameter concentrated the pathogens into a 22 times smaller area; the inserts were printed with high temperature resin and so were autoclavable; finally, the design included an upper layer which allows for a second larger pore-size filter to be used for dual filtration in future work.

Diagnostic accuracy (i.e., classification of infected vs uninfected samples) of 93.2 % was achieved in this work with sensitivity and specificity of 94.9 and 90% respectively. This diagnostic accuracy achieved here is superior to that of currently employed screening technologies such as urinalysis[4, 53, 191]. Direct comparison against other Raman-based technologies for uropathogen identification is not possible, as other published works have not included negative controls. This demonstrates a significant advantage of this work, afforded by the use of a handheld Raman spectrometer rather than Raman microscopes used in other works. This is of particular importance given the information of greatest value is afforded by rapid and accurate diagnosis rather than early pathogen classification. Spectral differences are demonstrated between infected and uninfected controls, as well as between pathogens.

Classification accuracy (i.e. identification of pathogen species within infected samples) of 91.7% is comparable to gold standard M, C&S and other classification technologies including mass spectrometry and PCR[5, 56, 215, 216]. The SERS-active filters developed here, however, have distinct advantages over these established technologies. Most notably, the 15-minute sample-to-result turn around provided by SERS-active filters is significantly better than the hours or days required by these established technologies[5]. Similarly, with no reagents and requiring widely available equipment, SERS-active filters are amenable to development into a point-of-care test, therein reducing turnaround time and logistical considerations. Finally, the equipment used here is considerably cheaper than that of these competitor technologies.

The classification performance achieved here is comparable with other published Raman research into uropathogen classification, with reported classification performances ranging from 83.5% to 100%[99, 110, 117, 149, 156, 158]. Some salient differences however differentiate these works. Firstly, only *Kloss et al., Schroder at al.* and *Yang et al.* tested their technologies on pathogens in urine, rather than pathogen suspensions[99, 117, 149]. Secondly, all but two of these published works used a Raman microscope rather than a spectrometer, and as such SERS-active filters combined with a handheld spectrometer (used in this study) suggest greater promise of a clinically implementable solution[110, 156].

Use of phantom urine samples is the primary limitation of this work. Composed of reference strain pathogens suspended at closely controlled pathogen loads in sterile urine, phantom urine samples were chosen to reduce samples variability during validation. Reference strain pathogens, in consistent stable growth phase and at controlled concentrations represent considerably less variation in Raman spectra as compared to that of clinical pathogens[101, 123, 137, 151, 170, 211]. Similarly, the single organism phantom samples may not accurately reflect the complexity of mixed infections frequently encountered in clinical samples.[87] The true diagnostic and classification performance may differ when challenged with the greater variability seen with clinical samples. Nevertheless, the results here warrant further investigation. As such, the diagnostic and classification performance of SERS-active filters requires assessment on clinical samples.

7.3 DIAGNOSTIC PERFORMANCE OF SERS-ACTIVE MEMBRANE FILTERS ON CLINICAL SAMPLES.

7.3.1 INTRODUCTION

Raman spectroscopy has the potential to act as an ideal diagnostic technology for UTIs. The ability to deliver highly resolved, information rich chemometric data without prior biomass expansion has potential to provide rapid and accurate UTI diagnosis with pathogen classification[45, 69, 70, 82, 88, 123, 156, 167]. Weak Raman scattering from uropathogens may however be overwhelmed by competing signal and fluorescence from urine. Despite numerous published works having developed methods capable of delivering highly resolved uropathogen Raman spectra with the ability to provide classification, few have assessed the performance of their technologies on clinical urine samples.

Kloss et al. were the first to assessed Raman classification of uropathogens in clinical samples[99]. An SVM classifier was trained on reference uropathogens cultured in sterile urine. Physical processing was limited to two cycles of centrifuge and washing before airdrying on nickel foil. Raman spectra were acquired from single cells using a Raman microscope. The same physical processing was applied to 10 infected clinical samples including 7 *Escherichia coli* and 3 *Enterococcus faecalis* and subsequently classified using the trained SVM. All 10 samples were correctly classified[99]. This work demonstrates the extraordinary power of Raman microscopy, with accurate classification achieved from spectra acquired from single pathogens with minimal processing. Not described however, is the time and technical skill required to focus the Raman microscopes on single pathogens.

Schroder et al. developed a dielectrophoresis chip that concentrated pathogens in the centre, therein reducing the challenge of focussing the Raman microscope on singe bacteria[117]. The technology was assessed using *Escherichia coli* and *Enterococcus faecalis* samples. An LDA classifier was trained on 600 spectra acquired from 5 batches of reference strain pathogens from each of the bacteria. Subsequently they tested their technology on three patient samples processed with a single centrifuge and wash. Each patient sample had 300 spectra acquired and assessed, with only 1 of 900 misclassified[117]. While this classification is excellent it is called to question given this work neglects that fact that data points need to be independent during validation[111]. While the classification performance achieved in both works is encouraging, the small number of patient samples and pathogens assessed limit the generalisability of these results beyond proof of principal.

Tien et al. assessed the SERS spectra from 108 clinical samples with pathogens including *Escherichia coli*, *Enterococcus faecalis*, *Proteus mirabilis*, *Pseudomonas aeruginosa* and *Citrobacter freundii*[124]. The uropathogens were concentrated through centrifugation prior to acquisition of SERS spectra using cylindrical Raman chips. The Raman equipment used for spectral acquisition is not documented, and as such, it is unclear whether a spectrometer or microscope was used[124]. The authors report identifying samples with single species, although the classification performance is not clearly documented. Despite the large number of samples, this work adds little to the Raman knowledge base. None of these published works included negative controls, and so were unable to assess diagnostic performance[99, 124, 160].

SERS-active filters achieved excellent diagnostic and classification accuracy on phantom urine samples. A pilot study to assess the performance on clinical samples is required prior to a full clinical trial of the technology.

Hypothesis: SERS-active filters can provide rapid UTI diagnosis with pathogen classification directly from clinical urine samples.

Objectives:

- Investigate the SERS spectra of clinical pathogens captured using SERS-active filters.
- Assess the diagnostic and classification performance provided by SERS-active filters for UTIs using clinical samples.

7.3.2 Methods

7.3.2.1 Clinical samples

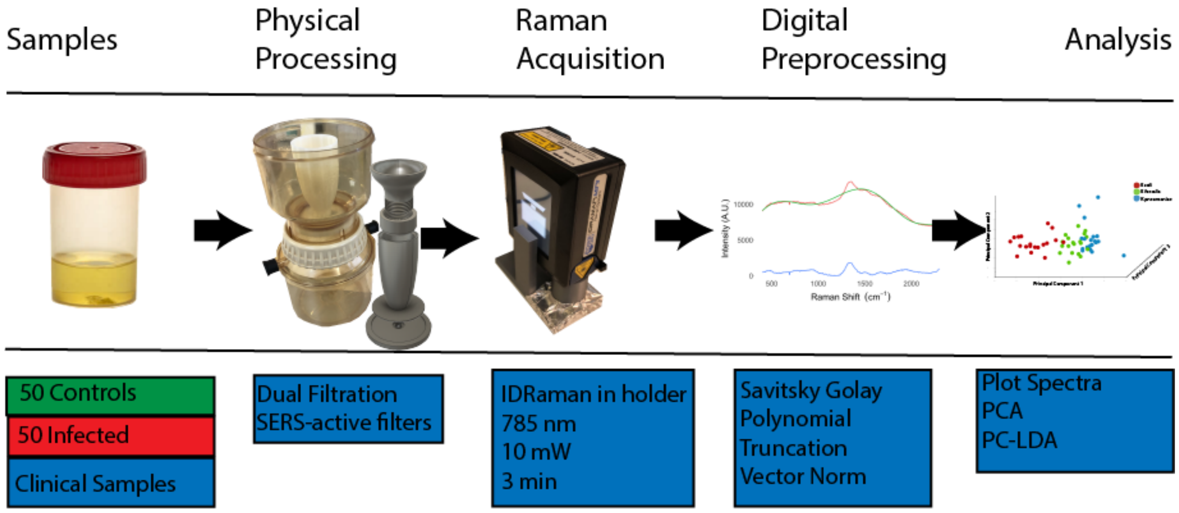

FIGURE 7. 13 METHODS FOR CLINICAL ASSESSMENT OF-SERS-ACTIVE FILTERS. 100 CLINICAL SAMPLES UNDERWENT PHYSICAL PROCESSING BY DUAL FILTRATION ONTO SERS-ACTIVE FILTERS. SERS SPECTRA WERE ACQUIRED WITH THE IDRAMAN IN THE 3D-PRINTED HOLDER. SPECTRA WERE DIGITALLY PRE-PROCESSED WITH SAVITSKY-GOLAY FILTERING, POLYNOMIAL SUBTRACTION AND VECTOR NORMALISATION BEFORE ANALYSIS WITH SPECTRAL PLOTS PCA AND PC-LDA.

The methods used are summarised in **Figure 7.13**. One hundred Clinical samples were acquired from Northwest London Pathology (NWLP) Microbiology Laboratory. Samples were processed according to NWLP stand operating procedures, with all samples screened using a Sysmex UF4000 flow cytometer and cultured on chromogenic agar. Positive (infected) samples were defined as those greater than or equal to 10^5 CFU/ml of one or more uropathogens. An augmented convenience sample set was acquired with consecutive samples at a ratio of 1:1 infected to infected to uninfected samples. After clinical processing, all samples were stored at 4 degrees Celsius, and were processed for SERS analysis within 72hours of collection. Infected samples included in this study included *Escherichia coli*, *Enterococci*, Group B *Streptococci*, *Proteus* species and mixed infection.

7.3.2.2 Dual filtration and SERS spectral acquisition

Samples were processed using the 3D printed dual filtration vacuum filter insert. A 10 mm diameter SERS-active 0.45 µm PVDF filter with a 50 nm gold nanocoating was loaded into the lower level, while the upper level had a 25mm diameter, 5 µm pore size PVDF filter. 10 ml of urine was vacuum filtered through the dual filtration system, followed by 5 ml of PBS to wash of residual urine. The upper 5 µm filter was discarded, while the lower SERS-active filter was air-dried before Raman spectral capture.

7.3.2.3 SPECTRAL DIGITAL PRE-PROCESSING AND ANALYSIS

Raman spectra were acquired using the IDRaman mini 2.0 handheld spectrometer loaded into the 3D printed mount. Spectra were acquired with laser wavelength of 785 nm and laser power set to 50 mW. Spectra were acquired for 2 seconds, with 60 scans averaged for a total acquisition time of 2 minutes.

Spectra were processed and analysed with scripts developed in R programming language. Mean spectra with standard error ribbons were plotted for infected and uninfected samples, as well as for the specific uropathogens. Diagnostic and classification performance were assessed using supervised learning through PC-LDA. To assess the diagnostic contribution of spectra bands to infected samples were centred and scaled by negative samples. Similarly, pairwise assessment of the contribution of spectra bands to classification single species infected samples were centred and scaled by other single species infected samples.

7.3.3 RESULTS

7.3.3.1 SATURATED SPECTRA

On visual assessment of the unprocessed spectra, 7 spectra were identified to have saturated the CCD leading to corrupted spectra (**Figure 7.14**). The samples from which the saturated spectra originated contained several infected and uninfected samples with different pathogens and collected on different days. In all cases the IDRaman had undergone calibration (**Table 7.5**). The CCD saturated when greater than 50000 intensity units were present. The 7 saturated spectra were removed from further analysis, leaving spectra from 93 samples.

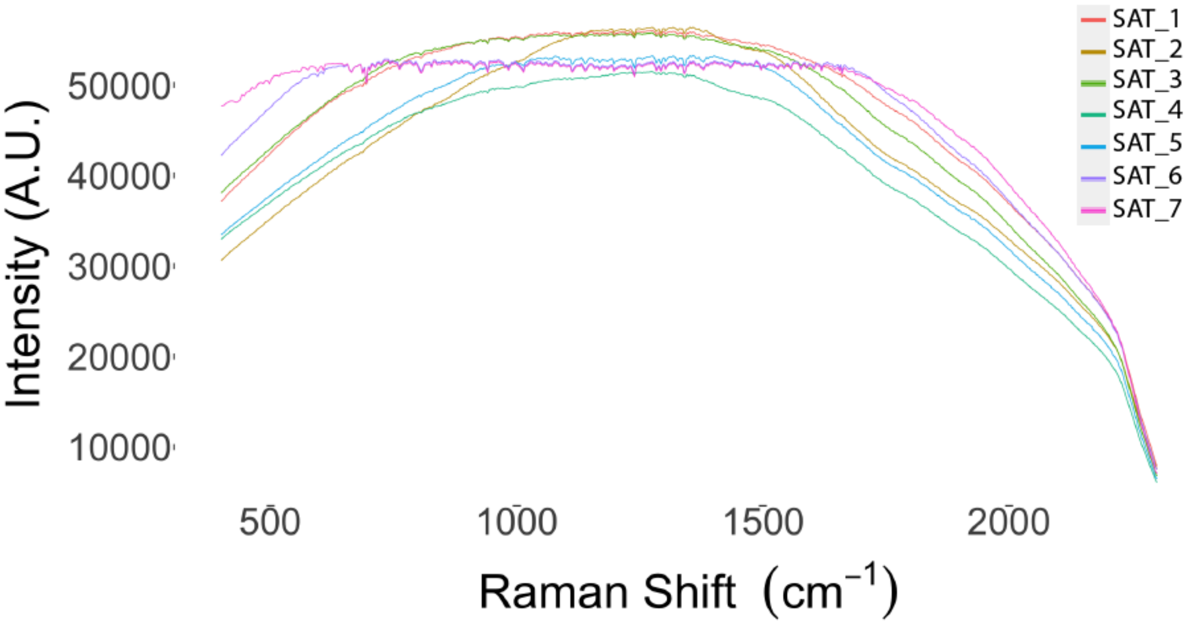

FIGURE 7. 14 RAMAN SPECTRA DEMONSTRATING CCD SATURATION.

TABLE 7. 5 SAMPLE CHARACTERISTICS FOR SATURATED SPECTRA.

Sample	Pathogen	Collection Date	Device calibration
SAT_1	None	21/05/2021	Completed
SAT_2	None	21/05/2021	Completed
SAT_3	None	11/06/2021	Completed
SAT_4	Group B Streptococcus	11/06/2021	Completed
SAT_5	None	18/06/2021	Completed
SAT_6	Enterococcus species	18/06/2021	Completed
SAT_7	Enterococcus species	18/06/2021	Completed

7.2.3.2 DIAGNOSIS OF INFECTED VS UNINFECTED CLINICAL SAMPLES

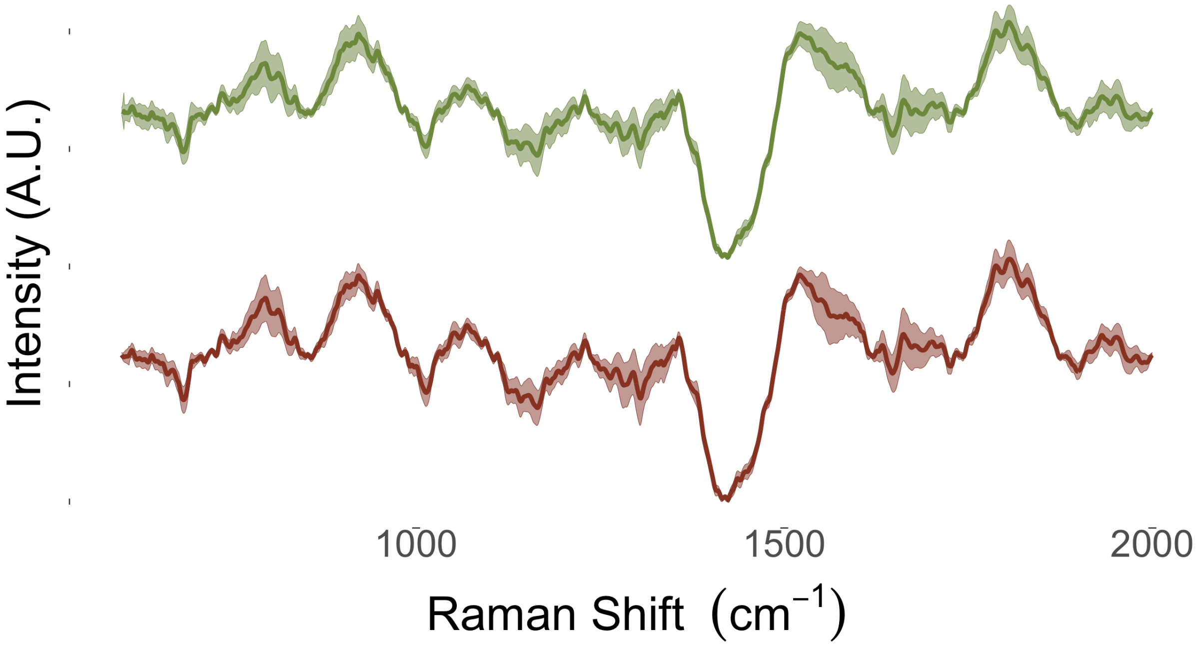

FIGURE 7. 15 MEAN SPECTRA WITH STANDARD ERROR RIBBONS FOR INFECTED AND UNINFECTED CLINICAL SAMPLES VACUUM FILTERED THROUGH SERS-ACTIVE MEMBRANE FILTERS. NO SPECTRAL DIFFERENCES ARE VISIBLE, WHILE WIDE STANDARD ERROR RIBBONS INDICATE A HIGH DEGREE OF SPECTRA VARIABILITY IN BOTH INFECTED AND UNINFECTED SAMPLES

Figure 7.15 presents the mean spectra, with standard error ribbons, for infected and uninfected clinical samples vacuum filtered through SERS-active membrane filters. On visual examination there are no discernible differences between the spectra of infected and uninfected samples. The plot also demonstrates relatively wide standard error ribbons representative of a high degree of spectral variability.

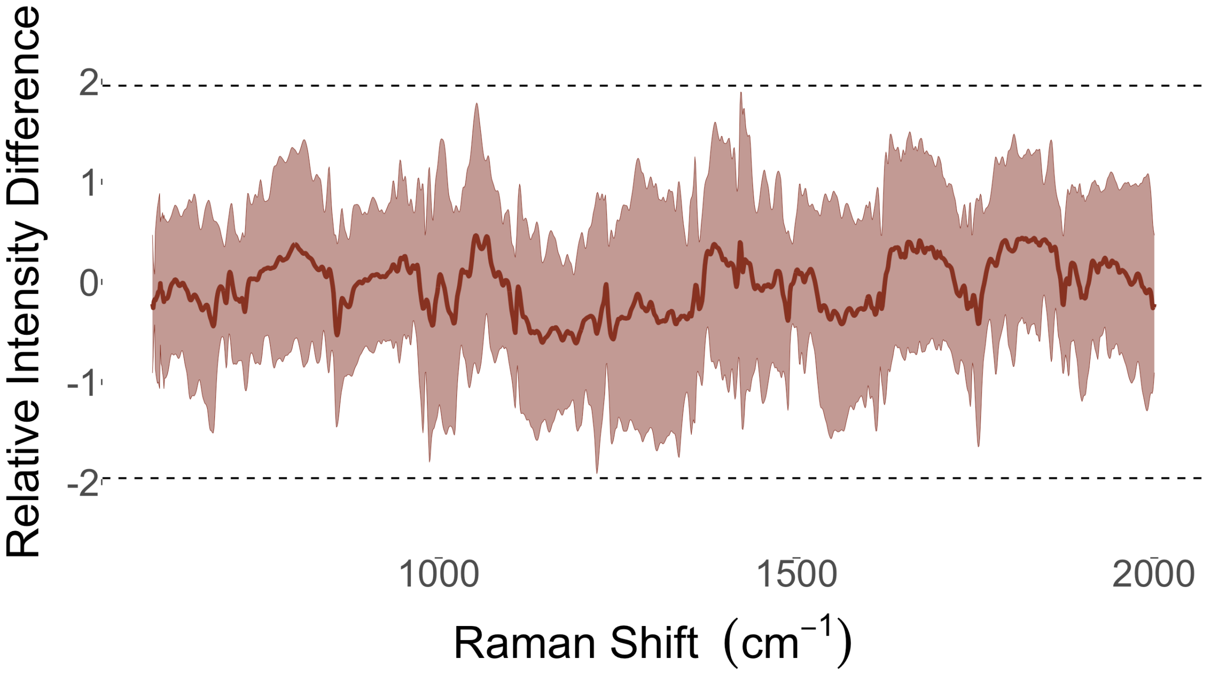

FIGURE 7. 16 MEAN SPECTRUM WITH STANDARD ERROR RIBBON FOR INFECTED CLINICAL SAMPLES CENTRED AND SCALED ON SPECTRA FROM UNINFECTED CLINICAL SAMPLES VACUUM FILTERED ONTO SERS-ACTIVE MEMBRANES. HORIZONTAL DASHED LINES DELINEATE THE BORDER AT WHICH DIFFERENCES WOULD BE SIGNIFICANT AT $\alpha = 0.05$

Figure 7.16 presents the mean spectrum with standard error ribbons for infected clinical samples centred and scaled on uninfected clinical samples. The spectra plot provides a depiction of the spectral differences relative to the local variability. Horizontal dashed lines delineate the bound where bands differ significantly with $\alpha = 0.05$. This plot demonstrates no peaks at which spectra acquired from infected differ significantly from those of spectra acquired from uninfected samples.

Figure 7.17 presents unsupervised learning through PCA of spectra acquired from samples vacuum filtered onto SERS-active membranes. The plot of the first 3 principal components demonstrates widely dispersed points with no natural clustering nor visible separation according to infection status.

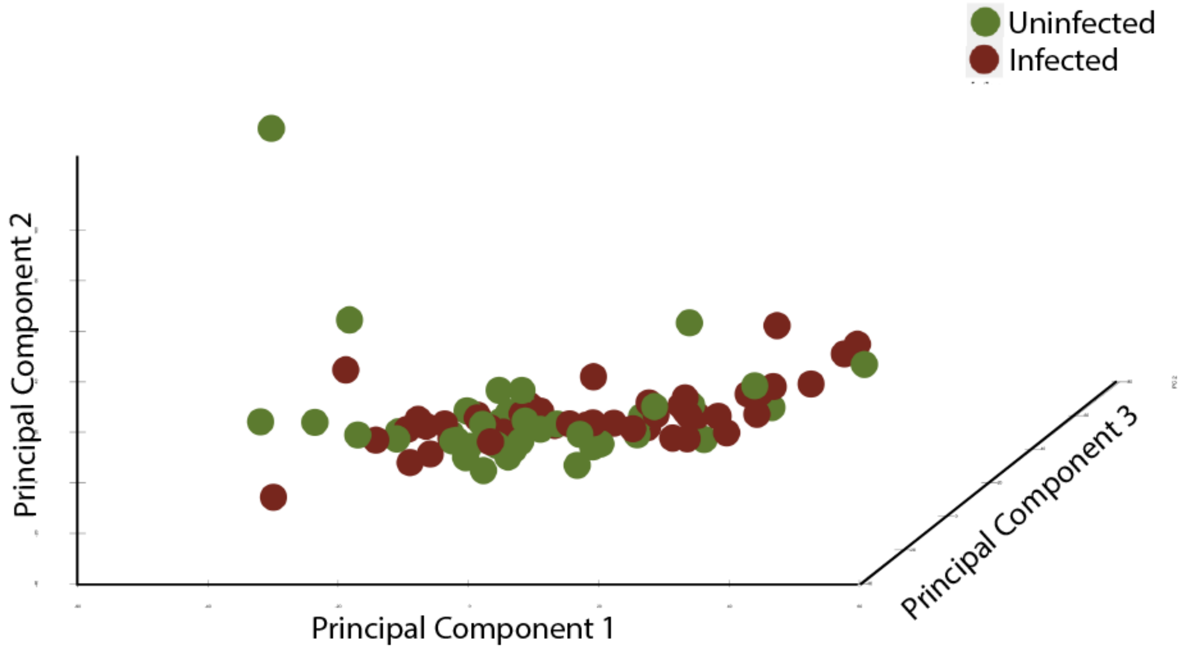

FIGURE 7. 17 PCA PLOT FOR UNSUPERVISED CLASSIFICATION OF INFECTED AND UNINFECTED SAMPLES VACUUM FILTERED THROUGH SERS-ACTIVE MEMBRANES

TABLE 7. 6 DIAGNOSTIC PERFORMANCE OF RAMAN SPECTROSCOPY WITH SERS-ACTIVE MEMBRANES ON CLINICAL SAMPLES

		Reference Pathogen	
		Uninfected control	**Infected**
Predicted pathogen	**Uninfected control**	25	16
	Infected	20	32
Diagnostic performance			
Accuracy		61.3% (95% CI: 50.6- 71.2%; p-value: 0.61)	
Cohen’s kappa		0.22	
Sensitivity		66.7%	
Specificity		55.6%	

The results of supervised learning through PC-LDA are presented in **Table 7.6**. The diagnostic performance had an accuracy of 61.3% (95% CI: 50.6-71.2%. p-value 0.61). The diagnostic sensitivity and specificity were 66.7% and 55.6% respectively.

7.3.3.3 CLASSIFICATION OF UROPATHOGENS IN CLINICAL SAMPLES

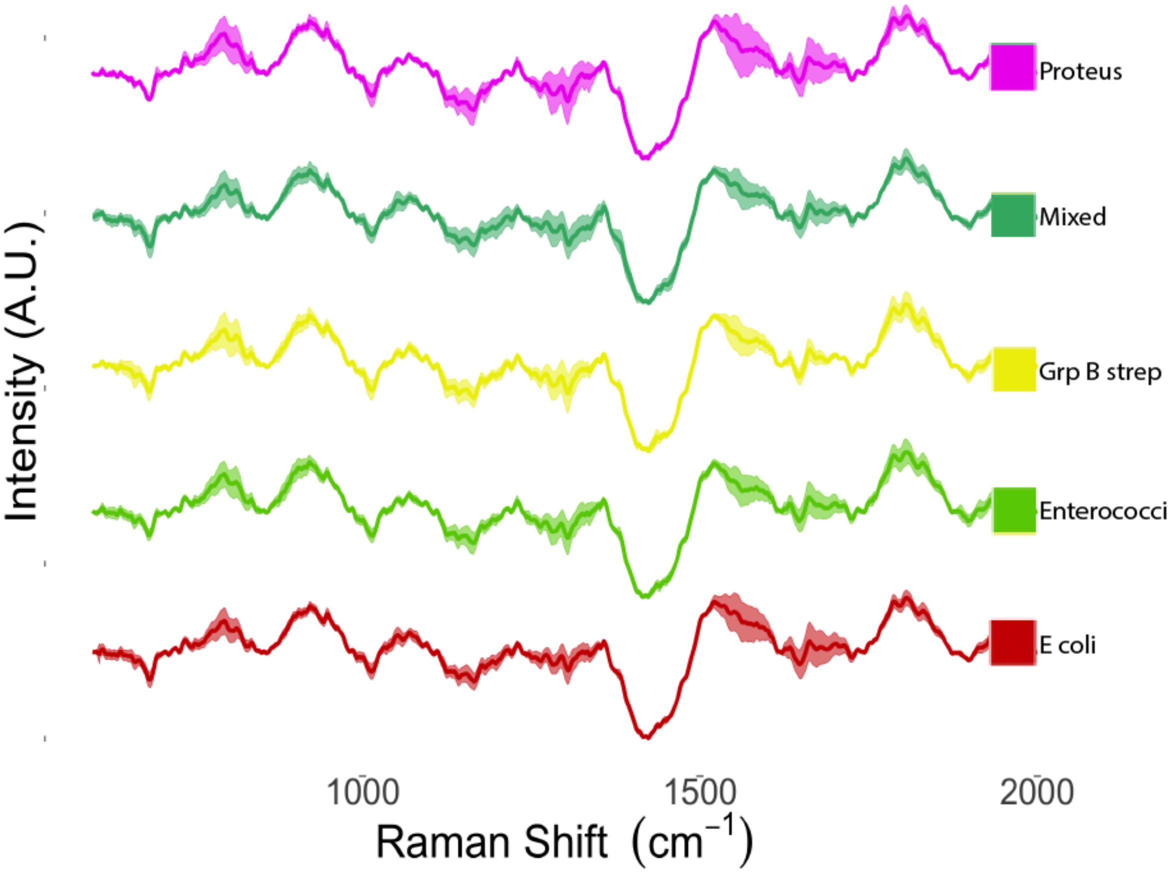

FIGURE 7. 18 MEAN SPECTRA WITH STANDARD ERROR RIBBONS FOR PATHOGENS FROM CLINICAL URINE SAMPLES VACUUM FILTERED ONTO SERS-ACTIVE MEMBRANES. NO DIFFERENCES ARE VISIBLE IN THE SPECTRA, WHILE WIDE STANDARD ERROR RIBBONS INDICATE A HIGH DEGREE OF SPECTRAL VARIABILITY.

Figure 7.18 presents the mean spectra with standard error ribbons acquired from clinical samples vacuum filtered through SERS-active membrane filters. No discernible differences are visible on the plotted spectra. Relatively wide standard error ribbons indicate a high degree of within group spectral variability.

Figure 7.19 present pairwise comparisons of spectra acquired from clinical samples vacuum filtered through SERS-active membranes. Horizontal lines delineate the boundary at which point differences are statistically significant at $\alpha = 0.05$. With the exception of the spectra referenced on Proteus spectra, none of the spectra demonstrate statistically significant peaks. The peaks arising from the Proteus spectra may reflect outliers in the small number of samples (n=3).

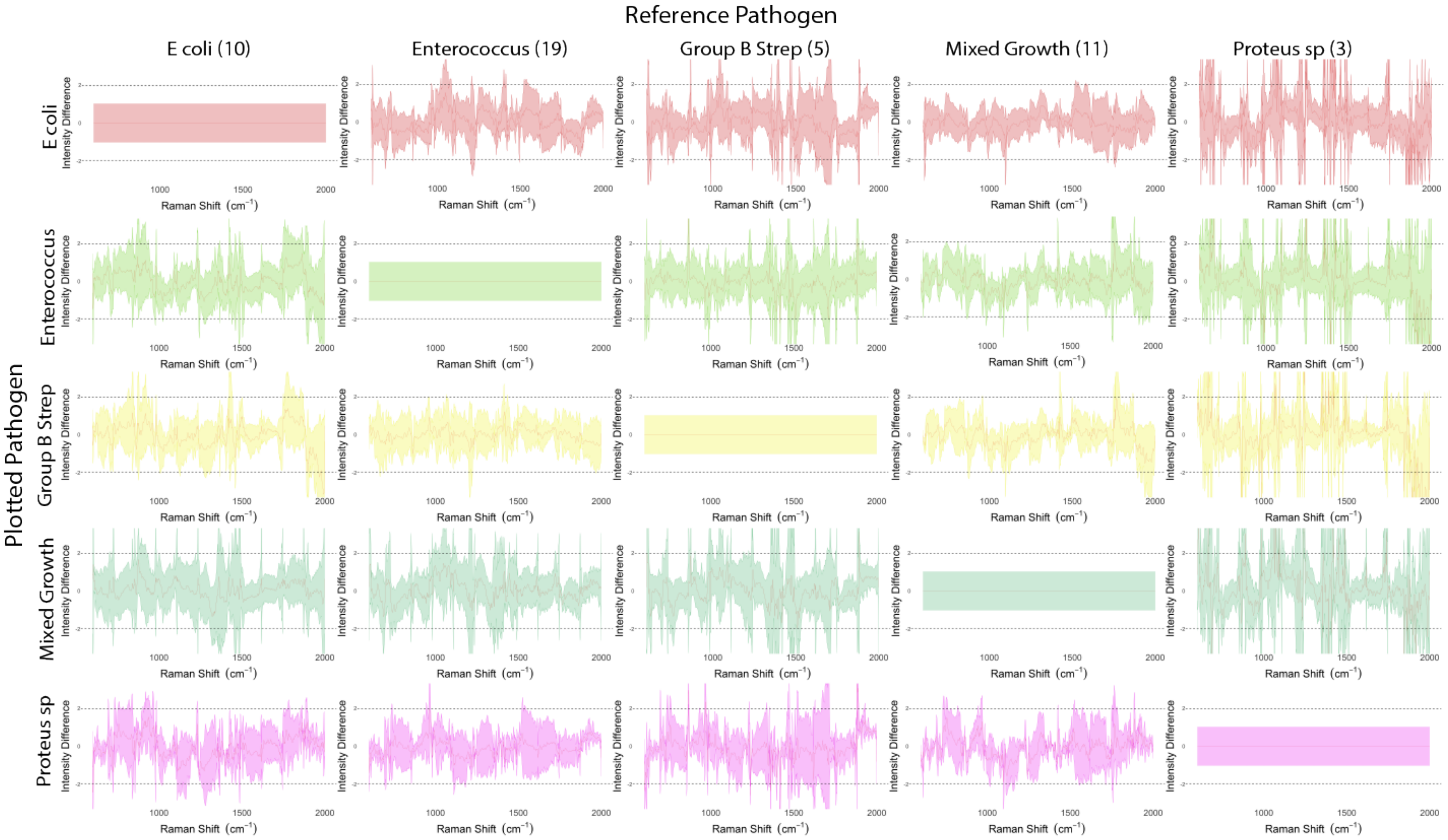

FIGURE 7. 19 MEAN SPECTRUM WITH STANDARD ERROR RIBBON OF ALL PATHOGEN SPECTRA CENTRED AND SCALED BY ALL OTHER PATHOGEN SPECTRA. HORIZONTAL DASHED LINES DELINEAT THE BORDER AT WHICH DIFFERENCE WOULD BE SIGNIFICANT AT α = 0.05. NO SIGNIFANT PEAKS ARE PRESENT WHILE WIDE STANDARD ERROR RIBBONS INDICATE A HIGH DEGREE OF SPECTRAL VARIABILITY.

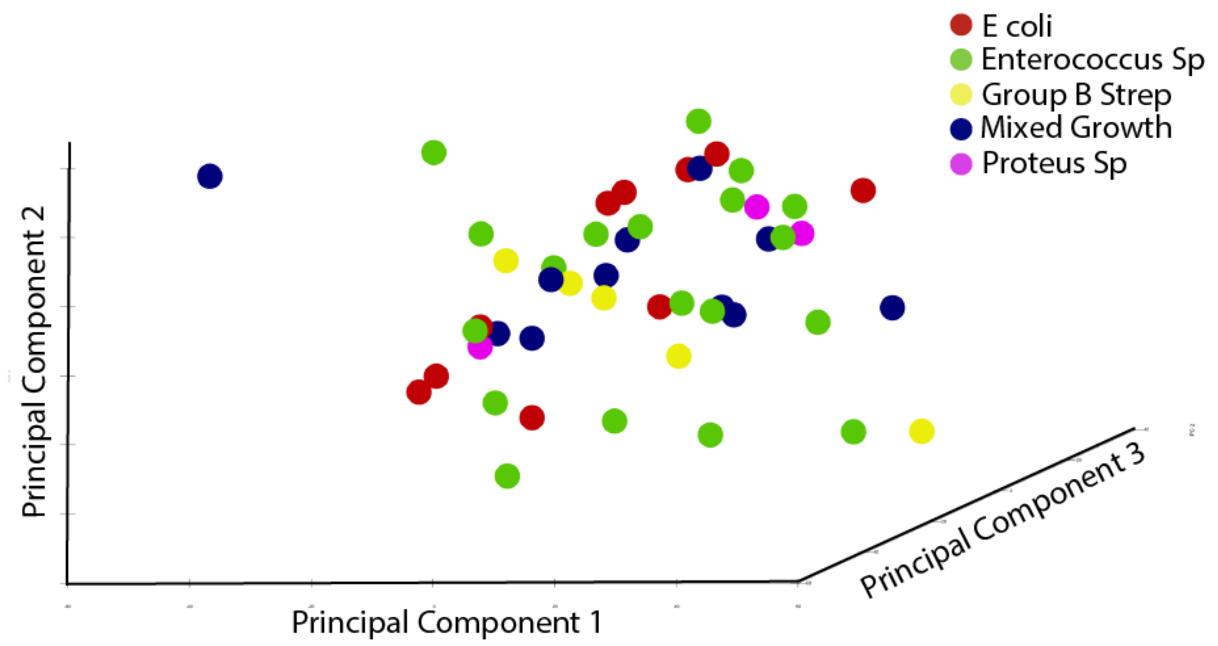

FIGURE 7. 20 PCA PLOT FOR SPECTRA ACQUIRED FROM INFECTED CLINICAL SAMPLES VACUUM FILTERED THROUGH SERS-ACTIVE FILTERS

Figure 7.20 presents unsupervised learning using PCA for spectra acquired from infected clinical samples vacuum filtered onto SERS-active membranes. The plot of the first three principal components demonstrates no natural clustering or separation by pathogen type.

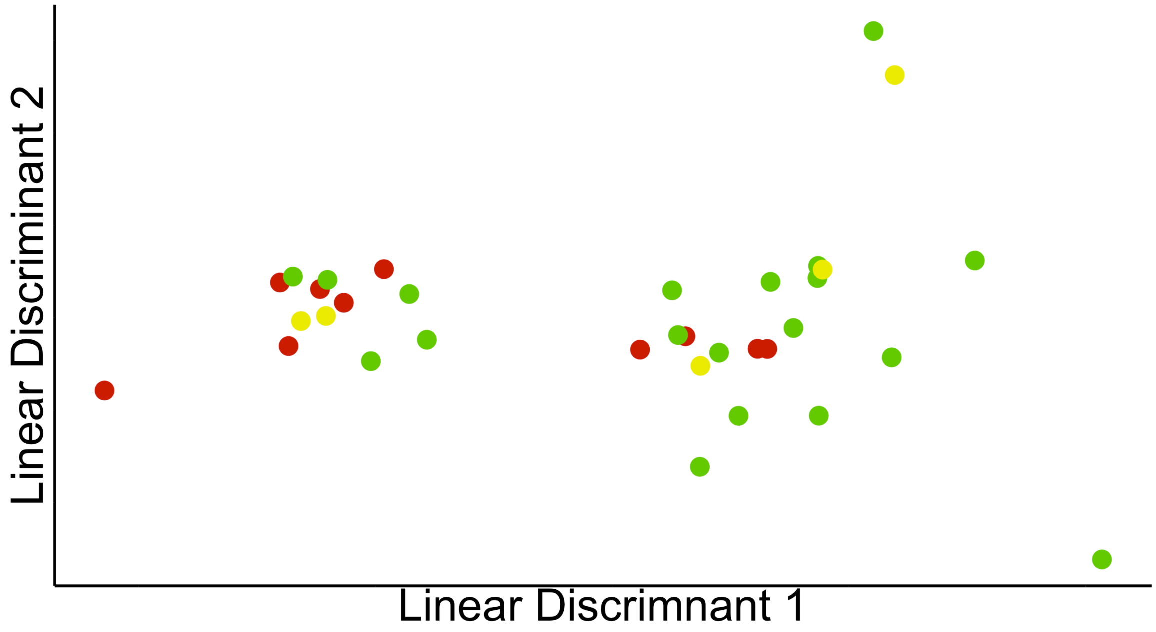

FIGURE 7. 21 PC-LDA CLASSIFICATION OF SPECTRA ACQUIRED FROM CLINICAL UROPATHOGENS ON SERS-ACTIVE MEMBRANES. MIXED SAMPLES WERE EXCLUDED FROM THE ANALYSIS IN LIGHT OF THE INCREASED COMPLEXITY OF MIXED ORGANISM SAMPLES WHILE PROTEUS SPECIES WERE EXCLUDED IN LIGHT OF SMALL SAMPLE NUMBERS.

Figure 7.21 presents supervised learning through PC-LDA for spectra acquired from infected clinical samples vacuum filtered onto SERS-active membrane filters. Mixed infection samples were excluded from analysis due to the challenges of multi-organism classification as well as the potential for a correct classification appearing incorrect. Proteus species samples were excluded due to the small number of samples available for analysis (n=3). Samples were classified with 64.7% (95% CI: 46.5;80.25. p-value 0.37) accuracy (**Table 7.7**). The high number of misclassifications led to species level sensitivities ranging from 20 to 84%, with specificities ranging from 53 to 97%.

TABLE 7. 7 PC-LDA CLASSIFICATION OF SPECTRA ACQUIRED FROM CLINICAL UROPATHOGENS.

		Reference Pathogen		
		Escherichia coli	***Enterococcus species***	***Group B Strep***
Predicted Pathogen	***Escherichia coli***	5	3	1
	Enterococcus species	4	16	3
	Group B streptococci	1	0	1
Classification performance				
Overall	**Accuracy**		64.7% (95% CI: 46.5-80.25%; p-value 0.37)	
	Cohen's Kappa		0.34	
Escherichia coli	**Sensitivity**		50%	
	Specificity		83%	
Enterococcus species	**Sensitivity**		84%	
	Specificity		53%	
Group B Streptococci	**Sensitivity**		20%	
	Specificity		97%	

7.3.5 DISCUSSION

Accurate diagnosis of UTIs with pathogen classification was not achieved using SERS-active filters in this pilot study.

The diagnostic accuracy of 61.3% (95% CI: 50.6-71.2%. p-value 0.61) is not statistically different to random assignment. The diagnostic performance here is inferior to current screening technologies such as urinalysis.

Similarly, the classification performance of 64.7% (95% CI: 46.5-80.25%; p-value 0.37) was not statistically better than random assignment and is inferior to currently implemented classification technologies.

Kloss et al. and *Schroder et al.* both achieved perfect classification of clinical samples in their published works[99, 117]. Direct comparison however is challenging, both because the small number of samples assessed in these studies limits generalisability, and more importantly spectra were acquired with a Raman microscope. The use of a Raman microscope in these works has the advantage of much higher resolution spectra afforded by the narrow focal volume, but with the disadvantage of limited room for clinical translation given the cost, physical footprint and technical expertise required to for Raman microscopes[88, 100, 101].

While SERS-active filter did not achieve sufficient signal for diagnosis and classification, there appears to be similar signal to that seen in the earlier work using phantom urine samples. The spectral plots of infected and uninfected samples (**Figures 7.6 and 7.15**) demonstrate similar peaks however large degree of variability evidenced by the wide standard error ribbons. This is more clearly presented in the relative difference plots (**Figures 7.7 and 7.16** which display similar form which has been flattened during scaling by the considerable variability present in the uninfected samples.

Understanding the factors that lead to this variability is important for planning further research and potentially improving the technology. Pathogens used in earlier works were controlled to minimise variability by using a single reference strain for each species, control the growth phase of the pathogen, and control of the pathogen load. Clinical samples vary with regards to all these factors. Clinical samples represent an array of uropathogen strains. Raman spectroscopy has been demonstrated to provide sensitive classification down to strain level, and similarly misclassification may be attributed to components such as O-antigens[101]. Clinical samples contain pathogens across the spectrum of growth phases. As pathogens progress through the growth cycle the cell envelope undergoes dynamic changes to fulfil the different metabolic requirements. These dynamic changes are reflected by changes in the Raman spectra[123, 151].

UTI samples are frequently polymicrobial. These mixed infections have important clinical ramifications, and as such are important to diagnose. Mixed infections present a substantial classification challenge to Raman spectroscopy[87]. The Raman spectrum is composed of the sum of the peaks arising from the Raman scattered photons[217]. While achieving classification of infected samples should be possible, pathogen classification is likely to be highly challenging.

Experimental parameters of the phantoms study were used in this study to avoid overfitting, however these parameters led to 7 saturated spectra. Review of the sample did not reveal a pattern, as these included both negative and positive samples, with multiple pathogens and on different days. The device was calibrated for all samples. Reduced power or acquisition time will avoid this in future work.

A representative assessment of the diagnostic and classification performance of this technology will require a larger study population. This study may be optimised in a few ways. In the first instance, sampling could be optimised using augmented sampling to provide equal numbers of infected and uninfected sample. Potentially augmented sampling could limit positive samples to two uropathogens, again with an even split. Even numbers, while not truly representative maximises statistical efficiency of the study[218]. The gold standard comparator can be reconsidered, as while culture provides definitive diagnosis of infection, the classification provided by chromogenic agar provides broad classification to uropathogen groups[6]. The ideal gold standard comparator would provide granular strain-level classification, allowing for identification of possible sources of misclassification. Finally, the larger sample size will allow for a SVM classifier to be used. Using the findings here the sample size required to assess whether SERS-active filters can diagnose UTIs with 85% sensitivity and specificity is 392 samples (See appendix).

In addition to optimising the structure of a clinical trial to better characterise the diagnostic and classification performance of the SERS technology, the technology may too be optimised to improve this performance. Most notably, a more up-to-date handheld spectrometer than the IDRaman mini 2.0 may be used. Newer handheld spectrometers offer a smaller focal volume, therein allowing the uropathogens to constitute a greater proportion of this volume which is likely to improve the SNR. To make best use of this smaller focal volume changes, an autofocus may developed to ensure this is properly focussed on the pathogens. Finally, a newer spectrometer is likely to have a more sensitive CCD which will improve spectral resolution.

7.4 CONCLUSION

Uropathogens have unique Raman spectra, that potentially allow for Raman spectroscopy to fulfil the role of an ideal diagnostic technology for UTIs. Fulfilling this role, however, is dependent on methods to physically capture and concentrate pathogens and enhance the Raman signal. Membrane filters paired with SERS enhancement provided signal using colloidal nanoparticles in **Chapter 6** allowed for identification of infected samples, however spectral variability did not allow for classification of uropathogens in infected samples. It was postulated nanoparticles may have induced variable enhancement through inconsistent application[98].

SERS-active filters were developed with the intention of providing more consistent enhancement, and therein better classification. PVDF membrane filters identified in **Chapter 6** as contributing minimal competing signal had a gold nanolayer applied through PVD. PVD was used due to its ability to apply a high purity gold coating with extremely fine control of the nanocoating thickness[213, 214]. The optimal thickness providing the greatest signal enhancement was identified as 50 nm.

A vacuum flask insert was also developed that reduced the filter diameter from 47mm to 10 mm. This was primarily to allow for more efficient filter production but provided additional roles of concentrating the pathogens into a smaller area, as well as allowing for dual filtration.

The diagnostic and classification performance were validated using phantom urine samples. Diagnostic accuracy of 93.2% exceeds that of currently implemented screening technologies, while the classification accuracy 91.7% is comparable to gold standard culture and emerging technologies such as mass spectrometry[5, 56, 215, 216, 219].

Following on from this success, a pilot was performed attempting diagnosis and classification of clinical samples using SERS-active filters. While SERS-active filters were unable to identify infected samples, the pilot demonstrated a similar signal to that seen in the phantoms. In future work, the findings of the pilot clinical study will be used to guide further development and improvement of the Raman acquisition system as well as inform the design of a representative clinical trial.

CHAPTER 8: CONCLUSION

8.1 SYNOPSIS OF THE COMPLETED WORK

The considerable disease burden caused by UTIs is severely exacerbated by an outdated diagnostic paradigm characterised by inaccuracy and diagnostic delay. A new UTI diagnostic paradigm was proposed by *Davenport et al.* in which accurate recognition of infected samples is provided near the point of care, with pathogen classification and AST following in the hours thereafter[5]. This paradigm likely falls short too, as it fails to deliver the diagnostic information required for precision antimicrobial therapy to be prescribed at the correct time and place. An ideal diagnostic technology upon which a new diagnostic paradigm can be built would deliver accurate UTI diagnosis with pathogen classification at the point of care therein allowing precision antimicrobial therapy to be tailored from the outset.

Raman spectroscopy has potential to perform as a suitable technology to achieve rapid and accurate UTI diagnosis with pathogen classification. The sensitivity of Raman spectroscopy allows for strain level pathogen classification without prior biomass expansion through cultivation, with minimal physical processing or reagents. As such, Raman spectroscopy is amenable to development into a point-of-care device. Handheld Raman spectrometers in particular have additional benefits in their small physical footprint and relatively low cost.

This thesis proves the hypothesis that Raman spectroscopy can provide rapid and accurate UTI diagnosis with pathogen classification, using a compact handheld device suitable for use at the point of care. In so doing, it takes the first steps in the development of a diagnostic technology that may reduce the burden of disease caused by UTIs.

The narrative review of **Chapter 2** demonstrates that the immense burden of disease caused by UTI is attributable to the massive rate at which UTIs occur. Implicit to this massive extent of disease, is that deficiencies in the diagnostic approach are similarly amplified by the massive rate the tests are required. A simple extrapolation would indicate that if urinary Dipstix are used for screening for the 150 million UTIs occurring each year, then the 80% sensitivity would lead to 30 million false negatives that incur diagnostic delays. While this is likely to be an oversimplification the point remains that staggering numbers of UTIs require a better diagnostic paradigm than currently implemented. **Chapter 2** applies the unique epidemiologic and clinical characteristics of UTIs to define the ideal diagnostic that prioritises rapid and accurate diagnosis with pathogen classification.

Raman spectroscopy is identified in **Chapter 3** as a suitable technology to fulfil the requirements of an ideal UTI diagnostic technology. Most importantly, its ability to provide highly resolved spectra without prior biomass expansion through cultivation underlies potential to be adapted to a point-of-care diagnostic. The state of the art of Raman based UTI diagnosis is addressed in the systematic review, demonstrating Raman spectroscopy's undoubtable ability to provide rapid uropathogen identification. Barriers to translation are also highlighted in the review, most notably an overreliance on powerful, yet clinically unfeasible, Raman microscopes.

Having established Raman spectroscopy as a technology with potential to provide rapid uropathogen identification **Chapter 3** also highlights the massive number of parameters under control and the extraordinary sensitivity to these. Systematic isolation and interrogation of these parameters was used in **Chapter 4** to develop a robust method that allowed for rapid evaluation of the Raman-based technologies employed in the subsequent experimental work.

Concentrated suspensions demonstrate unique Raman spectra allowing for accurate classification in **Chapter 5**. These spectra also demonstrate some substantial challenges with using handheld Raman spectroscopes: the relatively large focal volume and lower resolution result in relatively small peaks with a retained baseline.

Nonetheless, cross-validated supervised learning achieved excellent classification accuracy of 95% Extending this to clinically relevant concentrations demonstrates the weak biologic signal of pathogens is insufficient for classification, even when augmented by extended acquisition time, increased concentration and targeted analysis. Additional experimental work demonstrates the extreme spectral variation of unprocessed clinical urine samples. Combined, these findings confirm uropathogens have descriptive Raman spectra, however utilising Raman spectra for clinical diagnosis will require capture and separation of the pathogens and enhancement of the spectra.

The massive signal enhancement provided by SERS makes this the logical modality for achieving sufficient pathogen Raman signal enhancement for clinical diagnosis. The SERS spectra acquired from uropathogen suspensions using gold and silver nanoparticles of differing size were assessed in **Chapter 6**. Successful differentiation using SERS nanoparticles despite low sample numbers prompted an extension to an assessment at clinically relevant concentration. To maximise the likelihood of success, the uropathogens were first rapidly aggregated using vacuum filtration, a widely utilised microbiologic technique. Preliminary work demonstrated PVDF membrane filters to contribute minimal competing signal. Combining vacuum filtration with SERS enhancement provided by colloidal nanoparticles demonstrated acceptable diagnosis of infected samples, although suboptimal classification of the aetiologic uropathogen. The suboptimal classification performance is postulated to result from colloidal nanoparticles where consistent apposition cannot be ensured.

SERS-active membrane filters created by application of a gold-nanolayer to PVDF membrane filters using sputtered PVD were postulated to overcome the challenges of nanoparticles as agglomeration does not occur and pathogen apposition can be ensured by simple airdrying. An optimal gold nanolayer of 50 nm was established in **Chapter 7**, before validation of the SERS-active membrane filters using phantom urine samples. Excellent diagnostic and classification performance of 93.2% and 91.7% respectively were achieved. To assess clinical samples, a dual filtration device was developed to separate urine particulate matter before uropathogen capture on the SERS-active membranes. Using this device, a clinical pilot of 100 samples was performed, which, although underpowered to assess diagnostic performance provided valuable insights used to inform future work (see below).

This thesis has demonstrated that the significant burden of disease caused by UTIs and exacerbated by suboptimal diagnostic technologies may be ameliorated by Raman spectroscopy. Having demonstrated uropathogens have unique Raman spectra with classification potential, a method was sought to develop a technology that could provide rapid and accurate diagnosis at clinically relevant concentrations using a low-cost handheld Raman spectrometer. This culminated in the development and validation of SERS-active filters, capable of providing accurate diagnosis and classification direct from urine samples in minutes.

The most notable limitation of this work is the reliance on strictly controlled laboratory specimens of reference strain pathogens. Substantial methodologic work was undertaken to ensure that while the samples contained pathogens representative of UTIs, all other variation from bacterial load to pathogen stain and background solution was minimised. This is an important and necessary step while developing a Raman based technology as the researcher cannot be left to wonder if spectral variability (and ensuing misclassification) arises from the samples or from the technology. Nevertheless, reliance on these contrived samples remains a substantial barrier to furtherment of a Raman-based diagnostic technology for UTI diagnosis as the massive variation arising from multiple strains of multiple species at different pathogen loads poses a stepwise challenge in classification. Theoretically, once a technology is delivering consistent Raman spectra from pathogens overcoming the variation arising from clinical samples is a matter of acquiring a sufficiently large dataset.

Carefully controlled, cultured reference strain uropathogens were used for the majority of the studies included in this thesis. The requirement for a paired gold standard testing was therein obviated as the uropathogen was already known. The final study evaluating the performance of the SERS active filters on clinical samples was an exception, in which chromogenic urine culture was used as a gold standard reference test. Urine culture is the established gold standard diagnostic test for UTIs, however it has several limitations as a research reference standard[220].

The bladder was considered a sterile compartment until the development of highly sensitive molecular techniques has led to the recognition of the urinary microbiome[221, 222]. The urine, in fact, contains a wide range of organisms which are commensal in the urinary tract. While these organisms are non-cultivable on standard culture, they may be recognized by a novel diagnostic technology leading to an incorrectly defined false positive[54]. The recognition of commensal organism demonstrates further value to rapid and granular classification. A diagnostic test need not only identify whether a urine sample contains microbe but whether the microbe has the potential to cause disease.

Urine culture as a reference standard may be limited in providing reference classification. The laborious processes required for granular strain level classification are costly and time consuming. These processes may be reduced to limit costs, however at the expense of precision of classification. Pairing culture with mass spectrometry provides more granular classification without laborious processes to isolate and identify pathogens, however, is still reliant on successful cultivation of the microbes[58].

Composite reference standards are an eloquent mechanism for overcoming the shortcomings of any one reference test. An understanding of the relative strengths and weaknesses of reference diagnostics allows these to be combined to avoid bias arising from the reference[223, 224]. Applied to UTIs the reference test could combine mass spectrometry with PCR to provide granular classification with the potential to identify commensal organisms.

Ultimately, the performance of diagnostics needs to be assessed on clinical outcomes including such as resolution, progression and recurrence. Evermore granular diagnostics will warrant a reevaluation of the UTI paradigm linking specific microbes, both pathogenic and commensal, to specific outcomes such that the diagnostics can empower precision management.

Another potential limitation of this work is the use of PC-LDA for classification. PC-LDA suffers from inferior generalisability when compared to other supervised learning techniques such as SVM and ANNs. These supervised learning methods however require substantially larger training data and so are not feasible for the rapid prototyping required during development. Overfitting was reduced as much as possible through LOOCV of the number of components passed to LDA.

A similar argument of overfitting may be levelled against acquisition parameters and digital pre-processing where the massive parameter permutations could be adjusted to fit the data. This pitfall was avoided through the extensive methodologic work in **Chapter 4** which allowed for *a priori* selection of these parameters on pilot data. Nevertheless, the deep understanding of these parameters was developed over the entire time course, and so some of the earlier works in **Chapter 5** required *post hoc* revision of the pre-processing steps to adequately demonstrate the performance of the technology.

Estimating sample sizes for clinical studies is an important aspect of planning clinical research. Selecting an appropriate sample size is required to accurately address a research question while avoiding the harms of collecting excess data. These harms may include exposing patients to valueless testing, or subjecting them to inappropriate testing[225].

A thorough understanding of type I and type II error and it's and how these apply to the planned research are required. Type I error occurs when the null hypothesis is incorrectly rejected, and the alternative hypothesis is accepted. Applied to exploratory research assessing the diagnostic capabilities of a Raman based technology, the occurrence of type I error will lead the researcher to incorrectly conclude the technology has diagnostic capabilities. In this case the technology is likely to be subjected to further research which is likely to fail, therein consuming resources[226].

In contrast, type II error occurs when a null hypothesis is incorrectly accepted, and the alternative hypothesis is rejected. Applied to exploratory research assessing the diagnostic capabilities of a Raman-based diagnostic technology, the occurrence of a type II error will lead the researcher to incorrectly conclude a technology does not have diagnostic capability. In this case, the researcher is likely to discontinue a line of research into a technology with potential diagnostic capabilities.[226]

In exploratory research, where the aim is to identify research lines of potential value, type II error is more costly. Type I errors are less costly as these will be corrected in subsequent studies when the null hypothesis is accepted, and research lines are correctly discontinued. It is therefore preferable to overpower these exploratory studies by including increased numbers of samples.

In addition to the risk of type I and II errors, sample size estimation is determined by estimates of precision and variance as well as a clinically relevant endpoint. A challenge arises in exploratory research in that estimates of precision and variance are not known[226]. The challenge caused by the absence of precision and variance estimates is particularly stark in Raman research as small experimental variation leads to massive changes in classification performance. Therefore, performance estimates from earlier studies cannot be used as reliable estimates of precision and variance in subsequent studies.

A final challenge arises in using machine learning algorithms with cross validation to assess diagnostic performance. Using machine learning with cross validation means the data are not used only to assess the diagnostic performance, but also define the diagnostic performance. Therefore, there is no closed form solution for sample size estimation when using machine learning with cross validation[227]. Similarly, performing pilots to inform precision and variance estimates was not feasible as the estimates or precision and variance are influenced by the pilot size therein not reflecting the precision and variance that would be attained in an adequately sized study

In light of the exploratory nature of the studies as well as cross-validated PC-LDA, it was not possible to perform sample size estimation for the experimental work in this thesis. Rather interim analyses informed decisions to terminate or proceed with further data collection. A limitation of this work, therefore, is a substantial risk of selection bias in these works. While the concordance of the results of subsequent studies may somewhat mitigate the risk of selection bias, the veracity of these results cannot be relied upon in isolation and without more comprehensive assessment.

Future work should therefore provide a robust assessment of the diagnostic performance of the Raman-based diagnostic using independent data. Sample size estimates for the independent test set may be performed using the training set cross-validation performance to estimate the precision and variance.

Despite these limitations, the work presented in this thesis demonstrates the potential of SERS combined with vacuum filtration for point-of-care diagnosis of UTIs. As discussed in the following section, future work will aim to further develop this approach to improve the diagnostic and classification capabilities, therein moving it toward a clinically implementable technology.

8.2 STATE OF DEVELOPMENT AND FUTURE WORK

The work presented in this PhD has demonstrated the potential of Raman spectroscopy (deployed via the combination of SERS and vacuum filtration) to provide point-of-care diagnosis of UTI, including pathogen classification. Nonetheless, further work is required to develop this technique towards a clinically implementable technology.

In **Section 2.4** a minimum viable technology which may substantially improve the UTI paradigm was identified as one that delivers low-cost accurate diagnosis of UTIs at the point of care, with specificity having important value for community acquired UTIs which account for the majority of cases. Additional benefit is provided by accurate microbial classification and a digitalisation of results.

While rapid AST and pathogen load quantification will undoubtedly deliver benefits as the improved diagnostics empower precision management, this is secondary to the primary research targets. Nevertheless, it is an important benefit where a potential route toward delivering AST and load quantification is possible.

The key attribute of a UTI diagnostic is to be able to deliver accurate differentiation of infected from uninfected samples, with improved specificity being of value in uncomplicated community acquired UTIs. SERS-active filters differentiated infected from uninfected samples with 93.2% accuracy in phantom urine samples, providing 90% specificity. Achieving accurate diagnosis on phantom urine infections samples provides an excellent proof of concept for the technology. Attempted extension beyond proof of principal to clinical samples demonstrated the size of the challenge placed by the complexity of clinical pathogens.

Rapid turnaround was identified as a key attribute. The time taken from sample to result was achieved in minutes using the SERS-active filters. The current state of the technology required laboratory equipment which is amenable to development into a medical device. Further development toward a medical device may further improve the turnaround time by reducing the number of steps involved.

In the current early stage of development, SERS-active filters were used for UTI diagnosis in a laboratory setting. The widely employed techniques utilised in these processes are however amenable to development, and as such, the technology may be further developed to meet this key requirement.

The epidemiologic characteristics of UTI necessitate a diagnostic be low-cost. The SERS-active filters, which constitute the main consumable cost were produced at a low-cost. In the research setting the preparation a single SERS-active filter cost a few pennies. Importantly, the PVD process is used on industrial scale in other sectors (e.g. chip manufacture, jewelry, industrial hardware), and so is amenable to scaling with cost reduction. Handheld Raman spectrometers cost thousands of pounds, which as a single capital expense may be offset by the high incidence and therefore high usage of these devices.

Pathogen identification was identified as a secondary, but highly important attribute for a UTI diagnostic. Pathogen classification accuracy of 91.7% was achieved in phantom urine samples, demonstrating proof of principle. Importantly, the same spectrum is used for diagnosis is classification, and as such no further processing time is incurred. Variation in clinical pathogens highlight the requirement for substantially larger training sets. An additional secondary benefit arises in that the spectra are digitally collected and processed, and therefore the results may be stored in a database for secondary research or disease surveillance.

In summary, this work has delivered a technology with a proof of principle capabilities in line with a minimum viable product for UTI diagnosis. Large scale research is required to develop the training sets required for clinical samples, and in so doing demonstrating the diagnostic performance. The technology is amenable to further development required to deliver a clinically implementable medical device.

TABLE 8. 1 STATE OF TECHNOLOGY AND FUTURE REQUIREMENTS TOWARD PREDEFINED FUNCTIONAL REQUIREMENT SPECIFICATION

Attribute	State of the technology	Future development required
Key attributes		
Accurate differentiation of infected from uninfected samples	Proof of principle achieved with 93.2% accuracy in phantom urine samples using SERS-active filters	Large clinical trial to assess the diagnostic performance in clinical samples
Rapid	Sample to result achieved in minutes	
Low cost	SERS-active filters produced for pennies.	Amenable to mass production with likely further cost improvements
Point of care	Sample processing performed using widely-available laboratory equipment amenable to	Development toward a standalone medical device
Secondary attributes		
Uropathogen classification	Proof of principle achieved with 91.7% accuracy in phantom urine samples using SERS-active filters	Large clinical trial to assess the diagnostic performance in clinical samples
Digital results	Results are digital	

An appropriately powered clinical assessment of SERS-active filters is warranted. A challenge of Raman research for UTI diagnosis arises in that the extreme sensitivity of Raman spectra to technical and experimental parameter means that any change to these parameters limits the use of data collected prior to the change. As such, prior to initiation of a clinical trial the technology needs to be as close to fully optimised as feasible.

The IDRaman mini 2.0 used in this thesis is a low-cost handheld spectrometer first produced in 2013[166]. By way of comparison a more up to date, similarly priced handheld spectrometer the Metrohm Mira P may be used. Both spectrometers have a 100mW excitation power 785 nm laser source. The spectra resolution of the Mira P is 8-10 cm^{-1} as compared to 12-14 cm^{-1} on the IDRaman. The smallest attainable spot size on the Mira P is 0.042 mm as compared to 0.2 mm on the IDRaman. Spot size (controlled using focal length) was demonstrated in **Chapter 4** to provide a non-linear improvement in amplitude and quality of spectra. As such these two features alone should provide spectra with higher resolution and considerably higher signal-to-noise ratio, therein allowing for better classification.

In this thesis a spectrometer support was designed and 3D-printed to ensure consistent focal length and spot size. However, with the quality of the spectra demonstrated to vary substantially with as small as 0.5 mm differences, it is likely an autofocus will ensure greatest spectral intensity and resolution. This may be simply implemented with a moving sample stage that finds the maximal intensity as defined by AUC before starting the spectral acquisition. This would be of particular value should a spectrometer such as the Mira P be used, in which gaining the greatest benefit from the smaller spot size is contingent on accurate focussing.

The commercially available 0.45 μm PVDF filters used to create SERS-active filters are intended for sample sterilisation or pathogen isolation rather than spectral acquisition. The randomly arranged PVDF fibres, lead to some variation of gold deposition and apposition to pathogens. A preliminary specific-to-purpose has been designed using Fusion360 CAD and a prototype 3D printed using a Nanoscribe 3D printer (**Figure 8.1)**. The design consists of uniformly repeating filter pore units parametrically designed to allow fine tuning to optimally appose pathogens to the SERS gold layer. Further work is required to optimise the design parameters, and compare the enhancement against the current PVDF membrane filters. However, a custom filter designed specifically for pathogen measurements will have the potential to improve signal levels, and hence classification in future experiments in which SERS-active filters are used.

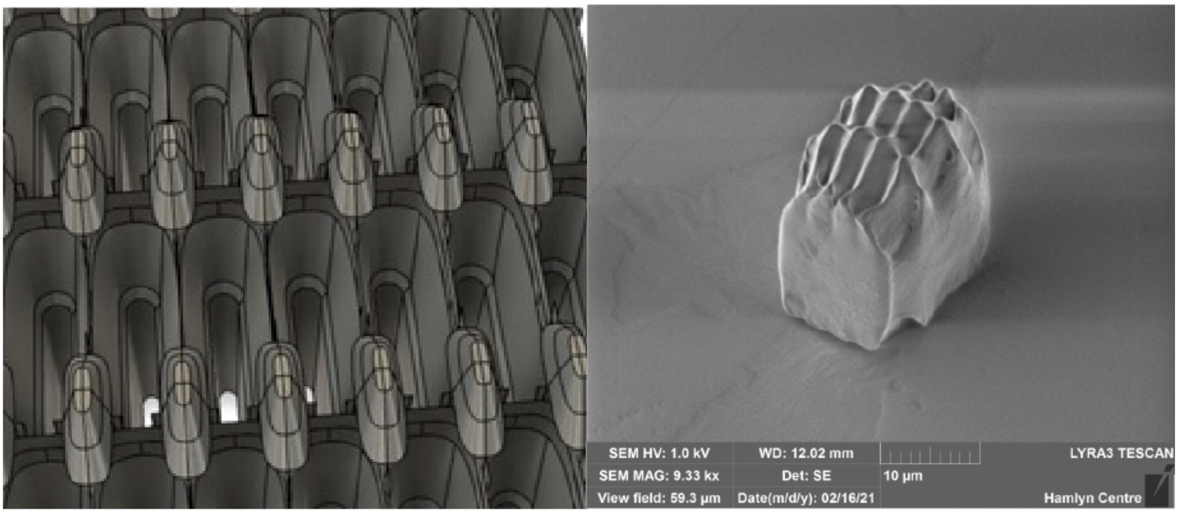

FIGURE 8. 1 A RATIONALLY DESIGNED FILTER. A CAD MODEL OF UNIFORMLY REPEATING UNITS PARAMETRICALLY DESIGNED FILTER PORES TO MAXIMISE PATHOGEN-SERS APPOSITION (LEFT PANEL). A SEM OF A NANOSCALE 3D-PRINTED FILTER USING A NANOSCRIBE 3D PRINTER (RIGHT PANEL).

Once optimised the performance of the Raman UTI diagnostic needs to be assessed, with several important considerations informed by the learnings of this thesis.

M, C&S is the established gold standard for clinical UTI diagnosis, however this may be suboptimal as a gold standard comparator. The primary outcome is likely to be infection defined as growth equal to or greater than 10^5 CFU/ml, for which M, C&S is ideal. A similarly important outcome however is the classification performance, for which standard culture is less appropriate. The high resolution of Raman spectra allows for much more granular classification than provided for by standard culture, which may lead to what appears as misclassification. An example of this is demonstrated by *Mircescu et al.,* where variations in O-antigens between strains led to misclassifications between *E. coli* and *P. mirabilis*[101]. A more appropriate gold standard comparator for classification performance may be PCR or mas spec. An additional consideration is that M, C&S correlates poorly with clinical outcomes, because of both asymptomatic bacteriuria leading to false positives and non-cultivable bacteria leading to false negatives. PCR has been demonstrated to correlate better with clinical outcomes.

PC-LDA was used for supervised learning in this thesis to allow for rapid assessment of classification performance with few samples. Supervised learning provided by SVMs or ANNs provide better generalisability, while ANNs are likely to require less pre-processing (and so retain greater signal). A substantially larger study population is required, both to overcome the variability anticipated in clinical samples, and to train these algorithms.

8.3 EXPANDING HORIZONS

Raman spectroscopy is uniquely suited to rapid phenotypic antimicrobial sensitivity testing (AST). Pathogen classification using Raman spectroscopy, and SERS in particular, is achieved through recognition of cell envelope components. The effects of antimicrobials are typically first evident in the cell envelope as this is where the majority of metabolism takes place. As such, chemometric evidence of antimicrobial efficacy typically precedes visual evidence. Theoretically, any Raman technology able to classify pathogens should similarly be able to differentiate antimicrobial resistant species from sensitive ones. Indeed, Raman AST has been demonstrated in a number of works[89, 156]. AST using SERS-active filters should therefore be interrogated in future work.

The processes that underpin SERS-active filters are not unique to urine, but rather can be applied to any biofluid at risk of infection. The diagnostic and classification performance of SERS-active filters should be assessed on biofluids including blood and cerebrospinal fluid. This may be contingent on additional physical processing, such as differential centrifugation of blood to separate eukaryotic cells from pathogens.

8.4 CONCLUSION

In summary, Raman spectroscopy is uniquely suited to alleviating the burden of disease caused UTIs in light of its ability to overcome the shortcomings of current diagnostic technologies. Specifically, the ability to achieve high resolution spectra without the need for prior biomass expansion allows for rapid and accurate classification. This thesis progressed to develop technology that may overcome both weak biologic Raman scattering from pathogens and the substantial noise present in urine. SERS-active filters are validated as a feasible technology to underpin a point of care diagnostic for UTIs. Future work will now seek to further develop this technique toward a clinically implementable solution.

APPENDIXES

SAMPLE SIZE CALCULATION FOR FUTURE CLINICAL WORK

$$n_{Se} = \frac{z^2\,\widehat{Se}(1-\widehat{Se})}{d^2\,Prev}$$

$$n_{Se} = \frac{1.96^2(0.85)(1-0.85)}{o.05^2(0.5)}$$

$$\underline{n_{Se} = 391.84 \approx 392}$$

$$n_{Sp} = \frac{z^2\,\widehat{Sp}(1-\widehat{Sp})}{d^2\,(1-Prev)}$$

$$n_{Sp} = \frac{1.96^2(0.85)(1-0.85)}{o.05^2(1-0.5)}$$

$$\underline{n_{Se} = 391.84 \approx 392}$$

n_{se} = Study sample size required for sensitivity

n_{sp} = study sample size required for specificity

z = Z cumulative (at $\alpha = 0.05$)

prev = prevalence

d = marginal error rate

R- SCRIPT

R code available at: https://github.com/simon-dryden/UTI-POCT-code

References

1. Flores-Mireles, A.L., et al., *Urinary tract infections: epidemiology, mechanisms of infection and treatment options.* Nature Reviews Microbiology, 2015. **13**(5): p. 269-284.
2. Foxman, B., *The epidemiology of urinary tract infection.* Nat Rev Urol, 2010. **7**(12): p. 653-60.
3. NICE, *UTI (Catheter): antimicrobial prescribing*. 2018.
4. D'eVille, W.L., et al., *The urine dipstick test useful to rule out infections. A meta-analysis of the accuracy.* BMC Urology, 2004. **4**.
5. Davenport, M., et al., *New and Developing Tehnologies for Urinary Tract Infections.* Nature Urology, 2017. **14**: p. 296-310.
6. Aspevall, O., et al., *Performance of four chromogenic urine culture media after one or two days of incubation compared with reference media.* J Clin Microbiol, 2002. **40**(4): p. 1500-3.
7. Granger, J.H., et al., *Prospects for point-of-care pathogen diagnostics using surface-enhanced Raman scattering (SERS).* Chem Soc Rev, 2016. **45**(14): p. 3865-82.
8. Foxman, B., *Urinary Tract Infection Syndromes.* Infectious Disease Clinics of North America, 2014. **28**(1): p. 1-13.
9. Zarb, P., et al., *The European Centre for Disease Prevention and Control Pilot Point Prevalence Survey of Healthcare-Associated Infections and Antimicrobial Use.* Euro Surveill, 2012. **17**(46).
10. Foxman, B., *Epidemiology of Urinary Tract Infections: Inciddence, Morbidity and Economic Costs.* The American Journal of Medicine, 2002. **113**(1A).
11. Chenoweth, C.E. and S. Saint, *Urinary Tract Infections.* Infect Dis Clin North Am, 2016. **30**(4): p. 869-885.
12. Al-Hasan, M.N., J.E. Eckel-Passow, and L.M. Baddour, *Bacteremia complicating gram-negative urinary tract infections: A population-based study.* Journal of Infection, 2010. **60**: p. 270-285.
13. Parker, V., et al., *Avoiding inappropriate urinary catheter use and catheter-associated urinary tract infection (CAUTI): a pre-post control intervention study.* BMC Health Serv Res, 2017. **17**(1): p. 314.
14. Magill, S.S., et al., *Multistate Point-Prevalence Survey of Health Care-Associated Infections.* N Engl J Med, 2014. **370**(13): p. 1198-1208.
15. Nicolle, L.E., *Catheter Associated Urinary Tract Infections.* Antimicrobial Resistance and Infection Control, 2014. **3**(23).
16. Saint, S., et al., *Are Physicians Aware Of Which of Their Patients Have Indwelling Urinary Catheters?* Am J. Med, 2000. **109**: p. 476-480.
17. Tiwari, M.M., et al., *Inappropriate use of urinary catheters: a prospective observational study.* Am J Infect Control, 2012. **40**(1): p. 51-4.
18. Rosenthal, V.D., et al., *International Nosocomial Infection Control Consortium (INICC) report, data summary of 36 countries, for 2004-2009.* Am J Infect Control, 2012. **40**(5): p. 396-407.
19. Salgado Yepez, E., et al., *Device-associated infection rates, mortality, length of stay and bacterial resistance in intensive care units in Ecuador: International Nosocomial Infection Control Consortium's findings.* World J Biol Chem, 2017. **8**(1): p. 95-101.
20. Melzer, M. and C. Welch, *Outcomes in UK patients with hospital-acquired bacteraemia and the risk of catheter-associated urinary tract infections.* Postgrad Med J, 2013. **89**(1052): p. 329-34.
21. Fortin, E., et al., *Healthcare-associated bloodstream infections secondary to a urinary focus: the Quebec provincial surveillance results.* Infect Control Hosp Epidemiol, 2012. **33**(5): p. 456-62.
22. Chant, C., et al., *Relationship of catheter-associated urinary tract infection to mortality and length of stay in critically ill patients: a systematic review and meta-analysis of observational studies.* Crit Care Med, 2011. **39**(5): p. 1167-73.
23. Saint, S., et al., *Cathter Associated Urinary Tract Infection and the Medicare Rule Changes.* Ann Intern Med, 2009. **150**(12): p. 877-884.
24. Weber, D.J., E.E. Sickbert-Bennett, and C.V. Gould, *Incidence of Catheter-Associated and Non-Catheter Associated Urinary Tract Infections in a Healthcare System.* Infect Control Hosp Epidemiol, 2011. **32**(8): p. 822-823.
25. Plowman, R., et al., *The rate and cost of hospital-acquired infections occurring in patients admitted to selected specialties of a district general hospital in England and the national burden imposed.* J Hosp Infect, 2001. **47**(3): p. 198-209.

26. Andersson, D.I. and D. Hughes, *Antibiotic resistance and its cost: is it possible to reverse resistance?* Nat Rev Microbiol, 2010. **8**(4): p. 260-71.
27. Nicolle, L.E., et al., *Infectious Diseases Society of America Guidelines for the Diagnosis and Treatment of Asymptomatic Bacteriuria in Adults.* Clin Infect Dis, 2005. **40**: p. 643-654.
28. I.W., S., *Biofilm exopolysaccharides: A Strong Stick Framework.* Microbiology, 2001. **147**: p. 3-9.
29. Weiner, L.M., et al., *Antimicrobial-Resistant Pathogens Associated With Healthcare-Associated Infections: Summary of Data Reported to the National Healthcare Safety Network at the Centers for Disease Control and Prevention, 2011-2014.* Infect Control Hosp Epidemiol, 2016. **37**(11): p. 1288-1301.
30. Scholes, D., et al., *Risk Factors Associated with Acute Pyelonephritis in Healthy Women.* Ann Intern Med, 2005. **142**: p. 20-27.
31. Lo, E., et al., *Strategies to prevent catheter-associated urinary tract infections in acute care hospitals: 2014 update.* Infect Control Hosp Epidemiol, 2014. **35**(5): p. 464-79.
32. Krein, S.L., et al., *Preventing device-associated infections in US hospitals: national surveys from 2005 to 2013.* BMJ Qual Saf, 2015. **24**(6): p. 385-92.
33. Tambyah, P.A., *Catheter-associated urinary tract infections: diagnosis and prophylaxis.* International Journal of Antimicrobial Agents, 2004. **24S**: p. S44-S48.
34. Nielubowicz, G.R. and H.L. Mobley, *Host-pathogen interactions in urinary tract infection.* Nat Rev Urol, 2010. **7**(8): p. 430-41.
35. Trautner, B.W. and R.O. Darouiche, *Role of biofilm in catheter-associated urinary tract infection.* Am J Infect Control, 2004. **32**(3): p. 177-83.
36. Donlan, R.M., *Biofilms Microbial Life on Surfaces.* Emerging Infectious Diseases, 2002. **8**(9): p. 881-890.
37. Sutherland, I., *Biofilm exopolysaccharides: A Strong Sticky Framework.* Microbiology, 2001. **147**: p. 3-9.
38. Stickler, D.J., *Clinical complications of urinary catheters caused by crystalline biofilms: something needs to be done.* J Intern Med, 2014. **276**(2): p. 120-9.
39. Jacobsen, S.M. and M.E. Shirtliff, *Proteus mirabilis biofilms and catheter-associated urinary tract infections.* Virulence, 2011. **2**(5): p. 460-5.
40. Weichhart, T., et al., *Current concepts of molecular defence mechanisms operative during urinary tract infection.* Eur J Clin Invest, 2008. **38 Suppl 2**: p. 29-38.
41. Chenoweth, C.E., C.V. Gould, and S. Saint, *Diagnosis, management, and prevention of catheter-associated urinary tract infections.* Infect Dis Clin North Am, 2014. **28**(1): p. 105-19.
42. Murray, P.R., K.S. Rosenthal, and M.A. Pfaller, *Medical Microbiology*. 7th ed. 2013, Philadelphia: elsevier.
43. Caroff, M. and D. Karibian, *Structure of bacterial lipopolysaccharides.* Carbohydr Res, 2003. **338**(23): p. 2431-47.
44. Silhavy, T.J., D. Kahne, and S. Walker, *The bacterial cell envelope.* Cold Spring Harb Perspect Biol, 2010. **2**(5): p. a000414.
45. Mosier-Boss, P.A., *Review on SERS of Bacteria.* Biosensors (Basel), 2017. **7**(4).
46. Vollmer, W., D. Blanot, and M.A. de Pedro, *Peptidoglycan structure and architecture.* FEMS Microbiol Rev, 2008. **32**(2): p. 149-67.
47. Lerouge, I. and J. Vanderleyden, *O-antigen structural variation: Mechanism and POssible Role in Animal/Plant INteractions.* FEMS Microbiol Rev, 2001. **26**: p. 17-47.
48. Kaper, J.B., J.P. Nataro, and H.L. Mobley, *Pathogenic Escherichia coli.* Nat Rev Microbiol, 2004. **2**(2): p. 123-40.
49. Mittal, R., et al., *Urinary tract infections caused by Pseudomonas aeruginosa: a minireview.* J Infect Public Health, 2009. **2**(3): p. 101-11.
50. NICE. *Urinary Tract INfection (Lower)*. 2015 July 2015 2019/01/04]; Available from: https://cks.nice.org.uk/urinary-tract-infection-lower-women#!scenario.
51. Schmiemann, G., et al., *The diagnosis of urinary tract infection: a systematic review.* Dtsch Arztebl Int, 2010. **107**(21): p. 361-7.
52. Stapleton, A.E., et al., *Performance of a New Rapid Immunoassay Test Kit for Point-of-Care Diagnosis of Significant Bacteriuria.* J Clin Microbiol, 2015. **53**(9): p. 2805-9.
53. Boonen, K.J.M., et al., *Urine flow cytometry as a primary screening method to exclude urinary tract infections.* World Journal of Urology, 2012. **31**(3): p. 547-551.

54. Sathiananthamoorthy, S., et al., *Reassessment of Routine Midstream Culture in Diagnosis of Urinary Tract Infection.* J Clin Microbiol, 2018.
55. Veron, L., et al., *Rapid urine preparation prior to identification of uropathogens by MALDI-TOF MS.* Eur J Clin Microbiol Infect Dis, 2015. **34**(9): p. 1787-95.
56. Lehmann, L.E., et al., *Rapid qualitative urinary tract infection pathogen identification by SeptiFast real-time PCR.* PLoS One, 2011. **6**(2): p. e17146.
57. Marialouis, X.A. and A. Santhanam, *Antibiotic Resistance, RAPD- PCR Typing of Multiple Drug Resistant Strains of Escherichia Coli From Urinary Tract Infection (UTI).* J Clin Diagn Res, 2016. **10**(3): p. DC05-9.
58. Wojno, K.J., et al., *Multiplex PCR Based Urinary Tract Infection (UTI) Analysis Compared to Traditional Urine Culture in Identifying Significant Pathogens in Symptomatic Patients.* Urology, 2020. **136**: p. 119-126.
59. Mach, K.E., et al., *Multiplex pathogen identification for polymicrobial urinary tract infections using biosensor technology: a prospective clinical study.* J Urol, 2009. **182**(6): p. 2735-41.
60. Mach, K.E., P.K. Wong, and J.C. Liao, *Biosensor diagnosis of urinary tract infections: a path to better treatment?* Trends Pharmacol Sci, 2011. **32**(6): p. 330-6.
61. Baltekin, O., et al., *Antibiotic susceptibility testing in less than 30 min using direct single-cell imaging.* Proc Natl Acad Sci U S A, 2017. **114**(34): p. 9170-9175.
62. Hooton, T.M., et al., *Diagnosis, Prevention, and Treatment of Catheter-Associated Urinary Tract Infection in Adults: 2009 International Clinical Practice Guidelines from the Infectious Diseases Society of America.* Clinical Infectious Diseases, 2010. **50**(5): p. 625-663.
63. NICE, *Lower UTI antimicrobial prescribing guideline.*
64. Meddings, J. and S. Saint, *Disrupting the life cycle of the urinary catheter.* Clin Infect Dis, 2011. **52**(11): p. 1291-3.
65. Lam, T.B., et al., *Types of indwelling urethral catheters for short-term catheterisation in hospitalised adults.* Cochrane Database Syst Rev, 2014(9): p. CD004013.
66. Pickard, R., et al., *Antimicrobial catheters for reduction of symptomatic urinary tract infection in adults requiring short-term catheterisation in hospital: a multicentre randomised controlled trial.* The Lancet, 2012. **380**(9857): p. 1927-1935.
67. Nace, D.A., P.J. Drinka, and C.J. Crnich, *Clinical uncertainties in the approach to long term care residents with possible urinary tract infection.* J Am Med Dir Assoc, 2014. **15**(2): p. 133-9.
68. Line, E., et al., *Overtreatment of Enterococcal Bbacteriuria.* Arch Int Med, 2012. **172**(1): p. 33-38.
69. Kastanos, E., et al., *A Novel Method for Bacterial UTI Diagnosis Using Raman Spectroscopy.* International Journal of Spectroscopy, 2012. **2012**: p. 1-13.
70. Kho, K.W., et al., *Clinical SERS: are we there yet?* J Biophotonics, 2011. **4**(10): p. 667-84.
71. Ferraro, J.R., K. Nakamoto, and C.W. Brown, *Introductory Raman Spectroscopy*. 2nd ed. 2003: Elsevier.
72. Haynes, C.L., A.D. McFarland, and R.P. Van Duyne, *Surface Enhanced Raman Spectroscopy.* Analytical Chemistry, 2005.
73. Smekal, A., *Zur Quantertheorie de Dispersion.* Naturwissenschaften, 1923. **11**: p. 873-875.
74. Raman, C.V., *A Change in Wavelength in Light Scattering.* Nature, 1928. **121**(3051): p. 619-620.
75. Raman, C.V. and K.S. Krishnan, *A New Type of Secondary Radiation.* Nature, 1928. **121**(3048): p. 501-502.
76. Maquelina, K., et al., *Identification of medically relevant microorganisms by vibrational spectroscopy.* Jourbal of Microbiolgic Methods, 2002. **51**: p. 255-271.
77. Chisanga, M., et al., *Enhancing Disease Diagnosis: Biomedical Applications of Surface-Enhanced Raman Scattering.* Applied Sciences, 2019. **9**(6).
78. Liu, T.Y., et al., *Functionalized arrays of Raman-enhancing nanoparticles for capture and culture-free analysis of bacteria in human blood.* Nat Commun, 2011. **2**: p. 538.
79. Fleischmann, M., P.J. Hendra, and A.J. McQuillan, *Raman Spectra of Pyridine Adsorbed at a Silver Electrode.* Chemical Physics Letters, 1974. **26**(2): p. 163-166.
80. Boardman, A.K., et al., *Rapid Detection of Bacteria from Blood with Surface-Enhanced Raman Spectroscopy.* Anal Chem, 2016. **88**(16): p. 8026-35.
81. Jeanmarie, D.L. and R.P. Van Duyne, *Part 1: Heterocyclic Aromatic and Aliphatic AMines Absorbed on the Anodized Silver Electrode.* J Eletroanal Chem, 1977. **84**: p. 1-20.

82. Jarvis, R.M. and R. Goodacre, *Characterisation and identification of bacteria using SERS.* Chem Soc Rev, 2008. **37**(5): p. 931-6.
83. Lorenz, B., et al., *Cultivation-Free Raman Spectroscopic Investigations of Bacteria.* Trends Microbiol, 2017. **25**(5): p. 413-424.
84. Jarvis, R.M., A. Brooker, and R. Goodacre, *Surface-Enhanced Raman Spectroscopy for Bacterial Discrimination Utilizing a Scanning Electron Microscope with a Raman Spectroscopy Interface.* Analytical Chemistry, 2004. **76**: p. 5198-5202.
85. Jarvis, R.M., S. Clarke, and R. Goodacre, *Rapid Analysis of Microbiological Systems Using SERS.* Physics and Applications, 2006. **103**: p. 397-408.
86. Jarvis, R.M. and R. Goodacre, *Discrimination of Bacteria Using Surface-Enhanced Raman Spectroscopy.* Anal Chem, 2004. **76**: p. 40-47.
87. Guicheteau, J., et al., *Bacterial mixture identification using Raman and surface-enhanced Raman chemical imaging.* Journal of Raman Spectroscopy, 2010. **41**(12): p. 1632-1637.
88. Kahraman, M., et al., *Towards single-microorganism detection using surface-enhanced Raman spectroscopy.* International Journal of Environmental Analytical Chemistry, 2007. **87**(10-11): p. 763-770.
89. Novelli-Rousseau, A., et al., *Culture-free Antibiotic-susceptibility Determination From Single-bacterium Raman Spectra.* Sci Rep, 2018. **8**(1): p. 3957.
90. xie, C., et al., *Identification of Single Bacterial Cells in Aqueous Solution Using Confocal Laser Tweezers Raman Spectroscopy.* Analytical Chemistry, 2005. **77**: p. 4390-4397.
91. Kneipp, K., et al., *Single Molecule Detection using Surface Enhanced Raman Spectroscopy.* Physical Review Letters, 1997. **78**(9): p. 1667-1670.
92. Lopez-Dıez, E.C. and R. Goodacre, *Characterization of Microorganisms Using UV Resonance Raman Spectroscopy and Chemometrics.* Anal Chem, 2004. **76**: p. 585-591.
93. Wei, D., S. Chen, and Q. Liu, *Review of Fluorescence Suppression Techniques in Raman Spectroscopy.* Applied Spectroscopy Reviews, 2015. **50**(5): p. 387-406.
94. Kalasinsky, K.S., et al., *Raman Chemical Imaging Spectroscopy Reagentless Detection and Identification of Pathogens: Signature Development and Evaluation.* Anal Chem, 2007. **79**: p. 2658-2673.
95. Manoharan, R., et al., *Effect of Cultural Conditions on Deep UV Resonance Raman Spectra of Bacteria.* Applied Spectroscopy, 1993. **47**(12): p. 2145-2150.
96. Jarvis, R.M. and R. Goodacre, *Ultra-Violet Raman Spectroscopy for Rapid Discrimination of Urinary Tract Infection Bacteria.* FEMS Microbiology Letters, 2004.
97. Jarvis, R.M., A. Brooker, and R. Goodacre, *Surface-enhanced Raman scattering for the rapid discrimination of bacteria.* Faraday Discuss., 2006. **132**: p. 281-292.
98. Liu, T.-T., et al., *A High Speed Detection Platform Based on Surface- Enhanced Raman Scattering for Monitoring Antibiotic- Induced Chemical Changes in Bacteria Cell Wall.* PLoS One, 2009. **4**(5).
99. Kloss, S., et al., *Culture independent Raman spectroscopic identification of urinary tract infection pathogens: a proof of principle study.* Anal Chem, 2013. **85**(20): p. 9610-6.
100. Kotanen, C.N., et al., *Surface enhanced Raman scattering spectroscopy for detection and identification of microbial pathogens isolated from human serum.* Sensing and Bio-Sensing Research, 2016. **8**: p. 20-26.
101. Mircescu, N.E., et al., *Towards a receptor-free immobilization and SERS detection of urinary tract infections causative pathogens.* Anal Bioanal Chem, 2014. **406**(13): p. 3051-8.
102. Goodacre, R., et al., *Rapid identification of urinary tract infection bacteria using hyperspectral whole-organism fingerprinting and artificial neural networks.* Micrbiology, 1998. **144**: p. 1157-1170.
103. Mozharov, S., et al., *Automated Cosmic Spike Filter optimized for Process Raman Spectroscopy.* Applied Spectroscopy, 2012. **66**(11): p. 1326-1333.
104. Bocklitz, T., et al., *How to pre-process Raman spectra for reliable and stable models?* Analytica Chimica Acta, 2011. **704**(1-2): p. 47-56.
105. Khedr, A., *Signal Processing for Raman Spectrscopy*, O. Charleton UNiversity, Editor. 2018.
106. Smulko, J.M., et al., *Anatomy of Noise in quantitative biological Raman Spectrscopy.* Bioaalysis, 2014. **6**(3): p. 411-421.
107. Storey, E.E. and A.S. Helmy, *Optimized preprocessing and machine learning for quantitative Raman spectroscopy in biology.* Journal of Raman Spectroscopy, 2019.

108. Byrne, H.J., et al., *Spectral pre and post processing for infrared and Raman spectroscopy of biological tissues and cells.* Chem Soc Rev, 2016. **45**(7): p. 1865-78.
109. Savitsky, A. and M.J.E. Golay, *Smoothing and Differentiation of Data Simplifies by Least Squares Procedures.* Anal Chem, 1964. **36**(8): p. 1627-1639.
110. Oliviera, F., H. HGiana, and L. Silviera, *Discrimination of Selected Species of Pathogeni Bacteria Using Near-Infrared Raman Spectroscopy and Prinicipal Component Analysis.* Journal of Biomedical Optics, 2012. **17**(10).
111. Hastie, T., R. Tibshirani, and J. Friedman, *Elements of Statistical Learning*. 2nd Edition ed. 2008: Springer.
112. Talsky, G., L. Mayring, and H. Kreuzer, *High-Resolution, Higher-Order UV/VIS Derivative Spectrophotometry.* Angewandte Chemie International Edition in English, 1978. **17**(11): p. 785-799.
113. Martinez, A., *PCA Vs LDA.* IEEE Transactions on Pattern Analysis and Machine INtellignce, 2001. **23**(2): p. 228-233.
114. Li, C. and B. Wang, *Prinicpal Component Analysis.* 2014.
115. Wold, S., K. Esbensen, and P. Geladi, *Prinicpal Component Analysis.* Chemoemetrics and Intelligent Laboratory Systems, 1987. **2**: p. 37-52.
116. Seasholtz, M.B. and B. Kowalski, *The Parsimony Principle Applied to Multivariate Calibration.* Analytica Chemica Acta, 1993. **277**(165-177).
117. Schroder, U.C., et al., *Combined dielectrophoresis-Raman setup for the classification of pathogens recovered from the urinary tract.* Anal Chem, 2013. **85**(22): p. 10717-24.
118. Tharwat, A., et al., *Linear discriminant analysis: A detailed tutorial.* AI Communications, 2017. **30**(2): p. 169-190.
119. Hsu, C.-W. and C.-J. Lin, *A comparison of methods of Multi Support Vector Machines*, in *Department of Computer Science and INfromation Engineering*. National Taiwan University: Taipei, Taiwan.
120. Ghaddar, B. and J. Naoum-Sawaya, *High dimensional data classification and feature selection using support vector machines.* European Journal of Operational Research, 2018. **265**(3): p. 993-1004.
121. Liu, J., et al., *Deep convolutional neural networks for Raman spectrum recognition: a unified solution.* Analyst, 2017. **142**(21): p. 4067-4074.
122. Kyriakides, A., et al., *Classification of Raman Spectra using the Classification Kernel.* Journal of Raman Spectroscopy, 2011. **42**: p. 904-909.
123. Avci, E., et al., *Discrimination of urinary tract infection pathogens by means of their growth profiles using surface enhanced Raman scattering.* Anal Bioanal Chem, 2015. **407**(27): p. 8233-41.
124. Tien, N., et al., *Diagnosis of Bacterial Pathogens in the Urine of Urinary-Tract-Infection Patients Using Surface-Enhanced Raman Spectroscopy.* Molecules, 2018. **23**(12).
125. Manoharan, R., et al., *UV Resonance Raman of Bacteria, Bacterial SPores Protoplasts and Calcium Dipicolinate.* Journal of Microbiological Methods, 1990. **11**: p. 1-15.
126. Gao, S., Z. Zhang, and L. He, *Filter-based surface-enhanced Raman spectroscopy for rapid and sensitive detection of the fungicide ferbam in water.* International Journal of Environmental Analytical Chemistry, 2016. **96**(15): p. 1495-1506.
127. Van Duyne, R.P., J.C. Huktsen, and D.A. Treichel, *Atomic Force Microscopy and Sureface Enhanced Raman Spectrscopy. Ag Island and Ag Film over Polymer Nanosphere Surpfaces Supported on Glass.* J Chem Phys, 1993. **99**(3): p. 2101-2115.
128. Efrima, S. and L. Zeiri, *Understanding the SERS of Bacteria.* Journal of Raman Spectroscopy, 2009. **40**: p. 277-288.
129. Rojas, E.R., et al., *The outer membrane is an essential load-bearing element in Gram-negative bacteria.* Nature, 2018. **559**(7715): p. 617-621.
130. Braun, V. and U. Sieglin, *The covalent murein-lipoprotein structure of the Escherichia coli cell wall. The attachment site of the lipoprotein on the murein.* Eur J Biochem, 1970. **13**(2): p. 336-46.
131. Efrima, S. and B.V. Bronk, *Silver Colloids Impregnating or Coating Bacteria.* J Phys Chem, 1998. **102**: p. 5947-5950.
132. Zhou, H., et al., *Label-Free in Situ Discrimination of Live and Dead Bacteria by Surface-Enhanced Raman Scattering.* Analytical Chemistry, 2015. **87**(13): p. 6553-6561.
133. Tódor, I.S., et al., *Gold nanoparticle assemblies of controllable size obtained by hydroxylamine reduction at room temperature.* Journal of Nanoparticle Research, 2014. **16**(12).

134. Lee, P.C. and D. Meisel, *Adsorption and Surface-Enhanced Raman of Dyes on SIlve and Gold SOl.* J Phys Chem, 1982. **86**: p. 3391-3395.
135. Javed, R., et al., *Role of capping agents in the application of nanoparticles in biomedicine and environmental remediation: recent trends and future prospects.* J Nanobiotechnology, 2020. **18**(1): p. 172.
136. Lin, C.-C., et al., *A filter-like AuNPs@MS SERS substrate for Staphylococcus aureus detection.* Biosensors and Bioelectronics, 2014. **53**: p. 519-527.
137. Kahraman, M., K. Keseroglu, and M. Culha, *On sample preparation for surface-enhanced raman scattering (SERS) of bacteria and the source of spectral features of the spectra.* Appl Spectrosc, 2011. **65**(5): p. 500-6.
138. Ansari, M.A., et al., *Interaction of silver nanoparticles with Escherichia coli and their cell envelope biomolecules.* J Basic Microbiol, 2014. **54**(9): p. 905-15.
139. Naja, G., et al., *Raman-based detection of bacteria using silver nanoparticles conjugated with antibodies.* Analyst, 2007. **132**(7): p. 679-86.
140. Gao, W., et al., *Intuitive Label-Free SERS Detection of Bacteria Using Aptamer-Based in Situ Silver Nanoparticles Synthesis.* Anal Chem, 2017. **89**(18): p. 9836-9842.
141. Stephen, K.E., et al., *Surface enhanced Raman spectroscopy (SERS) for the discrimination of Arthrobacter strains based on variations in cell surface composition.* Analyst, 2012. **137**(18): p. 4280-6.
142. Pahlow, S., et al., *Isolation and enrichment of pathogens with a surface-modified aluminium chip for Raman spectroscopic applications.* Chemphyschem, 2013. **14**(15): p. 3600-5.
143. Premasiri, W.R., Y. Gebregziabher, and L.D. Ziegler, *On the difference between surface-enhanced raman scattering (SERS) spectra of cell growth media and whole bacterial cells.* Appl Spectrosc, 2011. **65**(5): p. 493-9.
144. Cho, I.H., et al., *Membrane filter-assisted surface enhanced Raman spectroscopy for the rapid detection of E. coli O157:H7 in ground beef.* Biosens Bioelectron, 2015. **64**: p. 171-6.
145. Gao, S., B. Pearson, and L. He, *Mapping bacteria on filter membranes, an innovative SERS approach.* J Microbiol Methods, 2018. **147**: p. 69-75.
146. Rule Wigginton, K. and P.J. Vikesland, *Gold-coated polycarbonate membrane filter for pathogen concentration and SERS-based detection.* Analyst, 2010. **135**(6): p. 1320-6.
147. Szymborski, T., et al., *Electrospun polymer mat as a SERS platform for the immobilization and detection of bacteria from fluids.* Analyst, 2014. **139**(20): p. 5061-4.
148. Dryden, S.D., et al., *Rapid uropathogen identification using surface enhanced Raman spectroscopy active filters.* Sci Rep, 2021. **11**(1): p. 8802.
149. Yang, D., et al., *Portable bacteria-capturing chip for direct surface-enhanced Raman scattering identification of urinary tract infection pathogens.* R Soc Open Sci, 2018. **5**(9): p. 180955.
150. Prakash, O., et al., *Direct Detection of Bacteria Using Positively Charged Ag/Au Bimetallic Nanoparticles: A Label-free Surface-Enhanced Raman Scattering Study Coupled with Multivariate Analysis.* The Journal of Physical Chemistry C, 2019. **124**(1): p. 861-869.
151. Mukherjee, R., et al., *Understanding the effects of culture conditions in bacterial growth: A biochemical perspective using Raman microscopy.* J Biophotonics, 2020. **13**(1): p. e201900233.
152. Miles, A.A., S.S. Misra, and J.O. Irwin, *Estimation of the bacericidal power of blood.* J Hyg (Lond), 1938. **38**(6): p. 732-749.
153. McFarland, J., *The Nephelometer: an Instrument for Estimating the Number of Bacteria in Suspensions Used for Calculating the Opsonic Index for Vaccines.* JAMA, 1907. **XLIX**(14): p. 1176-1178.
154. Beal, J., et al., *Robust estimation of bacterial cell count from optical density.* Commun Biol, 2020. **3**(1): p. 512.
155. Khan, Z.A., M.F. Siddiqui, and S. Park, *Current and Emerging Methods of Antibiotic Susceptibility Testing.* Diagnostics (Basel), 2019. **9**(2).
156. Kastanos, E.K., et al., *A novel method for urinary tract infection diagnosis and antibiogram using Raman spectroscopy.* Journal of Raman Spectroscopy, 2010. **41**(9): p. 958-963.
157. Nordstrom, R.J., et al., *Complete urinary tract infection (UTI) diagnosis and antibiogram using surface enhanced Raman spectroscopy (SERS)*, in *Optical Diagnostics and Sensing XII: Toward Point-of-Care Diagnostics; and Design and Performance Validation of Phantoms Used in Conjunction with Optical Measurement of Tissue IV*. 2012.

158. Yogesha, M., et al., *A micro-Raman and chemometric study of urinary tract infection-causing bacterial pathogens in mixed cultures.* Anal Bioanal Chem, 2019. **411**(14): p. 3165-3177.
159. Premasiri, W.R., et al., *Rapid urinary tract infection diagnostics by surface-enhanced Raman spectroscopy (SERS): identification and antibiotic susceptibilities.* Anal Bioanal Chem, 2017. **409**(11): p. 3043-3054.
160. Schroder, U.C., et al., *Rapid, culture-independent, optical diagnostics of centrifugally captured bacteria from urine samples.* Biomicrofluidics, 2015. **9**(4): p. 044118.
161. Kahraman, M., et al., *Convective Assembly of Bacteria for SUrface Enhanced Raman Scattering.* Langmuir, 2008. **24**: p. 894-901.
162. Cook, C., J. Cleleand, and P. Hujibregts, *Creation and Critique of Studies of Diagnostic Accuracy: Use of the STARD and QUADAS Methodological Quality Assessment Tools.* Journal of Manual and Manipulative Therpay, 2007. **15**(2): p. 93-102.
163. Whitting, P., et al., *The development of QUADAS: a tool for the quality assessment of studies of diagnostic accuracy included in systematic reviews§.* BMC Biomedical Reseach Methodology, 2003. **3**(25).
164. Whitting, P., et al., *QUADAS-2: A Revised Tool for the Quality Assessment of Diagnostic Accuracy Studies.* QUADAS-2: A Revised Tool for the Quality Assessment of Diagnostic Accuracy Studies, 2011. **155**(8): p. 529-536.
165. Marotta, N.E. and L.A. Bottomley, *Surface-Enhanced Raman Scattering of Bacterial Cell Culture Growth Media.* Applied Spectroscopy, 2010. **64**(6): p. 601-606.
166. Optics, O., *IDRaman mini 2 manual*. 2015.
167. Hudson, S.D. and G. Chumanov, *Bioanalytical applications of SERS (surface-enhanced Raman spectroscopy).* Anal Bioanal Chem, 2009. **394**(3): p. 679-86.
168. Nasseri, B., et al., *Point-of-care microfluidic devices for pathogen detection.* Biosens Bioelectron, 2018. **117**: p. 112-128.
169. Premasiri, W.R., et al., *Rapid Bacterial Diagnostics via Surface Enhanced Raman Microscopy.* Spectroscopy, 2012. **27**(6): p. S8-31.
170. Choo-Smith, L.P., et al., *Investigating microbial (micro)colony heterogeneity by vibrational spectroscopy.* Appl Environ Microbiol, 2001. **67**(4): p. 1461-9.
171. Guo, S., et al., *Towards an improvement of model transferability for Raman spectroscopy in biological applications.* Vibrational Spectroscopy, 2017. **91**: p. 111-118.
172. Guo, S., T. Bocklitz, and J. Popp, *Optimization of Raman-spectrum baseline correction in biological application.* Analyst, 2016. **141**(8): p. 2396-404.
173. Vapnik, V.N., *An Overview of Statistical Learning Theory.* IEEE Trans Neural Networks, 1999. **10**(5): p. 988-999.
174. Messacar, K., *Narrow-spectrum, compared with broad-spectrum, antibiotics equally effective with less adverse events.* J Pediatr, 2018. **196**: p. 324-327.
175. Shields, R.K., et al., *Burden of illness in US hospitals due to carbapenem-resistant Gram-negative urinary tract infections in patients with or without bacteraemia.* BMC Infect Dis, 2021. **21**(1): p. 572.
176. Dalterio, R.A., et al., *The Resonance Raman Microprobe Detection of a Single Bacterial Cells from a Chromobacterial Mixture.* Applied Spectroscopy, 1987. **41**(2): p. 240-243.
177. Dalterio, R.A., et al., *An Ultraviolet (242nm Excitation) Resonance Raman Study of Live Bacteriaand Bacterial Components.* Applied Spectroscopy, 1987. **41**(3): p. 417-422.
178. Harz, M., et al., *Direct analysis of clinical relevant single bacterial cells from cerebrospinal fluid during bacterial meningitis by means of micro-Raman spectroscopy.* J Biophotonics, 2009. **2**(1-2): p. 70-80.
179. de Souza Vieira, E.E., et al., *Discrimination model applied to urinalysis of patients with diabetes and hypertension aiming at diagnosis of chronic kidney disease by Raman spectroscopy.* Lasers Med Sci, 2017. **32**(7): p. 1605-1613.
180. Moreira, L.P., et al., *Raman spectroscopy applied to identify metabolites in urine of physically active subjects.* J Photochem Photobiol B, 2017. **176**: p. 92-99.
181. Premasiri, W.R., R.H. Clarke, and M.E. Womble, *Urina Analysis by Laser Raman Spectroscopy.* Lasers in Surgery and Medicine, 2001. **28**(330-334).
182. Saatkamp, C.J., et al., *Quantifying creatinine and urea in human urine through Raman spectroscopy aiming at diagnosis of kidney disease.* J Biomed Opt, 2016. **21**(3): p. 37001.

183. MCMURDY III, J.W. and A.J. BERGER, *Raman Spectroscopy- Based Creatinine Measurement in Urine Samples from a Multipatient Population.* Applied Spectrscopy, 2003. **57**(5): p. 522-525.

184. Guimarães, A.E., et al., *Near Infrared Raman Spectrscopy (NIRS) A technique for doping control.* Spectrscopy, 2006. **20**: p. 185-194.

185. Huttanus, H.M., et al., *Raman chemometric urinalysis (Rametrix) as a screen for bladder cancer.* PLoS One, 2020. **15**(8): p. e0237070.

186. Pahlow, S., et al., *Isolation and identification of bacteria by means of Raman spectroscopy.* Adv Drug Deliv Rev, 2015. **89**: p. 105-20.

187. Ho, C.S., et al., *Rapid identification of pathogenic bacteria using Raman spectroscopy and deep learning.* Nat Commun, 2019. **10**(1): p. 4927.

188. Wang, P., et al., *Label-free mapping of single bacterial cells using surface-enhanced Raman spectroscopy.* Analyst, 2016. **141**(4): p. 1356-62.

189. Lee, W., et al., *3D-printed microfluidic device for the detection of pathogenic bacteria using size-based separation in helical channel with trapezoid cross-section.* Sci Rep, 2015. **5**: p. 7717.

190. Movasaghi, Z., S. Rehman, and I.U. Rehman, *Raman Spectroscopy of Biological Tissues.* Applied Spectroscopy Reviews, 2007. **42**(5): p. 493-541.

191. Broeren, M.A., et al., *Screening for urinary tract infection with the Sysmex UF-1000i urine flow cytometer.* J Clin Microbiol, 2011. **49**(3): p. 1025-9.

192. Van Nostrand, J.D., A.D. Junkins, and R.K. Bartholdi, *Poor Predictive Ability of Urinalysis and Microscopic Examination to Detect Urinary Tract Infection.* Am J Clin Pathol, 2000. **113**: p. 709-713.

193. Larmour, I.A., K. Faulds, and D. Graham, *SERS activity and stability of the most frequently used silver colloids.* Journal of Raman Spectroscopy, 2012. **43**(2): p. 202-206.

194. Creighton, J.A., C.G. Blatchford, and M.G. Albrecht, *Plasma Resonance Enhancement of Raman Scattering by Pyridine Adsorbed on Silver or Gold Sol Particles of Size Comparable to the Excitation Wavelength.* J. Chem Soc. Faraday Trans, 1979(75): p. 790-798.

195. Sengupta, A., M. Laucks, and E. Davis, *Surface-Enhanced Raman Spectroscopy of Bacteria and Pollen. .* Applied Spectroscopy. , 2005. **59**(8).

196. Leopold, N. and B. Lendl, *A New Method for Fast Preparation of Highly Surface-Enhanced Raman Scattering (SERS) Active Silver Colloids at Room Temperature by Reduction of Silver Nitrate with Hydroxylamine Hydrochloride.* J Phys Chem, 2003(107): p. 5723-5727.

197. Chen, L., et al., *Surface-Enhanced Raman Scattering (SERS) Active Gold Nanoparticles Decorated on a Porous Polymer Filter.* Appl Spectrosc, 2017. **71**(7): p. 1543-1550.

198. Kamińska, A., et al., *Highly reproducible, stable and multiply regenerated surface-enhanced Raman scattering substrate for biomedical applications.* Journal of Materials Chemistry, 2011. **21**(24).

199. Kaminska, A., et al., *Detection of Circulating Tumor Cells Using Membrane-Based SERS Platform: A New Diagnostic Approach for 'Liquid Biopsy'.* Nanomaterials (Basel), 2019. **9**(3).

200. Lee, C.H., et al., *Highly sensitive surface enhanced Raman scattering substrates based on filter paper loaded with plasmonic nanostructures.* Anal Chem, 2011. **83**(23): p. 8953-8.

201. Xu, F., et al., *Surface enhanced Raman scattering analysis with filter-based enhancement substrates: A mini review.* Reviews in Analytical Chemistry, 2021. **40**(1): p. 75-92.

202. Little, P., et al., *Dipsticks and diagnostic algorithms in urinary tract infection: development and validation, randomised trial, economic analysis, observational cohort and qualitative study.* Health Technol Assess, 2009. **13**(19): p. iii-iv, ix-xi, 1-73.

203. Elzey, S. and V.H. Grassian, *Agglomeration, isolation and dissolution of commercially manufactured silver nanoparticles in aqueous environments.* Journal of Nanoparticle Research, 2009. **12**(5): p. 1945-1958.

204. Stebounova, L.V., E. Guio, and V.H. Grassian, *Silver nanoparticles in simulated biological media: a study of aggregation, sedimentation, and dissolution.* Journal of Nanoparticle Research, 2010. **13**(1): p. 233-244.

205. Bae, E., et al., *Bacterial cytotoxicity of the silver nanoparticle related to physicochemical metrics and agglomeration properties.* Environ Toxicol Chem, 2010. **29**(10): p. 2154-60.

206. Medina, M. and E. Castillo-Pino, *An introduction to the epidemiology and burden of urinary tract infections.* Ther Adv Urol, 2019. **11**: p. 1756287219832172.

207. Dryden, S., et al., *Toward point-of-care uropathogen detection using SERS active filters*, in *Optical Diagnostics and Sensing XX: Toward Point-of-Care Diagnostics*. 2020.
208. Kamińska, A., et al., *Rapid detection and identification of bacterial meningitis pathogens in ex vivo clinical samples by SERS method and principal component analysis.* Analytical Methods, 2016. **8**(22): p. 4521-4529.
209. Kao, P., et al., *Surface-Enhanced Raman Detection on Metalized Nanostructured Poly(p-xylylene) Films.* Advanced Materials, 2008. **20**(18): p. 3562-3565.
210. Wang, H.H., et al., *Highly Raman-Enhancing Substrates Based on Silver Nanoparticle Arrays with Tunable Sub-10nm Gaps.* Advanced Materials, 2006. **18**(4): p. 491-495.
211. Premasiri, W.R., et al., *The biochemical origins of the surface-enhanced Raman spectra of bacteria: a metabolomics profiling by SERS.* Anal Bioanal Chem, 2016. **408**(17): p. 4631-47.
212. Premasiri, W.R., et al., *Characterization of Surface Enhanced Raman Scattering of Bacteria.* J Phys Chem, 2005(109): p. 312-320.
213. Baptista, A., et al., *Sputtering Physical Vapour Deposition (PVD) Coatings: A Critical Review on Process Improvement and Market Trend Demands.* Coatings, 2018. **8**(11).
214. Semin, D.J. and K.L. Rowlen, *Influence on Vapor Deposition Paramteters on SERS Active Ag Film Morphology and Optical Properties.* 1994, 1994. **66**: p. 4324-4331.
215. Ferreira, L., et al., *Rapid method for direct identification of bacteria in urine and blood culture samples by matrix-assisted laser desorption ionization time-of-flight mass spectrometry: intact cell vs. extraction method.* Clin Microbiol Infect, 2011. **17**(7): p. 1007-12.
216. Fletcher, J.S., et al., *Rapid discrimination of the causal agents of urinary tract infection using ToF-SIMS with chemometric cluster analysis.* Applied Surface Science, 2006. **252**(19): p. 6869-6874.
217. Mosier-Boss, P.A., et al., *SERS substrates fabricated using ceramic filters for the detection of bacteria: Eliminating the citrate interference.* Spectrochim Acta A Mol Biomol Spectrosc, 2017. **180**: p. 161-167.
218. Hajian-Tilaki, K., *Sample size estimation in diagnostic test studies of biomedical informatics.* J Biomed Inform, 2014. **48**: p. 193-204.
219. Huang, B., et al., *Direct Detection and Identification of Bacterial Pathogens from Urine with Optimized Sepcimen Processing and Enhanced Testing Algorithm.* Journal of Clinical Microbiology, 2017. **55**(5).
220. Biesheuvel, C., L. Irwig, and P. Bossuyt, *Observed differences in diagnostic test accuracy between patient subgroups: is it real or due to reference standard misclassification?* Clin Chem, 2007. **53**(10): p. 1725-9.
221. Whiteside, S.A., et al., *The microbiome of the urinary tract--a role beyond infection.* Nat Rev Urol, 2015. **12**(2): p. 81-90.
222. Drake, M.J., et al., *The urinary microbiome and its contribution to lower urinary tract symptoms; ICI-RS 2015.* Neurourol Urodyn, 2017. **36**(4): p. 850-853.
223. Tang, S., et al., *Dual composite reference standards (dCRS) in molecular diagnostic research: A new approach to reduce bias in the presence of Imperfect reference.* J Biopharm Stat, 2018. **28**(5): p. 951-965.
224. Naaktgeboren, C.A., et al., *Value of composite reference standards in diagnostic research.* BMJ, 2013. **347**: p. f5605.
225. Wang, X. and X. Ji, *Sample Size Estimation in Clinical Research: From Randomized Controlled Trials to Observational Studies.* Chest, 2020. **158**(1S): p. S12-S20.
226. Jones, S.R., S. Carley, and M. Marrison, *An Introduction to Power and Sample Size Caculation.* Emerg Med J, 2003. **20**: p. 453-458.
227. Afendras, G. and M. Markatou, *Optimality of training/test size and resampling effectiveness in cross-validation.* Journal of Statistical Planning and Inference, 2019. **199**: p. 286-301.